PHOTOPRODUCTION OF π^- FROM DEUTERIUM AT LABORATORY ENERGIES 600 TO 1250 MeV AND C.M. π PRODUCTION ANGLES 6° TO 160°

Thesis by

Patrick Lorne Walden

In Partial Fulfillment of the Requirements

for the Degree of

Doctor of Philosophy

California Institute of Technology

Pasadena, California

1972

(Submitted December 1, 1971)

ACKNOWLEDGEMENTS

This experiment was suggested and supervised by Professor Robert L. Walker. His suggestions, criticisms and advice were greatly appreciated, especially during the many difficult moments encountered in the experiment.

I would like to thank Dr. Franklin B. Welverton for his aid during the setup period of this experiment.

The experiment was done in collaboration with another student, Mr. Paul E. Scheffler, and I would like to thank him for his collaboration in all phases of the experiment.

I would like to thank Earl Emery for his maintainance of the liquid deuterium target, and I would like to thank Alfred Neubiesser and the synchrotron crew for maintaining and running the synchrotron.

Craig Maxwell built the recoil counters which performed very well, and I would like to thank him for this work.

Finally, I would like to thank W. Metcalf, T. Humphrey, G. Murata, and C. Smith for their assistance in data collection.

ABSTRACT

The differential cross sections for reaction $\gamma + n \rightarrow \pi^- + p$ have been measured for laboratory photon energies between 600 and 1250 MeV, using a liquid deuterium target. The measurements were made using a magnetic spectrometer and a recoil counter in which π's and p's were detected in various combinations. Measurements of the π^- counting rate, the π^-/π^+ counting rate ratio, and the π^-, p coincidence counting rate were used to calculate three independent values for the π^- photoproduction cross section. The cross sections from the latter two measurements were less sensitive to deuterium effects and were averaged to form the set of final data. The most notable feature of the data is the absence of an enhancement near the $F_{15}(1688)$ resonance. This feature has been predicted from quark model calculations. The $D_{13}(1520)$ resonance appears to be excited by a helicity 3/2 amplitude as was the case in π^+ photoproduction.

To Christine

TABLE OF CONTENTS

APPENDICES

LIST OF TABLES

LIST OF FIGURES

PART I INTRODUCTION

There have been many π photoproduction experiments in the resonance region (below 2 GeV) since the first ones were done in 1955, and yet there remain large holes in the experimental data where interesting physics can still be discovered.

In the experiment described in this thesis the differential cross sections of the reaction $\gamma + n \rightarrow \pi^- + p$ were measured at laboratory energies 690 to 1200 MeV and c.m. π angles 6° to 160°. The experiment was done in response to a need to bring the experimental knowledge of the π^- photoproduction cross sections to a level comparable to the π^+ and π^0 photoproduction cross sections in the same energy region. Before this experiment there existed only measurements at a few energies below 1000 MeV [1], and the region above 1000 MeV had not previously been covered. The latter region was of special interest in order to observe the effects of the "third resonance", the $F_{15}(1688)$. The new measurements, when combined with other photoproduction data, will yield much information on how the baryon resonances interact electromagnetically.

The extensive measurements from this experiment were required in order to be able to carry out a meaningful partial wave analysis. This is the only way to produce a quantitative result for the amplitude to electromagnetically excite the baryon resonances. The notation for the partial wave amplitudes in this thesis will be the ones used by Walker [2]. For each (π, nucleon) final state of orbital angular momentum ℓ there are four amplitudes designated $A_{\ell\pm}$ and $B_{\ell\pm}$. A is the helicity 1/2 amplitude where the initial photon and nucleon

spins are opposite, and B is the helicity 3/2 amplitude where the spins are aligned. The total angular momentum j for each amplitude is given by

$$j = \ell \pm 1/2 \tag{1}$$

where the $\pm$ corresponds to the $\pm$ of the amplitude. The parity for each amplitude is given by $(-1)(-1)^{\ell}$ where the extra (-1) is needed to account for the intrinsic parity of the π. We see that in general there are two π photoproduction amplitudes for each resonance, in contrast to π elastic scattering where each resonance has only one amplitude.

As with π elastic scattering, various π photoproduction reactions can be related through isospin conservation. However, this involves some basic assumption about the nature of the photon. We use the Gell-Mann-Nishijima formula

$$Q = I_3 + Y/2 \tag{2}$$

which relates a particle's charge Q to its isospin component I_3 and hypercharge Y. In electromagnetic interactions the charge Q is conserved so the photon at least acts as a combination of an isovector, I_3, and an isoscaler, Y. With this assumption any photoproduction amplitude:

$$\begin{aligned} A^{+}: &\quad \gamma + p \rightarrow \pi^{+} + n \\ A^{o}: &\quad \gamma + p \rightarrow \pi^{o} + p \\ A^{-}: &\quad \gamma + n \rightarrow \pi^{-} + p \\ A^{no}: &\quad \gamma + n \rightarrow \pi^{o} + n \end{aligned} \tag{3}$$

can be decomposed into the isospin amplitudes

$$A^{v3}, \quad A^{vl}, \quad \text{and} \quad A^{s},$$

where A^{v3} is the isospin 3/2 amplitude produced from the isovector part of the photon, and A^{v1} and A^{s} are the isospin 1/2 amplitudes produced from the isovector and isoscaler parts of the photon respectively. The isospin decomposition is given by [3]

$$\begin{aligned} A^{+} &= \sqrt{1/3}\ A^{v3} - \sqrt{2/3}\ (A^{v1} - A^{s}) \\ A^{o} &= \sqrt{2/3}\ A^{v3} + \sqrt{1/3}\ (A^{v1} - A^{s}) \\ A^{-} &= \sqrt{1/3}\ A^{v3} - \sqrt{2/3}\ (A^{v1} + A^{s}) \\ A^{no} &= \sqrt{2/3}\ A^{v3} + \sqrt{1/3}\ (A^{v1} + A^{s}) \end{aligned} \qquad (4)$$

We see from (4) that the Δ baryon resonances have one isospin amplitude, whereas the N baryon resonances have two isospin amplitudes. An isospin decomposition of the N baryon resonant amplitudes will give the relative strength with which the isovector and isoscaler parts of the photon interact.

There are other reasons for doing π photoproduction experiments. If the photon has an isotensor part as well as isovector and isoscaler parts the equations in (4) are no longer valid. If amplitudes for all four photoproduction reactions were known, the existence of an isotensor term would be quickly determined. There has been an indication [4] that such an isotensor term exists from the comparison of π^{+} and π^{-} total photoproduction cross sections in the region of the "first resonance" where the A^{v3} amplitude should dominate if no isotensor terms were present.

One other feature of the π photoproduction reaction is the effect of the one pion exchange (OPE) diagram in charged π photoproduction. The cross section due to the OPE diagram alone is given by

$$\sigma(\theta_{cm}) = G_{\pi N}^2 e^2 \left(\frac{q_{cm}}{K_{cm}}\right) \frac{1}{4W^2} \frac{\beta_{cm}^2 \sin^2\theta_{cm}}{2K_{cm}^2(1-\beta_{cm}\cos\theta_{cm})^2}$$

$$\times \left[(M_1 - M_2)^2 - \mu^2 + 2K_{cm}\omega_{cm}(1-\beta_{cm}\cos\theta_{cm})\right], \tag{5}$$

where

$G_{\pi N}^2$ = π, nucleon coupling constant 14.7

e^2 = fine structure constant 1/137

q_{cm} = c.m. π momentum

K_{cm} = c.m. photon momentum

W = c.m. energy

μ = π mass

M_1 = initial nucleon mass

M_2 = final nucleon mass

and

θ_{cm} = π c.m. production angle .

The inclusion of (5) in fitting procedures with $G_{\pi N}^2$ considered as a fitting parameter [5] will yield an experimental value for $G_{\pi N}^2$.

Since π photoproduction has one vertex involving electromagnetic interactions, which are well understood, there is some hope of being able to interpret the results. A symmetric quark model in which 3 quarks are bound by simple harmonic oscillator potentials has had some success. The agreement between the baryon photoproduction amplitudes predicted by the quark model and the amplitudes available from the partial wave analysis is quite promising [6, 7]. The agreement is sufficiently good to warrant using the quark model amplitudes as an initial solution for the forthcoming partial wave analysis [8].

In this manner the quark model will be tested to see how well it is compatible with the experimental data. The π^- photoproduction cross sections of this experiment will be used in the new analysis.

The quark model predicted a result which was directly related to this experiment. The helicity 3/2 amplitude, B_{3-}, of the $F_{15}(1688)$ resonance was predicted to be 0 [9] by the quark model. This amplitude in π^+ photoproduction produces a very marked peak in the cross sections and its absence in π^- photoproduction would be very obvious. Qualitatively this is what has been seen.

The mathematical details of the symmetric quark model are presented from Walker. [6] The baryon is assumed to be composed of three quarks bound together by simple harmonic oscillator potentials. The Hamiltonian is

$$H = \sum_{j=1}^{3} \frac{1}{2M} \vec{P}_j^2 + \tfrac{1}{2} M\omega_0^2 \sum_{i<j} (\vec{r}_i - \vec{r}_j)^2$$

where

M = mass of the quark

$\vec{P}_j$ = quark momentum

$\vec{r}_j$ = quark position

ω_0 = harmonic oscillator constant .

Using the substitutions

$$\vec{R} = \frac{1}{3} (\vec{r}_1 + \vec{r}_2 + \vec{r}_3) ,$$

$$\vec{\lambda} = \frac{1}{\sqrt{6}} (\vec{r}_1 + \vec{r}_2 - 2\vec{r}_3) ,$$

and

$$\vec{\rho} = \frac{1}{\sqrt{2}} (\vec{r}_1 - \vec{r}_2) ,$$

gives

$$H = \left(\frac{\vec{P}_R^2}{2(3M)}\right) + \left(\frac{1}{2M}(\vec{P}_\lambda^2 + \vec{P}_\rho^2) + \tfrac{1}{2}M\omega^2(\lambda^2 + \rho^2)\right) \tag{6}$$

where

$$\vec{P}_N = M\dot{\vec{N}} \quad , \qquad \vec{N} = \vec{\lambda}, \vec{\rho} \text{ or } \vec{R}$$

and

$$\omega^2 = 3\omega_0^2 .$$

The Hamiltonian in (6) combined with the SU(6) quark states gives a reasonable spectrum of the baryon resonances if the total wave function is required to be totally symmetric. The photon-quark interaction is given by

$$H_{cm} = -\frac{\hat{Q}e}{M}\vec{A}\cdot\vec{P} - \frac{eg}{2M}(\vec{\sigma}\cdot\vec{\nabla}\times\vec{A}) \tag{7}$$

where

$\hat{Q}$ = quark charge operator (i. e., 1/3, -2/3)

e = electron charge

g = quark gyromagnetic ratio

and

$\vec{A}$ = photon wave function .

We calculate the amplitudes for radiative decay (i. e., time reversed photoproduction) for a photon emitted with momentum, $\vec{K}$, and polarization $\hat{\epsilon}$. The photon wave function is

$$\vec{A} = \sqrt{\frac{4\pi}{2K}}\,\epsilon^+ e^{-i\vec{K}\cdot\vec{r}}$$

where

$$\epsilon^+ = -(\hat{\epsilon}_x + i\hat{\epsilon}_y)/\sqrt{2} \ .$$

We need consider only photons emitted in the Z direction with positive helicity, because rotational matrices and parity will take care of the other cases.

Also, the symmetric symmetry of the baryon wave function reduces the baryon matrix element to three times the matrix element on one quark. Using (7) on the third quark we obtain

$$H_{em} = \left(\frac{eg}{2M}\right) 2\sqrt{\pi K}\ (H_S + H_0) \tag{8}$$

where $H_S = 3Q_3 S_{3-} \exp(i\sqrt{2/3}\ K\lambda_z)$ (spin-flip)

$$H_0 = 3Q_3 \left(-\frac{1}{gK}\sqrt{\frac{2}{3}}\right) \exp(i\sqrt{2/3}\ K\lambda_z)(P_{\lambda_x} - iP_{\lambda_y}) \quad \text{(orbital-flip)}$$

and $S_{3-} = S_{3x} - iS_{3y}$ (the spin lowering operator) .

Copley, Karl, and Obryk [9] predicted that the B_{3-} amplitude of the $F_{15}(1688)$ resonance in π^- photoproduction would be zero from the symmetric quark model. Using (8) we can quickly point out this prediction. The $F_{15}(1688)$ is assumed to be the Regge recurrence of the nucleon. In this case it has the same SU(6) wave function as the nucleon which makes it a member of a SU(6) $\left\{8\right\}$, spin 1/2 symmetric [56] super-multiplet. The space wave function is a symmetric 2^+ state. The B_{3-} amplitude requires a baryon helicity change of 3/2 to 1/2. This is not provided by H_s, because the initial quark state can only reach helicity 1/2. The H_0 amplitude is possible, but then the matrix element is proportional to the charge of all three quarks, which for

$$F_{15}(1688) \rightarrow n + \gamma$$

is $Q_1 + Q_2 + Q_3 = 0$. Hence $B_{3-} = 0$.

The partial success of the quark model to predict the electromagnetic behavior of the baryon resonances rests on the fact it is dealing with a well-understood interaction. The success of the quark model to predict strong decays of the baryons is somewhat more limited. We see then that the electromagnetic interactions such as photoproduction are perhaps the best tools in probing the structure of the hadrons. In fact the only clear evidence of the composite nature of the proton comes from electron scattering experiments.

PART II APPARATUS

The experiment was carried out with the California Institute of Technology 1.5 GeV synchrotron. An internal target placed in the path of the accelerated electrons produced the bremsstrahlung beam which illuminated a 3" diameter LD_2 target. For further discussion on the beam and target, see Appendix XI. An illustration of the beam and experimental area can be seen in Figure 1. In the experimental area there were two magnetic spectrometers available, HEMA and LEM, which are pictured in Figures 2 and 3. Both spectrometers were pivoted about a vertical axis concentric with the center of the target and could be rotated to different lab angles. The HEMA spectrometer had a maximum momentum of 1200 MeV/c and was restricted to lab angles $< 55^{\circ}$. The LEM's maximum momentum was 600 MeV/c and was restricted to lab angles $< 147.7^{\circ}$. The maximum momentum of the HEMA spectrometer could be increased to 1670 MeV/c by adding an extension onto the HEMA frame and moving the counters to the higher momentum focus. This rearrangement was referred to as the ØUTR configuration. The extended frame restricted the available lab angles to $< 39.1^{\circ}$. For the HEMA-ØUTR spectrometer the A1 counter defined the solid angle of the spectrometer and the small hodoscope S2(T, TC, BC, and B) were the momentum defining counters. The large freon gas Cherenkov counter, FC, and the smaller lucite Cherenkov counter LC, (see Appendix IX) could, with suitable electronics, separate triggers due to electrons, pions and protons. Muons were indistinguishable from pions in this scheme but since they originate from π decays there was no attempt to eliminate them. S1 provided time-of-flight measurements between A1 and A2. A2 and S3 were extra trajectory defining counters

which eliminated counts from scatteres and showers. The slab of lead in front of S3 eliminated low energy electrons which failed to fire FC. The FAN counters were used to veto the events where the particle scattered off the magnet pole tips.

For the LEM spectrometer A was the aperature-defining counter and P (T, TC, BC, and B) was the momentum hodoscope. S1 and S2 were used for time-of-flight and trajectory definition. The FAN counters served the same purpose as the ones on HEMA. Photomultiplier pulse sizes differentiated between π's and protons (see Appendix IX). No Cherenkov counters were used.

The equipment just described was already in existence [10,11,12,13, 15] at the commencement of this experiment and has been described in other sources. Added for this experiment were recoil counters. Their construction and design are discussed in Appendix IX. The counters were mounted on a rail surrounding the deuterium target which permitted the counters to be moved to any desired angle. This rail was built for the γ counters of Wolverton's π^o photoproduction experiment. [11]

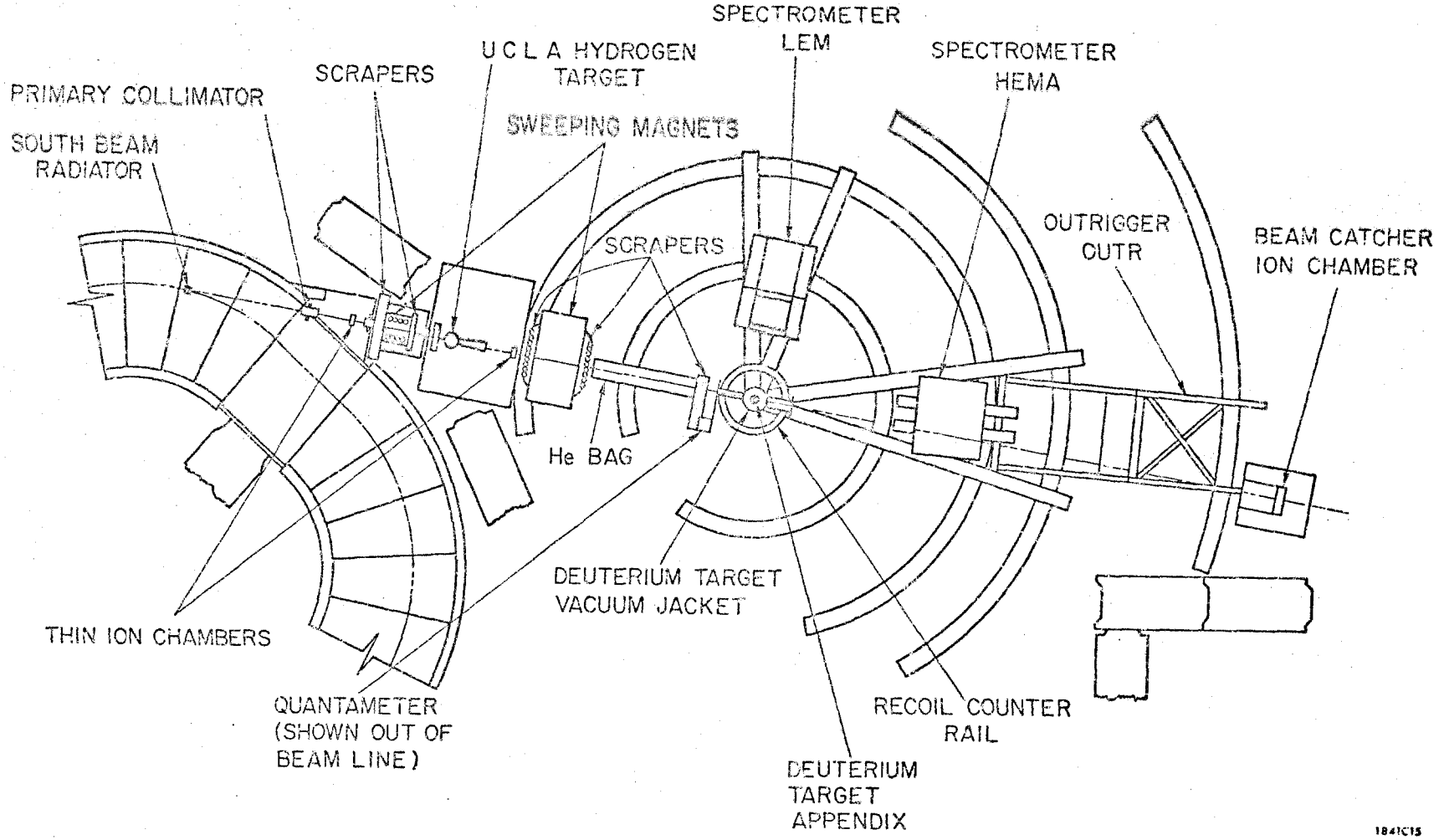

FIGURE 1

Beam and Experimental Area

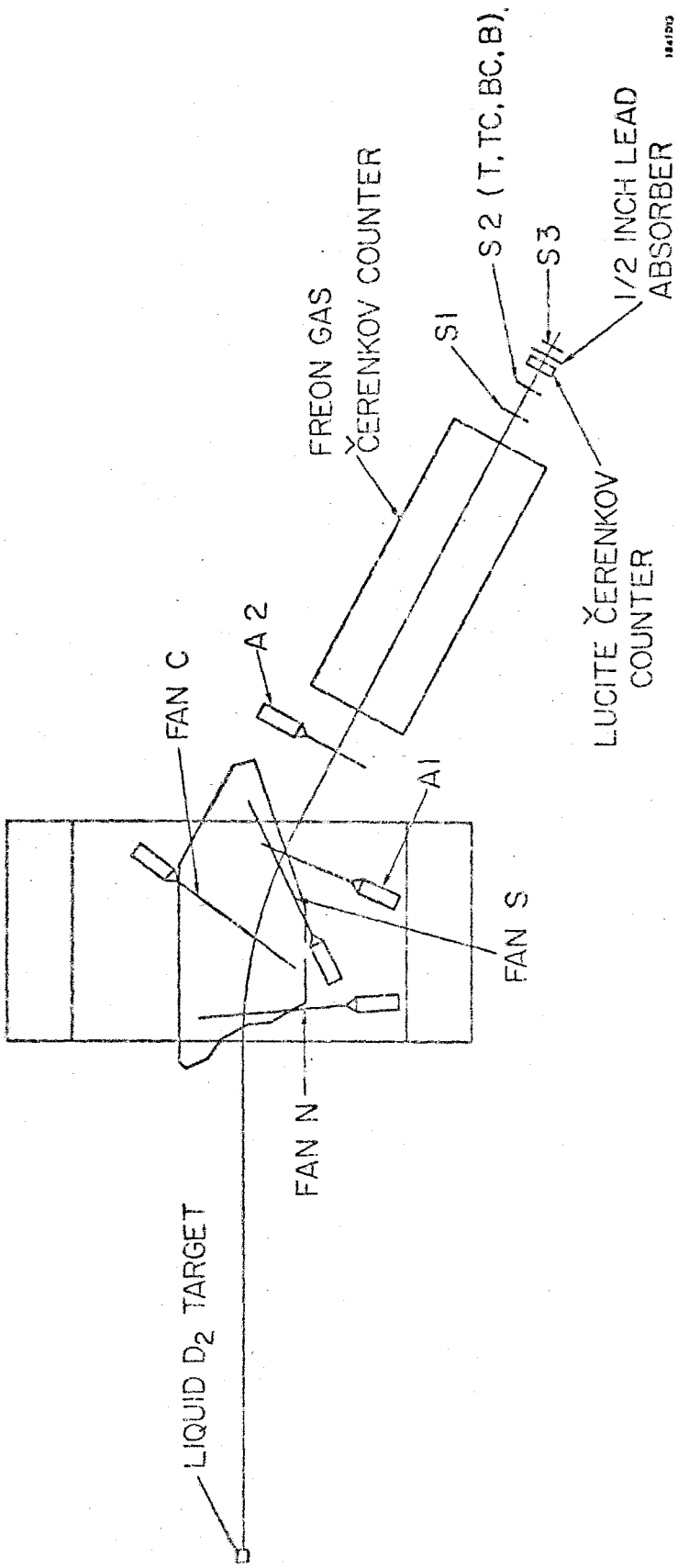

FIGURE 2

The HEMA Spectrometer

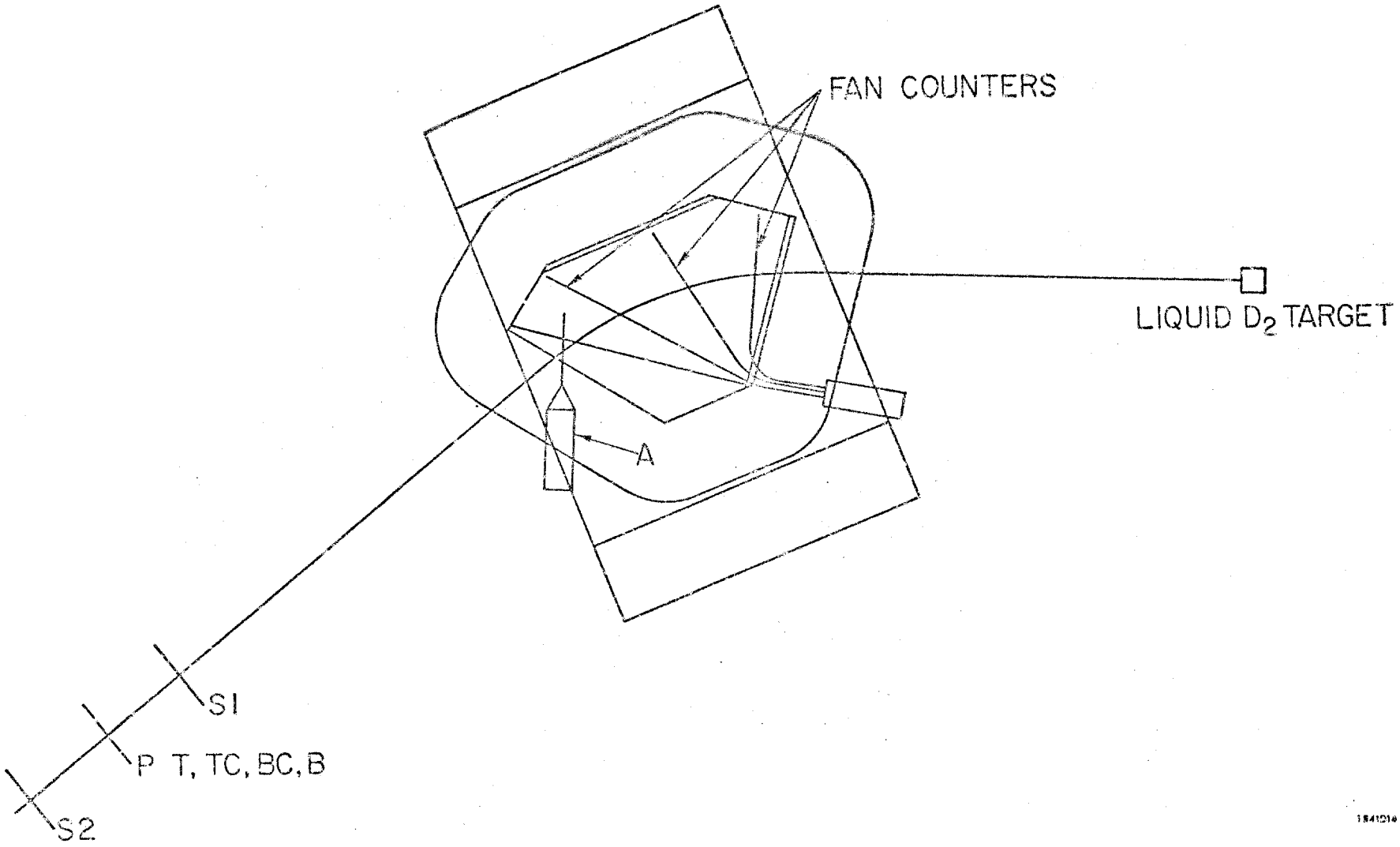

FIGURE 3

The LEM Spectrometer

PART III METHODS

Because there are no neutron targets, it is impossible to study the reaction

$$\gamma + n \rightarrow \pi^- + p \tag{9}$$

directly. One means of overcoming this difficulty is to measure the cross section for the inverse reaction [14, 15, 16]

$$\pi^- + p \rightarrow \gamma + n \tag{10}$$

and use detailed balancing to obtain the cross section for (9). This method suffers from the difficulties that there are two neutral particles in the final state to detect and there is a huge background contamination from the reaction

$$\begin{array}{l} \pi^- + p \rightarrow \pi^0 + n \\ \qquad\qquad\quad \hookrightarrow \gamma + \gamma \ . \end{array} \tag{11}$$

The method used for the present experiment was to use deuterium as a neutron target. The π^- from the reaction

$$\gamma + d \rightarrow \pi^- + p + p \tag{12}$$

is regarded as being photoproduced off the neutron which is loosely bound in the deuterium nucleus. The difficulties inherent with reaction (10) are now gone, but reaction (12) has problems of its own. There are numerous deuterium side effects associated with (12) which must be considered in order to obtain the π^- photoproduction cross section.

The largest overall effect is the increase in the number of restraints needed to completely determine the kinematics of an event. The reason is that reaction (9) has two particles in the final state whereas reaction (12) has three.

However, the extra proton in reaction (12) (the spectator proton) is almost at rest, having taken no part in the reaction, so that it is left with only its residual momentum inside the deuterium nucleus. Because of this, two-body kinematical restraints can be used for useful measurements. However, the undetermined spectator proton momentum greatly degrades the energy resolution of the experiment. There is a detailed discussion of this effect in Appendix II. The spectator proton momentum distribution used for calculations in this experiment was taken from the Hulthen wave function representation for the deuteron ground state. This function is given by

$$u(\rho) = \left[\frac{\alpha}{2\pi(1-\alpha\rho_1)}\right]^{\frac{1}{2}} \frac{(e^{-\alpha\rho} - e^{-\beta\rho})}{\rho} \tag{13}$$

where

$\vec{\rho} = \vec{r}_1 - \vec{r}_2$,

$\vec{r}_1, \vec{r}_2$ are the positions of the deuteron nucleon,

$\alpha = 45.69$ MeV ,

$\beta = 275.74$ MeV ,

and

$\rho_1 = 4/(\alpha+\beta) - 1/\beta$.

In the momentum representation the ground state is calculated by

$$\phi(K) = \int \exp(-i\vec{K}\cdot\vec{\rho})u(\rho)d^3\vec{\rho} \tag{14}$$

which is

$$\phi(K) = \left[\frac{8\pi\alpha}{(1-\alpha\rho_1)}\right]^{\frac{1}{2}} \frac{\beta^2 - \alpha^2}{(\alpha^2 + K^2)(\beta^2 + K^2)} . \tag{15}$$

The momentum distribution is then $|\phi(K)|^2$.

Another effect is the lowering of the cross section due to the Pauli exclusion principle. This arises because the two protons in the final state of reaction (12) are fermions; hence, the part of phase space where the two protons tend to be in the same state is restricted. The analytic expression for this effect is [17]

$$\frac{\partial\sigma}{\partial\Omega_D} = \left[1 - \tfrac{1}{3} F(D)\right] \frac{\partial\sigma_K}{\partial\Omega} + \left[1 - F(D)\right] \frac{\partial\sigma_L}{\partial\Omega} \tag{16}$$

where

$\partial\sigma/\partial\Omega_D$ = π^- photoproduction cross sections from LD_2.

$\partial\sigma_K/\partial\Omega$ = nucleon-spin dependent cross section,

$\partial\sigma_L/\partial\Omega$ = nucleon-spin independent cross section,

$\vec{D} = \vec{K} - \vec{q}$.

$\vec{K}$ = photon momentum,

$\vec{q}$ = π momentum,

and $F(D)$ is the deuteron form factor,

$$F(D) = \int \exp(-\vec{D}\cdot\vec{\rho})\, u^2(\rho) d^3\vec{\rho} \ . \tag{17}$$

The corresponding expression for a free neutron target is given by

$$\frac{\partial\sigma}{\partial\Omega_F} = \frac{\partial\sigma_K}{\partial\Omega} + \frac{\partial\sigma_L}{\partial\Omega} \ . \tag{18}$$

For small momentum transfers, i.e., small π production angles, $D \sim 0$ and $F(D) \sim 1$ so the photoproduction cross section from deuterium given by (16) is $2/3(\partial\sigma_K/\partial\Omega)$. The cross section for a free neutron target, on the other hand,

is $\partial\sigma_K/\partial\Omega$ because at 0^o the nucleon spin must flip, hence the spin independent cross section $\partial\sigma_L/\partial\Omega = 0$. Thus for forward π production angles, the Pauli exclusion principle lowers the deuterium cross sections by a factor of 2/3 with respect to the free neutron cross section.

The Glauber effect [18] lowers the cross section due to the shadowing of one nucleon by the other. Normally one would not expect such a shadowing effect to be large for the electromagnetic interactions because the photon has a mean free path of 500 fm in nuclear matter, which is far larger than any nucleus. However, the uncertainty principle presents the possibility that a photon can materialize into a ρ^o whose mean free path of 3 fm in nuclear matter allows a shadowing effect. Such an effect has been observed in total photoabsorption experiments [19,20]. In the present experiment the greatest shadowing would occur for the largest photon energy used, 1300 MeV. Using the uncertainty principle one can calculate that these photons could exist as ρ^o's for distances no more than 0.8 fm. Since the mean free path of ρ^o's in nuclear matter is 3 fm, the ρ^o's would disappear before they interacted. Hence the Glauber shadowing effect is not significant for this experiment.

There are numerous final state interactions which tend to make the interpretation of reaction (12) as π^- photoproduction ambiguous. Examples of such interactions are π^- scattering off of the second target nucleon,

$$\left.\begin{aligned} \gamma + n &\rightarrow \pi^- + p \\ \pi^- + p &\rightarrow \pi^- + p \end{aligned}\right\} \qquad (13)$$

and π^- absorption off of the second target nucleon,

$$\left.\begin{array}{l} \gamma + n \rightarrow \pi^- + p \\ \pi^- + p \rightarrow \pi^o + n \end{array}\right\} \qquad (20)$$

It is rather difficult to assess the effect of all these reactions although some attempts have been made [21,22,23,24]. Experimentally the effect of final state interactions seem small because single π^+ photoproduction cross section ratios from hydrogen and deuterium are not significantly different from 1, if one takes points not affected by the Pauli exclusion principle. Also, final state interactions involve both deuteron nucleons, hence one would expect that the spectator proton momentum distribution observed would significantly differ from that expected from a deuteron wave function such as the Hulthen wave function. This has not been seen* [26] (see Figure 4); thus it seems the final state interactions have a small effect.**

Finally, there is the possibility of contamination of the π^- rate from 2π photoproduction. If the nucleons are moving around the deuterium nucleus in the manner described by the Hulthen wave function, one can picture the 2π threshold being reduced by a high velocity deuteron nucleon striking a low energy bremsstrahlung photon. In this manner π^-'s from such reactions as

$$\gamma + d \rightarrow \pi^- + \pi^+ + p + n \qquad (21)$$

may significantly contaminate the single π^- photoproduction rates. However,

---

* This is only true for experiments at intermediate energies. For higher energy experiments there are some sizeable deviations. [46]

** In Part V, it is hinted that the systematically high LEM direct cross sections may be due to a final state rescattering effect.

a detailed Monte Carlo program to calculate this contamination produced a negligible result. This program is described in Appendix VII.

There are several experimental methods available to overcome the difficulties presented by the deuterium target. The best method is a Chew-Low extrapolation. Here the π^- photoproduction differential cross section is measured as a function of the photon energy, K, the c.m. production angle, θ_{cm}, and the relativistic invariant

$$\mathscr{P}_n^2 = (\mathscr{P}_D - \mathscr{P}_S)^2 = M_D^2 + M_P^2 - 2M_D E_S \qquad (22)$$

where

$\mathscr{P}_n$ = 4-momentum of the target neutron,

$\mathscr{P}_S$ = 4-momentum of the spectator proton,

$\mathscr{P}_D$ = 4-momentum of the target deuteron,

E_S = lab energy of the spectator proton,

M_D = mass of the deuteron,

and

M_P = mass of the proton.

The resulting curve is extrapolated to $\mathscr{P}_n^2 = M_n^2$ where M_n is the neutron mass. The cross section at this point should be the photoproduction cross section from free neutrons. This technique eliminates the effects due to kinematics and the Pauli exclusion principle. The one experimental difficulty of this method is the tremendous amount of statistics it requires. For experiments which try to cover a large kinematical region, such as this one, the demands on beam time would be entirely unreasonable.

There were several methods used in this experiment to eliminate the deuterium effects while achieving good statistics with short data runs. The simplest method used was to measure the π^-/π^+ ratio. This method assumes that the relative effects are the same for both π^- and π^+ photoproduction from deuterium. Then the ratio of the π^- and π^+ counting rates from deuterium will be equal to the ratio of the counting rates from free nucleons.

$$\left.\begin{aligned} R &= (\pi^- \text{ rate}/\pi^+ \text{ rate})_{\text{deut}} \\ &= (\pi^- \text{ rate}/\pi^+ \text{ rate})_{\text{free}} \end{aligned}\right\} \tag{23}$$

Multiplying the ratio by the π^+ photoproduction cross section from protons will yield the π^- photoproduction cross section from neutrons. With this method, the effect due to the Pauli exclusion principle is effectively removed*. However the energy resolution caused by the undetermined kinematics of the spectator proton is not improved, and the error from the statistics are degraded by the statistics of the π^+ rate and those of the π^+ cross section. Also the assumption that the π^+, π^- corrections are equal is suspect.

Another method tried in this experiment was to calculate the cross section from the π^- rates alone. This method is extensively discussed in Appendix II. The advantages here are that the statistical errors are better than the ratio method and asymmetric deuterium effects do not corrupt the π^- cross sections. However, again the energy resolution is not improved, and virtually every deuterium effect except for spectator proton momentum is ignored. Besides, the method is dependent on the deuterium model used.

---

* This assumes that the ratio of $(\partial\sigma_K/\partial\Omega)$ to $(\partial\sigma_L/\partial\Omega)$ is the same for both p and n.

An improvement on the previous method is obtained if one also detects the recoil proton as well as the π^-. A counter is placed at the position of the recoil proton corresponding to the target neutron at rest. In this manner the energy resolution of the experiment can easily be improved by 40%. Furthermore the production of π^- mesons in correlation with high velocity spectator protons is suppressed. However, this method ignores the Pauli principle, and produces larger errors due to statistics from the lower counting rates. Furtherfore the experimental situation restricted the use of the counter because for forward produced pions the proton did not get out of the target and for backward produced pions the counter was close to the photon beam. The latter restriction, however, was removed by detecting the proton in the spectrometer and the π^- in the recoil counter.

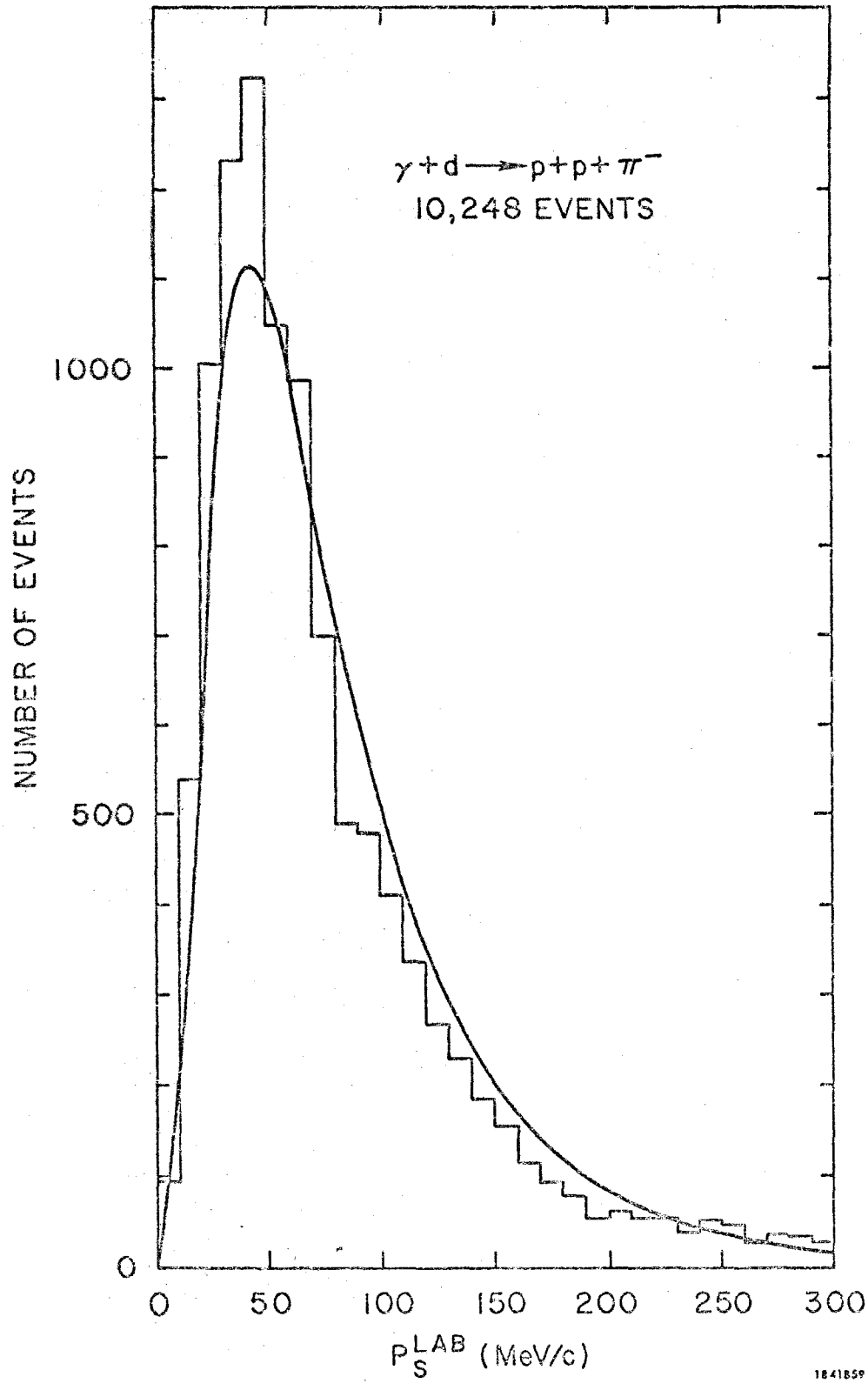

FIGURE 4. Distribution of the spectator proton lab momentum with the Hulthen wave function superimposed. Figure is taken from reference 26.

PART IV PROCEDURE

The present experiment consisted of 523 runs which covered a total of 104 spectrometer settings producing 416 measurements of the π^- photoproduction cross section. If the π^+ data are considered as separate measurements the number of data points is doubled to 832. The experiment covered 13 c. m. π production angles between 6° and 160° and 32 incident photon energies between 589 and 1256 MeV.

To record an event the time-of-flight counters (A1, A2, and S1 in HEMA; and A, S1, and S2 in LEM) were placed in a 6 ns fast coincidence. Then the Cherenkov counters on HEMA or the pulse height discrimination on LEM separated events into π, e, and p signals. Finally the desired signal (usually the π) was placed in coincidence with the momentum counters. A more detailed description of the electronics will be found in Appendix IX.

The basic daily run schedule began with a calibration of the quantameter integrater (see Appendix XI), after which the pulse height spectrum of each counter was checked. The basic run procedure consisted of data runs alternating with monitor runs. The monitor runs were required in order to calibrate the beam monitors with the Wilson type quantameter. (see Appendix XI)

There were four types of data runs:

(1) π^+ data run (PPD)

(2) π^- data run (PMD)

(3) π^- data run with recoil counter (PMDR)

(4) reverse π^- recoil data run (PMDPR).

The PPD and PMD were simply runs in which only the π was detected in the spectrometer. The PMDR runs detected the recoil proton in the recoil counters as well as the π^- in the spectrometer. The PMDPR runs were the reverse of the PMDR runs in that the proton was detected in the spectrometer and the π^- was detected in the recoil counters. The PPD, PMD, and PMDR runs used the HEMA for lab angles $< 50^o$ and the LEM for the larger angles. The PMDPR runs used the HEMA for bremsstrahlung end points < 916 MeV and the ØUTR for the higher end points.

There were three basic techniques used to measure the π^- photoproduction cross section: the π^-/π^+ ratio, the π^- direct cross section and the π^- recoil cross section (see Part III). The π^-/π^+ ratio measurement required consecutive PPD and PMD (or PMDR) data runs in which only the polarity of the magnet was changed. The direct cross section required the spectrometer counting rates from the PMD (or PMDR) runs. For the π^- recoil cross section it was originally planned to use only the PMDR runs. However, it turned out that only a limited number of measurements were possible with this arrangement because the recoil counters were saturated by the photon beam for lab angles $< 30^o$ and protons did not have sufficient energy to reach the recoil counters for lab angles $> 64^o$ (see Appendix IX). As a result recoil measurements would have been missing for the forward and backward π production angles. However, with the PMDPR runs it was possible to obtain the backward recoil data.

Empty target runs were taken for a scattering of the settings and interpolated for the settings that were not taken. This was done in order to save beam time for full target runs.

For the π^- data not requiring a recoil proton the empty target background was largest for the forward π^- production angles, where the spectrometer was very close to the beam. The runs accepted as final data had a background of 10% or less. The π^- background contamination at other settings ranged from 2% to 8%. The higher background occurred at the largest π^- production angles. For the recoil data there was no observable background.

The π^+ runs, which were required in order to calculate the π^-/π^+ ratio, could also be used for normalization purposes. With the use of a time-sharing computer console in the experimental bay the data runs could quickly be turned into cross sections. These cross sections could then be compared to the π^+ photoproduction cross sections from hydrogen as a check on the operation of the apparatus. This was only possible for the HEMA runs because the p efficiency for the LEM data was not available during run time. The reduction of the data to cross sections is described in Appendix X, Part E.

PART V RESULTS

As mentioned in Part IV, there exist four different cross section measurements. In order to avoid confusion when discussing these measurements the following names will be used:

1. direct cross sections — These are cross sections measured from the π spectrometer counting rates.

2. ratio cross sections — These are cross sections calculated from the ratio of the π^- and π^+ spectrometer counting rates.

3. recoil cross sections — These are cross sections calculated from the π^- spectrometer rates with the requirement that the p is detected in the recoil counters.

4. reverse recoil cross sections — These are cross sections calculated from the p spectrometer rates with the requirement that the π^- is detected in the recoil counters.

The best test of the capability of method (1) to extract

$$\gamma + n \rightarrow \pi^- + p \tag{24}$$

cross sections from the reaction

$$\gamma + d \rightarrow \pi^- + p + p \tag{25}$$

is to compare the cross sections from the reactions

$$\gamma + p \rightarrow \pi^+ + n \tag{26}$$

and

$$\gamma + d \rightarrow \pi^+ + n + n\,. \tag{27}$$

Such a comparison can be seen in Figures 5-7 where the π^+ direct cross sections from this experiment are compared to the π^+ cross sections from hydrogen calculated from Ecklund and Walker's fit [14]. The errors for this fit (not shown) are roughly equal to the errors shown with the data from this

experiment. In Figure 5, showing the comparison of the hydrogen and deuterium cross sections at c.m. π production angle, $\theta_{cm} = 10^{o}$, the deuterium data are noticeably lower. This behavior is expected from the Pauli exclusion principle effect [17] which lowers the π photoproduction cross sections from deuterium at small π production angles (see Part III). At $\theta_{cm} = 60^{o}$ (Figure 6) where the Pauli exclusion principle effect is not as strong, the agreement between the hydrogen and deuterium cross sections is very good. However, at $\theta_{cm} = 105^{o}$ (Figure 7) the deuterium cross sections are systematically high. This systematic shift is seen for all the π^{+} data from $\theta_{cm} = (90^{o}-160^{o})$. These points correspond exactly to the data taken by the LEM spectrometer. Consequently, the LEM results are suspect. Furthermore, for experimental points done with both the LEM and the HEMA spectrometers, the LEM direct cross sections were on the average 10% higher. A difference of this magnitude could account for the shift observed in Figure 7. However, a simple normalization correction of the LEM data would not help as the shift varies from 0-10%.

Several possible sources for the high LEM π^{+} direct cross sections were investigated. These were:

1. Contaminating backgrounds
2. Incorrect LEM acceptance calculations
3. Changes in the LEM solid angle
4. Electronics
5. Final state rescattering effects.

There is little reason to suspect contaminating backgrounds are responsible for the high cross sections. The possible contaminants, empty target background, 2π photoproduction, and electrons have already been subtracted from the deuterium data in Figure 7. The subtraction was fairly reliable. The empty target background was measured directly (see Part IV), the 2π contamination was calculated from known 2π cross sections (see Appendix VII), and the electron contaminant was estimated from this experiment's HEMA data and Thiessen's previous measurements [10]. It is difficult to imagine sources of other contaminants.

There were three checks made on the LEM acceptance calculation. First, the ratio of the experimental response, κ_π, and the total spectrometer acceptance, $\Delta P \Delta \Omega$, for both the HEMA and the LEM were compared. An error in either the κ_π or $\Delta P \Delta \Omega$ calculation for either spectrometer would produce disagreeing ratios. For close kinematical settings the agreement was better than 2%. Second, the Monte Carlo acceptance calculation was compared to more accurate methods (Table 16) and the agreement was well within the Monte Carlo error. Finally, the total LEM acceptance for this experiment was compared to Thiessen's [4] total acceptance (who used the same spectrometer) and the results were identical. These checks seem to preclude any errors in the acceptance calculation.

If the LEM solid angle were somehow larger than the acceptance calculations described, the result would be larger cross sections. However, there should also be a corresponding increase observed in the recoil rate for the π^- runs. This speculation was easily checked by a comparison of the

LEM π^- direct and recoil cross sections. Such a comparison is seen in Figure 8, and it is clear that there has been no increase in the recoil counting rate.

Electronic difficulties would be expected to produce more erratic data than the smooth results seen in Figures 7 and 8. The only imaginable electronic difficulty that could lead to higher cross sections would be triggering on events where the particles passed through only a fraction of the counters in the spectrometer telescope. If these particles originated from the target, the overall effect would be similar to an increase in aperture which has just been rejected. If the particles originated outside the target, they would have been removed by the background subtraction. Furthermore, the LEM electronics were frequently checked throughout the run and no major anomalies were ever seen.

Elastic and inelastic rescattering of the π off the deuterium spectator nucleon could cause an enhancement of the cross section. The lab momentum of backward photoproduced π's for the energy region of this experiment was around 300 MeV/c. This is just the right momentum required for the π to produce a $\Delta(1236)$ resonance with the spectator nucleon. Using a deuteron internucleon distance of r = 3.87 fm [*] and a cross section of $\sigma(\pi^- + p \rightarrow \Delta^0)$ = 68.3 mb [**] an order magnitude estimate of the rescattering correction is given by

---

* Taken from $< r^2 >$ produced by the Hulthen wave function.

** $\sigma(\pi^- + p \rightarrow \Delta^0) = \frac{1}{3}\sigma(\pi^+ + p \rightarrow \Delta^{++})$ at 300 MeV/c.

$$\frac{\sigma(\pi^- + p \rightarrow \Delta^0)}{4\pi < r^2 >} = 0.036 \qquad (28)$$

which means an effect as large at 10% can be expected. Unfortunately, present theories dealing with such rescattering problems [21, 22, 23, 24] are only valid for higher energy scattering at small momentum transfers.

It is unfortunate that the preceeding investigation produced no clear evidence to indicate a malfunction of the LEM spectrometer. Because of this fact it must be concluded that the direct cross sections might contain some deuterium side effects as large as 10%, and hence are unreliable. It was therefore decided to use the average of the ratio cross sections and both types of recoil cross sections as the final data. This is a reasonable decision as both of these measurements minimize the deuterium effects. To support this decision observe in Figure 9 that the ratio and reverse recoil cross sections are in fairly good agreement, whereas in Figure 10 the direct cross sections are systematically higher than the ratio results. It must be pointed out that some caution must be employed when using the ratio cross sections. For example, in Figure 11 which shows the π^+ direct cross sections from this experiment at $\theta_{cm} = 45^o$, the smearing effect of the deuterium has lowered the π^+ cross section below Ecklund and Walker's fit at 1000 MeV. This will cause a false enhancement in the π^- cross section at the same energy as can be seen in Figure 12. The π^- direct and recoil cross sections (Figure 13) show flatter distributions. In such cases the recoil measurement was taken as the final measurements and the ratio result was ignored.

The experimental cross sections are presented in Tables 1, 2, 3, 4, 5 and 6. The interpolated π^- cross sections, at constant lab photon energies,

are presented in Table 7, and Figure 14. The errors listed and shown result from statistics, raw data corrections (see Appendix X), and experimental response calculations. The total systematic error is taken from Ecklund [12] and is 10%. The fits seen in Figure 14 are Moravcsik fits.

Moravcsik fitting was used in order to obtain total cross sections and to extrapolate the data to special θ_{cm} angles. The fits themselves produce coefficients of which the physics content is difficult to interpret. A more scientific fitting procedure, which is an extension of Walker's earlier fits [2], is now being carried out, and will be reported in Scheffler's thesis. [8]

Moravcsik fits [27] have the form

$$(1-\beta_{cm}\cos\theta_{cm})^2\sigma(\theta_{cm}) = \sum_n A_n \cos^n\theta_{cm} \qquad (29)$$

where β_{cm} is the c.m. velocity of the π^-. The A_n's are determined by a least squares fit to the data. The term $(1-\beta_{cm}\cos\theta_{cm})^2$ in (29) takes into account the one pion exchange (OPE) diagram which contributes many high partial waves not included in a limited sum over $\cos^n\theta_{cm}$ terms. The forward peak in Figure 14 is produced by this diagram. β_{cm} in this experiment ranged from 0.940 to 0.978. At the (OPE) pole, $\cos\theta_{cm} = 1/\beta_{cm}$, the expression in (29) is directly calculable from the Born approximation. It is

$$(1-\beta_{cm}\cos\theta_{cm})^2\sigma(\theta_{cm})\Big|_{\cos\theta_{cm}=1/\beta_{cm}} = e^2 G^2_{\pi N}\left(\frac{q_{cm}}{K_{cm}}\right)\frac{(1-\beta^2_{cm})}{4WK_{cm}}\left[\mu^2-(M_n-M_p)^2\right] \qquad (30)$$

where

q_{cm} = c.m. π^- momentum

K_{cm} = c.m. photon momentum

W = c.m. energy

μ = π mass

M_n = neutron mass

M_p = proton mass

e^2 = fine structure constant 1/137

and

$G^2_{\pi N}$ = π - nucleon coupling constant 14.7 .

If the values in (30) are expressed in energy units of MeV, the conversion of units of $(1/\text{MeV}^2)$ into cross sections required is $(\hbar c)^2 = 3.89 \times 10^6 \mu b\ (\text{MeV})^2$. Adding the value from (30) to the set of experimental data, the Moravcsik fit can be interpolated [5] to obtain 0^o cross section. The fit coefficients are presented in Table 8. The resulting total cross sections and the differential cross sections at $\theta_{cm} = 0^o$, 90^o, and 180^o are shown in Figures 15-18. A listing of those cross sections is given in Table 9.

The total cross section in Figure 15 displays a peak at 700 MeV similar to the π^+ data. This peak in π^+ photoproduction is well known to be dominated by the B_{2-} amplitude of the $D_{13}(1520)$ [14] resonance and there is nothing to indicate that this is not true for π^- photoproduction.

A further examination of Figure 15 reveals an absence of a bump corresponding to the third resonance, the $F_{15}(1688)$ [28], which is very prominent near 1000 MeV [5] in π^+ photoproduction. This result is even more striking

when comparing Figures 11 and 13. The dominant amplitude for the $F_{15}(1688)$ resonance in π^+ photoproduction is the B_{3-} wave which has a maximum near 45° c.m. π angle. Figure 11 clearly shows a peak in the π^+ data, whereas the corresponding peak in Figure 13 is absent.

If the resonant B_{3-} amplitude is written as a sum of the isovector and isoscaler amplitudes,

$$\begin{aligned} B_{3-}(\pi^+) &= B_{3-}^{S} - B_{3-}^{V} \\ B_{3-}(\pi^-) &= B_{3-}^{S} + B_{3-}^{V} \end{aligned} \tag{31}$$

the experimental indication of $B_{3-}(\pi^-) \approx 0$ forces $B_{3-}^{S} \simeq -B_{3-}^{V}$. As stated in the introduction, the harmonic oscillator quark model predicts that the B_{3-} amplitude of the F_{15} resonance is proportional to the initial nucleon charge; since π^- is produced from a neutron, $B_{3-}(\pi^-) = 0$, [9] in agreement with the above observation.

π^+ photoproduction shows that the helicity $\frac{1}{2}$ amplitudes of the $D_{13}(1520)$ and $F_{15}(1688)$ resonances are small. [5] If the corresponding π^- amplitudes are larger, their effect would be most pronounced at 0° and 180° where the helicity 3/2 amplitudes are 0. The 180° data (Figure 18) show indications of bumps at 700 MeV near the $D_{13}(1520)$ and at 1000 MeV near the $F_{15}(1688)$, but the data are not convincing. The Tokyo data [29] at 180° show a much clearer bump at 1000 MeV. At 0° (Figure 16) there is no evidence for an $F_{15}(1688)$ effect, but there is clearly a sharp drop in the cross section at 700 MeV near the $D_{13}(1520)$. However, this effect has been seen in the π^+ photoproduction and is attributed to the η photoproduction threshold. [2] The quark

model mentioned in the introduction predicts a small A_{2-} amplitude for the $D_{13}(1520)$ and a moderate A_{3-} amplitude for the $F_{15}(1688)$ [6].

Also in the 0^{o} data there is a fairly rapid drop in cross section for 700-900 MeV. This has previously been speculated to be caused by the $S_{11}(1535)$ resonance, whose A_{0+} amplitude interfers with the Born terms and background to produce the effect [30].

In summary, the $D_{13}(1520)$ seems to behave as it does in π^{+} photoproduction. The $F_{15}(1688)$, B_{3-} amplitude is definitely much smaller than in π^{+} photproduction. The partial wave analysis currently being applied by Paul E. Scheffler to these data and other π photoproduction reactions will produce more conclusive results.

It was noted by Walker [2] that a simple electric Born approximation with the j = 1/2 and 3/2 waves absorbed reproduces the qualitative features of the π^{+} photoproduction cross section near 1200 MeV. In Figure 19 we see that this observation holds true for π^{-} photoproduction as well. However, when the anomalous magnetic Born terms are added, with the j = 1/2 and 3/2 waves also removed, (Figure 19) the backward angle distribution is improved somewhat but the forward angle features are destroyed. There has been no clear evidence yet in π photoproduction to indicate the presence of the anomalous magnetic Born terms.

TABLES 1-6

Notations

K = lab photon energy

θ_{cm} = c.m. π production angles in degrees

$\sigma(\theta)$ = cross section in μb/sr

$\Delta\sigma(\theta)$ = standard deviation of $\sigma(\theta)$

π^-/π^+ = π^-/π^+ counting rate ratio

$\Delta\pi^-/\pi^+$ = error in π^-/π^+

TABLE 1

π^- Direct Cross Sections

K	θ_{cm}	$\sigma(\theta)$	$\Delta\sigma(\theta)$	K	θ_{cm}	$\sigma(\theta)$	$\Delta\sigma(\theta)$
583.9	6.22	17.20	0.73	994.8	10.25	3.56	0.28
601.1	6.23	17.65	0.74	1025.2	10.31	2.86	0.25
614.1	6.27	17.54	0.71	1050.8	10.38	3.42	0.28
630.8	6.35	18.21	0.71	1073.3	10.07	3.35	0.18
641.0	6.21	19.23	0.91	1096.3	10.20	3.18	0.50
659.1	6.22	16.06	0.85	1121.7	10.29	3.09	0.20
674.2	6.30	16.93	0.84	1156.4	10.36	3.04	0.28
695.5	6.29	15.73	0.80	1170.3	10.24	2.84	0.31
713.4	6.20	14.98	0.68	1198.2	10.30	2.48	0.31
730.2	6.25	12.75	0.63	1216.7	10.46	2.65	0.32
748.0	6.30	10.84	0.58	1243.9	10.56	2.50	0.29
764.5	6.38	11.31	0.57	583.8	20.20	12.17	0.50
790.9	6.25	10.71	0.55	598.7	20.32	12.46	0.51
808.7	6.25	10.25	0.49	617.0	20.38	12.29	0.50
828.6	6.33	8.64	0.45	632.1	20.57	12.36	0.49
848.8	6.39	7.72	0.41	642.5	20.15	12.05	0.50
874.5	6.28	5.41	0.54	659.6	20.29	12.22	0.51
898.8	6.31	5.64	0.50	677.8	20.41	11.30	0.48
922.2	6.35	4.74	0.46	695.3	20.61	11.33	0.46
947.2	6.43	5.63	0.47	711.5	20.09	10.95	0.39
1070.8	6.14	3.80	0.36	731.3	20.21	9.72	0.36
1097.4	6.18	4.16	0.35	750.8	20.37	8.10	0.33
1123.7	6.26	3.41	0.52	768.0	20.53	7.27	0.31
1155.6	6.34	3.09	0.30	786.7	20.24	5.80	0.33
1170.0	6.41	4.13	0.45	808.8	20.40	5.47	0.32
1191.5	6.58	4.03	0.43	829.9	20.53	5.21	0.30
1213.7	6.69	3.30	0.44	850.8	20.72	4.47	0.28
1250.2	6.70	3.06	0.40	869.5	20.18	4.66	0.22
585.4	10.12	16.57	1.11	896.1	20.33	4.40	0.20
601.1	10.18	16.45	0.78	919.7	20.44	4.28	0.20
616.8	10.23	15.54	0.73	946.4	20.62	4.21	0.19
631.6	10.34	15.57	0.73	967.5	20.28	3.90	0.11
642.0	10.09	14.66	0.77	994.2	20.37	3.98	0.12
659.6	10.13	14.94	0.79	1026.1	20.45	3.77	0.11
675.8	10.18	13.58	0.75	1054.1	20.62	3.55	0.11
694.8	10.29	13.88	0.72	1069.8	20.24	3.85	0.19
711.4	10.00	13.41	0.66	1096.2	20.41	3.56	0.18
727.6	10.10	12.06	0.88	1124.9	20.64	3.50	0.18
747.8	10.18	11.16	0.67	1158.8	20.75	3.38	0.18
770.8	10.22	10.25	0.55	1166.1	20.24	3.14	0.29
790.1	10.18	7.20	0.39	1192.1	20.40	2.74	0.27
808.3	10.24	7.39	0.38	1220.6	20.56	2.94	0.28
831.3	10.28	6.22	0.35	1249.8	20.70	2.36	0.25
850.1	10.42	5.81	0.32	585.3	30.17	10.49	0.46
875.3	10.19	5.81	0.38	599.4	30.34	10.59	0.47
896.4	10.22	4.83	0.34	616.5	30.49	10.70	0.46
923.9	10.29	4.29	0.32	632.8	30.76	10.52	0.45
947.4	10.35	3.66	0.28	644.6	30.05	10.52	0.36
970.5	10.17	3.40	0.27	658.1	30.34	10.01	0.38

K	θ_{cm}	$\sigma(\theta)$	$\Delta\sigma(\theta)$	K	θ_{cm}	$\sigma(\theta)$	$\Delta\sigma(\theta)$
676.5	30.52	9.91	0.35	1058.4	45.84	3.77	0.14
693.1	30.84	9.82	0.35	1062.3	44.88	4.22	0.13
710.8	30.13	9.71	0.33	1098.5	45.02	3.89	0.15
728.4	30.37	9.17	0.32	1128.3	45.48	3.62	0.12
752.0	30.45	8.29	0.30	1161.6	45.79	3.37	0.12
771.2	30.79	6.96	0.27	1161.8	44.77	3.56	0.44
785.7	30.16	5.28	0.29	1194.2	45.22	3.44	0.15
810.9	30.20	5.70	0.30	1233.7	45.49	2.89	0.15
830.6	30.53	4.64	0.26	1270.1	45.83	2.72	0.14
856.3	30.72	4.63	0.27	585.5	59.89	8.48	0.32
874.0	30.04	4.61	0.15	599.2	60.38	8.03	0.32
899.2	30.19	4.49	0.15	619.3	60.54	8.35	0.32
923.9	30.44	4.54	0.15	636.2	60.97	8.25	0.31
949.9	30.71	4.18	0.15	640.1	59.87	8.14	0.30
968.9	30.03	4.72	0.18	659.6	60.14	8.42	0.41
998.1	30.18	4.44	0.16	679.2	60.48	7.84	0.30
1025.0	30.41	4.33	0.12	701.2	60.86	7.61	0.29
1056.7	30.62	4.50	0.13	707.6	59.89	7.41	0.23
1065.2	30.04	4.57	0.21	730.6	60.14	7.02	0.22
1094.0	30.26	4.28	0.21	751.1	60.59	6.11	0.24
1128.3	30.42	4.36	0.20	776.0	60.99	5.07	0.25
1160.3	30.68	4.47	0.21	786.1	59.70	4.65	0.21
1164.2	29.99	4.31	0.22	808.8	60.11	3.86	0.15
1195.2	30.15	3.76	0.21	835.3	60.52	3.35	0.14
1230.5	30.40	3.54	0.19	858.6	61.04	2.96	0.13
1264.6	30.68	3.54	0.19	872.7	59.74	2.92	0.13
585.0	45.07	9.28	0.65	898.9	60.22	3.01	0.13
602.5	45.13	9.48	0.65	925.2	60.57	2.84	0.13
617.7	45.57	9.15	0.63	957.7	60.96	2.44	0.12
633.3	45.99	10.36	0.66	967.5	59.60	2.70	0.09
640.8	45.15	8.82	0.37	999.1	60.02	2.73	0.08
659.6	45.34	7.99	0.35	1028.2	60.52	2.76	0.10
677.5	45.66	8.47	0.36	1063.0	60.88	2.66	0.12
696.8	45.98	7.88	0.34	1063.1	59.69	2.55	0.14
712.5	44.96	8.40	0.21	1102.7	59.90	2.47	0.13
729.4	45.30	8.13	0.20	1131.9	60.47	2.23	0.31
750.8	45.54	6.76	0.35	1160.3	59.43	2.07	0.11
773.3	45.87	5.79	0.17	1168.7	60.91	1.90	0.12
786.2	44.83	5.30	0.18	1196.2	59.89	1.84	0.10
807.4	45.20	4.67	0.17	1232.8	60.53	1.58	0.10
833.1	45.44	4.43	0.16	1276.9	60.75	1.44	0.10
854.8	45.90	3.96	0.30	581.8	74.78	7.19	0.24
875.0	44.92	4.27	0.20	599.4	75.30	7.41	0.25
898.0	45.19	3.87	0.15	617.5	75.53	7.24	0.61
922.0	45.63	3.82	0.15	638.4	75.86	7.12	0.73
949.8	45.99	4.02	0.31	639.6	74.66	7.19	0.53
971.5	44.78	4.32	0.15	659.1	75.23	7.13	0.19
996.8	45.24	4.41	0.18	680.0	75.53	7.45	0.37
1027.4	45.57	4.10	0.15	699.8	75.97	6.95	0.30

K	θ_{cm}	$\sigma(\theta)$	$\Delta\sigma(\theta)$	K	θ_{cm}	$\sigma(\theta)$	$\Delta\sigma(\theta)$
706.9	74.55	6.59	0.23	720.5	104.62	5.56	0.23
730.9	74.98	6.26	0.39	750.7	105.04	4.09	0.20
753.3	75.51	5.05	0.20	770.2	104.09	4.29	0.18
776.4	75.90	3.85	0.17	775.2	105.48	3.99	0.20
783.5	74.59	3.71	0.18	799.4	104.73	3.59	0.15
809.1	75.03	3.14	0.16	829.3	105.05	2.72	0.22
834.9	75.43	2.52	0.15	854.6	103.85	2.06	0.10
865.4	75.82	1.81	0.13	859.7	105.34	2.15	0.19
866.6	74.56	1.75	0.10	886.6	104.55	1.82	0.10
897.8	74.96	1.85	0.11	920.1	104.96	1.69	0.10
925.0	75.44	1.42	0.16	949.5	103.79	1.75	0.20
959.7	75.84	1.18	0.09	949.9	104.92	1.48	0.14
964.9	74.67	1.34	0.06	982.5	104.32	1.93	0.11
996.6	74.98	1.29	0.06	1014.8	104.84	1.53	0.11
1030.7	75.41	1.20	0.05	1051.1	105.26	1.42	0.16
1059.4	74.42	1.13	0.09	1035.6	108.59	1.62	0.09
1064.0	75.95	1.18	0.06	1075.1	109.12	1.27	0.11
1094.1	74.77	1.24	0.09	1115.8	109.63	1.14	0.10
1132.1	75.44	1.08	0.09	1154.3	109.85	0.84	0.12
1156.3	74.24	1.01	0.08	574.1	119.05	6.14	0.29
1169.4	75.76	0.89	0.17	592.5	119.62	6.34	0.29
1198.2	74.83	0.85	0.07	617.4	119.87	5.75	0.29
1233.7	75.41	0.81	0.07	628.0	118.90	6.39	0.30
1274.8	75.80	0.74	0.07	638.6	120.47	6.92	0.33
579.8	89.70	6.51	0.33	652.8	119.50	7.17	0.32
598.5	90.06	7.34	0.32	673.2	119.94	6.43	0.31
619.2	90.43	7.10	0.35	692.5	118.88	6.11	0.28
636.0	89.54	5.29	0.26	698.1	120.35	6.59	0.34
637.9	90.86	7.05	0.54	716.6	119.49	5.25	0.26
657.6	89.85	5.74	0.27	744.0	119.63	5.25	0.27
679.0	90.49	6.60	0.29	762.1	118.96	4.15	0.23
700.8	90.78	6.44	0.31	769.6	120.00	3.72	0.24
702.6	89.32	6.30	0.18	794.0	119.21	3.81	0.23
725.3	89.89	6.09	0.31	824.5	119.69	2.85	0.20
750.2	90.33	5.01	0.16	846.0	118.88	2.36	0.19
776.1	90.72	4.20	0.15	850.3	120.20	2.36	0.20
780.3	89.16	4.63	0.19	878.8	119.03	2.57	0.21
803.3	89.92	3.80	0.17	909.6	119.69	2.40	0.20
833.1	90.26	2.61	0.14	943.8	118.84	1.86	0.17
860.9	90.71	2.01	0.14	944.6	119.95	2.27	0.22
577.3	104.44	5.55	0.25	984.4	119.52	1.51	0.14
598.7	104.55	6.02	0.28	1020.2	118.31	1.50	0.09
617.3	105.18	5.89	0.28	1023.7	119.99	1.44	0.16
633.4	104.06	6.38	0.34	1071.0	118.74	1.26	0.12
637.0	105.61	6.63	0.31	1074.9	120.64	1.21	0.17
655.8	104.83	6.59	0.35	1105.1	119.27	1.32	0.12
676.9	105.07	5.74	0.33	1109.4	117.99	1.15	0.07
696.6	104.02	5.75	0.23	1147.0	119.69	0.98	0.15
698.3	105.70	6.64	0.37	1159.3	118.72	0.79	0.13

K	θ_{cm}	$\sigma(\theta)$	$\Delta\sigma(\theta)$	K	θ_{cm}	$\sigma(\theta)$	$\Delta\sigma(\theta)$
1205.4	119.05	0.91	0.09	755.4	149.30	5.94	0.41
1247.3	119.70	0.78	0.15	815.0	148.13	5.07	0.34
570.7	134.25	7.22	0.37	852.4	148.65	4.05	0.31
587.3	134.14	7.05	0.37	898.2	148.82	3.96	0.33
611.6	134.63	7.02	0.37	912.3	148.38	3.81	0.28
622.0	133.85	7.28	0.39	924.7	149.28	4.05	0.37
633.7	134.97	7.08	0.39	953.4	148.64	3.36	0.27
647.1	134.36	7.36	0.39	994.8	148.42	2.93	0.23
668.4	134.52	7.65	0.41	1006.6	149.17	3.29	0.27
681.3	133.71	6.39	0.35	1054.0	149.14	2.69	0.20
694.1	134.77	7.51	0.43	1057.8	149.72	2.41	0.25
710.3	134.23	6.01	0.34	1062.9	147.90	2.55	0.28
737.7	134.66	5.20	0.33	1103.6	149.40	2.44	0.20
750.4	133.59	5.79	0.32	1114.9	148.35	2.37	0.25
767.3	134.58	5.24	0.36	1155.6	148.51	2.02	0.26
787.3	133.93	4.03	0.28	1157.1	149.66	2.42	0.21
814.9	134.67	3.55	0.28	1211.9	148.81	1.62	0.31
847.2	134.63	3.14	0.28	610.4	158.50	7.58	0.41
831.2	133.51	3.70	0.25	636.6	158.57	8.45	0.46
865.3	133.87	3.67	0.25	660.4	158.82	9.51	0.50
901.8	134.20	3.07	0.25	673.4	158.62	8.37	0.51
926.0	134.76	2.44	0.27	688.0	158.94	10.34	0.59
926.8	133.58	2.56	0.22	698.4	158.75	8.33	0.53
974.8	134.31	2.42	0.20	725.8	158.80	7.73	0.52
1012.1	133.60	1.60	0.20	755.1	159.02	8.01	0.58
1017.6	134.54	2.03	0.20	821.3	158.53	5.48	0.38
1058.8	133.74	1.49	0.18	862.4	158.77	5.36	0.37
1063.1	134.57	1.53	0.20	898.5	158.29	4.85	0.35
1114.5	134.27	1.23	0.17	906.2	159.01	4.81	0.37
1166.4	134.85	1.29	0.20	945.7	159.32	4.56	0.39
563.6	148.96	6.96	0.38	949.3	158.79	4.80	0.36
584.3	149.06	7.49	0.41	992.4	158.69	3.55	0.46
611.5	149.25	7.89	0.42	1005.2	159.00	3.60	0.33
617.7	148.77	7.62	0.40	1024.7	158.58	3.35	0.37
629.4	149.46	8.23	0.46	1044.2	158.29	2.97	0.29
640.9	148.93	7.97	0.41	1046.4	159.14	3.64	0.35
666.8	149.32	8.24	0.44	1081.5	159.10	2.64	0.42
679.9	148.61	7.43	0.40	1104.4	158.42	2.53	0.31
690.5	149.29	7.75	0.44	1137.0	158.98	3.28	0.27
706.6	149.19	8.21	0.42	1146.7	158.41	2.45	0.36
733.8	149.11	6.63	0.39	1178.1	158.22	1.92	0.47

TABLE 2

π^- Recoil Cross Sections

K	θ_{cm}	$\sigma(\theta)$	$\Delta\sigma(\theta)$	K	θ_{cm}	$\sigma(\theta)$	$\Delta\sigma(\theta)$
608.5	44.85	14.22	4.11	906.1	59.86	2.40	0.30
615.6	45.32	17.22	4.09	932.1	60.29	2.27	0.17
632.6	45.42	8.92	2.13	963.3	60.80	2.00	0.16
648.7	45.77	17.45	3.31	971.6	59.35	2.25	0.11
657.4	44.93	10.80	1.65	1004.7	59.79	2.46	0.12
673.1	45.18	11.50	1.52	1036.0	60.20	2.46	0.12
691.9	45.33	9.18	1.16	1067.2	59.58	2.42	0.19
708.0	45.74	10.20	1.15	1069.1	60.67	2.50	0.14
725.7	44.77	9.44	0.76	1101.8	59.89	2.30	0.21
738.9	45.07	8.89	0.71	1135.8	60.29	1.94	0.16
761.6	45.33	5.54	0.41	1163.1	59.41	1.73	0.16
783.4	45.62	5.26	0.50	1174.8	60.70	1.70	0.15
797.0	44.59	4.94	0.46	1199.2	59.73	1.63	0.14
818.7	44.92	4.18	0.36	1240.0	60.30	1.31	0.12
842.3	45.17	4.23	0.36	1281.6	60.70	1.22	0.12
867.6	45.48	3.54	0.32	586.2	74.41	4.84	0.93
882.7	44.67	5.18	0.47	604.1	74.84	5.91	0.61
904.7	44.92	3.62	0.35	622.6	75.21	5.79	0.39
930.7	45.34	4.20	0.38	641.5	75.66	5.65	0.64
960.8	45.61	3.77	0.35	642.7	74.55	5.95	0.27
976.9	44.60	3.96	0.28	662.9	74.96	5.26	0.41
1007.5	44.97	4.05	0.45	684.3	75.33	6.10	0.27
1038.8	45.26	4.32	0.31	706.3	75.76	5.97	0.27
1066.3	45.59	3.80	0.27	711.0	74.37	5.97	0.44
1072.7	44.57	4.14	0.26	733.5	74.86	6.53	0.48
1102.7	44.94	3.78	0.24	757.6	75.23	4.35	0.35
1138.2	45.17	3.27	0.25	782.3	75.68	3.54	0.32
1168.7	45.61	3.47	0.24	787.4	74.43	3.15	0.22
1166.5	44.61	3.03	0.29	812.5	74.93	2.60	0.20
1204.6	44.92	3.23	0.32	839.2	75.24	1.95	0.19
1239.2	45.33	2.81	0.23	869.1	75.75	1.32	0.13
1276.7	45.64	2.67	0.22	871.3	74.41	1.46	0.13
591.0	59.59	7.72	0.62	903.2	74.88	1.30	0.12
605.7	59.91	7.06	0.56	933.1	75.30	1.06	0.11
624.6	60.22	7.58	0.59	964.9	75.82	0.93	0.10
643.1	60.61	8.02	0.59	968.8	74.33	1.05	0.07
645.5	59.57	6.65	0.52	1001.3	74.88	1.00	0.07
665.1	59.82	7.05	0.71	1037.2	75.30	0.89	0.08
684.5	60.21	7.42	0.52	1064.3	74.32	0.75	0.09
706.3	60.68	6.66	0.47	1072.1	75.70	0.95	0.10
714.0	59.47	7.20	0.45	1098.5	74.77	0.90	0.09
735.1	59.83	5.86	0.44	1138.6	75.32	0.93	0.10
757.9	60.18	5.45	0.39	1159.7	74.31	0.78	0.09
782.7	60.58	4.66	0.31	1173.5	75.87	0.75	0.09
791.1	59.49	4.16	0.45	1199.3	74.88	0.72	0.10
811.2	59.93	3.37	0.41	1239.7	75.38	0.70	0.08
839.1	60.35	2.84	0.36	1281.4	75.82	0.67	0.09
866.0	60.75	2.21	0.31	583.0	89.50	5.42	0.58
876.4	59.93	1.77	0.49	601.8	89.87	5.28	0.38

K	θ_{cm}	$\sigma(\theta)$	$\Delta\sigma(\theta)$	K	θ_{cm}	$\sigma(\theta)$	$\Delta\sigma(\theta)$
623.2	90.38	5.40	0.38	806.4	104.89	2.21	0.22
639.8	89.53	4.35	0.32	834.9	105.29	1.67	0.42
641.5	90.74	5.94	0.46	858.2	104.32	1.38	0.10
660.4	89.85	4.79	0.34	866.7	105.70	1.30	0.22
681.5	90.35	5.49	0.36	892.7	104.76	1.29	0.09
703.9	90.71	5.03	0.34	926.2	105.13	1.21	0.09
705.5	89.31	5.21	0.24	953.7	104.23	0.94	0.13
730.2	89.73	4.78	0.21	958.0	105.46	1.12	0.11
754.6	90.23	3.91	0.18	991.2	104.57	1.14	0.11
780.4	90.60	3.08	0.41	1022.5	105.17	0.95	0.10
783.1	89.35	3.76	0.23	1058.9	105.58	0.77	0.20
810.6	89.79	2.95	0.19	1043.2	109.35	0.77	0.09
837.1	90.36	1.85	0.14	1082.1	109.66	0.62	0.09
866.2	90.80	1.26	0.12	1124.9	110.11	0.46	0.11
636.9	104.38	5.32	0.40	1165.8	110.48	0.30	0.06
658.7	104.88	5.81	0.42	1119.5	118.91	0.53	0.05
682.3	105.14	4.87	0.38	1169.6	119.47	0.29	0.04
706.4	105.56	6.42	0.45	1217.5	119.82	0.21	0.07
775.5	104.40	3.56	0.23	1262.2	120.02	0.23	0.05

TABLE 3

π^- Reverse Recoil Cross Sections

K	θ_{cm}	$\sigma(\theta)$	$\Delta\sigma(\theta)$	K	θ_{cm}	$\sigma(\theta)$	$\Delta\sigma(\theta)$
594.1	119.77	4.71	0.50	659.1	149.76	8.83	0.69
605.5	119.74	5.47	0.38	683.0	149.87	9.47	0.74
626.3	120.00	4.98	0.33	707.1	149.97	7.48	0.75
647.0	119.64	5.58	0.55	713.0	149.71	7.84	0.67
648.2	120.06	5.52	0.44	732.1	149.74	6.27	0.52
666.7	119.71	6.07	0.49	756.1	149.73	5.85	0.50
688.2	119.99	5.43	0.42	781.1	149.77	5.20	0.47
709.9	120.14	5.96	0.46	786.9	149.78	5.49	0.50
713.6	119.56	5.11	0.35	816.1	149.70	4.48	0.41
735.4	119.75	4.95	0.33	837.6	149.77	4.42	0.40
758.7	119.93	4.10	0.34	866.7	149.83	3.48	0.32
782.9	120.07	3.42	0.31	870.8	149.80	3.26	0.31
789.9	120.11	2.91	0.28	906.4	149.83	3.59	0.35
816.7	120.28	2.34	0.24	923.2	149.62	3.29	0.31
842.0	120.20	2.13	0.23	957.6	149.79	2.78	0.27
864.0	120.21	1.56	0.18	976.8	149.74	2.29	0.28
876.2	119.80	1.64	0.17	1000.0	149.79	2.35	0.30
903.9	119.75	1.56	0.17	1023.8	149.74	2.53	0.33
929.8	119.75	1.46	0.16	1046.9	149.71	2.08	0.29
964.6	119.94	1.22	0.15	1061.5	149.74	1.26	0.19
972.5	119.61	1.38	0.16	1096.1	149.77	1.79	0.23
1000.0	119.71	1.40	0.16	1128.0	149.80	1.66	0.22
1040.7	119.79	0.92	0.13	1153.8	149.76	1.19	0.20
1068.4	119.55	0.88	0.12	1172.8	149.94	1.12	0.20
587.6	134.77	5.76	0.48	1203.8	149.82	0.68	0.15
613.4	134.85	5.55	0.45	1231.0	149.82	1.06	0.19
628.6	134.95	5.22	0.42	1259.3	149.69	1.05	0.20
645.0	134.68	6.40	0.58	592.4	159.82	7.27	0.68
646.8	135.06	6.46	0.50	609.5	159.81	8.50	0.75
665.7	134.96	6.74	0.55	623.9	159.71	7.44	0.57
694.8	134.99	5.95	0.43	640.5	159.69	9.35	0.76
703.6	134.83	5.73	0.44	642.1	159.86	7.60	0.73
716.7	134.79	5.64	0.47	657.9	159.74	8.56	0.62
726.9	134.58	5.17	0.43	673.9	159.58	8.67	0.66
756.4	134.72	3.95	0.32	702.5	159.66	9.17	0.78
786.3	135.06	3.86	0.36	705.6	159.63	8.72	0.73
790.6	134.66	3.67	0.29	733.2	159.68	9.32	0.80
812.9	134.83	3.24	0.26	756.5	159.62	7.32	0.59
841.3	134.82	2.55	0.21	779.6	159.51	6.01	0.53
870.1	134.95	1.97	0.19	782.9	159.76	6.78	0.58
874.9	134.72	1.94	0.17	817.4	159.65	6.24	0.57
898.3	134.85	2.12	0.18	834.8	159.74	5.39	0.49
933.0	134.87	2.02	0.18	853.4	159.64	5.09	0.46
970.3	135.00	1.68	0.16	875.0	159.81	3.80	0.40
590.0	149.73	7.20	0.57	893.9	159.81	4.94	0.57
604.4	149.70	6.95	0.53	925.0	159.83	4.53	0.47
629.8	149.87	8.36	0.67	938.1	159.70	4.02	0.47
644.0	149.80	7.81	0.61	981.3	159.82	3.63	0.41
646.3	149.93	8.28	0.81	1002.5	159.69	3.92	0.46

K	θ_{cm}	$\sigma(\theta)$	$\Delta\sigma(\theta)$	K	θ_{cm}	$\sigma(\theta)$	$\Delta\sigma(\theta)$
1028.8	159.79	3.61	0.45	1145.2	159.68	1.86	0.28
1056.8	159.75	2.72	0.34	1171.7	159.93	1.36	0.24
1071.0	159.70	2.66	0.33	1205.2	159.83	1.68	0.27
1098.8	159.71	3.13	0.38	1219.3	159.77	1.82	0.30
1124.4	159.71	1.91	0.27	1253.0	159.62	1.06	0.23

TABLE 4

π^+ Direct Cross Sections

K	θ_{cm}	$\sigma(\theta)$	$\Delta\sigma(\theta)$	K	θ_{cm}	$\sigma(\theta)$	$\Delta\sigma(\theta)$
583.9	6.22	14.78	0.75	659.6	20.29	10.14	0.46
601.1	6.23	14.75	0.74	677.8	20.41	10.23	0.46
614.1	6.27	14.96	0.79	695.3	20.61	9.30	0.43
630.8	6.35	14.73	0.71	711.5	20.09	9.38	0.33
641.0	6.21	14.92	0.80	731.3	20.21	8.82	0.32
659.1	6.22	15.01	0.80	750.8	20.37	8.03	0.30
674.2	6.30	14.51	1.66	768.0	20.53	7.95	0.30
695.5	6.29	12.09	0.69	786.7	20.24	7.58	0.69
713.4	6.20	14.29	0.74	808.8	20.40	7.29	0.28
730.2	6.25	13.04	0.69	829.9	20.53	7.25	0.28
748.0	6.30	12.14	0.65	850.8	20.72	6.99	0.27
764.5	6.38	11.13	0.62	869.5	20.18	7.53	0.27
874.5	6.28	10.23	0.84	896.1	20.23	7.29	0.26
898.8	6.31	9.17	0.78	919.7	20.44	7.35	0.26
922.2	6.35	8.61	0.74	946.4	20.62	6.91	0.25
947.2	6.43	7.58	0.68	967.5	20.28	6.76	0.25
585.4	10.12	12.68	0.72	994.2	20.37	6.88	0.25
601.1	10.18	13.72	0.75	1026.1	20.45	6.43	0.24
616.8	10.23	12.55	0.70	1054.1	20.62	5.60	0.22
631.6	10.34	13.84	0.73	1069.8	20.24	5.80	0.22
642.0	10.09	13.46	0.72	1096.2	20.41	4.79	0.20
659.6	10.13	11.73	0.67	1124.9	20.64	4.95	0.20
675.8	10.18	12.55	0.69	1158.8	20.75	4.31	0.19
694.8	10.29	11.76	0.65	1166.1	20.24	3.75	0.23
711.4	10.00	10.85	0.65	1192.1	20.40	3.06	0.20
727.6	10.10	10.26	0.63	1220.6	20.56	3.27	0.21
747.8	10.18	11.36	0.66	1249.8	20.70	2.62	0.19
770.8	10.22	10.21	0.62	585.3	30.17	9.25	0.44
790.1	10.18	10.28	0.47	599.4	30.34	9.87	0.45
808.3	10.24	9.77	0.45	616.5	30.49	9.71	0.44
831.3	10.28	9.46	0.44	632.8	30.76	9.56	0.43
850.1	10.42	9.16	0.43	644.6	30.05	9.67	0.35
875.3	10.19	8.85	0.44	658.1	30.34	9.87	0.68
896.4	10.22	8.05	0.41	676.5	30.52	9.24	0.34
923.9	10.29	8.05	0.40	693.1	30.84	9.37	0.33
947.4	10.35	7.60	0.39	710.8	30.13	10.05	0.34
1073.3	10.07	5.04	0.28	728.4	30.37	10.23	0.35
1096.3	10.20	4.14	0.25	752.0	30.45	8.52	0.31
1121.7	10.29	3.91	0.24	771.2	30.79	8.25	0.30
1156.4	10.36	3.90	0.24	785.7	30.16	7.73	0.46
1170.3	10.24	3.73	0.34	810.9	30.20	6.97	0.44
1198.2	10.30	3.91	0.36	830.6	30.53	6.98	0.43
1216.7	10.46	3.54	0.34	856.3	30.72	7.26	0.44
1243.9	10.56	3.11	0.31	874.1	30.03	6.72	0.18
583.8	20.20	11.02	0.49	899.2	30.19	6.91	0.19
598.7	20.32	10.64	0.47	923.9	30.44	7.09	0.20
617.0	20.38	9.87	0.45	949.9	30.71	7.06	0.18
632.1	20.57	10.42	0.46	968.9	30.03	7.90	0.29
642.5	20.15	10.77	0.48	998.1	30.18	7.64	0.28

K	θ_{cm}	$\sigma(\theta)$	$\Delta\sigma(\theta)$	K	θ_{cm}	$\sigma(\theta)$	$\Delta\sigma(\theta)$
1025.0	30.41	7.62	0.28	701.2	60.86	10.45	0.35
1056.7	30.62	6.57	0.26	707.6	59.89	10.05	0.59
1064.9	30.02	6.49	0.25	730.6	60.14	9.13	0.55
1095.8	30.24	6.06	0.24	751.1	60.59	8.44	0.53
1126.8	30.44	5.24	0.22	776.0	60.99	6.69	0.47
1160.2	30.70	4.67	0.21	786.1	59.70	6.73	0.22
1164.2	29.99	4.91	0.22	808.8	60.11	6.30	0.24
1195.2	30.15	4.29	0.20	835.3	60.52	5.42	0.20
1230.5	30.40	3.94	0.19	858.6	61.04	5.36	0.20
1264.6	30.68	3.75	0.19	872.7	59.74	5.06	0.28
585.0	45.07	9.65	0.46	898.9	60.22	5.01	0.27
602.5	45.13	9.99	0.46	925.2	60.57	5.50	0.29
617.7	45.57	10.25	0.46	957.7	60.96	5.74	0.30
633.3	45.99	11.08	0.48	967.3	59.60	5.82	0.26
640.8	45.15	10.56	0.42	998.7	60.03	5.88	0.26
659.6	45.34	9.59	0.39	1028.8	60.49	5.80	0.26
677.5	45.66	10.10	0.40	1063.1	59.69	5.36	0.25
696.8	45.98	9.80	0.39	1064.5	60.82	4.83	0.25
712.5	44.96	10.23	0.49	1102.7	59.90	3.97	0.21
729.4	45.30	10.05	0.48	1131.9	60.47	3.54	0.20
750.8	45.54	9.04	0.44	1160.3	59.43	2.90	0.19
773.3	45.87	8.84	0.44	1168.7	60.91	2.30	0.16
786.2	44.83	7.65	0.25	1196.2	59.89	2.22	0.17
807.4	45.20	6.65	0.46	1232.8	60.53	1.89	0.15
833.1	45.44	6.50	0.33	1276.9	60.75	1.57	0.15
854.8	45.90	6.58	0.24	581.8	74.79	8.54	0.26
875.0	44.92	6.49	0.30	598.8	75.32	8.99	0.26
898.0	45.19	7.21	0.32	617.3	75.51	8.99	0.26
922.0	45.63	6.88	0.31	638.3	75.85	9.17	0.59
949.8	45.99	7.77	0.34	639.5	74.64	8.58	0.26
971.5	44.75	7.78	0.21	659.1	75.23	9.73	0.91
997.5	45.21	8.03	0.21	680.0	75.52	9.01	0.22
1027.1	45.55	7.52	0.20	699.7	75.97	8.44	0.22
1059.1	45.81	6.58	0.19	706.1	74.47	8.66	0.36
1063.3	44.84	6.80	0.42	731.5	74.96	8.24	0.36
1097.9	45.02	6.04	0.23	752.1	75.59	7.26	0.33
1128.5	45.46	4.72	0.20	774.4	76.03	6.26	0.31
1161.8	44.77	4.02	0.21	783.5	74.59	5.72	0.38
1162.1	45.78	4.39	0.24	809.1	75.03	5.22	0.37
1194.2	45.22	3.62	0.20	834.9	75.43	3.96	0.32
1233.7	45.49	3.17	0.18	865.4	75.82	3.37	0.30
1270.1	45.83	3.19	0.19	866.6	74.56	3.93	0.21
585.5	59.89	9.41	0.53	897.8	74.96	3.32	0.20
599.2	60.38	8.83	0.51	925.0	75.44	3.64	0.21
619.3	60.54	9.31	0.51	959.7	75.84	3.37	0.37
636.2	60.97	9.79	0.52	964.9	74.67	3.84	0.25
640.1	59.87	9.84	0.46	996.6	74.98	3.31	0.23
659.6	60.14	11.05	0.32	1030.7	75.41	3.31	0.23
679.2	60.48	10.24	0.46	1059.4	74.42	3.05	0.20

K	θ_{cm}	$\sigma(\theta)$	$\Delta\sigma(\theta)$	K	θ_{cm}	$\sigma(\theta)$	$\Delta\sigma(\theta)$
1064.0	75.95	2.89	0.24	1075.1	109.12	2.04	0.14
1094.1	74.77	2.48	0.18	1115.8	109.63	1.71	0.11
1132.1	75.44	1.68	0.15	1154.3	109.85	1.59	0.12
1156.3	74.24	1.65	0.15	574.1	119.05	4.32	0.22
1169.4	75.76	1.35	0.14	592.5	119.62	4.37	0.21
1198.2	74.83	1.28	0.13	617.4	119.87	4.75	0.21
1233.7	75.41	1.01	0.12	628.0	118.90	4.43	0.23
1274.8	75.80	0.90	0.12	638.6	120.47	4.69	0.22
579.8	89.70	7.18	0.32	652.8	119.50	4.65	0.24
598.5	90.06	7.22	0.33	673.2	119.94	5.23	0.26
619.2	90.43	7.30	0.33	692.5	118.88	5.48	0.26
636.0	89.54	7.56	0.32	698.1	120.35	5.88	0.31
637.9	90.86	7.62	0.34	716.6	119.49	5.43	0.26
657.6	89.85	7.58	0.33	744.0	119.63	5.25	0.27
679.6	90.49	8.47	0.35	762.1	118.96	4.58	0.24
700.8	90.78	8.60	0.37	769.6	120.00	4.31	0.25
702.6	89.32	8.37	0.21	794.0	119.21	4.63	0.25
725.4	89.88	8.10	0.21	824.5	119.69	4.08	0.24
750.3	90.32	6.79	0.36	846.0	118.88	3.74	0.23
776.0	90.72	5.92	0.24	850.3	120.20	3.61	0.24
780.3	89.16	6.43	0.24	878.8	119.03	4.00	0.25
803.3	89.92	5.55	0.22	909.6	119.69	3.97	0.26
833.1	90.26	4.39	0.19	943.8	118.84	3.12	0.23
860.9	90.71	3.72	0.18	944.6	119.95	4.05	0.29
577.3	104.44	5.27	0.29	984.4	119.52	2.73	0.21
598.7	104.55	5.49	0.59	1020.2	118.31	2.58	0.16
617.3	105.18	5.66	0.31	1023.7	119.99	2.84	0.22
633.4	104.06	6.02	0.32	1071.0	118.74	2.43	0.16
637.0	105.61	6.38	0.35	1074.9	120.64	2.31	0.20
655.8	104.83	6.41	0.49	1105.1	119.27	1.82	0.21
676.9	105.07	6.87	0.71	1109.4	117.99	1.61	0.15
698.0	104.40	6.52	0.26	1147.0	119.69	1.89	0.16
698.3	105.70	6.93	0.36	1159.3	118.72	1.33	0.12
723.7	104.77	7.03	0.27	1205.4	119.05	1.20	0.12
749.1	105.25	6.18	0.26	1247.3	119.70	1.11	0.13
769.6	104.10	5.79	0.24	570.7	134.25	3.29	0.23
775.5	105.45	5.09	0.25	587.3	134.14	3.72	0.24
799.5	104.70	4.93	0.22	611.6	134.63	3.80	0.25
829.2	105.12	4.27	0.21	622.0	133.85	3.64	0.25
854.6	103.85	3.52	0.19	633.7	134.97	3.52	0.25
857.9	105.48	3.54	0.20	647.1	134.36	4.00	0.26
886.6	104.55	3.21	0.18	668.4	134.52	4.63	0.30
920.1	104.96	3.02	0.18	681.3	133.71	4.35	0.27
949.5	103.79	2.99	0.16	694.1	134.77	4.14	0.29
949.9	104.92	3.03	0.20	710.3	134.23	4.67	0.28
982.5	104.32	3.16	0.17	737.7	134.66	4.53	0.29
1014.8	104.84	3.10	0.18	750.4	133.59	3.73	0.25
1051.1	105.26	2.43	0.17	767.3	134.58	3.67	0.27
1035.6	106.59	2.26	0.13	787.3	133.93	3.74	0.25

K	θ_{cm}	$\sigma(\theta)$	$\Delta\sigma(\theta)$	K	θ_{cm}	$\sigma(\theta)$	$\Delta\sigma(\theta)$
814.9	134.67	3.55	0.26	1006.6	149.17	2.74	0.26
831.2	133.51	3.39	0.24	1053.9	149.22	2.70	0.25
847.2	134.63	3.53	0.28	1057.8	149.72	2.69	0.27
865.3	133.87	3.54	0.25	1062.9	147.90	2.68	0.27
901.8	134.20	3.00	0.24	1104.0	149.49	2.43	0.25
926.0	134.76	3.37	0.30	1114.9	148.35	2.34	0.27
926.8	133.58	3.31	0.25	1155.6	148.51	2.06	0.27
974.8	134.31	2.98	0.24	1162.2	149.72	2.13	0.26
1012.1	133.60	2.74	0.25	1211.9	148.81	2.69	0.38
1017.6	134.54	2.95	0.24	610.4	158.50	3.01	0.25
1058.8	133.74	2.48	0.24	636.6	158.57	3.18	0.25
1063.1	134.97	2.51	0.23	660.4	158.82	2.89	0.25
1114.5	134.27	2.13	0.22	673.4	158.62	3.24	0.31
1166.4	134.85	1.71	0.21	688.0	158.94	3.35	0.30
563.6	148.96	3.33	0.24	698.4	158.75	2.93	0.29
584.3	149.06	3.20	0.24	725.8	158.80	3.58	0.34
611.5	149.25	3.44	0.26	755.1	159.02	3.70	0.38
617.7	148.77	3.42	0.25	821.3	158.53	2.64	0.25
629.4	149.46	2.97	0.25	862.4	158.77	2.93	0.27
640.9	148.93	3.25	0.24	898.5	158.29	2.51	0.25
666.8	149.32	3.29	0.25	906.2	159.01	2.89	0.27
679.9	148.61	3.98	0.33	945.7	159.32	2.70	0.27
690.5	149.29	3.26	0.26	949.3	158.79	3.02	0.27
706.6	149.19	4.18	0.34	992.4	158.69	2.50	0.32
733.8	149.11	3.12	0.29	1005.2	159.00	2.10	0.23
755.4	149.30	3.52	0.33	1024.7	158.58	2.13	0.23
815.0	148.13	3.03	0.25	1044.2	158.29	1.81	0.25
852.4	148.65	3.19	0.26	1046.4	159.14	2.13	0.25
898.2	148.82	3.11	0.27	1081.5	159.10	2.00	0.23
912.3	148.38	2.68	0.25	1104.4	158.42	1.81	0.26
924.7	149.28	3.20	0.32	1137.0	158.98	1.68	0.22
953.4	148.64	3.08	0.27	1146.7	158.41	1.87	0.28
993.6	148.32	2.48	0.24	1178.1	158.22	2.28	0.38

TABLE 5

π^-/π^+ Ratios

K	θ_{cm}	π^-/π^+	$\Delta\pi^-/\pi^+$	K	θ_{cm}	π^-/π^+	$\Delta\pi^-/\pi^+$
583.9	6.22	1.17	0.07	731.3	20.21	1.10	0.05
601.1	6.23	1.21	0.07	750.8	20.37	1.02	0.05
614.1	6.27	1.16	0.07	768.0	20.53	0.92	0.05
630.8	6.35	1.23	0.07	786.7	20.24	0.77	0.08
641.0	6.21	1.28	0.08	808.8	20.40	0.74	0.05
659.1	6.22	1.09	0.07	829.9	20.53	0.71	0.04
674.2	6.30	1.16	0.13	850.8	20.72	0.65	0.04
695.5	6.29	1.29	0.08	869.5	20.18	0.63	0.03
713.4	6.20	1.04	0.06	896.1	20.23	0.59	0.03
730.2	6.25	0.99	0.06	919.7	20.44	0.59	0.03
748.0	6.30	0.91	0.06	946.4	20.62	0.60	0.03
764.5	6.38	1.00	0.06	967.5	20.28	0.59	0.03
585.4	10.12	1.31	0.11	994.2	20.37	0.58	0.03
601.1	10.18	1.20	0.08	1026.1	20.45	0.59	0.03
616.8	10.23	1.24	0.08	1054.1	20.62	0.63	0.03
631.6	10.34	1.13	0.07	1069.8	20.24	0.66	0.04
642.0	10.09	1.08	0.07	1096.2	20.41	0.74	0.04
659.6	10.13	1.28	0.09	1124.9	20.64	0.71	0.04
675.8	10.18	1.10	0.08	1158.8	20.75	0.80	0.05
694.8	10.29	1.17	0.08	1166.1	20.24	0.84	0.09
711.4	10.00	1.26	0.09	1192.1	20.40	0.90	0.10
727.6	10.10	1.17	0.11	1220.6	20.56	0.90	0.10
747.8	10.18	0.97	0.08	1249.8	20.70	0.89	0.11
770.8	10.22	1.00	0.07	585.3	30.17	1.12	0.07
790.1	10.18	0.71	0.04	599.4	30.34	1.08	0.06
808.3	10.24	0.75	0.05	616.5	30.49	1.11	0.07
831.3	10.28	0.66	0.04	632.8	30.76	1.10	0.06
850.1	10.42	0.62	0.04	644.6	30.05	1.08	0.05
875.3	10.19	0.66	0.05	658.1	30.34	1.03	0.08
896.4	10.22	0.60	0.05	676.5	30.52	1.07	0.05
923.9	10.29	0.54	0.04	693.1	30.84	1.04	0.05
947.4	10.35	0.47	0.04	710.8	30.13	0.97	0.04
1073.3	10.07	0.65	0.04	728.4	30.37	0.90	0.04
1096.3	10.20	0.76	0.12	752.0	30.45	0.97	0.05
1121.7	10.29	0.80	0.06	771.2	30.79	0.84	0.04
1156.4	10.36	0.74	0.07	785.7	30.16	0.69	0.05
1170.3	10.24	0.74	0.10	810.9	30.20	0.81	0.06
1198.2	10.30	0.64	0.09	830.6	30.53	0.66	0.05
1216.7	10.46	0.78	0.11	856.3	30.72	0.64	0.05
1243.9	10.56	0.79	0.11	874.1	30.03	0.68	0.03
583.8	20.20	1.10	0.06	899.2	30.19	0.65	0.03
598.7	20.32	1.17	0.06	923.9	30.44	0.65	0.02
617.0	20.38	1.25	0.07	949.9	30.71	0.59	0.02
632.1	20.57	1.19	0.06	968.9	30.03	0.61	0.03
642.5	20.15	1.11	0.06	998.1	30.18	0.60	0.03
659.6	20.29	1.21	0.07	1025.0	30.41	0.58	0.03
677.8	20.41	1.11	0.06	1056.7	30.62	0.69	0.03
695.3	20.61	1.21	0.07	1164.2	29.99	0.88	0.05
711.5	20.09	1.16	0.05	1195.2	30.15	0.92	0.06

K	θ_{cm}	π^-/π^+	$\Delta\pi^-/\pi^+$	K	θ_{cm}	π^-/π^+	$\Delta\pi^-/\pi^+$
1230.5	30.40	0.88	0.06	858.6	61.04	0.55	0.03
1264.6	30.68	0.92	0.06	872.7	59.74	0.59	0.05
585.0	45.07	0.96	0.08	898.9	60.22	0.60	0.05
602.5	45.13	0.96	0.08	925.2	60.57	0.52	0.04
617.7	45.57	0.89	0.07	957.7	60.96	0.43	0.04
633.3	45.99	0.93	0.07	967.3	59.60	0.44	0.03
640.8	45.15	0.83	0.05	998.7	60.03	0.47	0.03
659.6	45.34	0.84	0.05	1028.8	60.49	0.44	0.03
677.5	45.66	0.84	0.05	1063.1	59.69	0.48	0.03
696.8	45.98	0.80	0.04	1064.5	60.82	0.51	0.03
712.5	44.96	0.81	0.04	1102.7	59.90	0.62	0.04
729.4	45.30	0.80	0.04	1131.9	60.47	0.63	0.09
750.8	45.54	0.76	0.05	1160.3	59.43	0.71	0.06
773.3	45.87	0.66	0.04	1168.7	60.91	0.82	0.07
786.2	44.83	0.70	0.03	1196.2	59.89	0.83	0.08
807.4	45.20	0.71	0.05	1232.8	60.53	0.84	0.08
833.1	45.44	0.70	0.04	1276.9	60.75	0.92	0.10
854.8	45.90	0.63	0.03	581.8	74.78	0.85	0.03
875.0	44.92	0.62	0.04	599.0	75.32	0.82	0.03
898.0	45.19	0.57	0.04	617.4	75.52	0.82	0.05
922.0	45.63	0.54	0.03	638.3	75.85	0.79	0.03
949.8	45.99	0.53	0.08	639.6	74.67	0.83	0.06
971.5	44.78	0.55	0.03	659.1	75.15	0.70	0.07
996.8	45.24	0.57	0.03	680.0	75.51	0.82	0.05
1027.4	45.57	0.55	0.03	699.7	75.97	0.81	0.04
1058.4	45.84	0.57	0.03	706.1	74.47	0.76	0.04
1062.3	44.88	0.64	0.03	731.5	74.96	0.80	0.05
1098.5	45.02	0.65	0.03	752.1	75.59	0.70	0.04
1128.3	45.48	0.77	0.04	774.4	76.03	0.60	0.04
1161.6	45.79	0.79	0.04	783.5	74.59	0.66	0.06
1161.8	44.77	0.90	0.11	809.1	75.03	0.56	0.06
1194.2	45.22	0.93	0.06	834.9	75.43	0.63	0.07
1233.7	45.49	0.93	0.06	865.4	75.82	0.58	0.07
1270.1	45.83	0.83	0.06	866.6	74.56	0.45	0.03
585.5	59.89	0.89	0.06	897.8	74.96	0.55	0.04
599.2	60.38	0.92	0.06	925.0	75.44	0.39	0.05
619.3	60.54	0.90	0.06	959.7	75.84	0.35	0.04
636.2	60.97	0.84	0.05	964.9	74.67	0.35	0.03
640.1	59.87	0.83	0.03	996.6	74.98	0.40	0.03
659.6	60.14	0.76	0.03	1030.7	75.41	0.36	0.03
679.2	60.48	0.75	0.03	1059.4	74.42	0.38	0.04
701.2	60.86	0.71	0.02	1064.0	75.95	0.42	0.04
707.6	59.89	0.74	0.03	1094.1	74.77	0.50	0.05
730.6	60.14	0.71	0.06	1132.1	75.44	0.65	0.07
751.1	60.59	0.69	0.04	1156.3	74.24	0.66	0.10
776.0	60.99	0.73	0.04	1169.4	75.76	0.65	0.14
786.1	59.70	0.70	0.04	1198.2	74.83	0.70	0.12
808.8	60.11	0.62	0.03	1233.7	75.41	0.82	0.15
835.3	60.52	0.63	0.03	1274.8	75.80	0.89	0.18

K	θ_{cm}	π^-/π^+	$\Delta\pi^-/\pi^+$	K	θ_{cm}	π^-/π^+	$\Delta\pi^-/\pi^+$
579.8	89.70	0.92	0.06	716.6	119.49	0.97	0.06
598.5	90.06	1.01	0.06	744.0	119.63	1.00	0.06
619.2	90.43	0.97	0.06	762.1	118.96	0.90	0.06
636.0	89.54	0.70	0.04	769.6	120.00	0.87	0.06
637.9	90.86	0.92	0.08	794.0	119.21	0.82	0.06
657.6	89.85	0.76	0.04	824.5	119.69	0.70	0.05
679.0	90.49	0.77	0.04	846.0	118.88	0.63	0.06
700.8	90.78	0.75	0.04	850.3	120.20	0.67	0.06
702.6	89.32	0.75	0.03	878.8	119.03	0.64	0.06
725.3	89.89	0.76	0.03	909.6	119.69	0.60	0.06
750.2	90.33	0.74	0.05	943.8	118.84	0.58	0.05
776.1	90.72	0.70	0.03	944.6	119.95	0.56	0.06
780.3	89.16	0.72	0.03	984.4	119.52	0.52	0.05
803.3	89.92	0.68	0.03	1020.2	118.31	0.55	0.03
833.1	90.26	0.59	0.04	1023.7	119.99	0.52	0.05
860.9	90.71	0.56	0.04	1071.0	118.74	0.53	0.04
577.3	104.44	1.04	0.07	1074.9	120.64	0.57	0.06
598.7	104.55	1.10	0.12	1105.1	119.27	0.71	0.08
617.3	105.18	1.06	0.07	1109.4	117.99	0.64	0.05
633.4	104.06	1.06	0.07	1147.0	119.69	0.56	0.06
637.0	105.61	1.03	0.06	1159.3	118.72	0.72	0.06
655.8	104.83	1.02	0.09	1205.4	119.05	0.70	0.07
676.9	105.07	0.83	0.09	1247.3	119.70	0.72	0.11
698.3	105.70	0.97	0.06	570.7	134.25	2.20	0.16
769.6	104.10	0.72	0.04	587.3	134.14	1.90	0.14
799.5	104.70	0.74	0.04	611.6	134.63	1.85	0.13
829.2	105.12	0.59	0.05	622.0	133.85	2.00	0.15
854.6	103.85	0.59	0.04	633.7	134.97	2.01	0.15
857.9	105.48	0.60	0.08	647.1	134.36	1.84	0.13
886.6	104.55	0.54	0.05	668.4	134.52	1.65	0.12
920.1	104.56	0.55	0.05	681.3	133.71	1.46	0.10
949.5	103.79	0.56	0.07	694.1	134.77	1.81	0.14
949.9	104.92	0.55	0.05	710.3	134.23	1.29	0.09
982.5	104.32	0.59	0.04	737.7	134.66	1.15	0.09
1014.8	104.84	0.50	0.04	750.4	133.59	1.53	0.11
1051.1	105.26	0.63	0.07	767.3	134.58	1.44	0.12
1035.6	108.59	0.67	0.04	787.3	133.93	1.08	0.09
1075.1	109.12	0.64	0.04	814.9	134.67	1.01	0.09
1115.8	109.63	0.66	0.05	831.2	133.51	1.06	0.09
1154.3	109.85	0.58	0.04	847.2	134.63	0.91	0.09
574.1	119.05	1.42	0.09	865.3	133.87	0.99	0.08
592.5	119.62	1.45	0.08	901.8	134.20	1.05	0.10
617.4	119.87	1.21	0.07	926.0	134.76	0.77	0.08
628.0	118.90	1.45	0.09	926.8	133.58	0.76	0.07
638.6	120.47	1.47	0.08	974.8	134.31	0.78	0.08
652.8	119.50	1.54	0.09	1012.1	133.60	0.60	0.07
673.2	119.94	1.23	0.08	1017.6	134.54	0.70	0.07
692.5	118.88	1.11	0.06	1058.8	133.74	0.58	0.07
698.1	120.39	1.12	0.07	1063.1	134.97	0.66	0.08

K	θ_{cm}	π^-/π^+	$\Delta\pi^-/\pi^+$	K	θ_{cm}	π^-/π^+	$\Delta\pi^-/\pi^+$
1114.5	134.27	0.57	0.08	1155.6	148.51	0.95	0.16
1166.4	134.85	0.77	0.12	1162.2	149.72	1.17	0.18
563.6	148.96	2.10	0.17	1211.9	148.81	0.63	0.12
584.3	149.06	2.34	0.19	610.4	158.50	2.50	0.22
611.5	149.25	2.29	0.19	636.6	158.57	2.72	0.23
617.7	148.77	2.23	0.18	660.4	158.82	3.24	0.30
629.4	149.46	2.76	0.24	673.4	158.62	2.58	0.27
640.9	148.93	2.45	0.20	688.0	158.94	3.10	0.28
666.8	149.32	2.50	0.21	698.4	158.75	2.84	0.31
679.9	148.61	1.86	0.17	725.8	158.80	2.16	0.23
690.5	149.29	2.38	0.21	755.1	159.02	2.17	0.24
706.6	149.19	1.96	0.18	821.3	158.53	2.11	0.21
733.8	149.11	2.13	0.22	862.4	158.77	1.79	0.18
755.4	149.30	1.70	0.18	898.5	158.29	1.92	0.21
815.0	148.13	1.66	0.16	906.2	159.01	1.66	0.17
852.4	148.65	1.27	0.13	945.7	159.32	1.70	0.19
838.2	148.82	1.28	0.13	949.3	158.79	1.58	0.16
912.3	148.38	1.41	0.15	992.4	158.69	1.48	0.17
924.7	149.28	1.27	0.15	1005.2	159.00	1.74	0.22
953.4	148.64	1.09	0.12	1024.7	158.58	1.56	0.15
993.6	148.32	1.11	0.13	1044.2	158.29	1.47	0.21
1006.6	149.17	1.20	0.13	1046.4	159.14	1.70	0.23
1053.9	149.22	0.94	0.11	1081.5	159.10	1.43	0.16
1057.8	149.72	0.91	0.12	1104.4	158.42	1.33	0.21
1062.9	147.90	0.98	0.12	1137.0	158.98	1.75	0.18
1104.0	149.49	0.98	0.13	1146.7	158.41	1.34	0.22
1114.9	148.35	0.97	0.14	1178.1	158.22	1.01	0.19

TABLE 6

π^- Ratio Cross Sections

Cross are computed from

$$\sigma(\gamma + n \rightarrow \pi^- + p) = (\pi^-/\pi^+) \times \sigma(\gamma + p \rightarrow \pi^+ + n)$$

$\sigma(\gamma + p \rightarrow \pi^+ + n)$ is taken from Ecklund's fit [12]

K	θ_{cm}	$\sigma(\theta)$	$\Delta\sigma(\theta)$	K	θ_{cm}	$\sigma(\theta)$	$\Delta\sigma(\theta)$
583.9	6.22	20.72	1.21	994.8	10.25	4.43	0.26
601.1	6.23	21.44	1.24	1025.2	10.31	3.78	0.23
614.1	6.27	21.13	1.26	1050.8	10.38	4.14	0.28
630.8	6.35	22.00	1.22	1073.3	10.07	3.83	0.25
641.0	6.21	23.12	1.39	1096.3	10.20	4.11	0.63
659.1	6.22	20.26	1.26	1121.7	10.29	3.86	0.28
674.2	6.30	21.29	2.38	1156.4	10.36	3.17	0.32
695.5	6.29	22.54	1.45	1170.3	10.24	3.21	0.43
713.4	6.20	17.82	1.01	1198.2	10.30	2.62	0.37
730.2	6.25	15.30	0.91	1216.7	10.46	2.99	0.41
748.0	6.30	13.47	0.84	1243.9	10.56	2.77	0.39
764.5	6.38	14.59	0.92	583.8	20.20	13.02	0.73
790.9	6.25	13.15	0.48	598.7	20.32	13.81	0.76
808.7	6.25	12.13	0.44	617.0	20.38	14.32	0.79
828.6	6.33	10.54	0.41	632.1	20.57	13.71	0.73
848.8	6.39	9.41	0.38	642.5	20.15	13.15	0.73
874.5	6.28	7.76	0.75	659.6	20.29	14.17	0.78
898.8	6.31	7.59	0.76	677.8	20.41	13.03	0.72
922.2	6.35	6.78	0.70	695.3	20.61	13.98	0.78
947.2	6.43	7.39	0.76	711.5	20.09	13.24	0.58
1070.8	6.14	5.03	0.33	731.3	20.21	11.62	0.53
1097.4	6.18	5.48	0.30	750.8	20.37	9.86	0.47
1123.7	6.26	4.41	0.51	768.0	20.53	8.30	0.41
1155.6	6.34	4.34	0.26	786.7	20.24	6.87	0.68
1170.0	6.41	4.92	0.35	808.8	20.40	6.62	0.41
1191.5	6.58	4.67	0.35	829.9	20.53	5.90	0.37
1213.7	6.69	4.30	0.33	850.8	20.72	5.31	0.35
1250.2	6.70	3.86	0.30	869.5	20.18	5.34	0.27
585.4	10.12	20.33	1.68	896.1	20.23	4.96	0.26
601.1	10.18	18.63	1.24	919.7	20.44	4.75	0.24
616.8	10.23	19.42	1.31	946.4	20.62	4.76	0.25
631.6	10.34	17.38	1.13	967.5	20.28	4.73	0.21
642.0	10.09	17.00	1.16	994.2	20.37	4.57	0.21
659.6	10.13	20.27	1.43	1026.1	20.45	4.40	0.24
675.8	10.18	17.17	1.19	1054.1	20.62	4.25	0.20
694.8	10.29	17.55	1.21	1069.8	20.24	4.32	0.24
711.4	10.00	18.57	1.32	1096.2	20.41	4.42	0.26
727.6	10.10	15.90	1.43	1124.9	20.64	3.72	0.22
747.8	10.18	12.30	0.96	1158.8	20.75	3.69	0.22
770.8	10.22	12.07	0.90	1166.1	20.24	3.80	0.40
790.1	10.18	8.55	0.52	1192.1	20.40	4.00	0.45
808.3	10.24	9.01	0.55	1220.6	20.56	3.81	0.42
831.3	10.28	7.67	0.49	1249.8	20.70	3.62	0.45
850.1	10.42	6.89	0.45	585.3	30.17	12.26	0.76
875.3	10.19	7.29	0.51	599.4	30.34	11.71	0.70
896.4	10.22	6.31	0.47	616.5	30.49	11.86	0.70
923.9	10.29	5.42	0.42	632.8	30.76	11.82	0.69
947.4	10.35	4.17	0.35	644.6	30.05	11.95	0.56
970.5	10.17	4.27	0.25	658.1	30.34	11.40	0.84

K	θ_{cm}	$\sigma(\theta)$	$\Delta\sigma(\theta)$	K	θ_{cm}	$\sigma(\theta)$	$\Delta\sigma(\theta)$
676.5	30.52	12.12	0.57	1058.4	45.84	3.73	0.24
693.1	30.84	11.78	0.55	1062.3	44.88	4.38	0.24
710.8	30.13	10.80	0.48	1098.5	45.02	4.20	0.22
728.4	30.37	9.30	0.41	1128.3	45.48	4.02	0.21
752.0	30.45	9.09	0.42	1161.6	45.79	3.36	0.19
771.2	30.79	7.32	0.35	1161.8	44.77	3.91	0.49
785.7	30.16	5.76	0.44	1194.2	45.22	3.50	0.23
810.9	30.20	6.55	0.51	1233.7	45.49	3.05	0.21
830.6	30.53	5.02	0.40	1270.1	45.83	2.63	0.19
856.3	30.72	4.87	0.38	585.5	59.89	8.50	0.55
874.1	30.03	5.38	0.20	599.2	60.38	8.96	0.59
899.2	30.19	5.32	0.26	619.3	60.54	8.92	0.56
923.9	30.44	5.25	0.19	636.2	60.97	8.63	0.53
949.9	30.71	5.00	0.18	640.1	59.87	8.69	0.33
968.9	30.03	5.41	0.31	659.6	60.14	8.18	0.30
998.1	30.18	5.43	0.24	679.2	60.48	8.42	0.37
1025.0	30.41	5.19	0.23	701.2	60.86	8.03	0.27
1056.7	30.62	5.62	0.26	707.6	59.89	8.35	0.38
1065.2	30.04	5.08	0.21	730.6	60.14	7.26	0.58
1094.0	30.26	4.85	0.20	751.1	60.59	6.28	0.32
1128.3	30.42	4.81	0.20	776.0	60.99	5.57	0.31
1160.3	30.68	4.90	0.21	786.1	59.70	4.83	0.30
1164.2	29.99	4.44	0.27	808.8	60.11	3.50	0.18
1195.2	30.15	4.32	0.27	835.3	60.52	3.12	0.17
1230.5	30.40	3.85	0.26	858.6	61.04	2.56	0.14
1264.6	30.68	3.94	0.27	872.7	59.74	2.81	0.23
585.0	45.07	10.08	0.82	898.9	60.22	3.01	0.24
602.5	45.13	10.21	0.80	925.2	60.57	2.76	0.22
617.7	45.57	9.53	0.75	957.7	60.96	2.45	0.20
633.3	45.99	9.97	0.74	967.3	59.60	2.63	0.19
640.8	45.15	9.07	0.50	998.7	60.03	2.82	0.19
659.6	45.34	9.57	0.54	1028.8	60.49	2.59	0.17
677.5	45.66	9.95	0.54	1063.1	59.69	2.84	0.18
696.8	45.98	9.29	0.52	1064.5	60.82	2.88	0.19
712.5	44.96	9.39	0.47	1102.7	59.90	2.74	0.19
729.4	45.30	8.34	0.41	1131.9	60.47	2.17	0.31
750.8	45.54	7.16	0.48	1160.3	59.43	2.03	0.17
773.3	45.87	5.65	0.30	1168.7	60.91	2.04	0.18
786.2	44.83	5.50	0.24	1196.2	59.89	1.84	0.17
807.4	45.20	5.04	0.37	1232.8	60.53	1.47	0.14
833.1	45.44	4.57	0.26	1276.9	60.75	1.46	0.16
854.8	45.90	4.00	0.19	581.8	74.78	6.71	0.27
875.0	44.92	4.17	0.27	599.0	75.32	6.62	0.24
838.0	45.19	4.08	0.26	617.4	75.52	6.77	0.42
922.0	45.63	4.00	0.25	638.3	75.85	6.95	0.27
949.8	45.99	4.12	0.61	639.6	74.67	7.47	0.56
971.5	44.78	4.33	0.23	659.1	75.15	6.42	0.65
996.8	45.24	4.67	0.26	680.0	75.51	7.98	0.50
1027.4	45.57	4.29	0.24	699.7	75.97	7.97	0.42

K	θ_{cm}	$\sigma(\theta)$	$\Delta\sigma(\theta)$	K	θ_{cm}	$\sigma(\theta)$	$\Delta\sigma(\theta)$
706.1	74.47	7.62	0.44	799.5	104.70	3.18	0.18
731.5	74.96	7.69	0.45	829.2	105.12	2.05	0.16
752.1	75.59	5.67	0.36	854.6	103.85	1.63	0.12
774.4	76.03	4.03	0.29	857.9	105.48	1.64	0.23
783.5	74.59	3.98	0.36	886.6	104.55	1.35	0.11
809.1	75.03	2.54	0.26	920.1	104.96	1.36	0.12
834.9	75.43	2.28	0.25	949.5	103.79	1.38	0.17
865.4	75.82	1.77	0.22	949.9	104.92	1.38	0.13
866.6	74.56	1.42	0.11	982.5	104.32	1.43	0.10
897.8	74.96	1.63	0.13	1014.8	104.84	1.15	0.09
925.0	75.44	1.21	0.14	1051.1	105.26	1.15	0.13
959.7	75.84	1.12	0.14	1035.6	108.59	1.49	0.08
964.9	74.67	1.19	0.10	1075.1	109.12	1.01	0.06
996.6	74.98	1.46	0.12	1115.8	109.63	0.62	0.04
1030.7	75.41	1.28	0.12	1154.3	109.85	0.35	0.03
1059.4	74.42	1.27	0.12	574.1	119.05	5.09	0.32
1064.0	75.95	1.26	0.12	592.5	119.62	5.49	0.32
1094.1	74.77	1.29	0.13	617.4	119.87	4.75	0.27
1132.1	75.44	1.25	0.14	628.0	118.90	5.86	0.37
1156.3	74.24	1.09	0.17	638.6	120.47	6.03	0.33
1169.4	75.76	0.83	0.18	652.8	119.50	6.86	0.42
1198.2	74.83	0.85	0.14	673.2	119.94	5.84	0.36
1233.7	75.41	0.74	0.14	692.5	118.88	5.76	0.34
1274.8	75.80	0.68	0.14	698.1	120.35	5.84	0.36
579.8	89.70	5.73	0.36	716.6	119.49	5.41	0.33
598.5	90.06	6.19	0.36	744.0	119.63	5.08	0.32
619.2	90.43	6.34	0.39	762.1	118.96	4.22	0.28
636.0	89.54	4.87	0.28	769.6	120.00	3.91	0.29
637.9	90.86	6.26	0.52	794.0	119.21	3.30	0.23
657.6	89.85	5.48	0.31	824.5	119.69	2.31	0.18
679.0	90.49	6.09	0.32	846.0	118.88	1.92	0.17
700.8	90.78	6.07	0.33	850.3	120.20	1.98	0.18
702.6	89.32	6.20	0.21	878.8	119.03	1.83	0.17
725.3	89.89	6.31	0.29	909.6	119.69	1.77	0.17
750.2	90.33	5.16	0.34	943.8	118.84	1.71	0.16
776.1	90.72	3.99	0.17	944.6	119.95	1.68	0.17
780.3	89.16	3.96	0.19	984.4	119.52	1.67	0.17
803.3	89.92	2.90	0.15	1020.2	118.31	1.60	0.10
833.1	90.26	1.95	0.12	1023.7	119.99	1.53	0.15
860.9	90.71	1.40	0.10	1071.0	118.74	1.06	0.07
577.3	104.44	5.08	0.33	1074.9	120.64	1.13	0.13
598.7	104.55	5.17	0.57	1105.1	119.27	0.93	0.10
617.3	105.18	5.30	0.33	1109.4	117.99	0.77	0.06
633.4	104.06	5.57	0.38	1147.0	119.69	0.42	0.04
637.0	105.61	5.36	0.33	1159.3	118.72	0.46	0.04
655.8	104.83	5.77	0.50	1205.4	119.05	0.25	0.03
676.9	105.07	5.12	0.56	1247.3	119.70	0.25	0.04
698.3	105.70	6.14	0.41	570.7	134.25	5.61	0.42
769.6	104.10	3.84	0.21	587.3	134.14	5.70	0.41

K	θ_{cm}	$\sigma(\theta)$	$\Delta\sigma(\theta)$	K	θ_{cm}	$\sigma(\theta)$	$\Delta\sigma(\theta)$
611.6	134.63	6.03	0.43	852.4	148.65	2.94	0.29
622.0	133.85	6.41	0.49	898.2	148.82	3.14	0.33
633.7	134.97	6.50	0.50	912.3	148.38	3.50	0.38
647.1	134.36	6.35	0.46	924.7	149.28	3.14	0.36
668.4	134.52	6.19	0.44	953.4	148.64	2.67	0.29
681.3	133.71	5.81	0.41	993.6	148.32	2.76	0.33
694.1	134.77	7.64	0.59	1006.6	149.17	2.99	0.33
710.3	134.23	5.69	0.39	1053.9	149.22	2.13	0.26
737.7	134.66	4.79	0.35	1057.8	149.72	2.00	0.26
750.4	133.59	6.07	0.45	1062.9	147.90	2.17	0.27
767.3	134.58	5.28	0.43	1104.0	149.49	1.63	0.22
787.3	133.93	3.52	0.28	1114.9	148.35	1.50	0.21
814.9	134.67	2.78	0.24	1155.6	148.51	1.15	0.19
831.2	133.51	2.79	0.23	1162.2	149.72	1.38	0.21
847.2	134.63	2.39	0.23	1211.9	148.81	0.70	0.13
865.3	133.87	2.75	0.23	610.4	158.50	7.18	0.64
901.8	134.20	2.95	0.28	636.6	158.57	7.63	0.66
926.0	134.76	2.21	0.24	660.4	158.82	9.32	0.86
926.8	133.58	2.20	0.21	673.4	158.62	7.32	0.75
974.8	134.31	2.34	0.23	688.0	158.94	9.08	0.83
1012.1	133.60	1.84	0.22	698.4	158.75	8.88	0.96
1017.6	134.54	2.11	0.22	725.8	158.80	6.04	0.63
1058.8	133.74	1.47	0.19	755.1	159.02	5.46	0.60
1063.1	134.97	1.62	0.19	821.3	158.53	4.76	0.48
1114.5	134.27	0.86	0.12	862.4	158.77	3.94	0.40
1166.4	134.85	0.75	0.11	898.5	158.29	4.41	0.48
563.6	148.96	4.99	0.40	906.2	159.01	3.83	0.40
584.3	149.06	6.35	0.53	945.7	159.32	4.00	0.45
611.5	149.25	6.69	0.54	949.3	158.79	3.72	0.39
617.7	148.77	6.40	0.52	992.4	158.69	3.31	0.38
629.4	149.46	7.88	0.69	1005.2	159.00	3.86	0.49
640.9	148.93	7.00	0.58	1024.7	158.58	3.31	0.32
656.8	149.32	7.74	0.65	1044.2	158.29	2.87	0.41
679.9	148.61	5.97	0.54	1046.4	159.14	3.22	0.43
690.5	149.29	8.03	0.70	1081.5	159.10	2.24	0.25
706.6	149.19	6.84	0.62	1104.4	158.42	1.87	0.29
733.8	149.11	6.92	0.70	1137.0	158.98	2.02	0.21
755.4	149.30	4.97	0.52	1146.7	158.41	1.51	0.24
815.0	148.13	3.81	0.36	1178.1	158.22	1.01	0.19

TABLE 7

π^- Photoproduction Angular Distributions

K = lab photon energy in MeV

θ_{cm} = c.m. π^- production angle in degrees

$\sigma(\theta)$ = cross section in μb/sr

$\Delta\sigma(\theta)$ = standard deviation of $\sigma(\theta)$

All cross sections have been interpolated to constant energy values. The standard deviation is derived from a quadrature addition of the errors from statistics, raw data corrections, and acceptance calculations.

K	θ_{cm}	$\sigma(\theta)$	$\Delta\sigma(\theta)$
600	6.2	21.39	1.24
600	10.2	18.75	1.27
600	20.3	13.85	0.76
600	30.3	11.72	0.70
600	45.1	10.19	0.81
600	60.4	8.95	0.58
600	75.3	6.63	0.25
600	90.1	6.21	0.36
600	104.6	5.18	0.55
600	119.7	5.22	0.25
600	134.6	5.78	0.31
600	149.4	6.78	0.38
600	159.8	7.82	0.71
620	6.3	21.44	1.24
620	10.3	18.98	1.27
620	20.4	14.20	0.78
620	30.5	11.86	0.70
620	45.6	9.59	0.75
620	60.6	8.91	0.56
620	75.6	6.79	0.40
620	90.4	6.34	0.39
620	105.2	5.31	0.33
620	119.9	4.99	0.22
620	134.8	5.79	0.40
620	149.3	7.09	0.40
620	159.2	7.54	0.45
640	6.2	23.01	1.38
640	10.1	17.07	1.15
640	20.3	13.29	0.73
640	30.3	11.90	0.62
640	45.2	9.17	0.52
640	59.9	8.68	0.34
640	74.7	7.45	0.56
640	89.6	4.99	0.29
640	104.3	5.63	0.42
640	119.6	5.84	0.51
640	134.6	6.18	0.33
640	149.3	7.46	0.64
640	159.2	7.73	0.50

K	θ_{cm}	$\sigma(\theta)$	$\Delta\sigma(\theta)$
660	6.2	20.33	1.32
660	10.1	20.19	1.42
660	20.3	14.15	0.78
660	30.4	11.48	0.82
660	45.3	9.58	0.54
660	60.1	8.18	0.30
660	75.2	6.49	0.65
660	89.9	5.55	0.31
660	104.9	5.64	0.51
660	119.7	6.27	0.31
660	134.6	6.41	0.35
660	149.5	8.14	0.65
660	159.4	8.82	0.51
680	6.3	21.63	2.13
680	10.2	17.25	1.20
680	20.4	13.15	0.72
680	30.6	12.05	0.57
680	45.7	9.86	0.54
680	60.5	8.41	0.37
680	75.5	7.98	0.50
680	90.5	6.09	0.32
680	105.2	5.27	0.54
680	120.0	5.77	0.28
680	134.8	6.59	0.35
680	149.1	7.40	1.00
680	159.1	8.56	0.44
700	6.3	21.35	1.34
700	10.2	17.87	1.25
700	20.5	13.77	0.72
700	30.6	11.40	0.52
700	45.8	9.31	0.51
700	60.8	8.05	0.28
700	75.9	7.96	0.42
700	90.8	6.07	0.33
700	119.4	5.67	0.27
700	134.4	5.77	0.29
700	149.4	7.19	0.70
700	159.3	8.96	0.60

K	θ_{cm}	$\sigma(\theta)$	$\Delta\sigma(\theta)$
720	6.2	16.83	0.97
720	10.0	17.15	1.38
720	20.1	12.55	0.56
720	30.3	10.01	0.44
720	45.1	8.92	0.44
720	60.0	7.76	0.49
720	74.7	7.66	0.44
720	89.8	6.28	0.27
720	119.6	5.22	0.24
720	134.5	5.42	0.29
720	149.4	7.09	0.45
720	159.2	7.73	1.19
740	6.3	14.30	0.87
740	10.1	13.69	1.14
740	20.3	10.83	0.50
740	30.4	9.20	0.42
740	45.4	7.76	0.44
740	60.3	6.81	0.46
740	75.2	6.86	0.41
740	90.1	5.63	0.32
740	119.7	4.96	0.23
740	134.6	4.74	0.26
740	149.7	6.13	0.51
740	159.2	6.99	1.46
760	6.4	14.28	0.90
760	10.2	12.18	0.93
760	20.5	9.03	0.44
760	30.6	8.35	0.39
760	45.5	6.18	0.38
760	60.5	5.76	0.32
760	75.5	4.69	0.41
760	90.4	4.14	0.48
760	119.9	4.22	0.23
760	134.4	4.68	0.48
760	149.7	5.75	0.49
760	159.6	7.25	0.59

K	θ_{cm}	$\sigma(\theta)$	$\Delta\sigma(\theta)$
780	6.3	13.74	0.66
780	10.2	10.39	0.72
780	20.3	7.38	0.59
780	30.4	6.38	0.41
780	45.4	5.51	0.23
780	60.5	5.02	0.26
780	75.4	3.80	0.23
780	89.5	3.81	0.32
780	104.4	3.50	0.15
780	119.5	3.63	0.20
780	134.4	3.96	0.23
780	149.8	5.23	0.47
780	159.6	6.30	0.41
800	6.3	12.63	0.46
800	10.2	8.80	0.54
800	20.3	6.72	0.52
800	30.2	6.21	0.48
800	44.9	5.07	0.26
800	59.9	3.97	0.20
800	74.7	2.93	0.17
800	89.7	3.13	0.12
800	104.7	2.88	0.33
800	119.7	2.94	0.20
800	134.5	3.33	0.19
800	149.7	5.03	0.46
800	159.6	6.13	0.56
825	6.3	10.83	0.41
825	10.3	8.04	0.50
825	20.5	6.06	0.38
825	30.4	5.46	0.43
825	45.2	4.50	0.25
825	60.3	3.24	0.16
825	75.1	2.33	0.16
825	90.1	2.26	0.10
825	105.1	2.15	0.15
825	119.9	2.29	0.14
825	134.7	2.80	0.17
825	148.9	8.94	0.43
825	159.0	5.20	0.59

K	θ_{cm}	$\sigma(\theta)$	$\Delta\sigma(\theta)$
850	6.4	9.33	0.39
850	10.4	6.90	0.45
850	20.7	5.33	0.35
850	30.7	4.91	0.39
850	45.7	4.10	0.18
850	60.8	2.74	0.14
850	75.5	1.83	0.14
850	90.5	1.60	0.08
850	105.4	1.68	0.18
850	119.7	1.94	0.11
850	134.4	2.54	0.19
850	149.1	3.40	0.50
850	159.1	4.62	0.48
875	6.3	7.76	0.75
875	10.2	7.29	0.51
875	20.2	5.27	0.27
875	30.0	5.38	0.20
875	45.0	4.23	0.22
875	59.8	2.64	0.39
875	74.6	1.46	0.08
875	104.4	1.38	0.07
875	119.4	1.74	0.12
875	134.5	2.21	0.40
875	149.3	3.17	0.22
875	159.3	3.85	0.28
900	6.3	7.55	0.75
900	10.2	6.19	0.47
900	20.3	4.93	0.26
900	30.2	5.32	0.25
900	45.1	4.04	0.21
900	60.1	2.76	0.34
900	74.9	1.45	0.14
900	104.8	1.31	0.07
900	119.6	1.68	0.12
900	134.6	2.36	0.38
900	149.3	3.33	0.24
900	159.0	4.25	0.29
925	6.4	6.85	0.71
925	10.3	5.36	0.41
925	20.5	4.75	0.25
925	30.4	5.24	0.19
925	45.5	4.03	0.23
925	60.4	2.52	0.23
925	75.3	1.16	0.09
925	105.1	1.27	0.07
925	119.8	1.60	0.13
925	134.8	2.11	0.14
925	149.1	3.26	0.23
925	159.1	4.14	0.25
950	10.3	4.18	0.34
950	20.6	4.75	0.24
950	30.7	5.00	0.19
950	45.6	3.97	0.31
950	60.7	2.28	0.20
950	75.6	1.04	0.08
950	104.9	1.21	0.10
950	119.4	1.51	0.19
950	134.5	2.02	0.19
950	149.2	2.82	0.20
950	159.2	3.80	0.29
975	10.2	4.30	0.25
975	20.3	4.68	0.21
975	30.1	5.42	0.30
975	44.8	4.21	0.22
975	59.5	2.38	0.18
975	74.5	1.11	0.11
975	104.3	1.23	0.18
975	119.5	1.53	0.15
975	134.3	2.34	0.23
975	149.3	2.55	0.23
975	159.4	3.73	0.30

K	θ_{cm}	$\sigma(\theta)$	$\Delta\sigma(\theta)$
1000	10.3	4.32	0.25
1000	20.4	4.54	0.21
1000	30.2	5.41	0.24
1000	45.2	4.46	0.27
1000	59.8	2.54	0.17
1000	74.9	1.10	0.18
1000	104.7	1.19	0.10
1000	119.7	1.50	0.12
1000	134.4	2.20	0.23
1000	149.1	2.64	0.18
1000	159.0	3.62	0.24
1025	10.3	3.78	0.23
1025	20.4	4.41	0.24
1025	30.4	5.19	0.23
1025	45.4	4.29	0.20
1025	60.2	2.51	0.10
1025	75.2	1.03	0.17
1025	105.1	1.05	0.11
1025	119.1	1.43	0.13
1025	134.1	1.88	0.15
1025	149.3	2.52	0.18
1025	159.0	3.45	0.22
1050	10.4	4.13	0.28
1050	20.6	4.27	0.21
1050	30.6	5.53	0.25
1050	45.6	3.97	0.19
1050	60.5	2.57	0.13
1050	75.5	1.03	0.17
1050	105.3	1.04	0.16
1050	109.0	1.08	0.28
1050	119.2	1.20	0.12
1050	134.3	1.65	0.14
1050	149.5	2.08	0.15
1050	159.0	2.85	0.20

K	θ_{cm}	$\sigma(\theta)$	$\Delta\sigma(\theta)$
1075	6.1	5.10	0.33
1075	10.1	3.85	0.28
1075	20.3	4.34	0.25
1075	30.1	5.00	0.21
1075	44.8	4.22	0.17
1075	59.7	2.61	0.21
1075	74.5	0.96	0.23
1075	109.3	0.88	0.17
1075	118.8	1.04	0.08
1075	133.9	1.29	0.17
1075	149.1	1.75	0.18
1075	159.0	2.46	0.18
1100	6.2	5.37	0.32
1100	10.2	4.07	0.58
1100	20.4	4.33	0.25
1100	30.3	4.84	0.20
1100	45.0	4.02	0.19
1100	59.9	2.54	0.22
1100	74.8	1.04	0.18
1100	109.5	0.72	0.09
1100	119.2	0.95	0.10
1100	134.1	1.02	0.14
1100	149.2	1.71	0.13
1100	159.0	2.27	0.29
1125	6.3	4.41	0.50
1125	10.3	3.79	0.28
1125	20.6	3.72	0.22
1125	30.4	4.82	0.20
1125	45.3	3.79	0.28
1125	60.2	2.13	0.15
1125	75.2	1.03	0.16
1125	109.7	0.54	0.04
1125	118.8	0.60	0.06
1125	134.4	0.84	0.12
1125	149.2	1.53	0.12
1125	159.0	1.91	0.14

K	θ_{cm}	$\sigma(\theta)$	$\Delta\sigma(\theta)$
1150	6.3	4.35	0.31
1150	10.3	3.30	0.31
1150	20.7	3.69	0.22
1150	30.6	4.87	0.21
1150	45.5	3.50	0.15
1150	60.5	1.93	0.13
1150	75.5	0.92	0.08
1150	109.9	0.38	0.03
1150	118.9	0.45	0.07
1150	134.7	0.78	0.12
1150	149.3	1.29	0.12
1150	159.0	1.59	0.18
1175	6.4	4.86	0.35
1175	10.3	3.11	0.42
1175	20.3	3.87	0.42
1175	30.0	4.40	0.27
1175	44.8	3.32	0.32
1175	59.6	1.81	0.13
1175	74.5	0.81	0.10
1175	119.1	0.35	0.05
1175	149.2	1.04	0.13
1175	158.9	1.19	0.16
1200	6.6	4.53	0.34
1200	10.3	2.66	0.37
1200	20.4	3.94	0.44
1200	30.2	4.25	0.27
1200	45.1	3.36	0.18
1200	59.8	1.70	0.11
1200	74.9	0.76	0.08
1200	119.1	0.27	0.02
1200	149.3	0.77	0.11
1200	159.8	1.63	0.27
1225	6.7	4.17	0.32
1225	10.5	2.92	0.40
1225	20.6	3.78	0.42
1225	30.4	3.92	0.26
1225	45.3	3.09	0.17
1225	60.2	1.48	0.10
1225	75.2	0.72	0.07
1225	119.4	0.24	0.03
1225	149.8	0.97	0.18
1225	159.7	1.69	0.29
1250	6.7	3.86	0.30
1250	30.6	3.90	0.26
1250	45.5	2.82	0.15
1250	60.5	1.35	0.09
1250	75.5	0.70	0.07
1250	120.0	0.23	0.05
1250	149.7	1.05	0.20
1250	159.6	1.13	0.24

TABLE 8

Coefficients for the Moravcsik Fits

K = lab photon energy in MeV

g = χ^2/(number of degrees of freedom)

Units for the A_i are in μb/sr

K	χ^2	g	A_0	A_1	A_2	A_3	A_4	A_5	A_6	A_7
600	4.88	0.542	5.689	-7.408	3.878	-6.866	4.795			
620	8.66	0.962	5.687	-7.299	3.875	-7.209	5.026			
640	15.49	1.726	5.538	-7.679	5.071	-7.982	5.125			
660	6.43	0.714	5.663	-8.515	6.471	-8.788	5.238			
680	7.30	0.811	5.991	-8.569	5.382	-7.865	5.120			
700	6.76	1.126	6.566	-9.513	-0.243	2.839	7.102	-12.285	5.592	
720	7.33	1.221	6.464	-9.397	-1.251	4.798	6.604	-13.363	6.190	
740	5.77	0.961	6.000	-9.666	-0.482	7.528	2.794	-13.081	6.943	
760	4.02	0.670	4.402	-7.165	2.263	0.376	4.125	- 8.336	4.367	
780	5.71	0.815	3.725	-5.754	1.717	-1.247	5.062	- 6.330	2.855	
800	13.57	1.938	3.020	-4.940	1.196	1.129	4.077	- 9.298	4.841	
825	1.75	0.291	2.209	-4.159	3.322	1.986	- 4.574	- 6.327	11.648	-4.084
850	0.88	0.146	1.592	-3.034	4.168	-0.892	- 4.175	- 3.376	9.308	-3.575
875	2.42	0.484	1.151	-2.483	5.489	-2.255	- 6.106	- 0.810	8.584	-3.555
900	1.70	0.340	1.120	-2.205	4.952	-2.577	- 4.625	- 1.814	8.628	-3.467
925	1.23	0.245	0.940	-2.476	6.330	-0.986	-10.072	- 1.148	13.225	-5.802
950	0.81	0.202	0.887	-2.411	5.926	-0.787	- 8.840	- 1.390	11.151	-4.532
975	4.58	1.145	0.852	-2.398	6.614	-1.941	- 9.147	0.265	10.118	-4.356
1000	2.80	0.701	0.775	-2.295	7.601	-2.090	-13.019	2.164	13.503	-6.633
1025	0.89	0.223	0.693	-1.885	7.070	-2.776	-11.469	2.317	12.036	-5.980
1050	8.95	1.790	0.732	-1.588	5.868	-2.386	-10.072	2.272	10.341	-5.161
1075	1.09	0.218	0.554	-1.244	5.993	-2.149	-11.865	3.156	11.555	-5.994
1100	1.53	0.306	0.561	-0.852	4.640	-2.029	- 9.322	2.071	9.989	-5.053
1125	20.79	2.969	0.543	0.304	1.860	-5.380	1.284	1.393		
1150	16.44	2.348	0.358	0.502	2.068	-5.262	0.554	1.784		
1175	4.26	0.852	0.158	0.833	1.869	-5.098	0.508	1.734		
1200	15.44	3.087	0.117	0.944	1.688	-4.879	0.361	1.772		
1225	10.77	2.154	0.055	1.100	1.491	-5.244	1.363	1.239		
1250	10.02	3.338	0.071	0.968	1.416	-4.717	0.972	1.292		

TABLE 9

Cross Section from Moravcsik Fits

K = lab photon energy in MeV

σ_{tot} = total cross section in μb

$\sigma(\theta)$ = differential cross section in μb/sr

θ = c.m. π^- production angle in degrees

$\Delta\sigma(\theta)$ = error from the fit

K	σ_{tot}	$\Delta\sigma_{tot}$	$\sigma(0^{o})$	$\Delta\sigma(0^{o})$	$\sigma(90^{o})$	$\Delta\sigma(90^{o})$	$\sigma(180^{o})$	$\Delta\sigma(180^{o})$
600.0	93.63	1.63	23.49	1.00	5.69	0.18	7.62	0.37
620.0	94.48	1.77	23.74	1.02	5.69	0.19	7.72	0.34
640.0	93.28	1.65	23.49	1.02	5.54	0.20	8.30	0.38
660.0	96.15	1.64	24.33	1.09	5.66	0.21	9.15	0.40
680.0	97.98	1.64	22.67	1.23	5.99	0.20	8.67	0.39
700.0	96.64	1.69	23.91	1.25	6.57	0.28	9.98	0.75
720.0	91.15	1.58	20.22	1.04	6.46	0.24	9.43	0.86
740.0	81.65	1.63	16.87	0.94	6.00	0.27	7.98	0.95
760.0	68.72	1.68	16.63	0.92	4.40	0.35	7.91	0.67
780.0	58.43	1.01	16.04	0.69	3.72	0.15	6.96	0.51
800.0	49.96	0.93	14.30	0.52	3.02	0.11	6.84	0.59
825.0	41.46	0.83	13.12	0.51	2.21	0.08	6.55	0.78
850.0	35.31	0.74	11.61	0.48	1.59	0.07	5.65	0.67
875.0	32.05	0.65	10.50	0.72	1.15	0.09	4.72	0.44
900.0	31.73	0.74	9.66	0.72	1.12	0.11	5.21	0.46
925.0	30.15	0.60	8.71	0.66	0.94	0.09	5.39	0.39
950.0	28.18	0.68	6.60	0.76	0.89	0.10	4.71	0.46
975.0	28.56	0.76	6.56	0.63	0.85	0.14	4.35	0.48
1000.0	28.84	0.72	7.03	0.65	0.77	0.14	4.56	0.41
1025.0	27.49	0.64	6.26	0.61	0.69	0.14	4.29	0.37
1050.0	26.16	0.70	6.85	0.71	0.73	0.15	3.53	0.34
1075.0	24.06	0.91	6.82	0.41	0.55	0.20	3.20	0.34
1100.0	23.03	0.76	7.32	0.45	0.56	0.16	3.01	0.40
1125.0	20.88	0.57	6.21	0.46	0.54	0.07	1.89	0.13
1150.0	18.71	0.42	5.82	0.37	0.36	0.05	1.53	0.13
1175.0	16.11	0.56	6.50	0.44	0.16	0.07	1.30	0.15
1200.0	15.17	0.44	6.00	0.43	0.12	0.06	1.11	0.16
1225.0	14.41	0.44	6.13	0.42	0.05	0.06	1.49	0.23
1250.0	13.54	0.49	6.01	0.44	0.07	0.06	1.26	0.22

FIGURES 5 - 13

Uninterpolated π^+ and π^- cross sections from Deuterium.

Ecklund's Fit is taken from Reference 12.

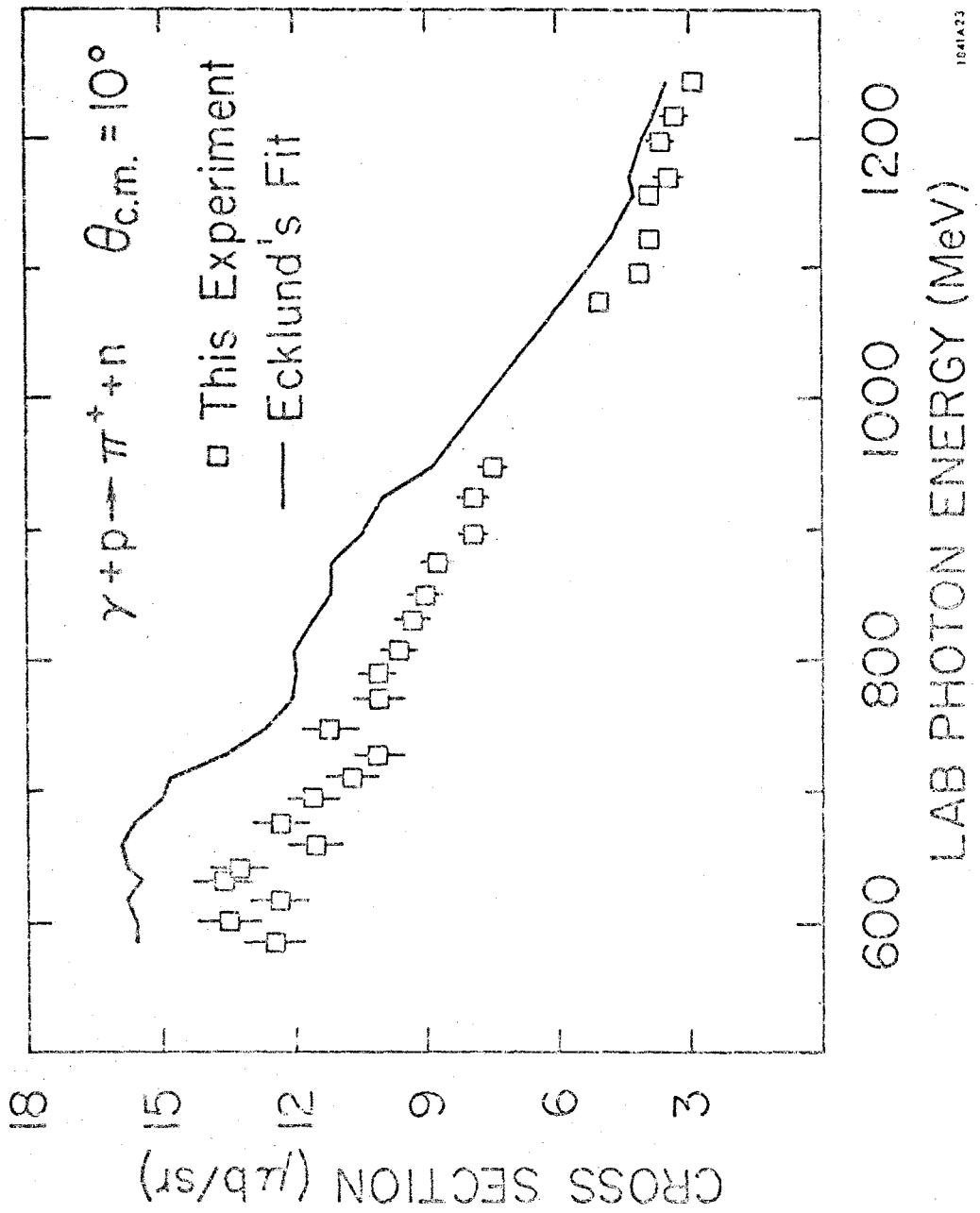
$\gamma + p \rightarrow \pi^+ + n$ $\theta_{c.m.} = 10°$
This Experiment
Ecklund's Fit
CROSS SECTION (μb/sr)
LAB PHOTON ENERGY (MeV)
1641A23

FIGURE 5

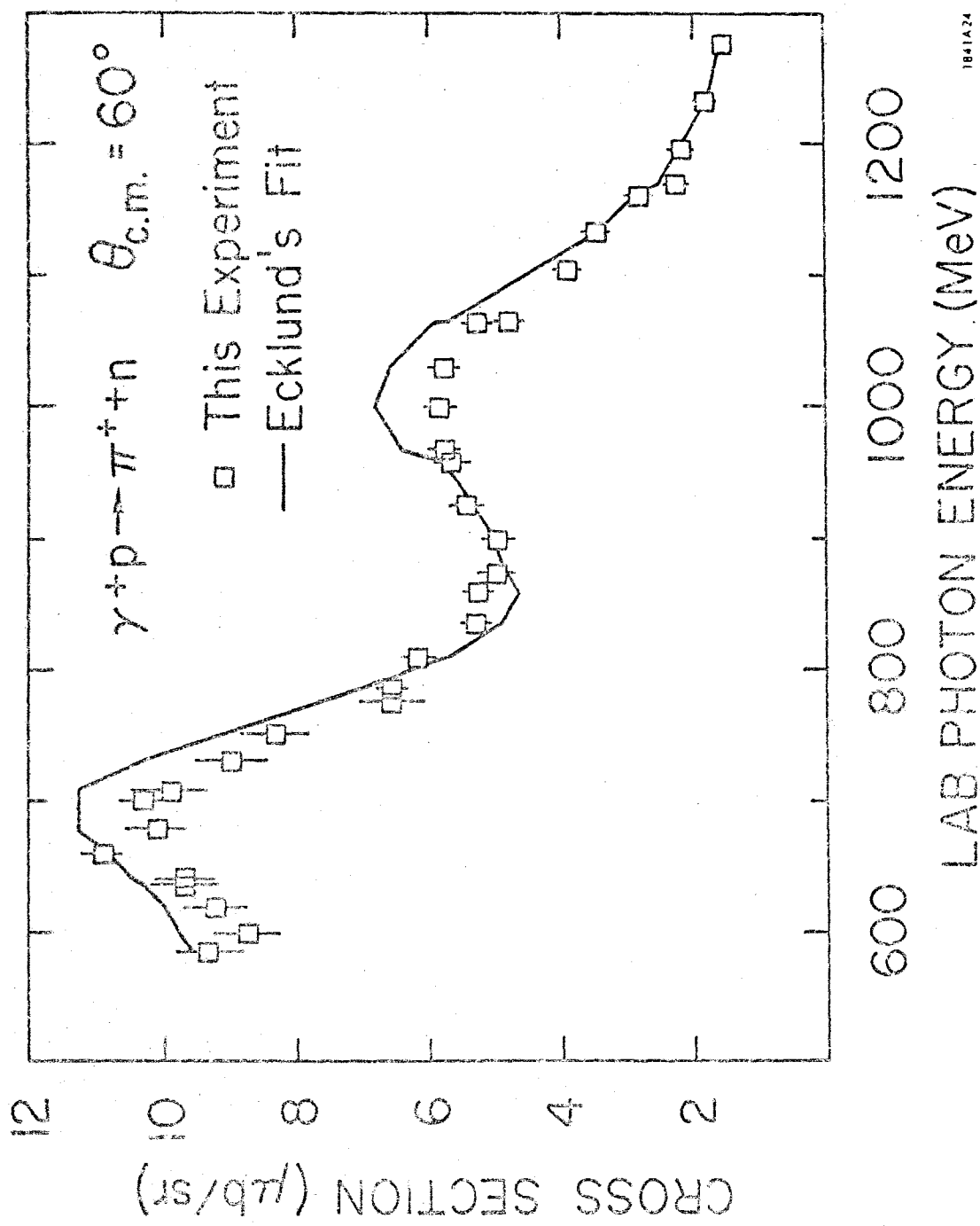
$\gamma + p \rightarrow \pi^+ + n$
$\theta_{c.m.} = 60°$
This Experiment
Ecklund's Fit
CROSS SECTION (μb/sr)
12
10
8
6
4
2
600
800
1000
1200
LAB PHOTON ENERGY (MeV)
1841A24

FIGURE 6

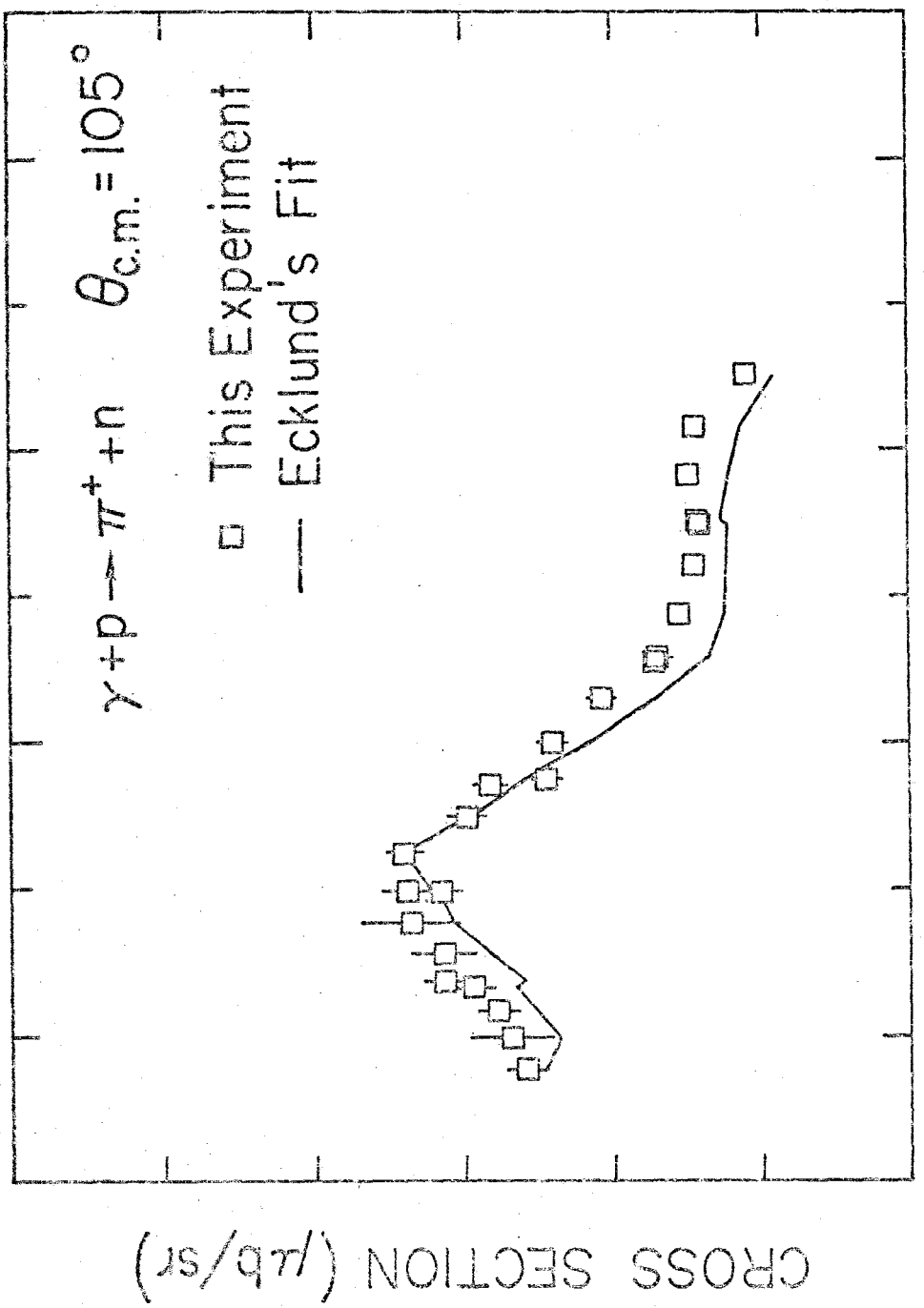
$\gamma + p \rightarrow \pi^+ + n$
$\theta_{c.m.} = 105°$
This Experiment
Ecklund's Fit
CROSS SECTION (μb/sr)
600
800
1000
1200
LAB PHOTON ENERGY (MeV)
1841A25

FIGURE 7

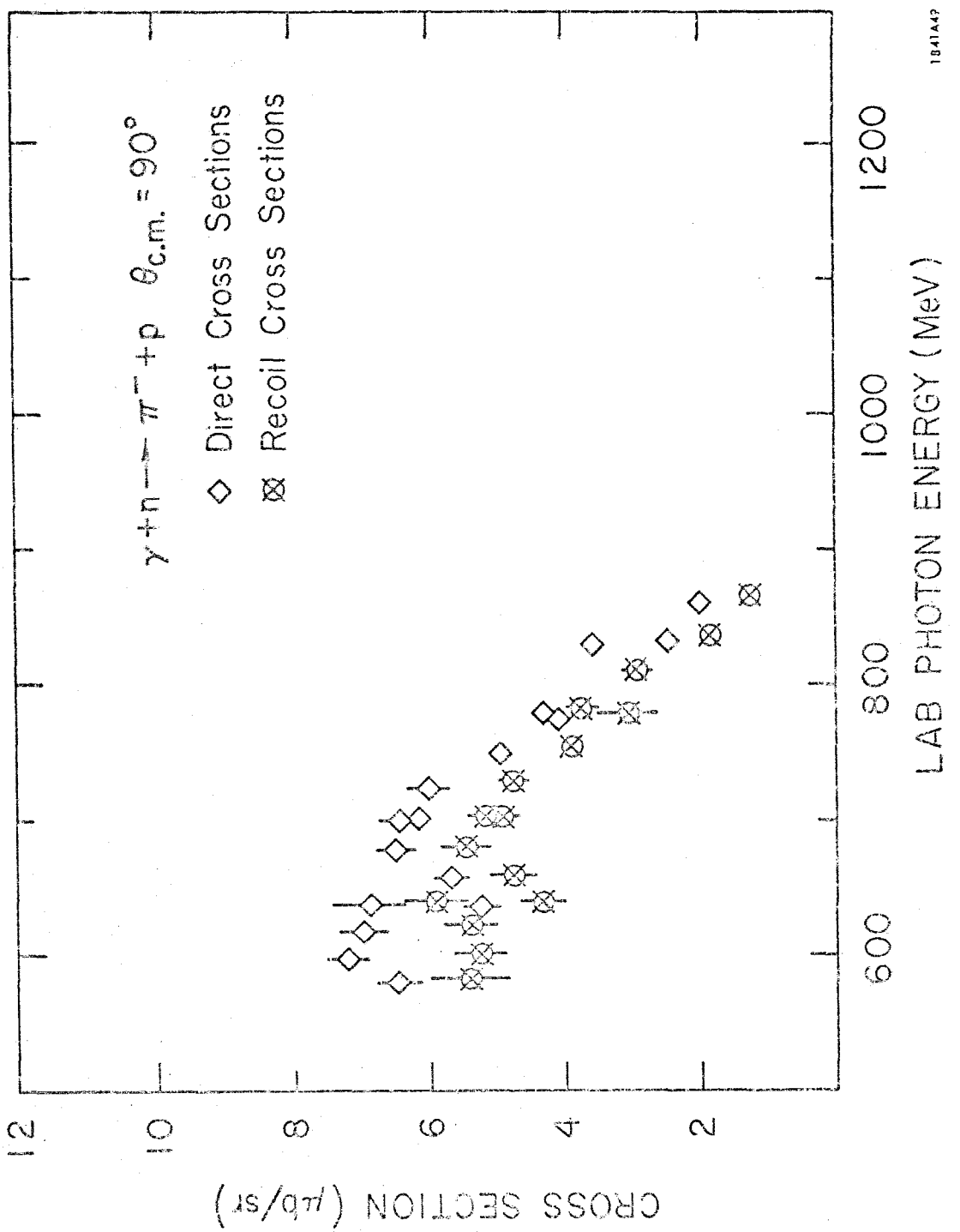
$\gamma + n \rightarrow \pi^- + p$ $\theta_{c.m.} = 90°$
◇ Direct Cross Sections
⊠ Recoil Cross Sections
CROSS SECTION ($\mu b/sr$)
12
10
8
6
4
2
600
800
1000
1200
LAB PHOTON ENERGY (MeV)
1841A49

FIGURE 8

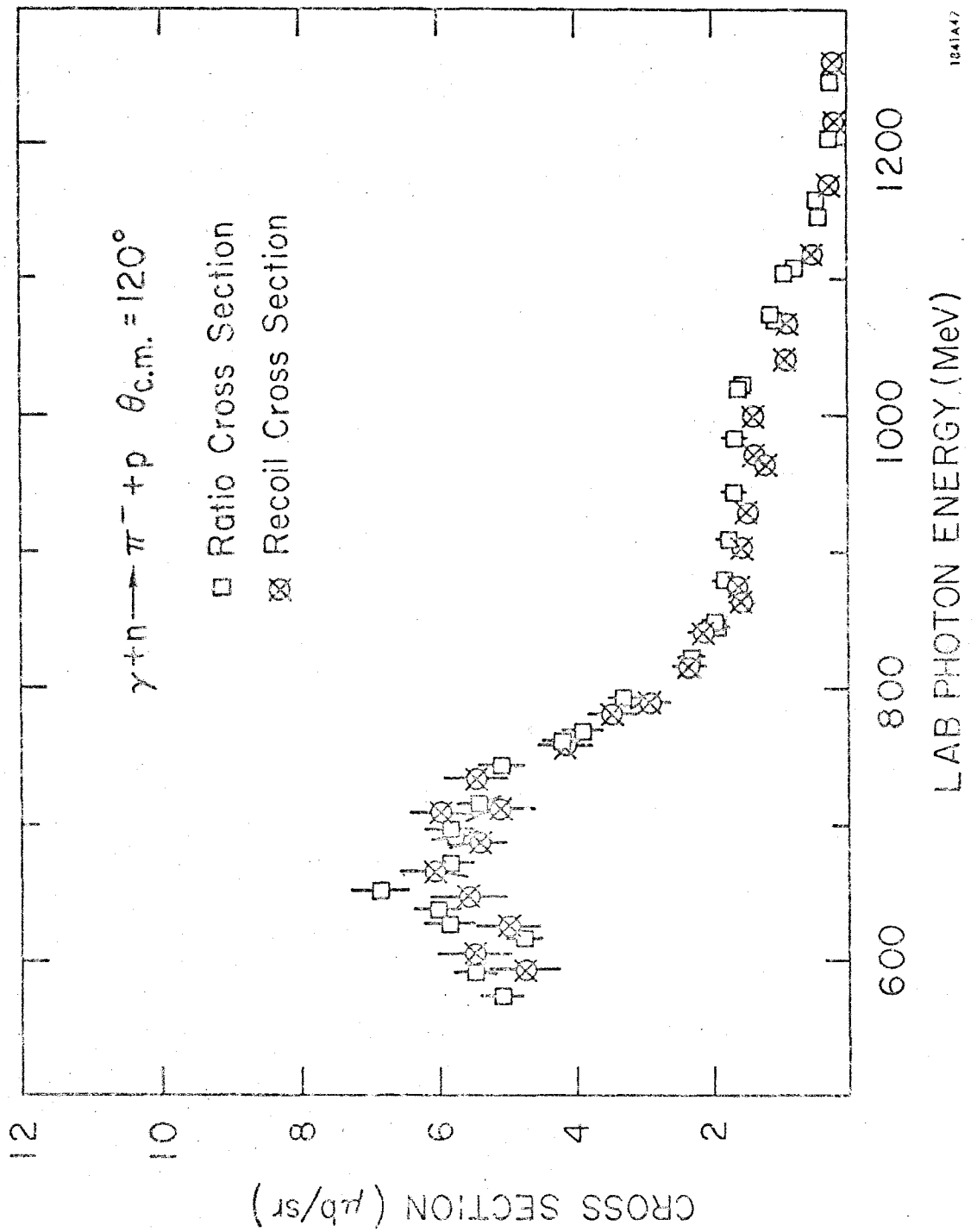
$\gamma + n \longrightarrow \pi^- + p$ $\theta_{c.m.} = 120°$
□ Ratio Cross Section
⊗ Recoil Cross Section
CROSS SECTION ($\mu b/sr$)
LAB PHOTON ENERGY (MeV)
12
10
8
6
4
2
600
800
1000
1200
1841A47

FIGURE 9

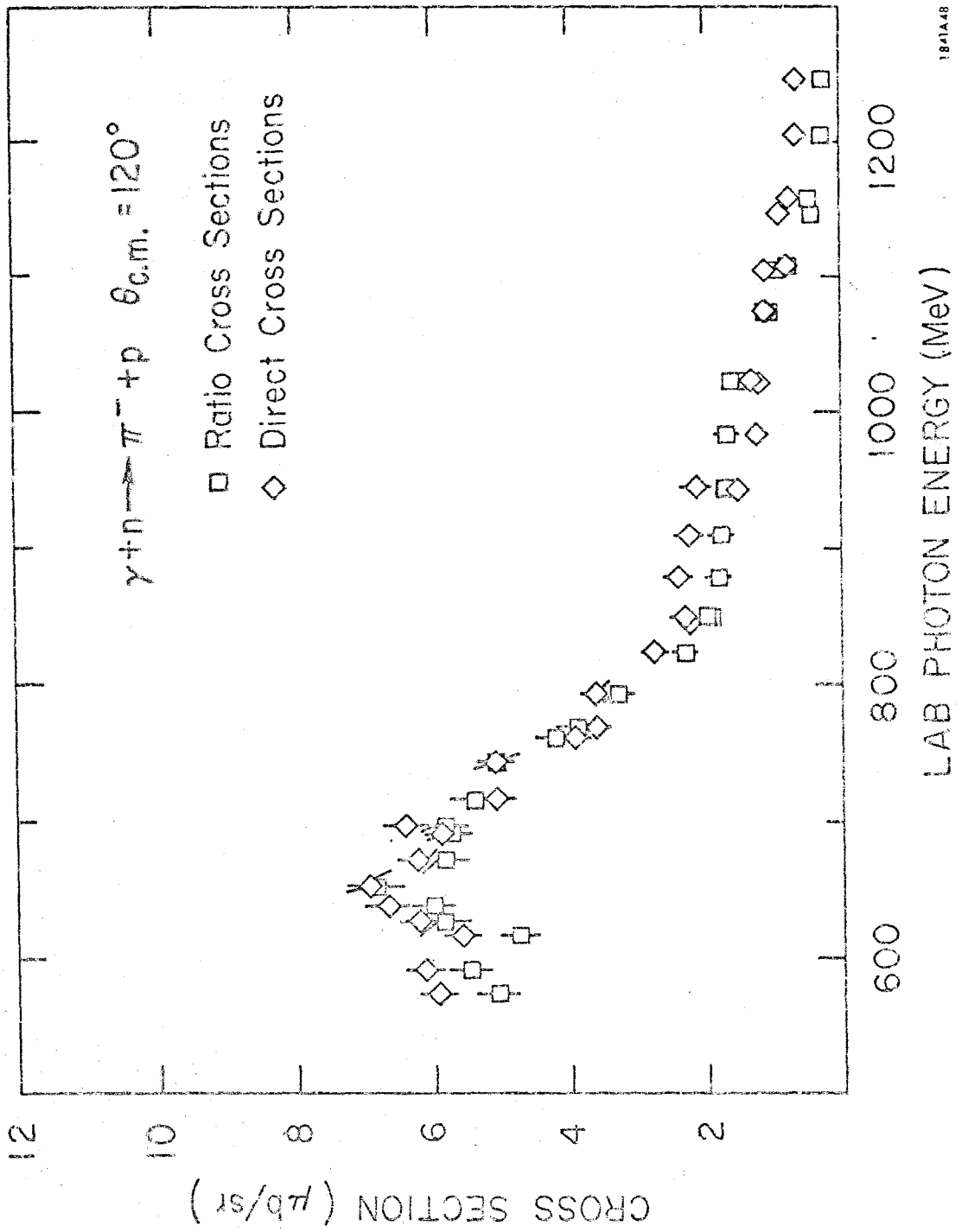
$\gamma + n \rightarrow \pi^- + p$ $\theta_{c.m.} = 120°$
Ratio Cross Sections
Direct Cross Sections
CROSS SECTION (μb/sr)
12
10
8
6
4
2
600
800
1000
1200
LAB PHOTON ENERGY (MeV)
1841A48

FIGURE 10

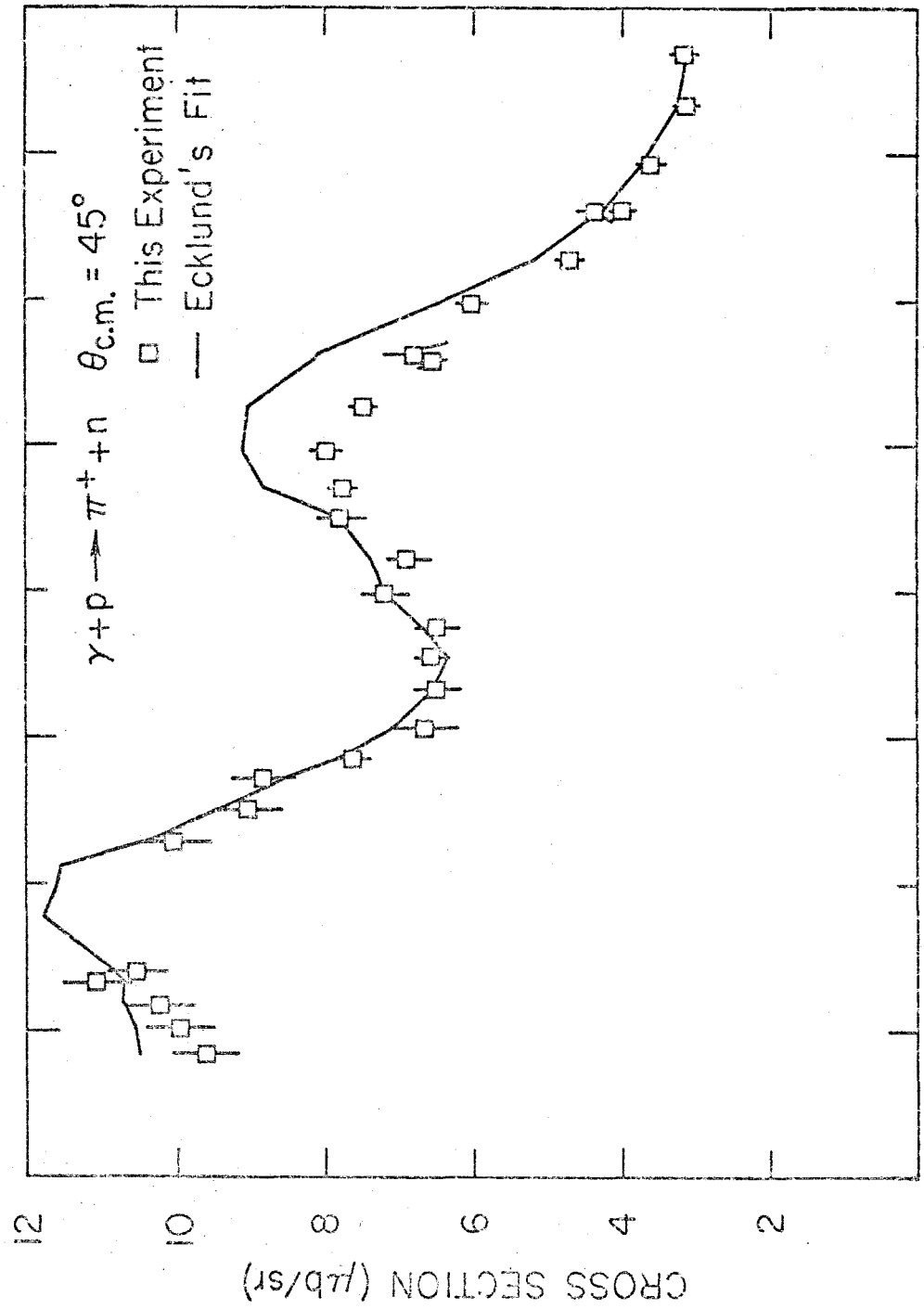
$\gamma + p \rightarrow \pi^+ + n$ $\theta_{c.m.} = 45°$
This Experiment
Ecklund's Fit
CROSS SECTION (μb/sr)
LAB PHOTON ENERGY (MeV)
12
10
8
6
4
2
600
800
1000
1200
1841A46

FIGURE 11

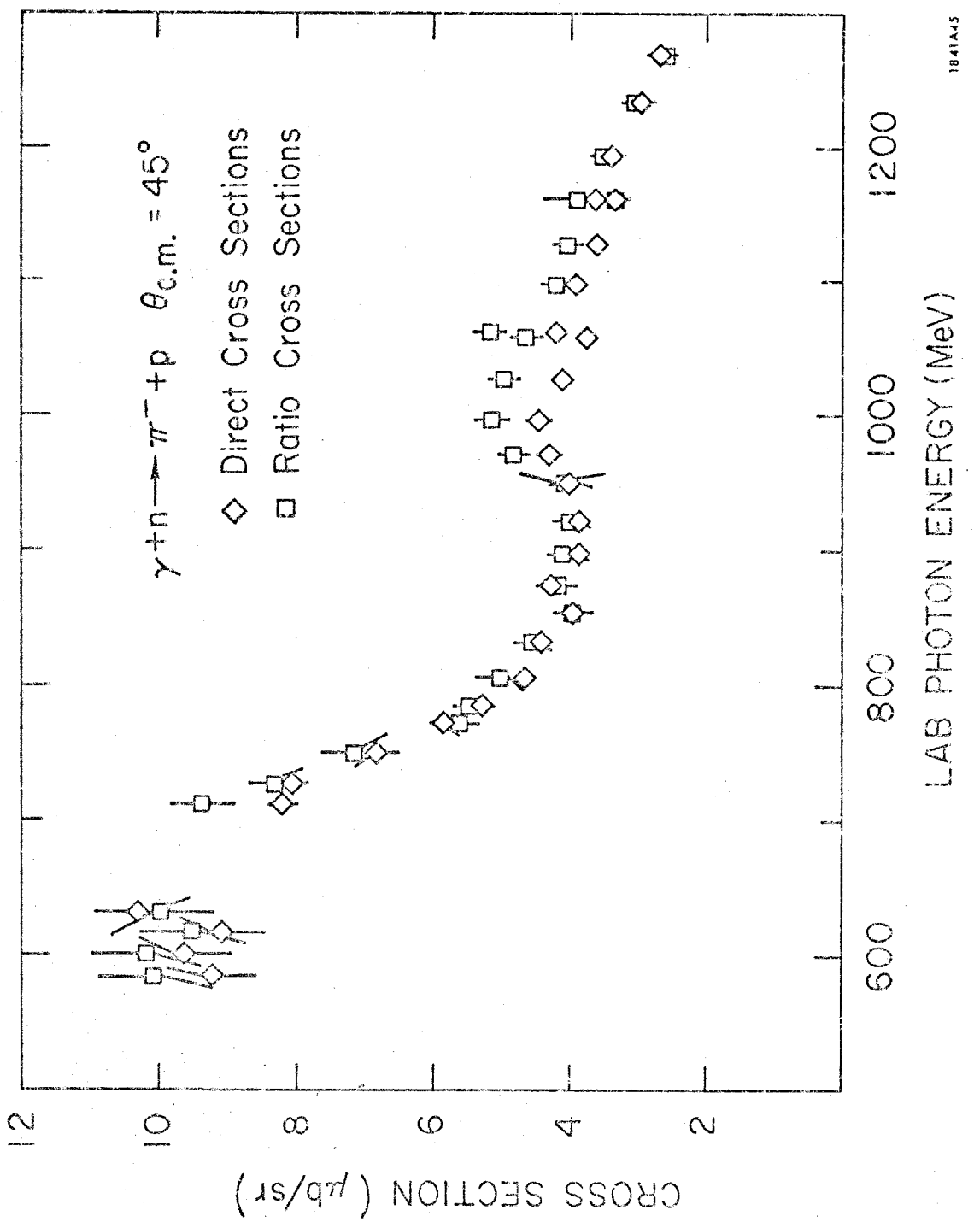
$\gamma + n \longrightarrow \pi^- + p \quad \theta_{c.m.} = 45°$
Direct Cross Sections
Ratio Cross Sections
CROSS SECTION ($\mu b/sr$)
LAB PHOTON ENERGY (MeV)
12
10
8
6
4
2
600
800
1000
1200
1841A45

FIGURE 12

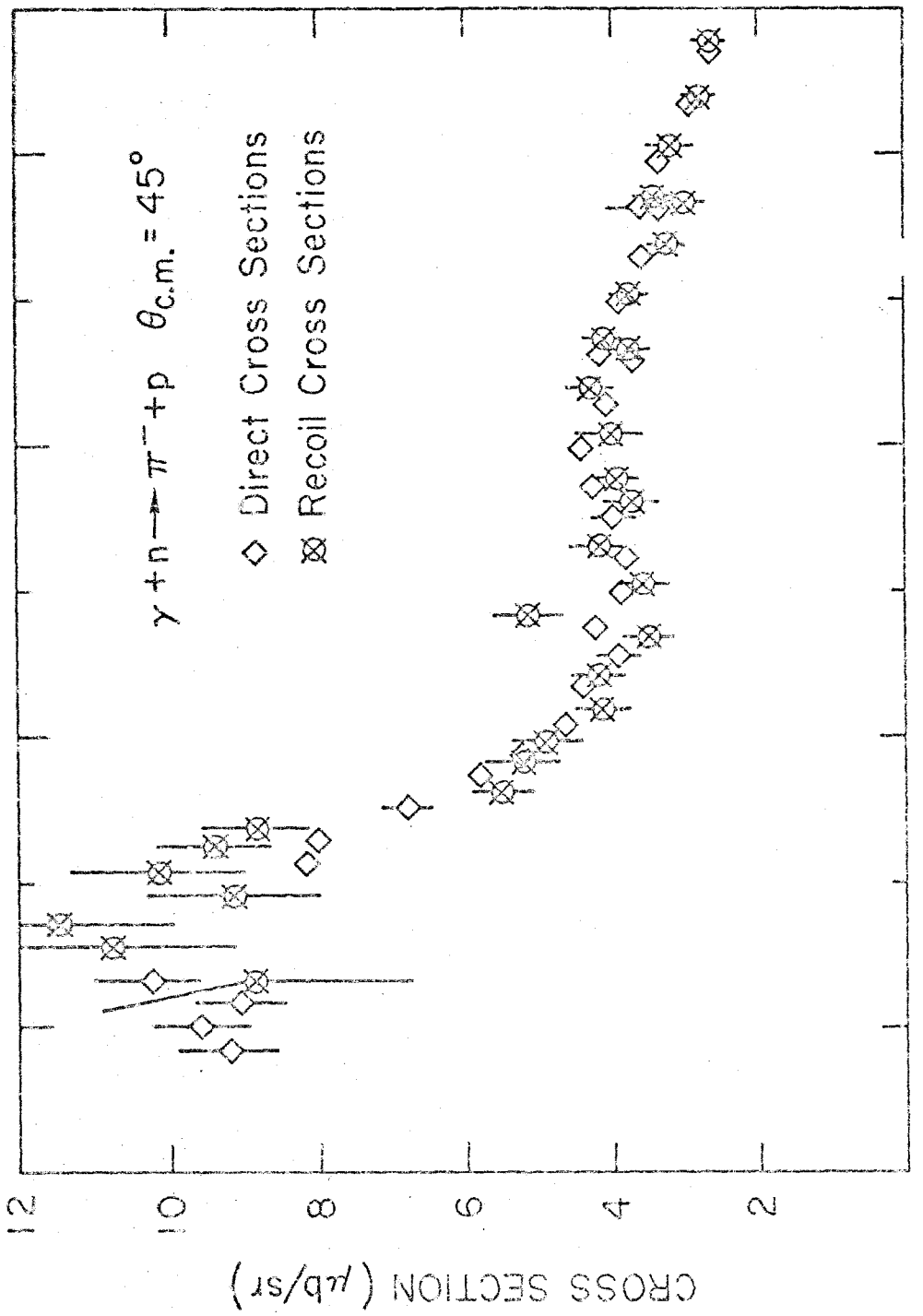
$\gamma + n \rightarrow \pi^- + p$ $\theta_{c.m.} = 45°$
◇ Direct Cross Sections
⊗ Recoil Cross Sections
CROSS SECTION (μb/sr)
12
10
8
6
4
2
600
800
1000
1200
LAB PHOTON ENERGY (MeV)
1841A44

FIGURE 18

FIGURE 14

π^- Photoproduction from Deuterium, Angular Distributions

The measured cross sections have been interpolated to constant lab photon energy values. The data are presented with the Moravcsik fits.

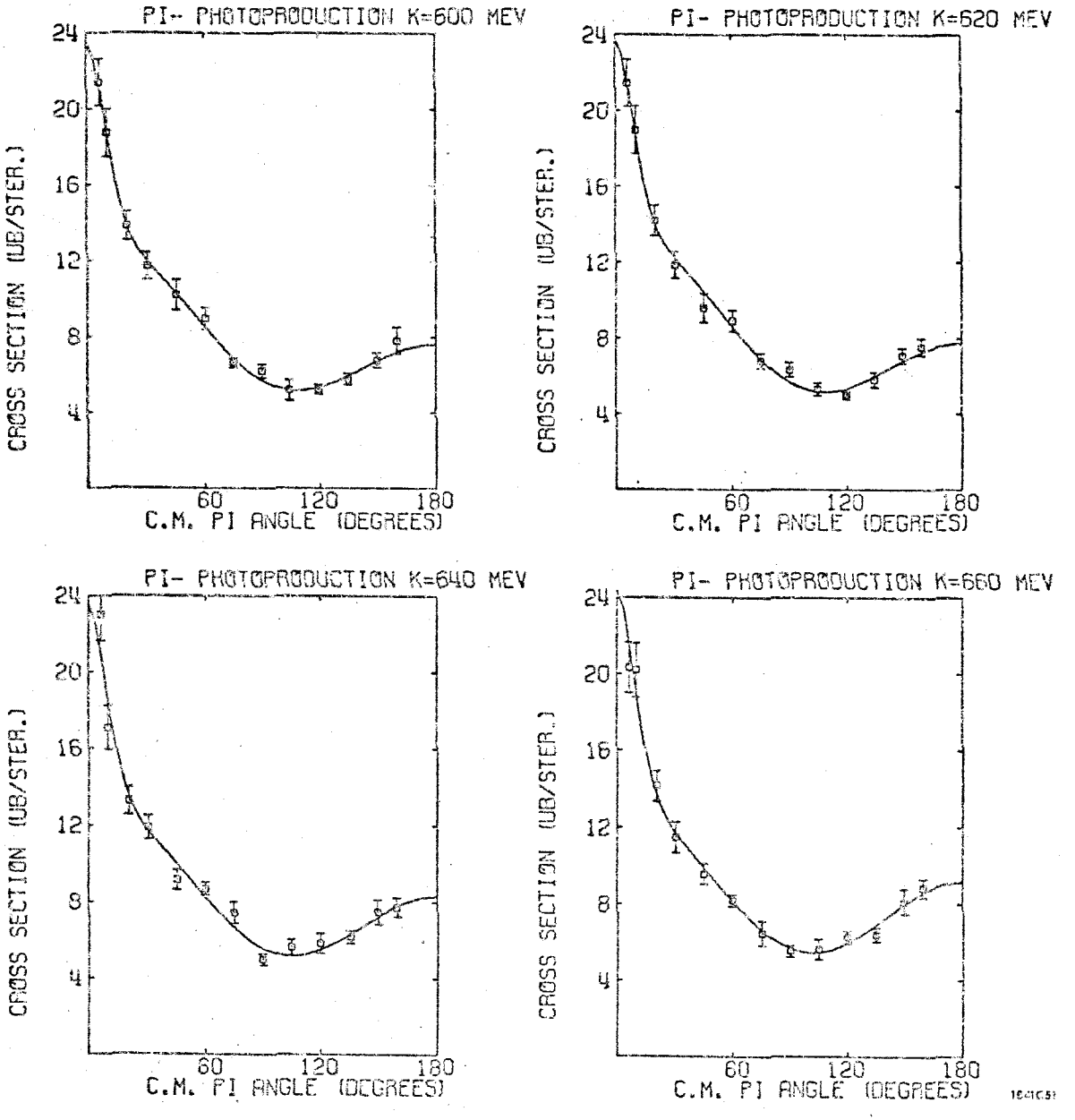
PI- PHOTOPRODUCTION K=600 MEV
PI- PHOTOPRODUCTION K=620 MEV
PI- PHOTOPRODUCTION K=640 MEV
PI- PHOTOPRODUCTION K=660 MEV
CROSS SECTION (UB/STER.)
C.M. PI ANGLE (DEGREES)
24
20
16
12
8
4
60
120
180

FIGURE 14.1

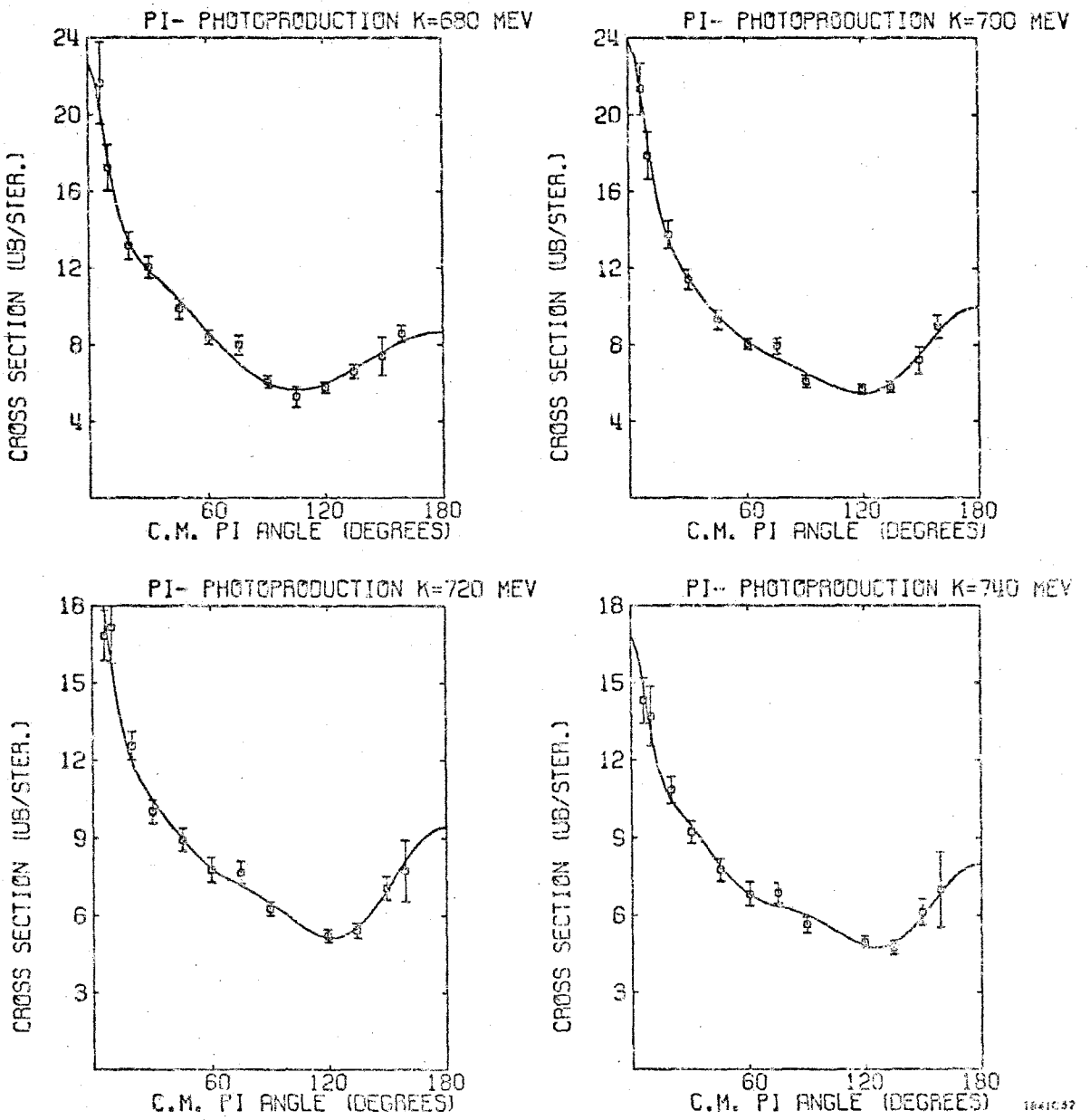
PI- PHOTOPRODUCTION K=680 MEV
PI- PHOTOPRODUCTION K=700 MEV
PI- PHOTOPRODUCTION K=720 MEV
PI- PHOTOPRODUCTION K=740 MEV
CROSS SECTION (UB/STER.)
C.M. PI ANGLE (DEGREES)
60
120
180
4
8
12
16
20
24
3
6
9
15
18

FIGURE 14.2

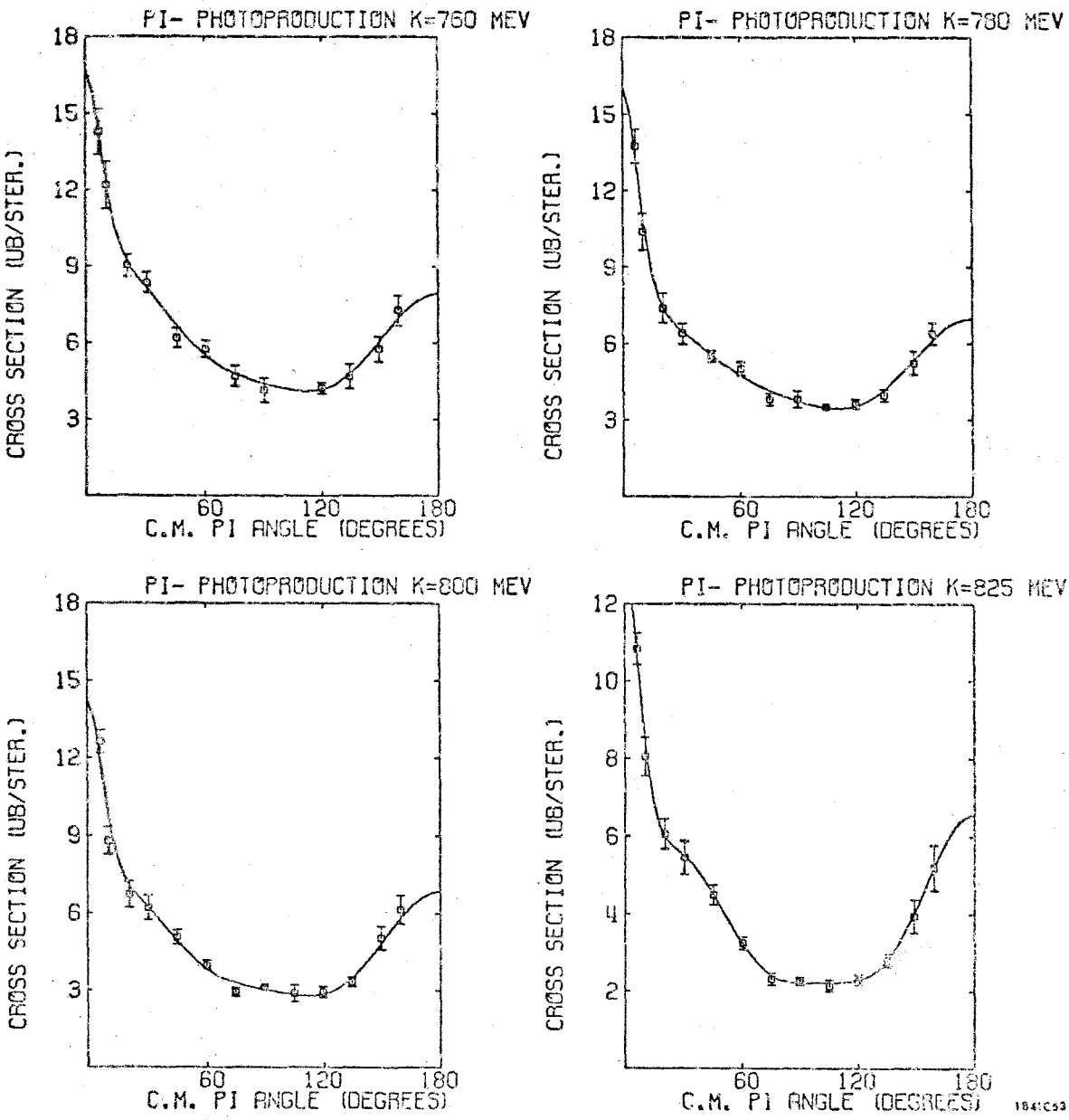
PI- PHOTOPRODUCTION K=760 MEV
CROSS SECTION (UB/STER.)
C.M. PI ANGLE (DEGREES)
PI- PHOTOPRODUCTION K=780 MEV
CROSS SECTION (UB/STER.)
C.M. PI ANGLE (DEGREES)
PI- PHOTOPRODUCTION K=800 MEV
CROSS SECTION (UB/STER.)
C.M. PI ANGLE (DEGREES)
PI- PHOTOPRODUCTION K=825 MEV
CROSS SECTION (UB/STER.)
C.M. PI ANGLE (DEGREES)
184C53

FIGURE 14.3

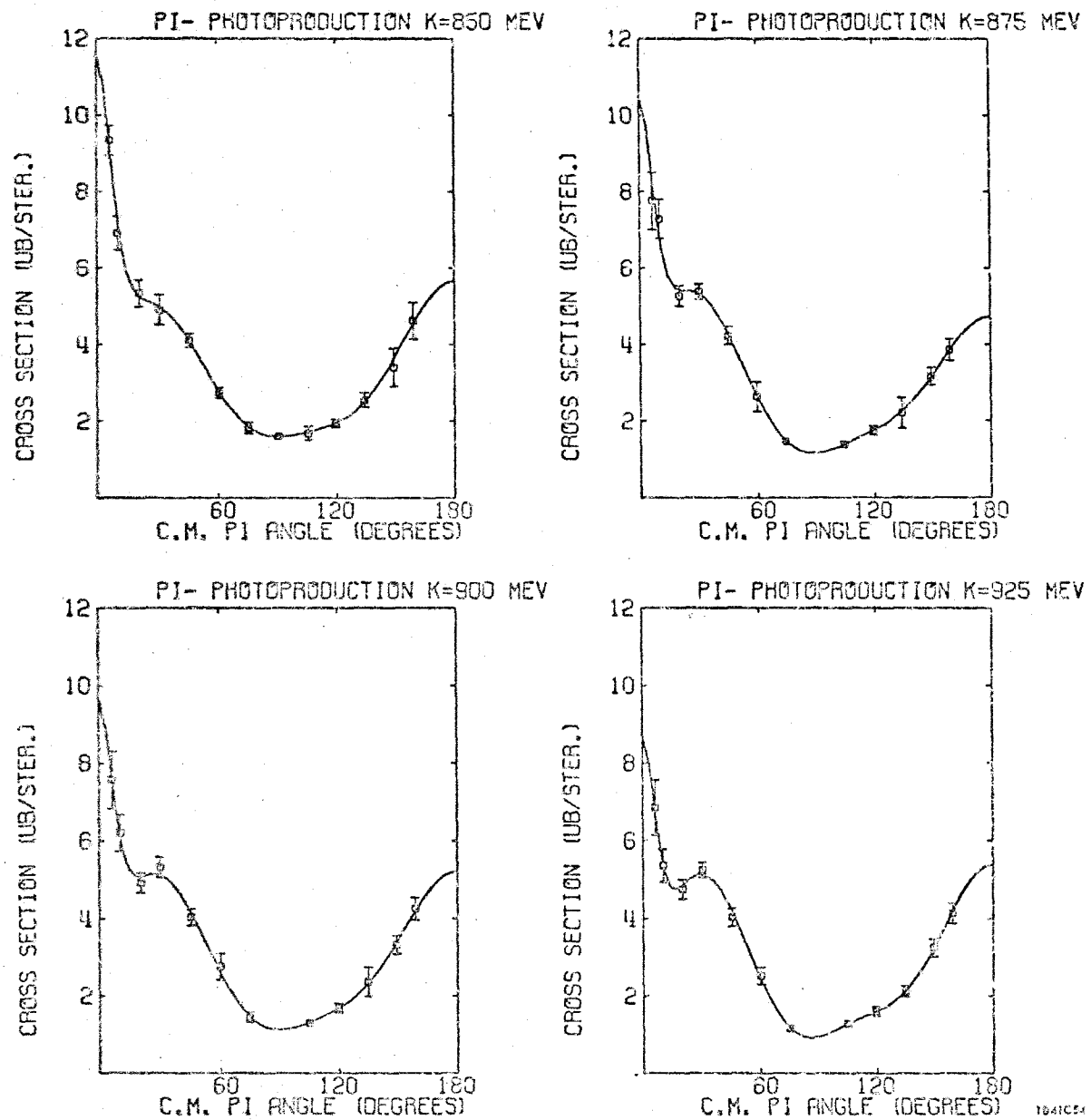
PI- PHOTOPRODUCTION K=850 MEV
CROSS SECTION (UB/STER.)
C.M. PI ANGLE (DEGREES)
PI- PHOTOPRODUCTION K=875 MEV
CROSS SECTION (UB/STER.)
C.M. PI ANGLE (DEGREES)
PI- PHOTOPRODUCTION K=900 MEV
CROSS SECTION (UB/STER.)
C.M. PI ANGLE (DEGREES)
PI- PHOTOPRODUCTION K=925 MEV
CROSS SECTION (UB/STER.)
C.M. PI ANGLE (DEGREES)

FIGURE 14.4

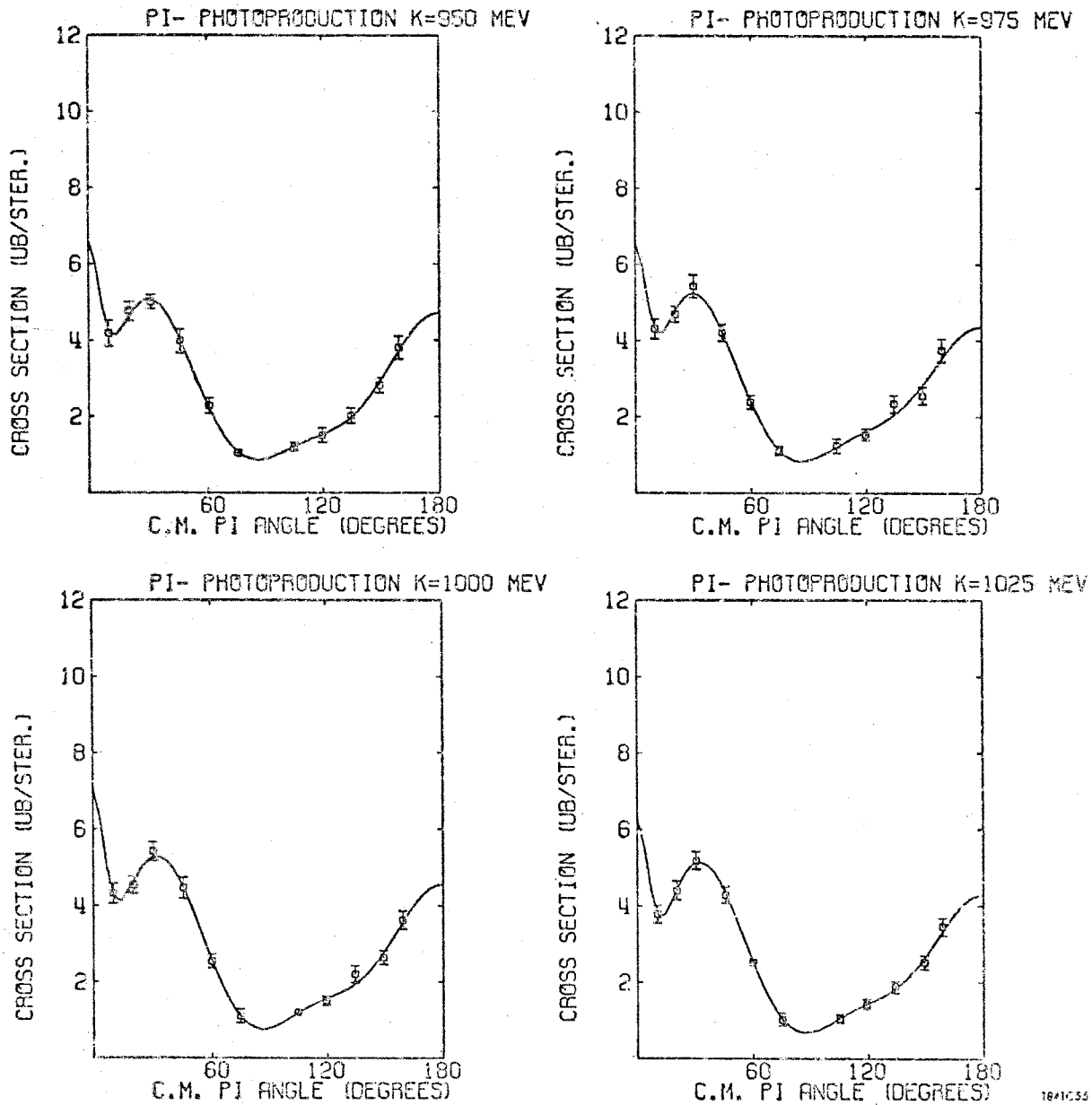
PI- PHOTOPRODUCTION K=950 MEV
PI- PHOTOPRODUCTION K=975 MEV
PI- PHOTOPRODUCTION K=1000 MEV
PI- PHOTOPRODUCTION K=1025 MEV
CROSS SECTION (UB/STER.)
C.M. PI ANGLE (DEGREES)
12
10
8
6
4
2
60
120
180
18410-55

FIGURE 14.5

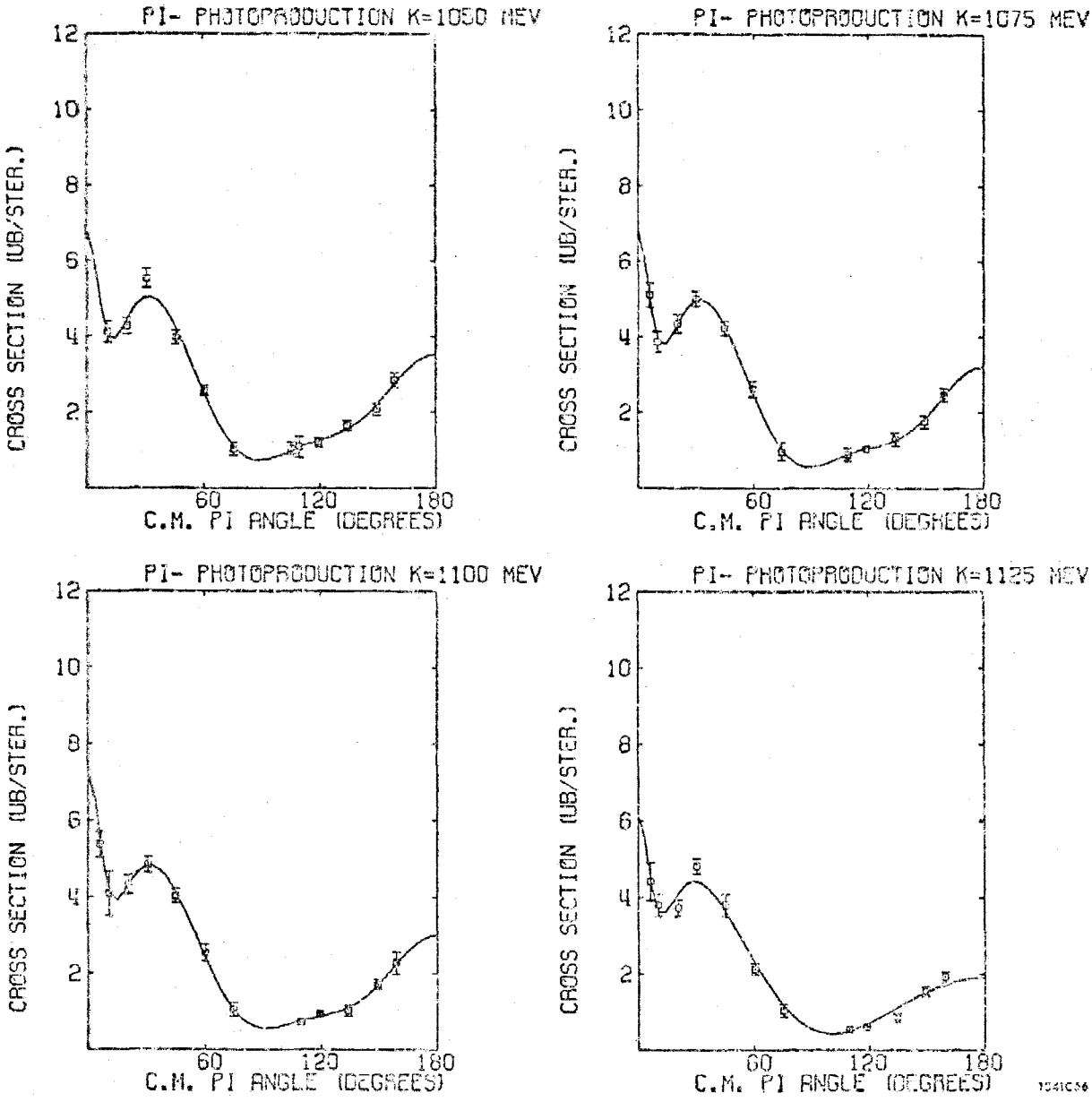
PI- PHOTOPRODUCTION K=1050 MEV
PI- PHOTOPRODUCTION K=1075 MEV
PI- PHOTOPRODUCTION K=1100 MEV
PI- PHOTOPRODUCTION K=1125 MEV
CROSS SECTION (UB/STER.)
C.M. PI ANGLE (DEGREES)
0
2
4
6
8
10
12
60
120
180

FIGURE 14.6

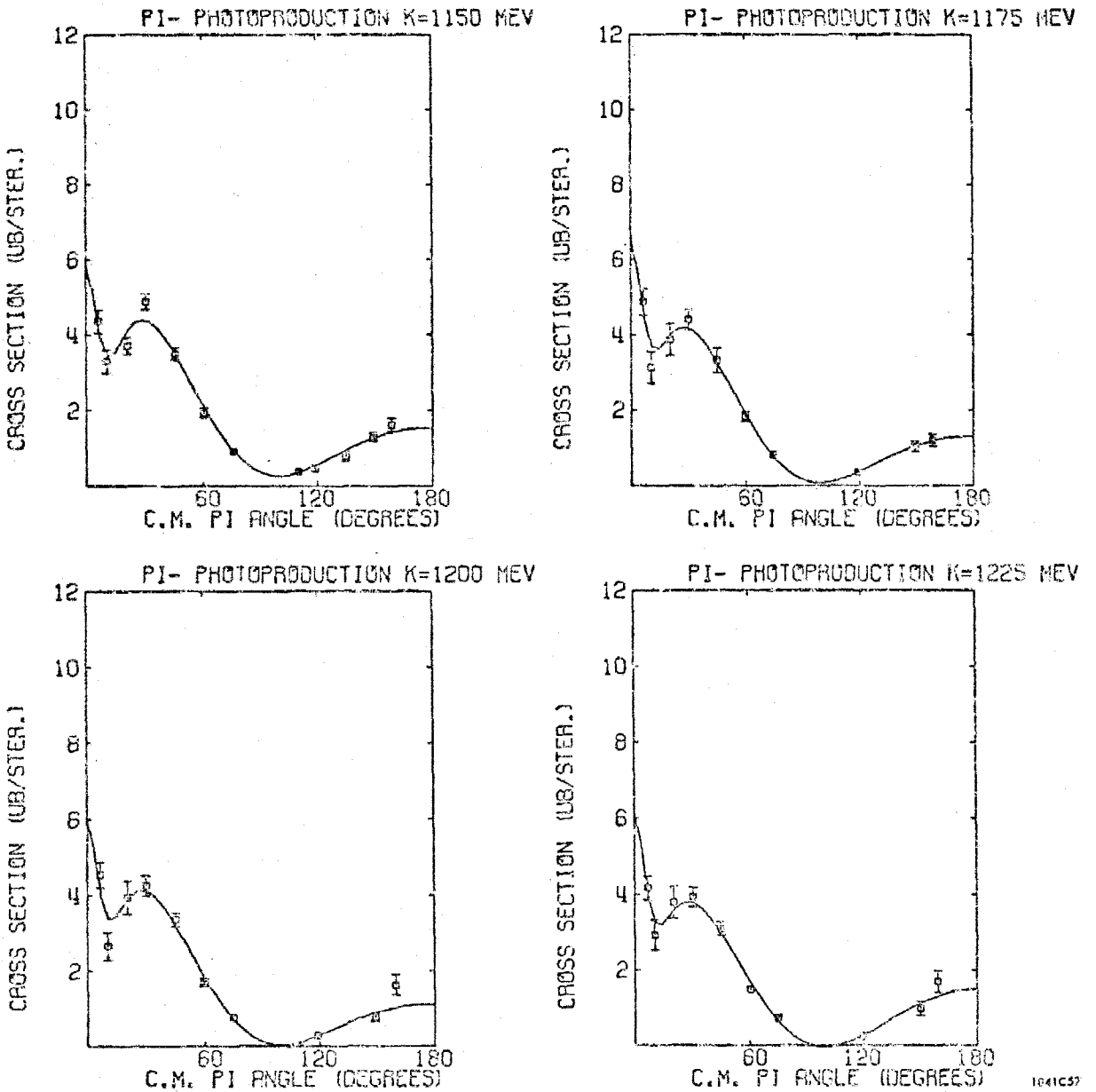
PI- PHOTOPRODUCTION K=1150 MEV
PI- PHOTOPRODUCTION K=1175 MEV
PI- PHOTOPRODUCTION K=1200 MEV
PI- PHOTOPRODUCTION K=1225 MEV
CROSS SECTION (UB/STER.)
C.M. PI ANGLE (DEGREES)
12
10
8
6
4
2
60
120
180
1041C57

FIGURE 14.7

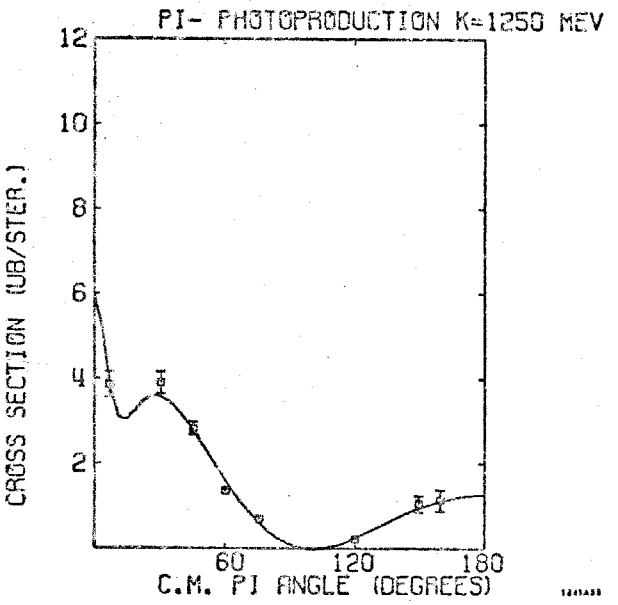
PI- PHOTOPRODUCTION K=1250 MEV
CROSS SECTION (UB/STER.)
12
10
8
6
4
2
60
120
180
C.M. PI ANGLE (DEGREES)

FIGURE 14.8

FIGURES 15 - 18

Cross Sections From the Moravcsik Fits.

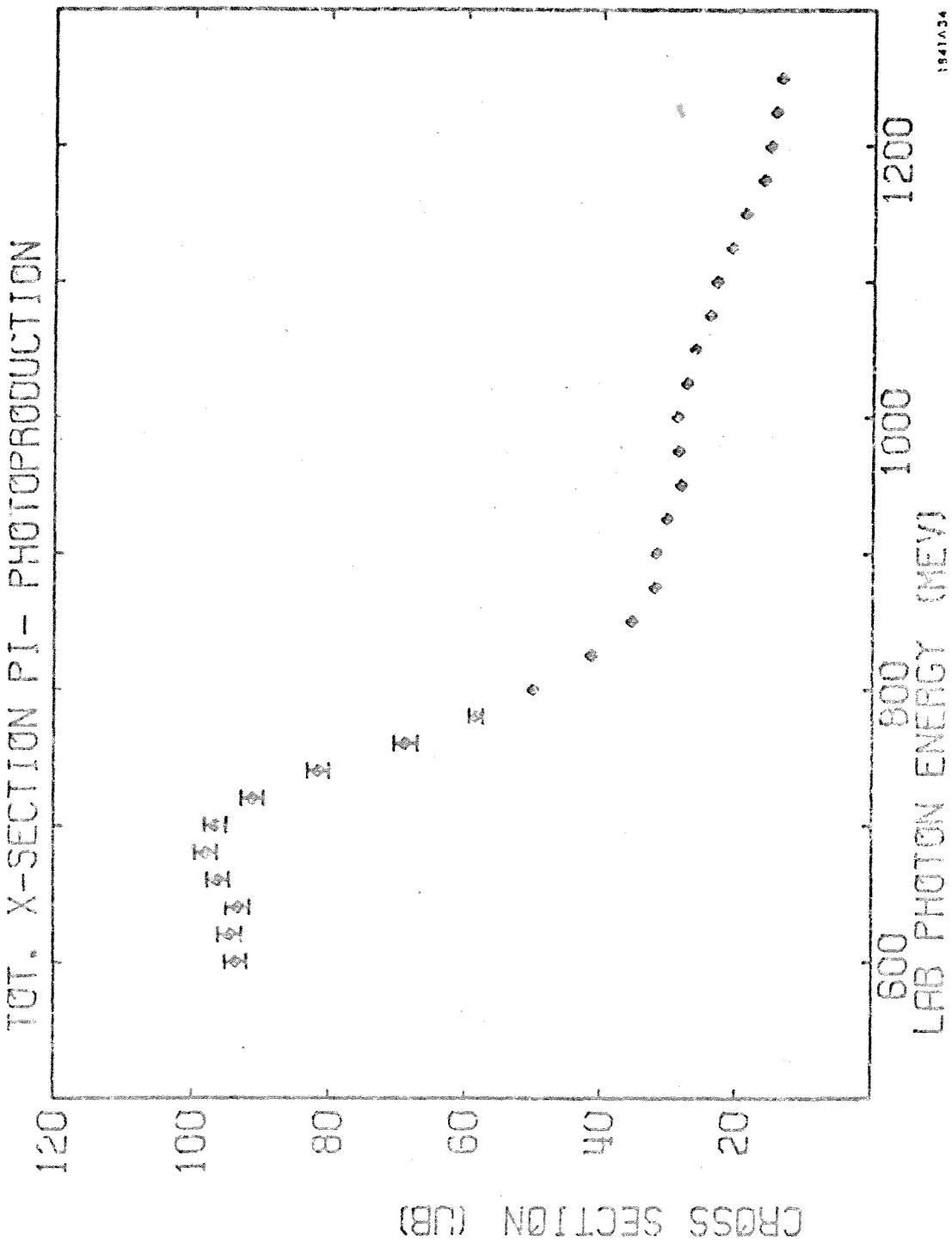
TOT. X-SECTION PI- PHOTOPRODUCTION
CROSS SECTION (UB)
120
100
80
60
40
20
600
800
1000
1200
LAB PHOTON ENERGY (MEV)
1841A34

FIGURE 15

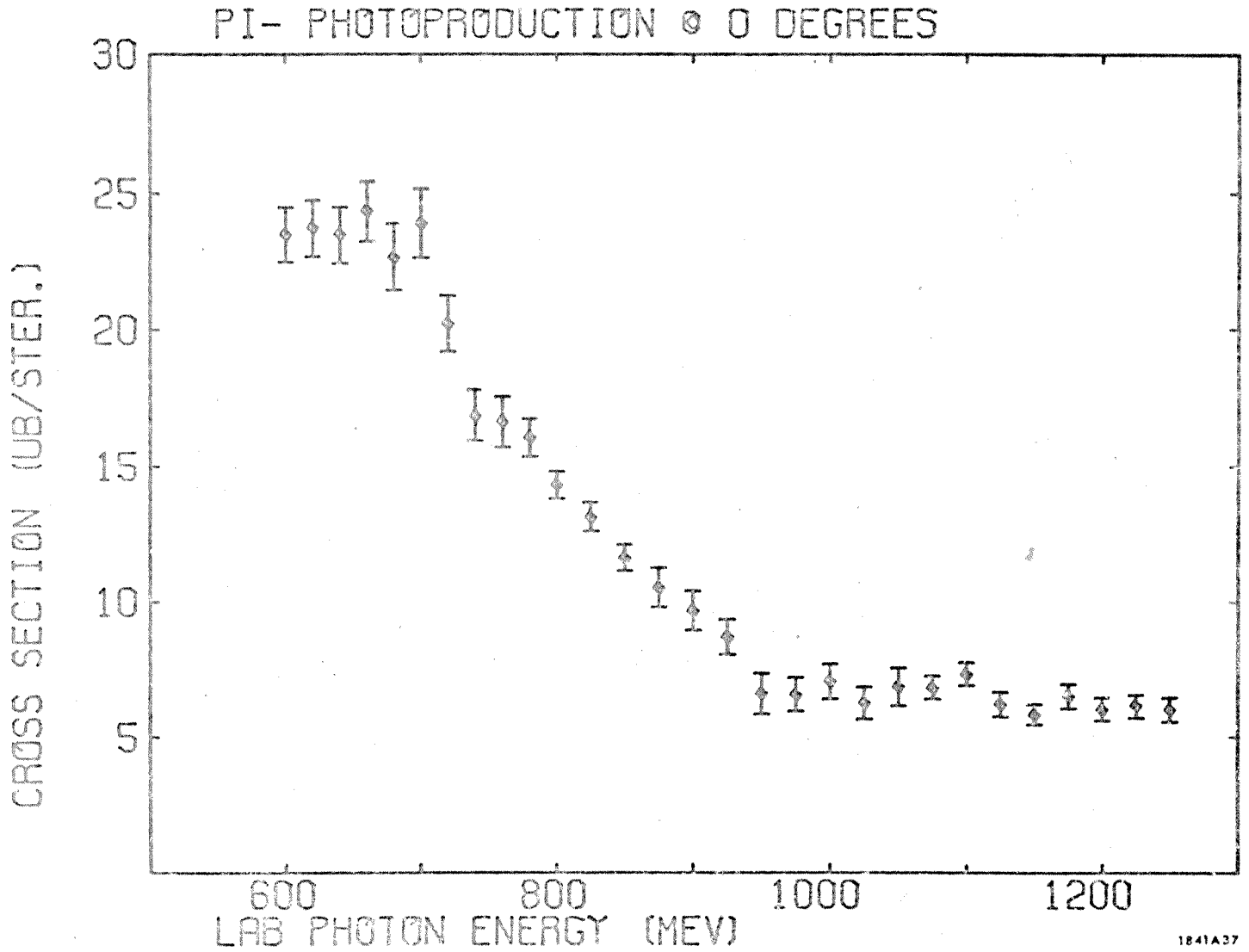
PI- PHOTOPRODUCTION @ 0 DEGREES
CROSS SECTION (UB/STER.)
30
25
20
15
10
5
600
800
1000
1200
LAB PHOTON ENERGY (MEV)
1841A37

FIGURE 16

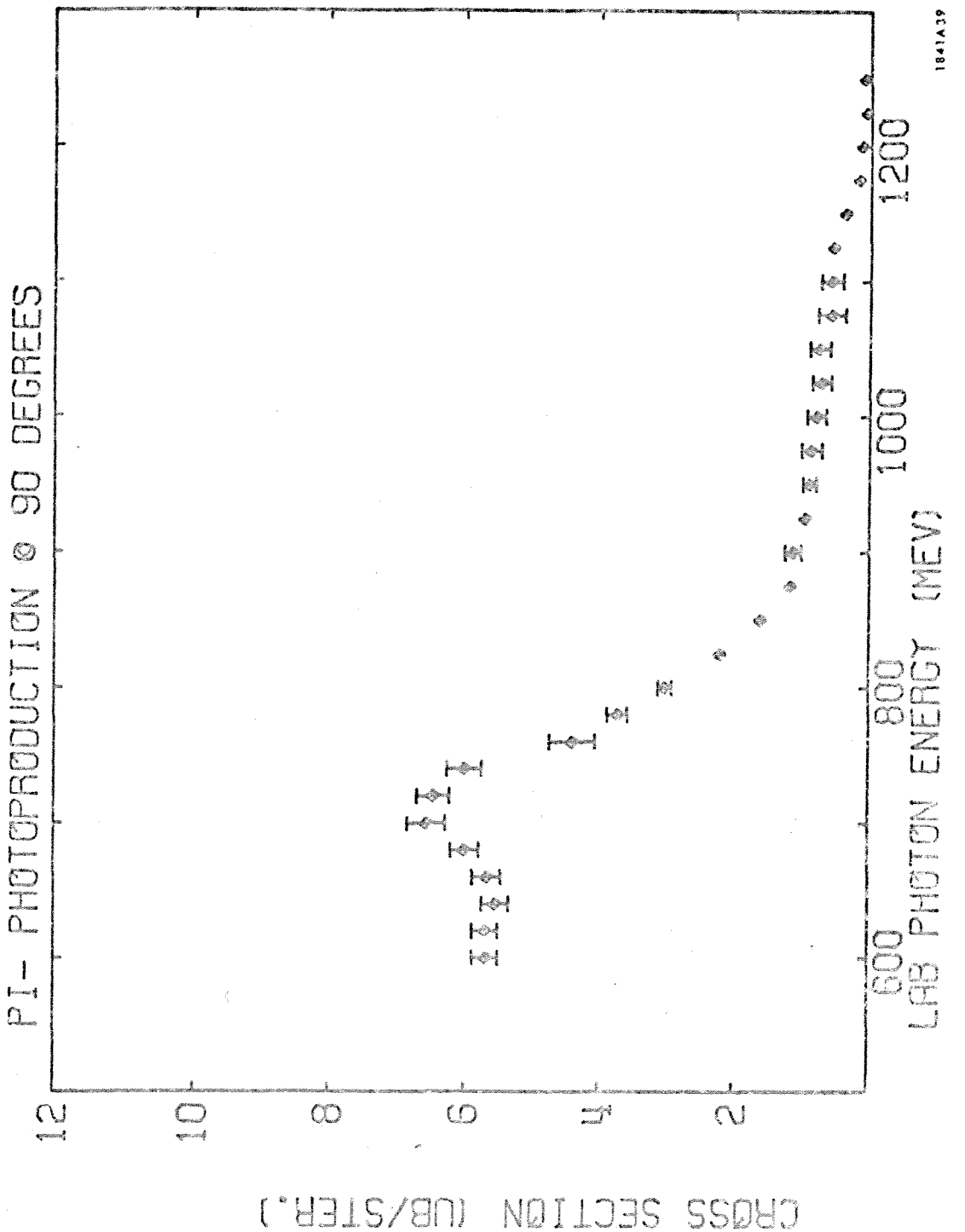
PI- PHOTOPRODUCTION @ 90 DEGREES
CROSS SECTION (UB/STER.)
12
10
8
6
4
2
600
800
1000
1200
LAB PHOTON ENERGY (MEV)
1841A39

FIGURE 17

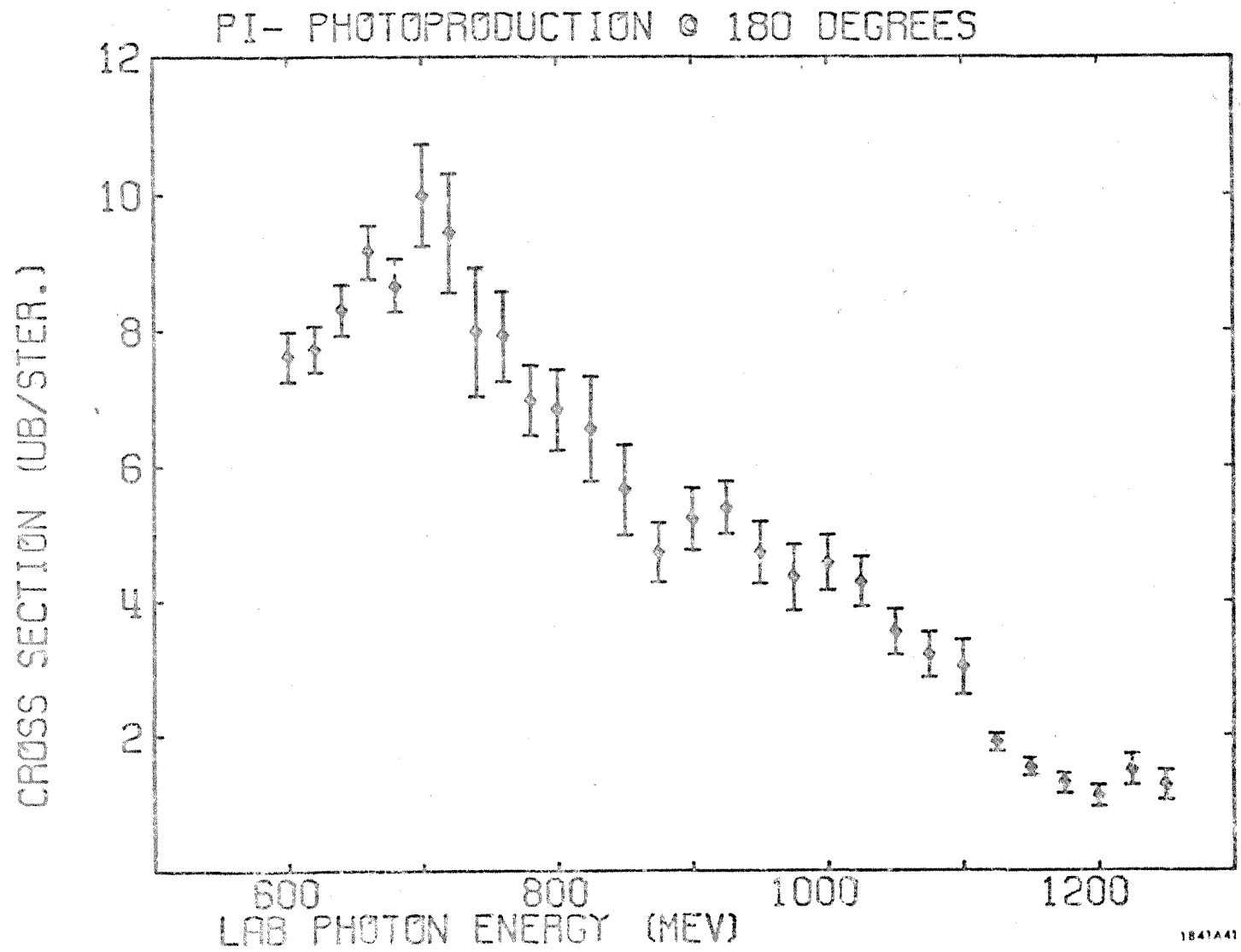
PI- PHOTOPRODUCTION @ 180 DEGREES
CROSS SECTION (UB/STER.)
12
10
8
6
4
2
600
800
1000
1200
LAB PHOTON ENERGY (MEV)
1841A41

FIGURE 18

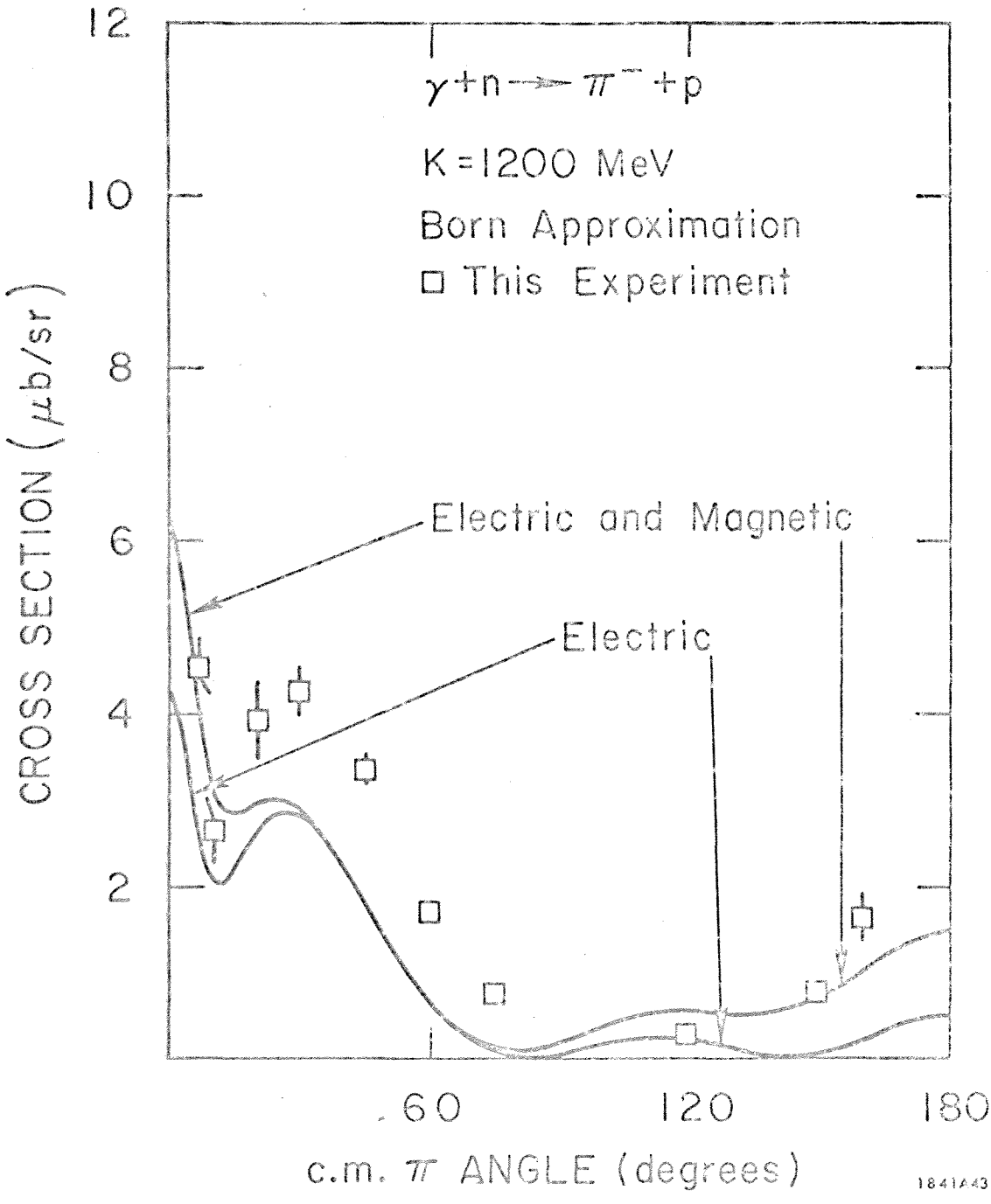
γ+n → π⁻+p
K=1200 MeV
Born Approximation
□ This Experiment
Electric and Magnetic
Electric
CROSS SECTION (μb/sr)
12
10
8
6
4
2
60
120
180
c.m. π ANGLE (degrees)
1841A43

FIGURE 19

PART VI COMPARISON TO OTHER EXPERIMENTS

After the data runs for this experiment the results of several other π^- photoproduction experiments became available. The comparison of these experiments can be seen in Figure 20. The data from this experiment seen in that figure are the results from the Moravcsik fits described in Part V. The overall comparison is quite good. The only serious discrepancy is with the Frascati bubble chamber experiment [48] shown in Figure 20.1. The shift in the data points between the two experiments indicates that one of us has made a serious error in the calculation of the lab photon energy. The favorable comparison of our experiment to the DESY experiment [26] (Figure 20.2) suggests that the error has been made by the Frascati group. In Figure 20.5 the results from this experiment are seen to be systematically lower than the Tokyo results [29]. Also, this experiment does not show the structure at 1000 MeV seen in the Tokyo data. However, the fitting program used to extrapolate this experiment's data to 180° had difficulty in producing the backward peak seen in the angular distributions of Figure 14. The closest measured point to 180° was at 160° and the fits at $\theta_{cm} > 160^{\circ}$ tended to fold over rapidly. The structure at 1000 MeV probably disappeared because of this experiment's poor resolution at backward π production angles ($\sim \pm 100$ MeV).

FIGURE 20

Comparison With Other Experiments

The solid line is from the Moravcsik fits for this experiment.

The references for the other experiments are given in the caption.

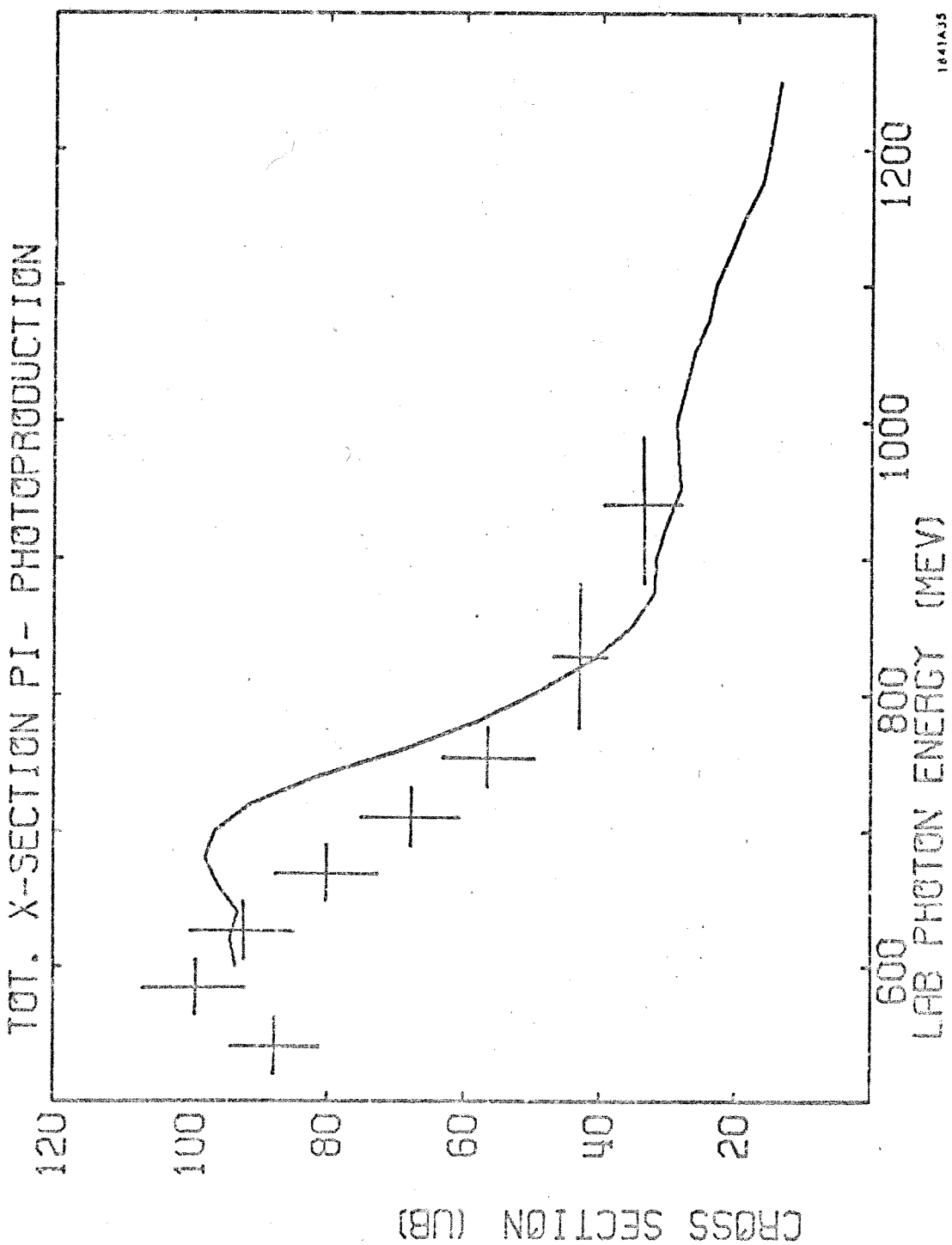

FIGURE 20.1

E. Lodi-Rizzini et al. [48]

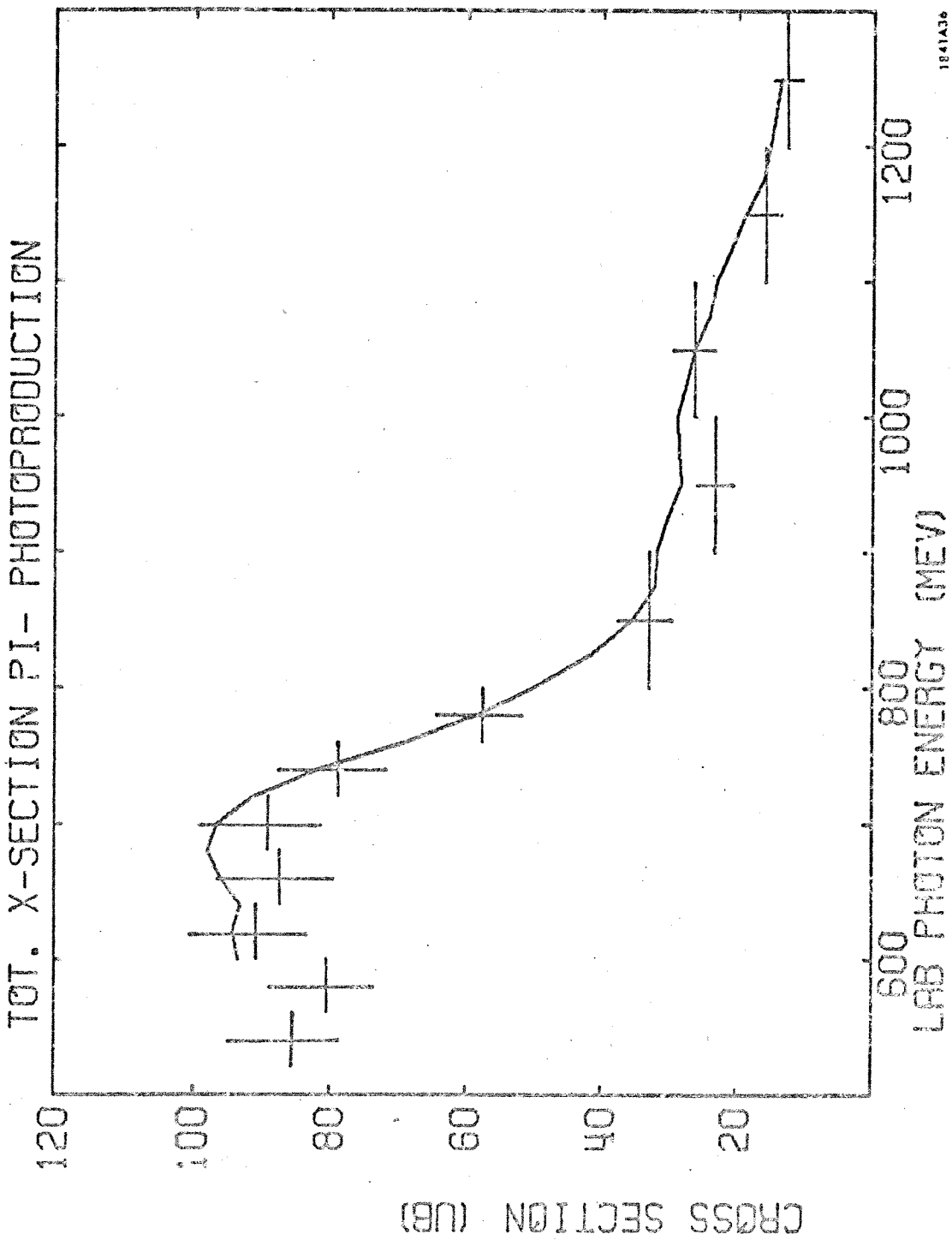

FIGURE 20.2

H. G. Hilpert et al. [26]

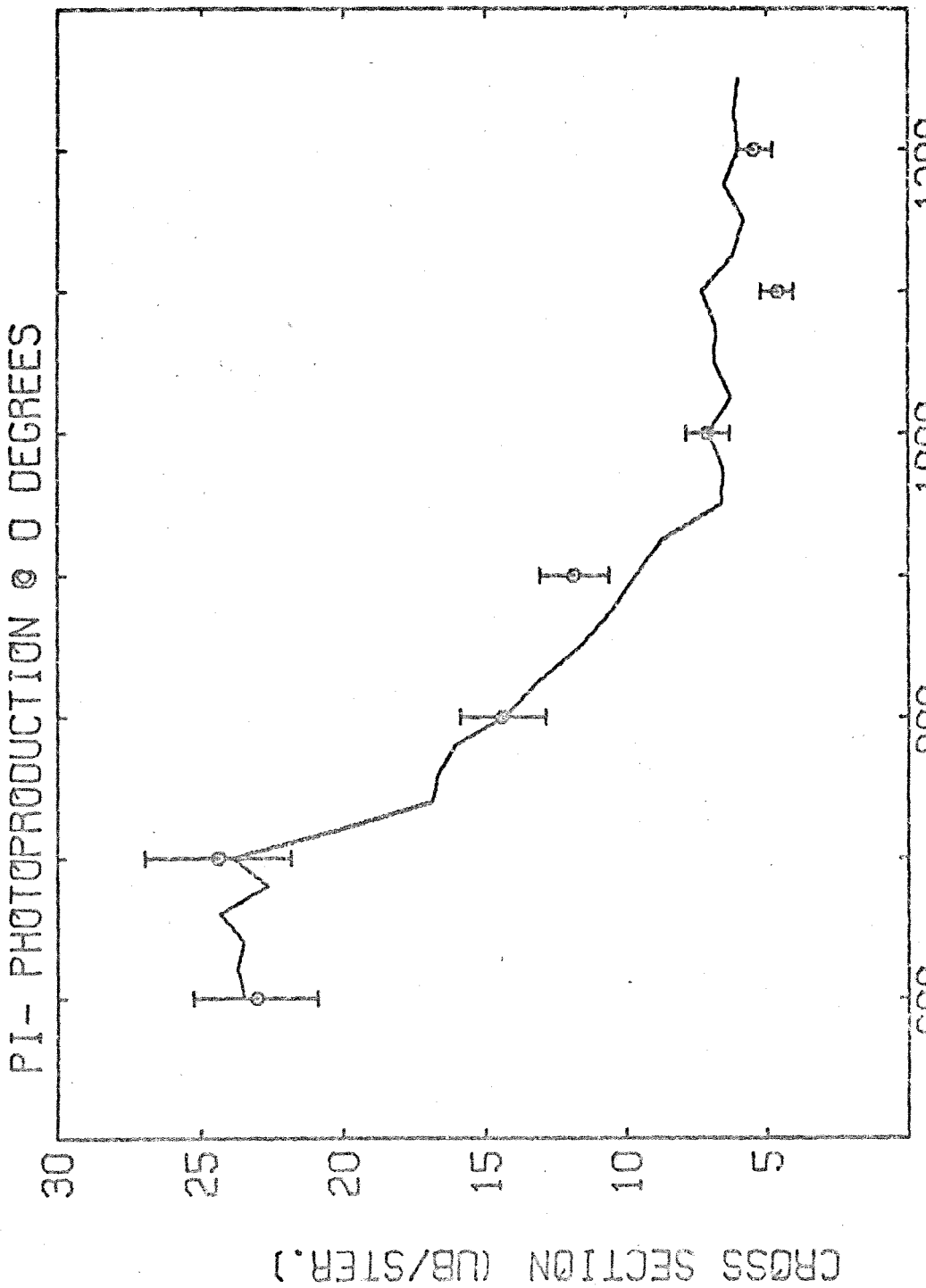

FIGURE 20.3

A. Ito et al. [47]

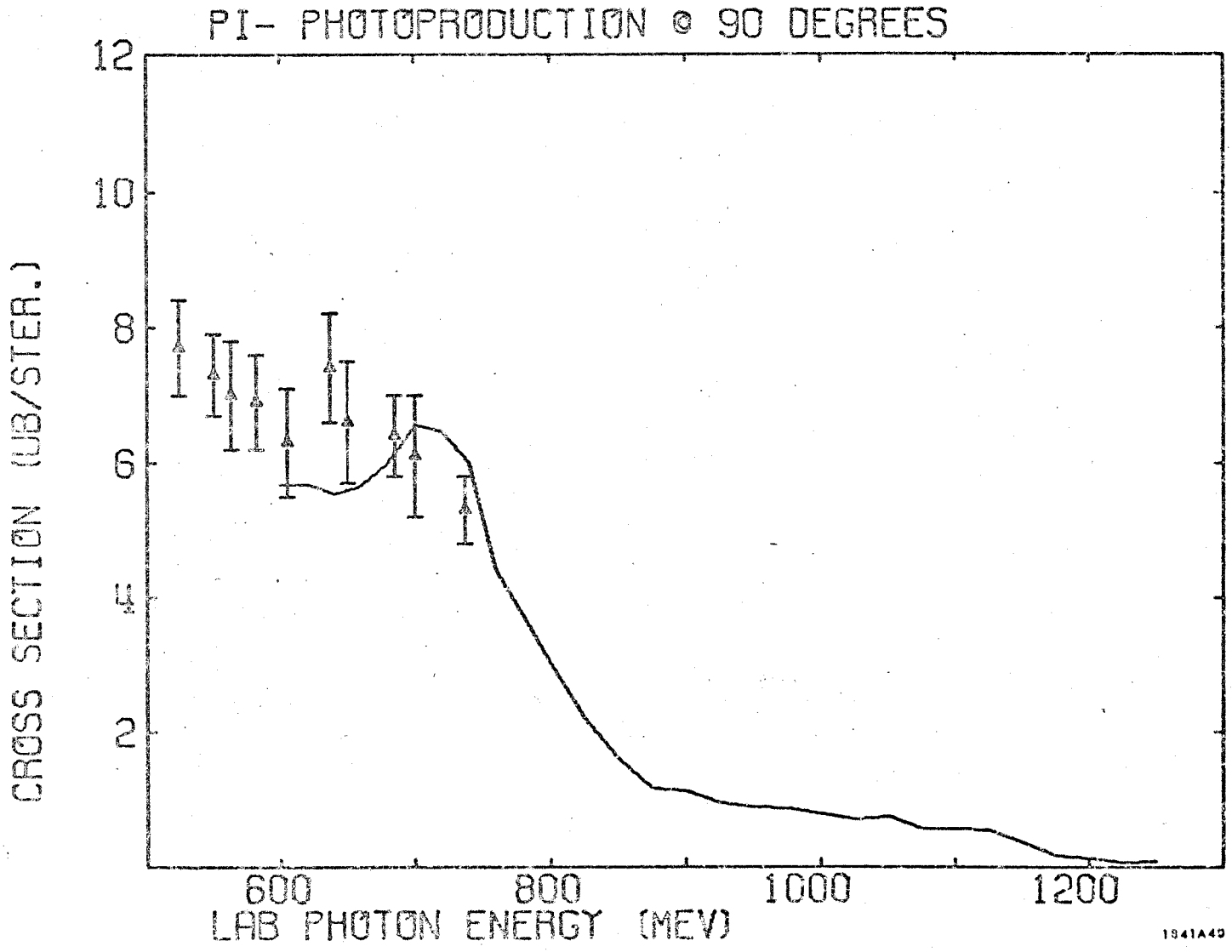

FIGURE 20.4

M. Beneventano et al. [49]

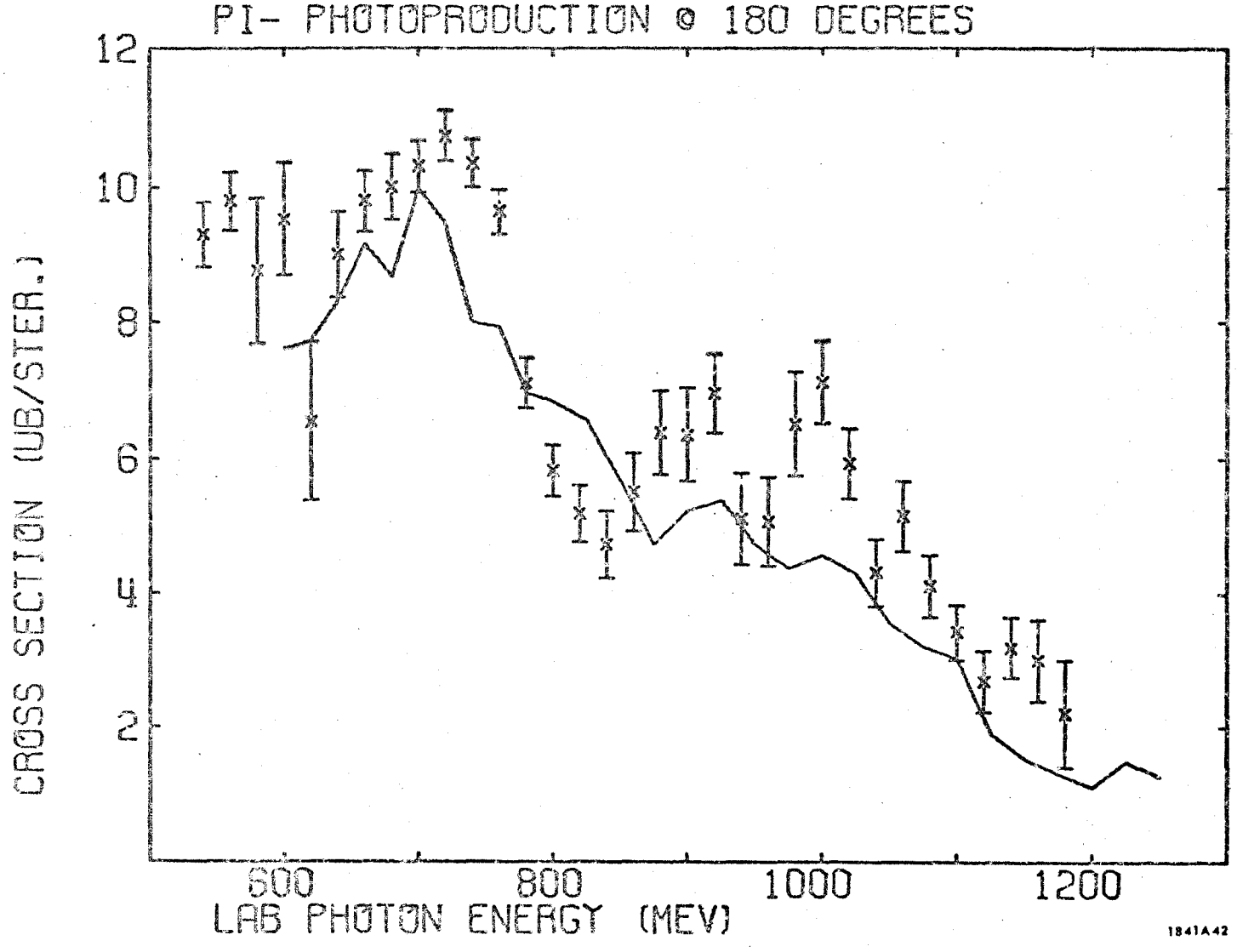

FIGURE 20.5

T. Fujii et al. [29]

PART VII CONCLUSIONS

This experiment has increased the experimental information on the π^- photoproduction differential cross section in the energy regions of the second and the third resonances to a level comparable to the information from π^+ and π^o photoproduction. Of the three types of cross section measurements, the direct cross sections measured with the LEM spectrometer were systematically higher than the ratio and recoil cross sections. There was no clear evidence to indicate that an error in the experimental technique produced this discrepancy. The ratio cross sections and the recoil cross sections were accepted as the final data as they were less influenced by deuterium effects.

There was a sufficient concentration of measurements at forward production angles to reveal a peak produced by the π exchange term which has previously been seen in π^+ photoproduction. However, the concentration of the data was such that the calculation of the π - nucleon coupling constant, $G^2_{\pi N}$, was not possible. The $D_{13}(1518)$ resonance is very noticeable in the data. At present it seems to behave as it does in π^+ photoproduction where its major contribution comes from the helicity (3/2) B_{2-} amplitude. The $F_{15}(1688)$ resonance, however, seems to be absent.

A quark model theory [9] has predicted that the dominant $F_{15}(1688)$ amplitude in π^+ photoproduction, B_{3-}, would be 0 in π^- photoproduction. The present experiment seems to confirm this prediction. The 0^o cross sections produced from Moravcsik fits to the data show a sharp drop in the energy region 700 - 740 MeV. There is a similar drop in the π^+ 0^o cross sections which has been associated with the η [2] photoproduction threshold.

Finally, the expected deuterium effect, the lowering of the cross section at small π production angles due to the Pauli principle [17], was seen by comparing the π^+ cross sections from hydrogen to the π^+ cross sections from deuterium.

The data from this experiment when added to the π photoproduction data from other experiments can by means of a partial wave analysis determine the electromagnetic amplitudes of the resonances. It will be interesting to see how compatible the quark model is with the results of these analyses.

APPENDIX I

KINEMATICS

There are a number of useful kinematic quantities and definitions which will be required for the cross section calculation. They will be described here in order that the derivation of the cross section formula is not obscured by these details.

In the calculations below it is assumed that the momentum and direction of both the pion and the spectator proton are known. Reasons for this choice will appear in Appendix II where the Monte Carlo integration variables are discussed. The deuteron is stationary in the lab frame, and the photon direction is known from the beam line. The virtual target neutron is given the opposite momentum of the spectator proton.

There are four frames of reference which will be of interest. They are:

1. the laboratory frame
2. the (π, recoil p) cm frame
3. the target neutron rest frame
4. the (γ, target n) cm frame .

Values associated with the first frame will be unmarked, the second frame will have subscripts "cm", the third frame will have primes, and the fourth frame will have both primes and subscripts "cm". The six particles considered and their 4-momenta in the lab frame are:

1. the photon $\quad \mathscr{K} = (K, \vec{K})$
2. the deuteron $\quad \mathscr{P}_D = (M_D, \vec{0})$
3. the pion $\quad \mathscr{Q} = (\omega, \vec{q})$
4. the recoil proton $\quad \mathscr{P}_R = (E_R, \vec{P}_R)$

5. the spectator proton $\mathscr{P}_S = (E_S, \vec{P}_S)$
6. the target neutron $\mathscr{P}_n = (E_n, \vec{P}_n)$.

The sympols for the particle masses are:

1. the proton mass M_p
2. the neutron mass M_n
3. the pion mass μ
4. the deuteron mass M_D.

Energy, momentum, and mass will be expressed in energy units of MeV. Units are such that c, the velocity of light, is 1. With these units 4-momentum dot products are defined as:

$$\mathscr{P}_1 \cdot \mathscr{P}_2 = E_1 E_2 - \vec{P}_1 \cdot \vec{P}_2$$

and

$$\mathscr{P}^2 = E^2 - P^2 = M^2 .$$

1. The Lab Photon Energy

The energy momentum conservation law for the reaction $\gamma + d \rightarrow \pi^- + p + p$ is expressed in the equation

$$\mathscr{K} + \mathscr{P}_D = \mathscr{Q} + \mathscr{P}_R + \mathscr{P}_S . \tag{1.1}$$

Both $\mathscr{Q}$ and $\mathscr{P}_S$ are assumed to be known, and together with $\mathscr{P}_D$, this is sufficient information to determine the lab photon energy K. For we have

$$\mathscr{K} + \mathscr{P}_D - \mathscr{Q} - \mathscr{P}_S = \mathscr{P}_R ,$$

and squaring both sides gives

$$M_D^2 + \mu^2 + M_p^2 + 2K(M_D - \omega + q\cos\theta - E_S + P_S\cos\theta_S) - 2M_D(\omega + E_S) + 2(\omega E_S - q P_S G) = M_p^2 \quad (1.2)$$

where

$$\cos\theta = \vec{q}\cdot\vec{K}/qK ,$$

$$\cos\theta_S = \vec{P}_S\cdot\vec{K}/P_S K ,$$

$$G = \vec{q}\cdot\vec{P}_S/qP_S .$$

The above equation can easily be solved for K. It is

$$K = \frac{2M_D(\omega + E_S) - 2(\omega E_S - qP_S G) - M_D^2 - \mu^2}{2(M_D - \omega + q\cos\theta - E_S + P_S\cos\theta_S)} \quad (1.3)$$

2. $(\partial K/\partial q)$ Photon Energy to π Momentum Transformation

In Appendix II there will be a need to transform from integration variables $d^3\vec{P}_S dK d\Omega$ to $d^3\vec{P}_S dq d\Omega$ where Ω is the π solid angle. The transformation required is $(\partial K/\partial q)_{\vec{P}_S\Omega}$. To do this we need to express K in terms of $\vec{P}_S$, q, and Ω. Such an expression is available in (1.3). Taking the derivative of (1.3) with respect to q we get

$$\frac{\partial K}{\partial q} = \frac{(M_D - E_S)\beta + P_S G + K(\beta - \cos\theta)}{M_D - \omega + q\cos\theta - E_S + P_S\cos\theta_S} \quad (1.4)$$

where $\beta = q/\omega$.

3. W, The (π^-, recoil p) c.m. Energy

W is a relativistic invariant and is given by the equation $(\mathscr{Q} + \mathscr{P}_R)^2 = W^2$. Using (1.1) this expression is equivalent to

$$(\mathcal{K} + \mathcal{P}_D - \mathcal{P}_S)^2 = W^2 .$$

Evaluating this expression in the lab frame gives

$$W^2 = M_D^2 + M_P^2 + 2M_D(K - E_S) - 2K(E_S - P_S \cos\theta_S) . \qquad (1.5)$$

4. **k'**, The Photon Energy in the Target Neutron Rest Frame

The differential cross section for single π photoproduction can be represented as a function of the c.m. energy W and the c.m. production angle θ_{cm}. However, for π^+ and π^o photoproduction where stationary proton targets are used it is sufficient to give the incident lab photon energy K instead of W because

$$K = \frac{W^2 - M_P^2}{2M_P} .$$

Most data are reported in terms of K.

For comparison purposes one would like to report π^- photoproduction from deuterium in the same manner. However, as seen in (1.5), K no longer defines W. Since the LH_2 proton target was stationary for π^+ and π^o photoproduction, it can be argued that K should be evaluated in the target neutron rest frame for π^- photoproduction. However, this is not obvious because the target neutron is a bound particle and $\mathcal{P}_n^2 \neq M_n^2$ which makes its rest frame rather ambiguous.

Keeping in mind that W is the important variable and that the K reported should relate to photoproduction from free neutrons, we define hypothetical 4-momenta for the photon ($\mathcal{k}$) and the neutron ($\mathcal{p}_n$) such that

$$k^2 = 0 ,$$

$$p_n^2 = M_n^2 ,$$

$$k + p_n = \mathcal{Q} + \mathcal{P}_R ,$$

and

$$(k + p_n)^2 = W^2 .$$

Evaluated in the neutron rest frame we have

$$k' = \frac{W^2 - M_n^2}{2M_n} . \tag{1.6}$$

5. $\partial\Omega_{cm}/\partial\Omega$, Solid Angle Transformation

Ω_{cm} and Ω are the solid angle variables for the pion in the (π^-, recoil p) c.m. frame and the lab frame, respectively. We begin the derivation of $(\partial\Omega_{cm}/\partial\Omega)$ by writing down the relativistic invariant differential

$$d^4\mathcal{Q}\, d^4\mathcal{P}_R\, \delta(\mathcal{Q}^2 - \mu^2)\delta(\mathcal{P}_R^2 - M_P^2)\delta^4(\mathcal{Q} + \mathcal{P}_R - \mathcal{P}_W) ,$$

where $\mathcal{P}_W = \mathcal{K} + \mathcal{P}_D - \mathcal{P}_S$. Cancelling $\delta^4(\mathcal{Q} + \mathcal{P}_R - \mathcal{P}_W)$ by integrating out $d^4\mathcal{P}_R$ gives the invariant

$$d^4\mathcal{Q}\, \delta(\mathcal{Q}^2 - \mu^2)\delta(\mathcal{P}_R^2 - M_P^2) . \tag{1.7}$$

because (1.7) is an invariant further integrations can be carried out with identical results in either the lab frame or the (π^-, recoil p) c.m. frame. Integrating out the π^- energy in $d^4\mathcal{Q} = d^3q\, d\omega = d^3q_{cm}\, d\omega_{cm}$ and cancelling $\delta(\mathcal{Q}^2 - \mu^2) = \delta(\omega^2 - q^2 - \mu^2) = \delta(\omega_{cm}^2 - q_{cm}^2 - \mu^2)$ gives

$$\frac{d^3q}{2\omega}\, \delta(\mathcal{P}_R^2 - M_P^2) = \frac{d^3q_{cm}}{2\omega_{cm}}\, \delta(\mathcal{P}_R^2 - M_P^2) .$$

Noting $d^3q = q^2 dq\, d\Omega$ and $d^3q_{cm} = q^2_{cm} dq_{cm} d\Omega_{cm}$, we can integrate over the π^- momentum and get the result

$$d\Omega \int \frac{q^2}{2\omega}\, dq\, \delta(\mathscr{P}_R^2 - M_P^2) = d\Omega_{cm} \frac{q^2_{cm}}{2\omega_{cm}} \left| \frac{\partial \mathscr{P}_R^2}{\partial q_{cm}} \right|^{-1} . \tag{1.8}$$

We leave the dq integration for now because this form will be useful in Appendix II. The quantity $\partial \mathscr{P}_R^2 / \partial q_{cm}$ is calculated as follows:

with
$$\mathscr{P}_W = \mathscr{Q} + \mathscr{P}_R \tag{1.9}$$

then
$$\mathscr{P}_R^2 = (\mathscr{P}_W - \mathscr{Q})^2 = W^2 - 2W\omega_{cm} + \mu^2 \tag{1.10}$$

hence
$$\frac{\partial \mathscr{P}_R^2}{\partial q_{cm}} = -\frac{2Wq_{cm}}{\omega_{cm}} . \tag{1.11}$$

Substituting (1.11) into (1.8) plus a little manipulation gives

$$\frac{\partial \Omega_{cm}}{\partial \Omega} = \int \frac{2Wq^2}{q_{cm}\omega}\, dq\, \delta(\mathscr{P}_R^2 - M_P^2) \tag{1.12}$$

The final result comes from the integration over dq and we have

$$\frac{\partial \Omega_{cm}}{\partial \Omega} = \frac{2Wq^2}{q_{cm}\omega} \left| \frac{\partial \mathscr{P}_R^2}{\partial q} \right|^{-1} \tag{1.13}$$

$\partial \mathscr{P}_R^2 / \partial q$ can be evaluated from $\mathscr{P}_R^2 = M_P^2$ and (1.2) and so the desired expression is

$$\frac{\partial \Omega_{cm}}{\partial \Omega} = \frac{Wq^2}{q_{cm} \left| M_D q + K(q - \omega \cos\vartheta) - qE_S + \omega P_S G \right|} . \tag{1.14}$$

6. $\cos\theta_{cm}$, Cosine of the c.m. Pion Scattering Angle

This quantity is defined by

$$\cos\theta_{cm} = \vec{K}_{cm} \cdot \vec{q}_{cm} / K_{cm} q_{cm} .$$

To evaluate this quantity we use the expression for the invariant $\mathcal{K} \cdot \mathcal{Q}$ in the c.m. frame

$$\mathcal{K} \cdot \mathcal{Q} = K_{cm}(\omega_{cm} - q_{cm}\cos\theta_{cm}) , \tag{1.15}$$

and its expression in the lab frame

$$\mathcal{K} \cdot \mathcal{Q} = K(\omega - q\cos\theta) . \tag{1.16}$$

Equating (1.15) and (1.16) gives

$$\cos\theta_{cm} = \frac{1}{q_{cm}}\left[\frac{Kq}{K_{cm}}\cos\theta + \omega_{cm} - \frac{K\omega}{K_{cm}}\right] . \tag{1.17}$$

We now need to know q_{cm}, K_{cm}, and ω_{cm}. From (1.10) we get

$$\omega_{cm} = \frac{W^2 + \mu^2 - M_P^2}{2W} , \tag{1.18}$$

and q_{cm} then comes from $\omega_{cm}^2 - q_{cm}^2 = \mu^2$. K_{cm} is found from $\mathcal{K} \cdot \mathcal{P}_W$ in the (π^-, recoil p) c.m. frame

$$\mathcal{K} \cdot \mathcal{P}_W = K_{cm} W , \tag{1.19}$$

and in the lab frame

$$\mathcal{K} \cdot \mathcal{P}_W = \mathcal{K} \cdot (\mathcal{P}_R + \mathcal{Q}) = \mathcal{K} \cdot (\mathcal{K} + \mathcal{P}_D - \mathcal{P}_S) = K(M_D - E_S + P_S\cos\theta_S) \tag{1.20}$$

Equating (1.19) and (1.20) we obtain

$$K_{cm} = K \frac{M_D - E_S + P_S \cos\theta_S}{W} \quad . \tag{1.21}$$

APPENDIX II

CROSS SECTION CALCULATION

The reaction actually observed in this experiment was $\gamma + d \rightarrow \pi^- + p + p$. This reaction has three particles in its final state. However, one of the protons, the spectator, is almost at rest (it only has the residual momentum left over from its motion inside the deuterium nucleus) so that the final state behaves like a fuzzy two-body state. This is the justification for pretending the reaction observed is $\gamma + n \rightarrow \pi^- + p$. However, in order to calculate the experimental observations accurately the fuzziness caused by the spectator proton must be included in the cross section formula.

To this end we write down a general expression relating the π^- yield in the spectrometer to the π^- cross section

$$C = \int_K \int_{\Delta\Omega} \int_{\Delta q} \Phi(K) \frac{\partial^2 \sigma(K, q, \Omega)}{\partial q \, \partial \Omega} \eta \, t \, dK \, dq \, d\Omega \qquad (2.1)$$

where

C = number of π^- that entered the spectrometer

$\Phi(K)$ = number of incident photons per unit energy

$\partial^2\sigma/\partial q \, \partial\Omega$ = π^- differential cross section in the lab frame

η = density of neutrons in the target

t = effective thickness of the target

K = lab photon energy

q = π^- lab momentum

Ω = π^- lab solid angle.

This formula is correct regardless of the number of particles in the final state. In part A the differential cross section $\partial^2\sigma(K, q, \Omega)/\partial q \, \partial\Omega$ is computed from the

π^- photoproduction cross section and the spectator model of the deuteron. In part B the rate integral (2.1) is completely developed; and in part C the Monte Carlo process used to compute the integral is described.

A. $\partial^2\sigma/\partial q\,\partial\Omega$ Calculation

All wave functions used in this section are normalized to $(2E)^{\frac{1}{2}}$ per unit volume. $\phi(P)$ will be the Hulthèn wave function of the deuteron ground state (see part III). The formulae (Appendix 1) on kinematics will be used.

We start by writing down the Golden Rule equation for the reaction $\gamma + d \rightarrow \pi^- + p + p$ with respect to the lab frame. It is

$$v d\sigma = \frac{1}{2K2M_D}(2\pi)^4 \delta^4(\mathscr{P}_f - \mathscr{P}_i)\,|B|^2 \times 2\pi\,\delta(\mathscr{Q}^2 - \mu^2)\frac{d^4\mathscr{Q}}{(2\pi)^4}\,2\pi\,\delta(\mathscr{P}_S^2 - M_P^2)\frac{d^4\mathscr{P}_S}{(2\pi)^4}\,2\pi\,\delta(\mathscr{P}_R^2 - M_P^2)\frac{d4\,\mathscr{P}_R}{(2\pi)^4} \tag{2.2}$$

where

B = the amplitude for the reaction $\gamma + d \rightarrow \pi^- + P + P$

$\mathscr{P}_f = \mathscr{Q} + \mathscr{P}_S + \mathscr{P}_R$

$\mathscr{P}_i = \mathscr{K} + \mathscr{P}_D$

v = relative velocity of the incoming particles (in this case $v = c = 1$).

The δ-functions $\delta(\mathscr{Q}^2 - M^2)$, $\delta(\mathscr{P}_S^2 - M_P^2)$, and $\delta^4(\mathscr{P}_f - \mathscr{P}_i)$ are eliminated by integrations over $d\omega$, dE_S, and $d^4\mathscr{P}_R$ respectively. These operations reduce (2.2) to

$$d\sigma = \frac{1}{2K2M_D}\,2\pi\,\delta(\mathscr{P}_R^2 - M_P^2)\,|B|^2\,\frac{d^3q}{2\omega(2\pi)^3}\,\frac{d^3P_S}{2E_S(2\pi)^3} \tag{2.3}$$

We now relate $|B|^2$ to the $\gamma + n \rightarrow \pi^- + p$ cross section by using the spectator model illustrated in Figure (21). The deuteron breaks up into a virtual neutron and a proton with equal but opposite momentum P_S and amplitude $\phi(P_S)$. The neutron interacts with the photon with amplitude A to form the π^- and recoil proton. If we let T be the interaction matrix between the initial and final states, then

$$B = \langle \mathcal{Q}, \mathcal{P}_R, \mathcal{P}_S | T | \mathcal{K}, \mathcal{P}_D \rangle . \tag{2.4}$$

Now the deuteron splits into a neutron and a proton, so

$$| \mathcal{P}_D \rangle = \sqrt{2M_D}\,\phi(P_S) \frac{| \mathcal{P}_S \rangle}{\sqrt{2E_S}} \frac{| \mathcal{P}_n \rangle}{\sqrt{2E_n}} \tag{2.5}$$

where $| \mathcal{P}_n \rangle$ is the wave function of the virtual neutron and is normalized to $\sqrt{2E_n} = \left(2(P_S^2 + M_n^2)\right)^{\frac{1}{2}}$. * These operations give

$$B = \frac{\langle \mathcal{Q}, \mathcal{P}_R | T | \mathcal{K}, \mathcal{P}_n \rangle}{\sqrt{2E_n}}\, \phi(P_S) \frac{\langle \mathcal{P}_S | \mathcal{P}_S \rangle}{\sqrt{2E_S}} \sqrt{2M_D} . \tag{2.6}$$

---

* There is a question as to what normalization to use for the neutron wave function. The total energy of the neutron is $E_n = M_D - E_S$ and this energy, not the one in the text, could have been used for normalization. However, we are trying to extract the $\gamma + n \rightarrow \pi^- + p$ amplitude A from the $\gamma + d \rightarrow \pi^- + p + p$ amplitude B, and A has for inputs free particle wave functions, so the wave function $| \mathcal{P}_n \rangle$ was altered a bit to make a free particle function normalized to $E_n = (P_S^2 + M_n^2)^{\frac{1}{2}}$. The normalizations do not change the results significantly. For the average $P_S = 80$ MeV/c we get a ratio

$$\frac{(P_S^2 + M_n^2)^{\frac{1}{2}}}{M_D - E_S} = 1.01$$

Now $\langle \mathscr{P}_S | \mathscr{P}_S \rangle = 2E_S$, and $\langle \mathscr{Q}, \mathscr{P}_R | T | \mathscr{K}, \mathscr{P}_n \rangle = A$ (the $\gamma + n \rightarrow \pi^- + p$ amplitude) thus (2.6) becomes

$$B = \left(\frac{2E_S M_D}{E_n}\right)^{\frac{1}{2}} A\phi(P_S) \,. \tag{2.7}$$

Substituting (2.7) into (2.3) we have

$$d\sigma = \frac{1}{2K} \frac{|A|^2}{2E_n} 2\pi\,\delta(\mathscr{P}_R^2 - M_P^2) \frac{q^2 dq\, d\Omega}{2\omega(2\pi)^3} \left[\phi^2(P_S) \frac{d^3P_S}{(2\pi)^3}\right] \tag{2.8}$$

A is a function of W and θ_{cm}. From Eq. (1.6), k', the photon energy in the target neutron rest frame, can be related to W for easy comparison with other data reported in this way.

Since A is the amplitude for $\gamma + n \rightarrow \pi^- + p$ we can write the Golden Rule for this reaction also

$$v_{cm} d\sigma = \frac{1}{2E_{n_{cm}} 2k_{cm}} (2\pi)^4 \delta^4(\mathscr{P}_f - \mathscr{P}_i) |A|^2 2\pi\,\delta(\mathscr{Q}^2 - \mu^2) \frac{d^4\mathscr{Q}}{(2\pi)^4} 2\pi\,\delta(\mathscr{P}_R^2 - M_P^2) \frac{d^4\mathscr{P}_R}{(2\pi)^4} \tag{2.9}$$

where v_{cm} is the relative velocity of the photon and neutron in their c. m. frame, $\mathscr{P}_f = \mathscr{Q} + \mathscr{P}_R$, and $\mathscr{P}_i = \mathscr{k} + \mathscr{p}_n$. This expression can be manipulated to give

$$\frac{\partial\sigma}{\partial\Omega_{cm}} = \frac{q_{cm}}{k'_{cm}} \frac{|A|^2}{(8\pi W)^2} \,. \tag{2.10}$$

Cancelling $|A|^2$ between (2.8) and (2.10) gives

$$d\sigma = \frac{k'_{cm} W}{K E_n} \frac{2Wq^2}{q_{cm}\omega} dq\, d\Omega \frac{d\sigma}{\partial\Omega_{cm}} \delta(\mathscr{P}_R^2 - M_P^2) \left[\phi^2(P_S) \frac{d^3P_S}{(2\pi)^3}\right] \tag{2.11}$$

Noting $k'_{cm} W = k \cdot (\mathcal{Q} + \mathcal{P}_R) = k \cdot (k + \mathcal{P}_n) = k'M_n$, we achieve the required result

$$\frac{\partial^2 \sigma}{\partial q \, \partial \Omega} = \int_{\vec{P}_S} \frac{k'M_n}{K E_n} \frac{2Wq^2}{q_{cm}\omega} \frac{\partial \sigma}{\partial \Omega_{cm}} \delta(\mathcal{P}_R^2 - M_P^2) \left[\phi^2(P_S) \frac{d^3 P_S}{(2\pi)^3} \right] \tag{2.12}$$

B. The Rate Integral

The integral developed in this section is a messy mass of symbols and involved a 9-fold integration. Furthermore, there are three kinds of these integrals which differ because they depend on the particle detected in the spectrometer, and on the spectrometer that was used. Because of an integration over the spectator proton momentum, a Monte Carlo technique was used to compute the integrals. Since the computational difficulties of this technique are not increased by increasing orders of integration there was no attempt to simplify the integrals. Hence the reason for the apparent complexity. Only one of the three integrals will be developed here. The others will be discussed in Section (2-C).

The specific case that will be treated here is for the pion detected in the HEMA spectrometer. Taking formula (2.1) we substitute (2.12) and get the following equation

$$C = \int_K \int_\Omega \int_q \int_{\vec{P}_S} \frac{k'M_n}{K E_n} \Phi(K) \frac{2Wq^2}{q_{cm}\omega} \frac{\partial \sigma}{\partial \Omega_{cm}} \delta(\mathcal{P}_R^2 - M_P^2) \left[\phi^2(P_S) \frac{d^3 P_S}{(2\pi)^3} \right] \eta \, t \, dK dq d\Omega \ . \tag{2.13}$$

We note that $\int_q (2Wq^2/q_{cm}\omega)\delta(\mathscr{P}_R^2 - M_P^2)dq$ of (2.13) is equivalent to the right-hand side of (1.13), and so when the integration is done we have $\partial\Omega_{cm}/\partial\Omega$. Having eliminated the integration in q we will bring it back again because the integration in K is not practical. We use the transformation

$$dK \rightarrow (\partial K/\partial q)\, dq \tag{2.14}$$

The integral is now reduced to

$$C = \int_{\Delta\Omega}\int_{\Delta q}\int_{\vec{P}_S} \frac{k'M_n}{K E_n}\Phi(K)\eta t \frac{\partial\sigma}{\partial\Omega_{cm}}\frac{\partial\Omega_{cm}}{\partial\Omega}\frac{\partial K}{\partial q}\left[\phi^2(P_S)\frac{d^3P_S}{(2\pi)^3}\right]dq\, d\Omega \ . \tag{2.15}$$

This integral, although correct, does not reflect the complexity of the experimental situation. The bremsstrahlung beam has a non-uniform shape at the target, the target itself is not uniform in thickness, and the spectrometer properties cannot be easily represented by independent integrations in q and Ω. Each part of (2.15) will therefore be altered to conform to the experimental setup. The coordinate system used in the following text is illustrated in Figure (22).

The bremsstrahlung beam function is transformed to

$$\Phi(K) \rightarrow \frac{H}{E_0}\frac{B(E_0, K, Y, Z)}{K}\, dY\, dZ \tag{2.16}$$

where

H = total energy in the beam

E_0 = bremsstrahlung end point

Y = target width coordinate (see Figure (22))

Z = target height coordinate (see Figure (22)).

The function $B(E_0, K, Y, Z)$ is defined so that

$$\int_0^{E_0} \int_{\Delta Y} \int_{\Delta Z} B(E_0, K, Y, Z) \frac{dK}{E_0} dY dZ = 1 \tag{2.17}$$

where ΔY and ΔZ define the size of the beam spot at the target. The function $B(E_0, K, Y, Z)$ was tabulated from the computer program BPAKI. [31]

The normalized pion counting rate, R = C/H (counts per beam energy), will be related to the cross section $d\sigma(k', \theta_{cm})/d\Omega_{cm}$.

We equate

$$dq\, d\Omega = P_0 dQ\, d\beta\, d\theta \tag{2.18}$$

where

$Q = (q - P_0)/P_0$

P_0 = central momentum of the spectrometer

β, θ are angular variables defining the spectrometer acceptance (see Figure (22)).

The limits on the Q and β integrations are very difficult to compute. A better choice is α and ζ, the verticle positions of the particle at the spectrometer aperature counter and momentum counter respectively (see Appendix V). These variables have simple limits (i.e., the size of the counter). Appendix 5 describes fits for Q and β as functions of Z, α, and ζ. We will represent the fits symbolically by

$$\left.\begin{aligned} Q &= f(Z, \alpha, \zeta) \\ \beta &= g(Z, \alpha, \zeta) \end{aligned}\right\} \tag{2.19}$$

This enables (2.18) to be put into the form

$$dq\,d\Omega = P_0 \frac{\partial(Q,\beta)}{\partial(\alpha,\xi)}\, d\alpha\, d\xi\, d\theta \quad , \tag{2.20}$$

where the Jacobian is computed from (2.19).

Finally, we must multiply (2.15) by the factor $\exp(-\mu L/q\tau)$ where τ is the π life time and L is the path length of the π from the target to the last spectrometer counter. This factor accounts for the loss of pions due to decay.

Making the preceeding changes to (2.15), we obtain the rate integral

$$R = \eta \frac{P_0}{E_0} \int_{\Delta Z}\int_{\Delta Y}\int_{X}\int_{\Delta\theta}\int_{\Delta\alpha}\int_{\Delta\xi}\int_{\vec{P}_S} \frac{k'M_n}{KE_n} \frac{B(K, E_0, Y, Z)}{K} \frac{\partial\sigma}{\partial\Omega_{cm}}(k', \theta_{cm}) \frac{\partial\Omega_{cm}}{\partial\Omega}$$

$$\times \frac{\partial K}{\partial q} \exp(-\mu L/q\tau) \left[\phi^2(P_S) \frac{d^3P_S}{(2\pi)^3}\right] \frac{\partial(Q,\beta)}{\partial(\alpha,\xi)}\, dZ\, dY\, dX\, d\alpha\, d\xi\, d\theta \tag{2.21}$$

C.

In this part the Monte Carlo process to evaluate the rate integral (2.21) is described. The process is extensively discussed in Appendix 3, and the results there will be applied without explanation. First there is need for a couple of definitions; the response integral

$$\kappa_\pi = \eta \frac{P_0}{E_0} \int_{\Delta Z}\int_{\Delta Y}\int_{X}\int_{\Delta\alpha}\int_{\Delta\xi}\int_{\Delta\theta}\int_{\vec{P}_S} \frac{k'M_n}{KE_n} \frac{B(K, E_0, Y, Z)}{K} \frac{\partial\Omega_{cm}}{\partial\Omega}$$

$$\times \frac{\partial K}{\partial q} \exp(-\mu L/q\tau) \left[\phi^2(P_S) \frac{d^3P_S}{(2\pi)^3}\right] \frac{\partial(Q,\beta)}{\beta(\alpha,\xi)}\, dZ\, dY\, dX\, d\alpha\, d\xi\, d\theta \tag{2.22}$$

and the average cross section $\overline{[\partial\sigma(\bar{k}', \bar{\theta}_{cm})/\partial\Omega_{cm}]}$, where

$$R = \overline{[\partial\sigma(\bar{k}', \bar{\theta}_{cm})/\partial\Omega_{cm}]}\,\kappa_{\pi} \quad . \tag{2.23}$$

The Monte Carlo process will evaluate κ_{π}. Then with (2.23) plus a few other complications, the average cross section can be calculated.

For each event in the Monte Carlo process the order in which the integration variables are picked and their limits are:

1. Z interval $-\Delta Z/2 < Z < \Delta Z/2$
2. Y interval $-\Delta Y/2 < Y < \Delta Y/2$
3. x interval $-(R^2-Y^2)^{\frac{1}{2}} < X < (R^2-Y^2)^{\frac{1}{2}}$
4. α interval $-\Delta\alpha/2 < \alpha < \Delta\alpha/2$
5. ζ interval $\zeta_0-\Delta\zeta/2 < \zeta < \zeta_0+\Delta\zeta/2$
6. θ interval $\theta_0-\Delta\theta/2 < \theta < \theta_0+\Delta\theta/2$
7. ϕ_S interval $0 < \phi_S < 2\pi$
8. $\cos\theta_S$ interval $-1 < \cos\theta_S < +1$
9. P_S interval $0 < P_S < \infty$

where R = radius of the target. The values of P_S are weighted according to the function $P_S^2\phi^2(P_S)/(2\pi)^3$. For each event we compute

$$ADD_i = (R^2-Y^2)^{\frac{1}{2}}\frac{k_i!M_n}{K_iE_{n_i}}\frac{B(K_i, E_0, Y_i, Z_i)}{K_i}\left(\frac{\partial\Omega_{cm}}{\partial\Omega}\right)_i\left(\frac{\partial K}{\partial q}\right)_i\exp(-\mu L/q_i\tau)\frac{\partial(Q_i, \beta_i)}{\zeta(\alpha_i, \zeta_i)}\,, \tag{2.24}$$

and defining

$$NORM = 2\eta\frac{P_0}{E_0}\frac{\Delta Y\,\Delta Z\,\Delta\alpha\,\Delta\zeta\,\Delta\theta}{N}\,, \tag{2.25}$$

where N = number of events, we compute (2.22) by

$$\kappa_\pi = \text{NORM} \sum_{i=1}^{N} \text{ADD}_i \tag{2.26}$$

The definitions for $\bar{k}'$ and $\bar{\theta}_{cm}$ are then given by

$$\bar{k}' = \sum_{i=1}^{N} k_i' \, \text{ADD}_i \Big/ \sum_{i=1}^{N} \text{ADD}_i \tag{2.27}$$

and

$$\bar{\theta}_{cm} = \sum_{i=1} \theta_{cm_i} \text{ADD}_i \Big/ \sum_{i=1}^{N} \text{ADD}_i \tag{2.28}$$

Equation (2.26) is also used when computing the response integral when the recoil proton is detected. In that case only the ADD_i's where the recoil proton hit the recoil counter are used.

For the cases where the proton is detected in the spectrometer and the pion in the recoil counter, all the preceeding formula are valid under the transformation of $\mathscr{Q} \longrightarrow \mathscr{P}_R$, except for the following cases. The decay factor $\exp(-\mu L/q\tau)$ is dropped, and the factor DP_{source}/DP_{mag} (see Appendix 8) must be included in ADD_i.

When the LEM is used, β is picked instead of α, and the Jacobian $\partial(Q, \beta)/\partial(\alpha, \xi)$ is replaced by $\partial Q/\partial \xi$.

In order to calculate the average cross section, nuclear absorption A_N, (see Appendix 6) and the muon contribution (κ_μ/κ_π) (see Appendix 4) must be included in (2.23). The equation becomes

$$R = \overline{\left[\partial\sigma(\bar{k}', \bar{\theta}_{cm}/\partial\Omega_{cm}\right]} \; A_N(1 + (\kappa_\mu/\kappa_\pi))\,\kappa_\pi \; . \tag{2.29}$$

From (2.27) the average cross section is obtained.

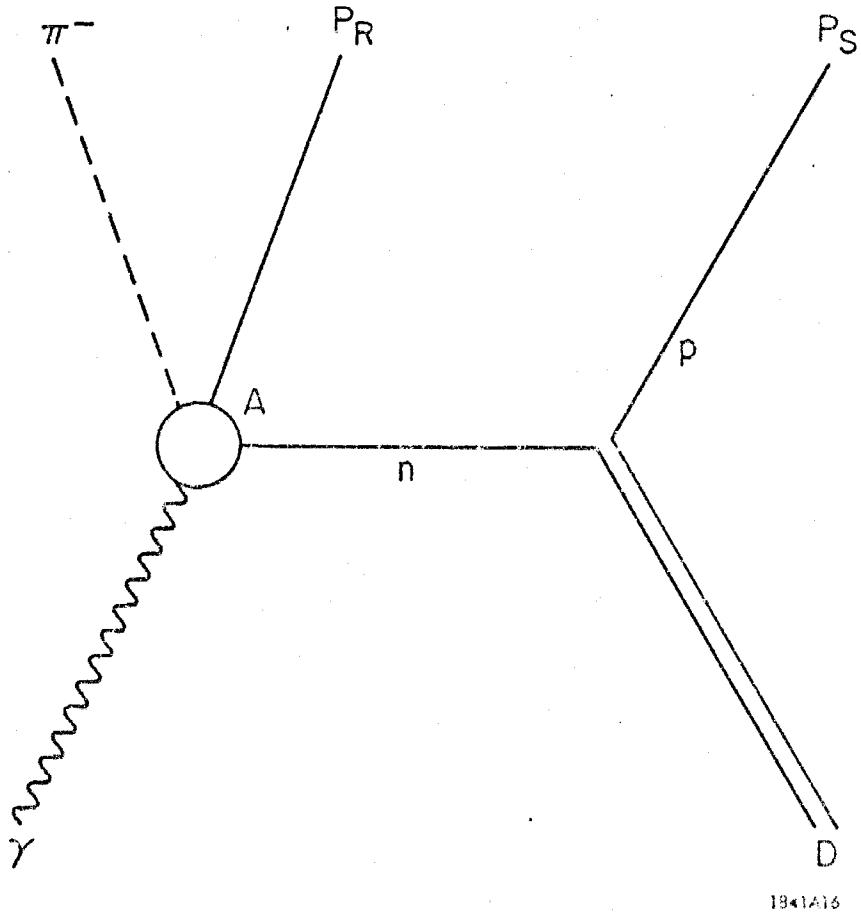

FIGURE 21

The Spectator Model

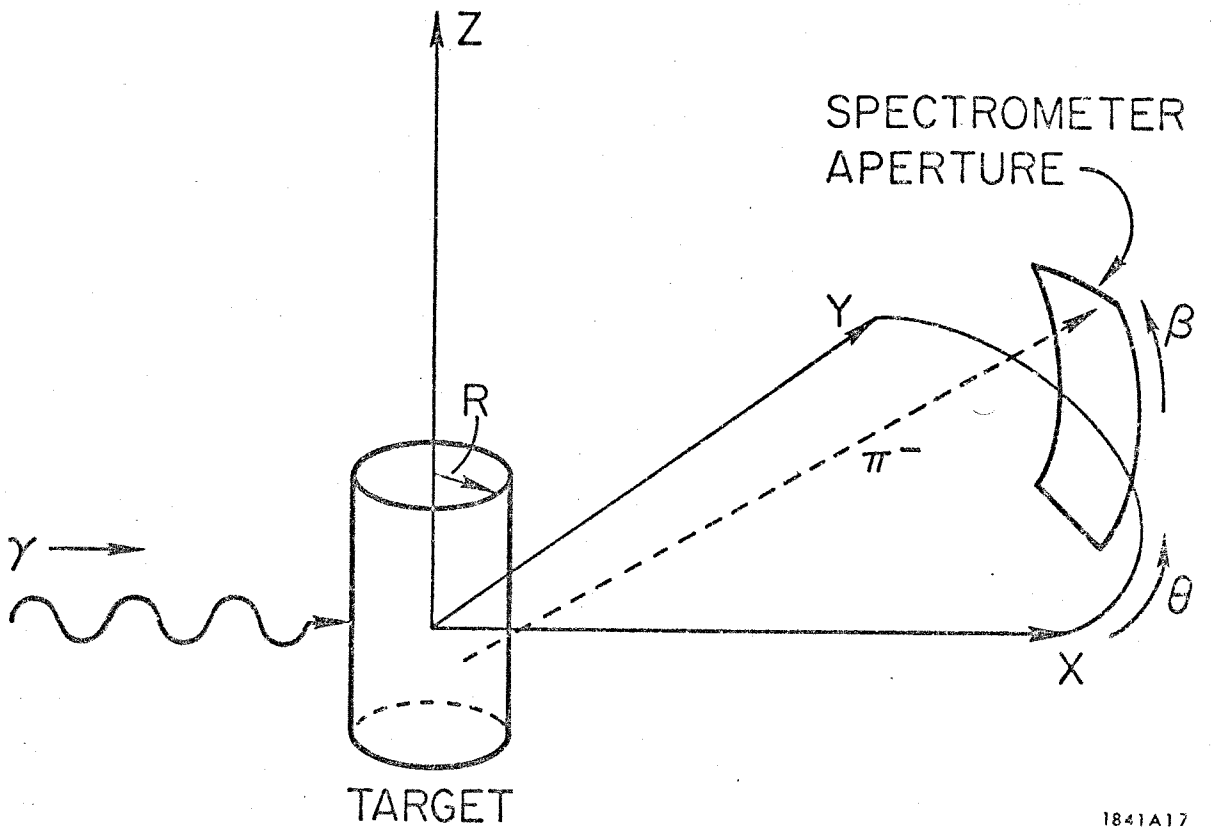

FIGURE 22

The Laboratory Frame

APPENDIX III

MONTE CARLO INTEGRATION

Monte Carlo integration has been used to compute the integrals described in Appendices II, IV, and VII. In this appendix a short proof of the method will be given along with a few examples to illustrate the usefulness of the technique.

We will evaluate the integral $\int_a^b f(x)dx$. It is assumed that this integral is difficult to do analytically. To begin we define

$$< f > = \frac{\int_a^b f(x)\,dx}{\int_a^b dx} = \frac{\int_a^b f(x)\,dx}{b-a} \tag{3.1}$$

In the Monte Carlo process N values of x are chosen randomly in $[a,b]$. From the f(x)'s associated with the chosen x's, the best estimate of $< f >$ is

$$\overline{f} = \frac{1}{N}\sum_{i=1}^{N} f(x_i) \ , \tag{3.2}$$

and

$$\lim_{N \to \infty} \overline{f} = < f > \ . \tag{3.3}$$

Comparing equations (3.1), (3.2), and (3.3) it is easy to see that

$$\lim_{N \to \infty} \frac{b-a}{N}\sum_{i=1}^{N} f(x_i) = \int_a^b f(x)\,dx \ , \tag{3.4}$$

which is the required result.

It is also useful to know what the expected deviation of the Monte Carlo result from the true result is after N trials. From standard error theory [32], the deviation in $\bar{f}$ after N trials is

$$\sigma = \frac{1}{\sqrt{N-1}} \left\{ \frac{1}{N} \sum_{i=1}^{N} f^2(x_i) - \bar{f}^2 \right\}^{\frac{1}{2}} , \tag{3.5}$$

so the error in the integral is

$$E = \frac{b-a}{\sqrt{N-1}} \left\{ \frac{1}{N} \sum_{i=1}^{N} f^2(x_i) - \bar{f}^2 \right\}^{\frac{1}{2}} . \tag{3.6}$$

For $N \gg 1$, Eq. (3.6) can be approximated by

$$E = \frac{b-a}{N} \left\{ \sum_{i=1}^{N} f^2(x_i) - \frac{1}{N} \left(\sum_{i=1}^{N} f(x_i) \right)^2 \right\}^{\frac{1}{2}} . \tag{3.7}$$

This is the expected deviation of the Monte Carlo calculation after N trials.

There are many numerical integration techniques that could be used to compute the integral used in the above proof. These techniques are also more accurate and less time-consuming than the Monte Carlo process just presented. However, as the number of dimensions in the integral increases, the numerical methods become very cumbersome and computation time increases as a power of the number of dimensions. The Monte Carlo technique, however, experiences no such difficulties. It is almost as easy to do a n-dimensional integration as it is to do a one-dimensional integration. For example, the equivalent of Eq. (3.4) for the two-dimensional integral $\int_a^b dx \int_c^d dy\, f(x, y)$ is

$$\lim_{N \to \infty} \frac{(b-a)(d-c)}{N} \sum_{i=1}^{N} f(x_i, y_i) = \int_a^b dx \int_c^d dy\, f(x,y) \,. \tag{3.8}$$

Extensions to higher dimensions should be clear. In Appendices II, IV, and VII, there were 9 and 12 dimensional integrations to compute. Here the Monte Carlo technique is clearly superior to the numerical methods.

Some other formulae using Monte Carlo integration are the following:

1. $$\int_a^b dx \int_{g(x)}^{h(x)} dy\, f(x,y) = \lim_{N \to \infty} \frac{b-a}{N} \sum_{i=1}^{N} [h(x_i) - g(x_i)] f(x_i, y_i) \,. \tag{3.9}$$

In this case x must be chosen first in the interval $[a, b]$. Let this x be x_i. They must be chosen in the interval $[h(x_i), g(x_i)]$.

2. $$\int_a^b f(x)g(x)\,dx = \lim_{N \to \infty} \frac{h(b)-h(a)}{N} \sum_{i=1}^{N} f(h^{-1}(u_i)) \tag{3.10}$$

where

$$u = \int_c^x g(t)\,dt = h(x) \,, \tag{3.11}$$

and c is an arbitrary constant. In this case it is assumed that the integral (3.11) can be done analytically. The u's are chosen randomly in the interval $[h(a), h(b)]$.

3. $$\int_a^b f(x)\,dx = \int_a^b \frac{f(x)}{g(x)}\, g(x)\,dx = \lim_{N \to \infty} \frac{h(b)-h(a)}{N} \sum_{i=1}^{N} \frac{f(h^{-1}(u_i))}{g(h^{-1}(u_i))} \,. \tag{3.12}$$

This equation uses the same substitution and evaluation process as in Eq. (3.10). Equation (3.12) is very useful when $[a, b]$ is $[-\infty, \infty]$. In this instance the Gaussian or other suitable functions are substituted for g(x).

APPENDIX IV

π-μ DECAY CORRECTION

In this experiment a significant number of pions decayed via the reaction $\pi \rightarrow \mu + \nu$. The detection system was unable to distinguish a π from a μ, so that a significant number of triggers were caused by μ's. This made necessary a computation of the experimental response to the μ's.

In the development of the response integral for muons and for the remainder of the appendix, the notations and definitions described in Appendices 1 and 2 will be used.

We will take Eqs. (2.15), (2.16), and (2.18) plus the substitutions $d\Omega = d\beta\, d\theta$ and $R = C/H$ to write the integral

$$R = \eta \frac{P_0}{E_0} \int_{\Delta Z}\int_{\Delta Y}\int_{X}\int_{Q}\int_{\Omega}\int_{P_S} \frac{k' M_n}{K E_n} \frac{B(K, E_0, Y, Z)}{K} \frac{\partial \sigma}{\partial \Omega_{cm}}(k', \theta_{cm}) \frac{\partial \Omega_{cm}}{\partial \Omega} \times \frac{\partial K}{\partial q}\left[\phi^2(P_S) \frac{d^3 P_S}{(2\pi)^3}\right] dX\, dY\, dZ\, dQ\, d\Omega \quad . \tag{4.1}$$

This integral is essentially another form of (2.21) except that the pion decay factor is not included. To turn (4.1) into a rate calculation for μ's we must include:

1. $\frac{\mu}{q\tau} \exp(-\mu L/q\tau)\, dL$ — the probability that a π decays in the path interval $(L, L + dL)$.
2. $\frac{d\Omega_\mu}{4\pi}$ — the probability that the μ decays into the solid angle $d\Omega_\mu$ in the π rest frame.
3. $S(q, \Omega, X, Y, Z, L, \Omega_\mu)$ — the success (either 1 or 0) of detecting a μ given a specified event.

Including factors in (4.1), we get the expression for the muon counting rate

$$R = \eta \frac{P_0}{E_0} \int_{\Delta Z} \int_{\Delta Y} \int_X \int_Q \int_\Omega \int_L \int_\Omega \int_{\mu} \int_{\vec{P}_S} \frac{k' M_n}{K E_n} \frac{B(K, E_0, Y, Z)}{K} \frac{\partial \sigma}{\partial \Omega_{cm}} (k', \theta_{cm}) \frac{\partial \Omega_{cm}}{\partial \Omega}$$

$$\times \frac{\partial K}{\partial q} \left[\phi^2 (P_S) \frac{d^3 P_S}{(2\pi)^3} \right] S(q, \Omega, X, Y, Z, L, \Omega_\mu) \frac{\mu}{q\tau} \exp(-\mu L / q\tau) \, dL \tag{4.2}$$

$$\times \frac{\partial \Omega_\mu}{4\pi} \, dX \, dY \, dZ \, dQ \, d\Omega \ .$$

Now the spectrometer detects the μ, so there is an uncertainty in the momentum and direction of the π it came from, hence the integrations over Q and Ω are not just limited to the spectrometer acceptance but extend over all values. With (4.2) we can define the muon response integral, κ_μ, in the same manner that the pion response, κ_π, was defined (see Appendix 2).

The muon response is then

$$\kappa_\mu = \eta \frac{P_0}{E_0} \int_{\Delta Z} \int_{\Delta Y} \int_X \int_Q \int_\Omega \int_L \int_\Omega \int_{\mu} \int_{\vec{P}_S} \frac{k' M_N}{K E_n} \frac{B(K, E_0, Y, Z)}{K} \frac{\partial \Omega_{cm}}{\partial \Omega} \frac{\partial K}{\partial q} \left[\phi^2 (P_S) \frac{d^3 P_S}{(2\pi)^3} \right]$$

$$\times S(q, \Omega, X, Y, Z, L, \Omega_\mu) \frac{\mu}{q\tau} \exp(-\mu L / q\tau) dL \frac{d\Omega_\mu}{4\pi} \, dX \, dY \, dZ \, dQ \, d\Omega \ , \tag{4.3}$$

which can be evaluated by Monte-Carlo integration.

There are two problems in computing κ_μ by Monte-Carlo methods. One is to find an efficient means of computing $\pi - \mu$ trajectories through the spectrometer, and the other is a means of picking the Q, Ω variables to be assured of getting a reasonable number of successful events.

Thiessen[33], Boyden[34], and Kilner[35] solved the first problem by using the effective edge model of the spectrometer. [36,37] The effective edge preserves the spectrometer's optical properties while allowing a minimum amount of trajectory computation. To test that the optical properties are indeed preserved,

Thiessen's ray tracing programs[33] for the effective edge were used to generate the spectrometer resolution functions which could then be compared to those computed correctly (see Appendix V). In Figure (23) are the results for the HEMA spectrometer. Although the effective edge curve is jagged, because of program inefficiencies, the comparison was close enough to justify the use of the model. Similar results were obtained for the other spectrometers.

To find a means of choosing the variable Q , a study was made of Thiessen's $\pi-\mu$ resolution functions.[10] An example of these functions can be seen in Figure (24).

It was found that the mean Q of the $\pi-\mu$ resolution functions was shifted on the average + 0.025 from the listed mean Q in Wolverton's spectrometer report [37] and in Appendix V. We shall define

$$< Q >_{\mu} = < Q > + 0.025 ,$$

where $< Q >$ is listed mean Q . It was also found that the ratio of the $\pi-\mu$ and π resolution widths, $(\sigma_{\mu}/\sigma_{\pi})$, was a linear function of the mean π momentum. (See Figure 25) The resolution width ratio was fitted to the equation

$$(\sigma_{\mu}/\sigma_{\pi}) = A + B \cdot < q > \qquad (4.4)$$

where

σ_{μ} RMS resolution width of $\pi-\mu$ events

σ_{π} RMS resolution width of π events

A, B fit parameters

$< q > = P_0(1 + < Q >)$

The results of this fit are in Table (10).

With the aid of (4.4) we can approximate the $\pi-\mu$ resolution function by a Gaussian with a mean $< Q >_{\mu}$, and standard deviation σ_{μ}. If the Q's for the Monte Carlo process are weighted by this Gaussian a reasonable number of successes is assured. Examining Figure (24) it is easy to see that a Guassian is a mediocre fit to that curve. However, to pick Q 's weighted by the curve in Figure (24), interpolation from a table would be required. Gaussian weighting is much faster and saves computer time. Errors are not induced into the Monte Carlo integration by the Gaussian approximation if the weighting curve is multiplied out as in (3.12) of the Monte Carlo appendix. This is done in (4.7) further on.

For choosing Ω, Thiessen's [33] prescription was used. For a given Q a π can either decay before reaching the spectrometer or after reaching it. If it decays before, it is possible to pick an Ω-window, $\Delta\Omega(Q, L)$, such that the μ has a non-zero possibility of entering the spectrometer's entrance aperature. If the π decays after the magnet, the Ω-window is defined to be the entrance aperature.

The integral κ_{μ} can now be evaluated. The results of the appendix on Monte Carlo integration will be applied without explanation. For each event, i, in the Monte Carlo process, the values for the integration variables are chosen in the following order.

1. Z_i limits $-\Delta Z/2 < Z_i < \Delta Z/2$
2. Y_i limits $-\Delta Y/2 < Y_i < \Delta Y/2$
3. X_i limits $-(r^2-Y^2)^{\frac{1}{2}} < X < (r^2-Y^2)^{\frac{1}{2}}$
4. Q_i limits $-\infty < Q_i < \infty$
5. L_i limits $0 < L_i < L_0$

6. θ_i } limits the Ω-window $\Delta\Omega(Q_i, L_i)$
7. β_i }
8. $\cos\theta_{\mu_i}$ limits $-1 < \cos\theta_{\mu_i} < +1$
9. ϕ_{μ_i} limits $0 < \phi_{\mu_i} < 2\pi$
10. $\cos\theta_{S_i}$ limits $-1 < \cos\theta_{S_i} < +1$
11. ϕ_{S_i} limits $0 < \phi_{S_i} < 2\pi$
12. P_{S_i} limits $0 < P_{S_i} < \infty$

where L_0 is the particle path length from the target to the momentum counters. The variable Q is weighted by the Gaussian.

$$G(Q) = \frac{1}{\sqrt{2\pi}} \exp\left[-\frac{(Q - \langle Q \rangle_\mu)^2}{2\sigma_\mu^2}\right] , \tag{4.5}$$

and the variable L is weighted by the exponential

$$F_{q_i}(L) = \frac{1}{q_i \tau} \exp\left[-\frac{\mu L}{q_i \tau}\right] . \tag{4.6}$$

As in Appendix 2 the values of P_S are weighted by $P_S^2 \phi^2(P_S)/(2\pi)^3$. If the event is successful (i.e., $S(q_i, \Omega_i, X_i, Y_i, Z_i, L_i, \Omega_{\mu_i}) = 1$) we compute

$$ADD_i = (r^2 - Y_i^2)^{\frac{1}{2}} \frac{k_i! M_n}{K_i E_{n_i}} \frac{B(K_i, E_0, Y_i, Z_i)}{K_i} \left(\frac{\partial\Omega_{cm}}{\partial\Omega}\right)_i \left(\frac{\partial K}{\partial q}\right)_i \exp\left[\frac{(Q_i - \langle Q \rangle_\mu)^2}{2\sigma_\mu^2}\right] \tag{4.7}$$

$$\times \Delta\Omega(Q_i, L_i)(1 - \exp[-\mu L_0/q_i \tau]) .$$

If $S(\ldots) = 0$ (i.e., the event was unsuccessful) ADD_i is set to zero. After a specified number of trials, N, κ_μ can be best approximated by

$$\kappa_\mu = \text{NORM} \sum_{i=1}^{N} ADD_i \tag{4.8}$$

where

$$\text{NORM} = 2\eta \frac{P_0}{E_0} \frac{\sqrt{2\pi}\ \sigma_\mu\ \Delta Y \Delta Z}{N} \tag{4.9}$$

The μ response, κ_μ, was calculated for a scattering of various experimental settings. These were compared to π response, κ_π, at the same settings and the ratios (κ_μ/κ_π) were formed. In Figure (26) the ratios κ_μ/κ_π are plotted as a function of $\mu L_0/\langle q \rangle \tau$ for channels T, TC, BC, and B respectively. The dependence is approximately linear. On this basis the fit

$$\left(\frac{\kappa_\mu}{\kappa_\pi}\right) = A + B \left(\frac{\mu L_0}{\langle q \rangle \tau}\right) \tag{4.10}$$

was made to represent the general result. This saved much computing time. The fits are printed in Table II. It is seen that these fits are almost identical except the fit for T which is slightly lower than the rest. One possible explanation for this could be the cutoff of the high Q tail (see Figure (24)) by the bremsstrahlung end-point.

TABLE 10

RMS Resolution Spread for the $\pi - \mu$ Decay Process

σ_μ RMS $\pi - \mu$ resolution width

σ_π π RMS resolution width

$< q > = P_0(1 + <Q>)$

SPECTROMETER	A	B
HEMA	7.40	- 0.00191
OUT R*	4.25	—
LEM	7.22	- 0.00484

* There were only 3 OUT R π settings used in this experiment. These had very close momentum settings so no fit was attempted.

TABLE 11

Muon-to-Pion Response Ratio

$$\frac{\kappa_\mu}{\kappa_\pi} = A + B \cdot \frac{\mu L_0}{< q > \tau}$$

κ_μ	muon	response
κ_π	pion	response
μ	pion	mass
L_0	pion	path length
τ	pion	lifetime

CHANNEL	A	B
T	-0.061805	0.52577
TC	-1.2071	0.65936
BC	-0.76085	0.62824
B	-0.84003	0.64890

FIGURE 23

Comparison of Monte Carlo and True Resolution Functions for HEMA

The smooth curve is the true resolution function.

The jagged curve is the Monte Carlo approximation to the resolution function.

β = verticle acceptance angle of HEMA

P_0 = the central momentum of HEMA

The areas under the curves are as follows:

	True (rad.)	Monte Carlo (rad.)
T	0.002723	0.002979
TC	0.002582	0.002704
BC	0.002460	0.002532
B	0.002361	0.002368

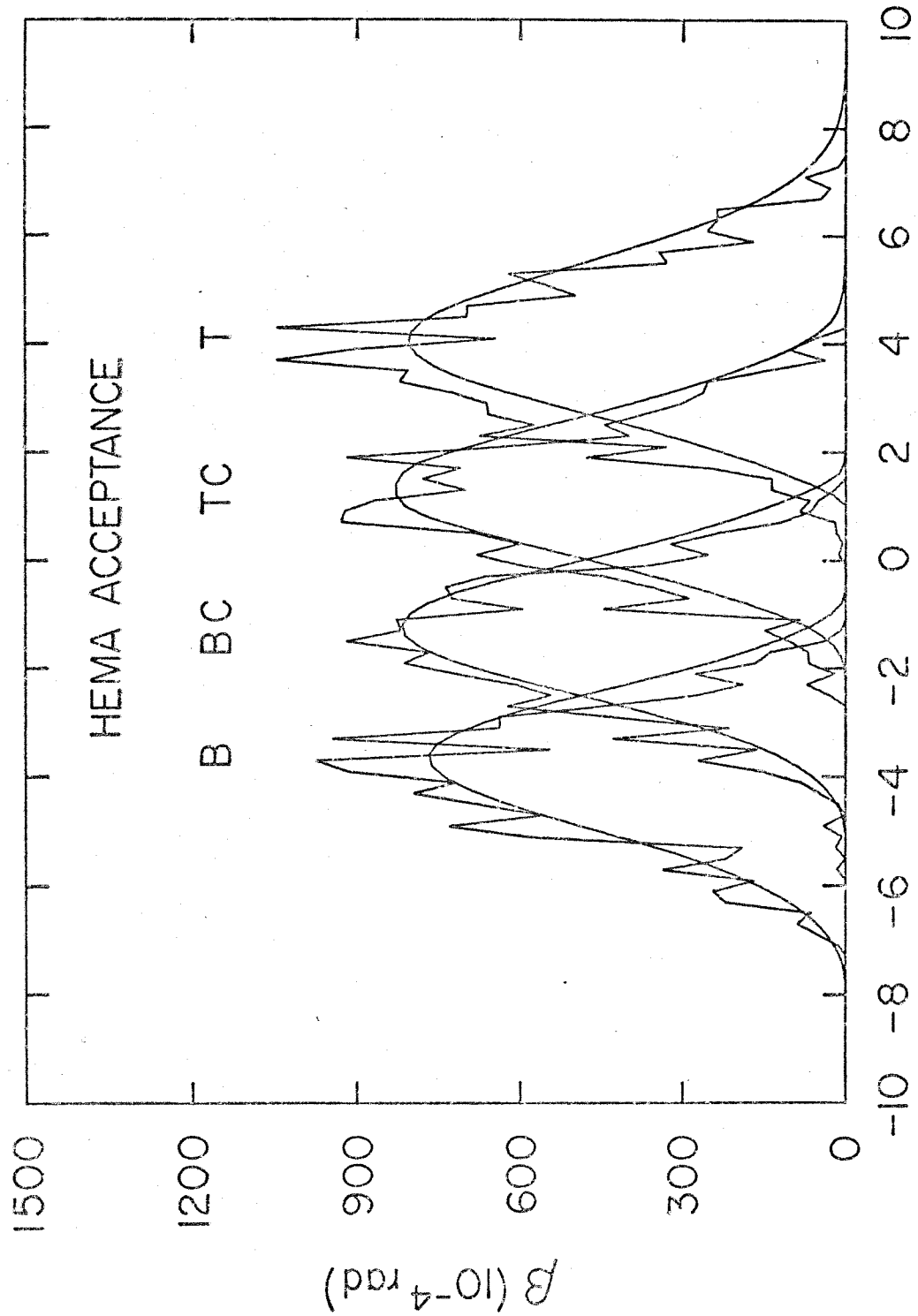
HEMA ACCEPTANCE
B BC TC T
β (10⁻⁴ rad)
Q=(P-P0)/P0(%)
1500
1200
900
600
300
0
-10 -8 -6 -4 -2 0 2 4 6 8 10
184850

FIGURE 23

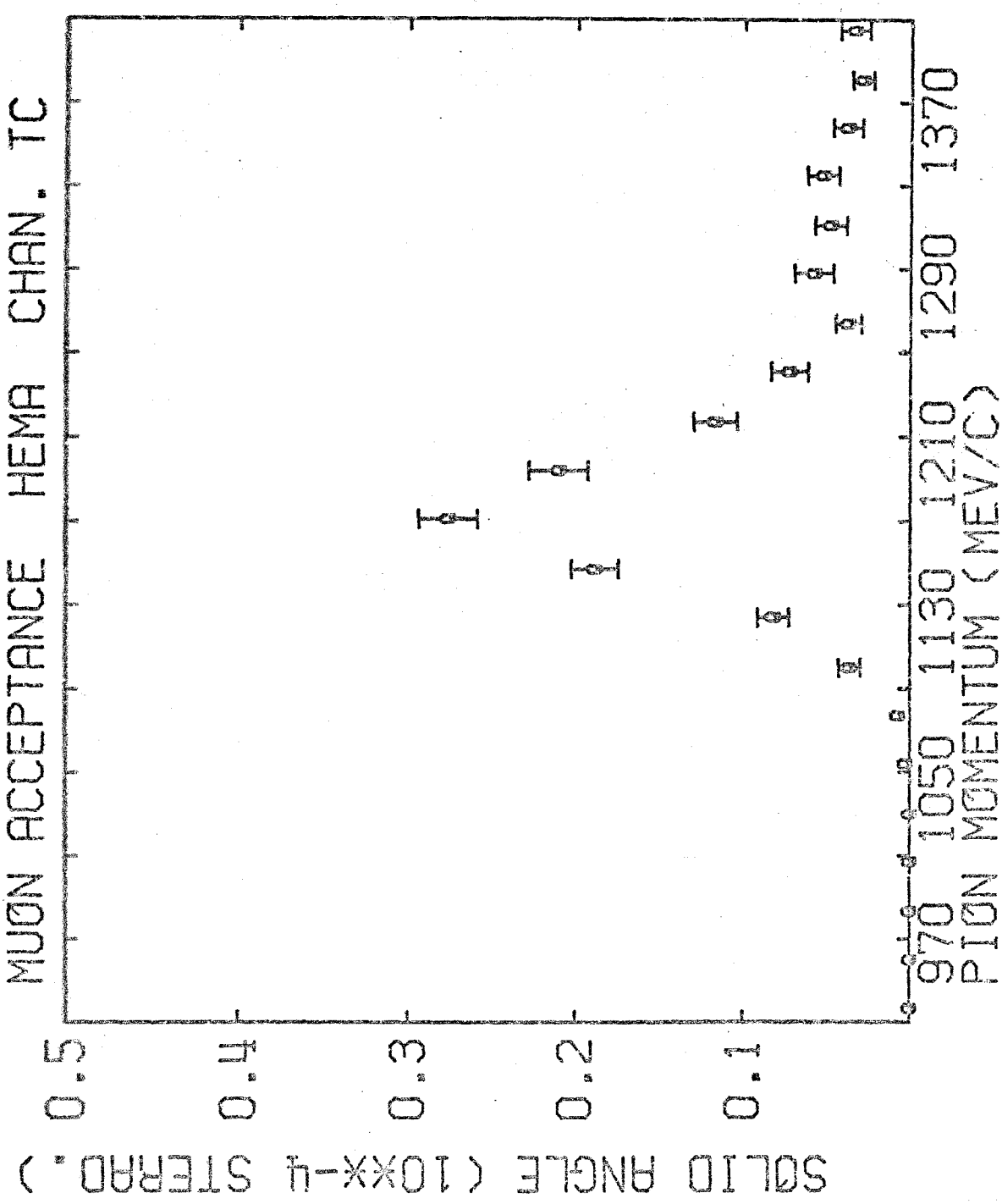

FIGURE 24

Muon Resolution Function

FIGURE 25

Muon-to-Pion RMS Resolution Spread Ratios

σ_{μ} = RMS resolution spread for μ's

σ_{π} = RMS resolution spread for π's

The π's are considered to have originated in the target. The μ's are considered to have originated from $\pi \rightarrow \mu + \nu$ decays.

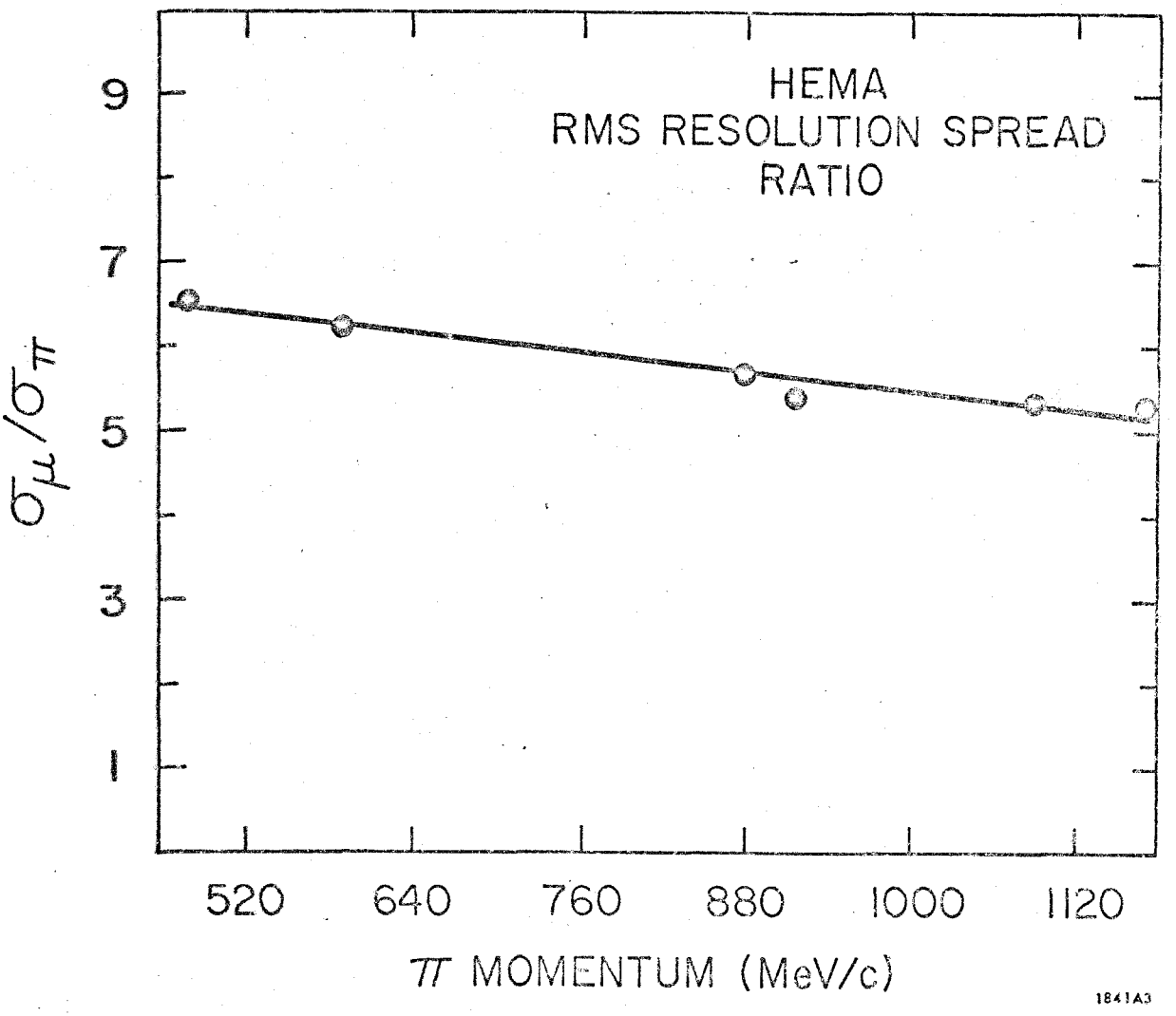
HEMA
RMS RESOLUTION SPREAD
RATIO
σ_μ/σ_π
9
7
5
3
1
520
640
760
880
1000
1120
π MOMENTUM (MeV/c)
1841A3

FIGURE 25.1

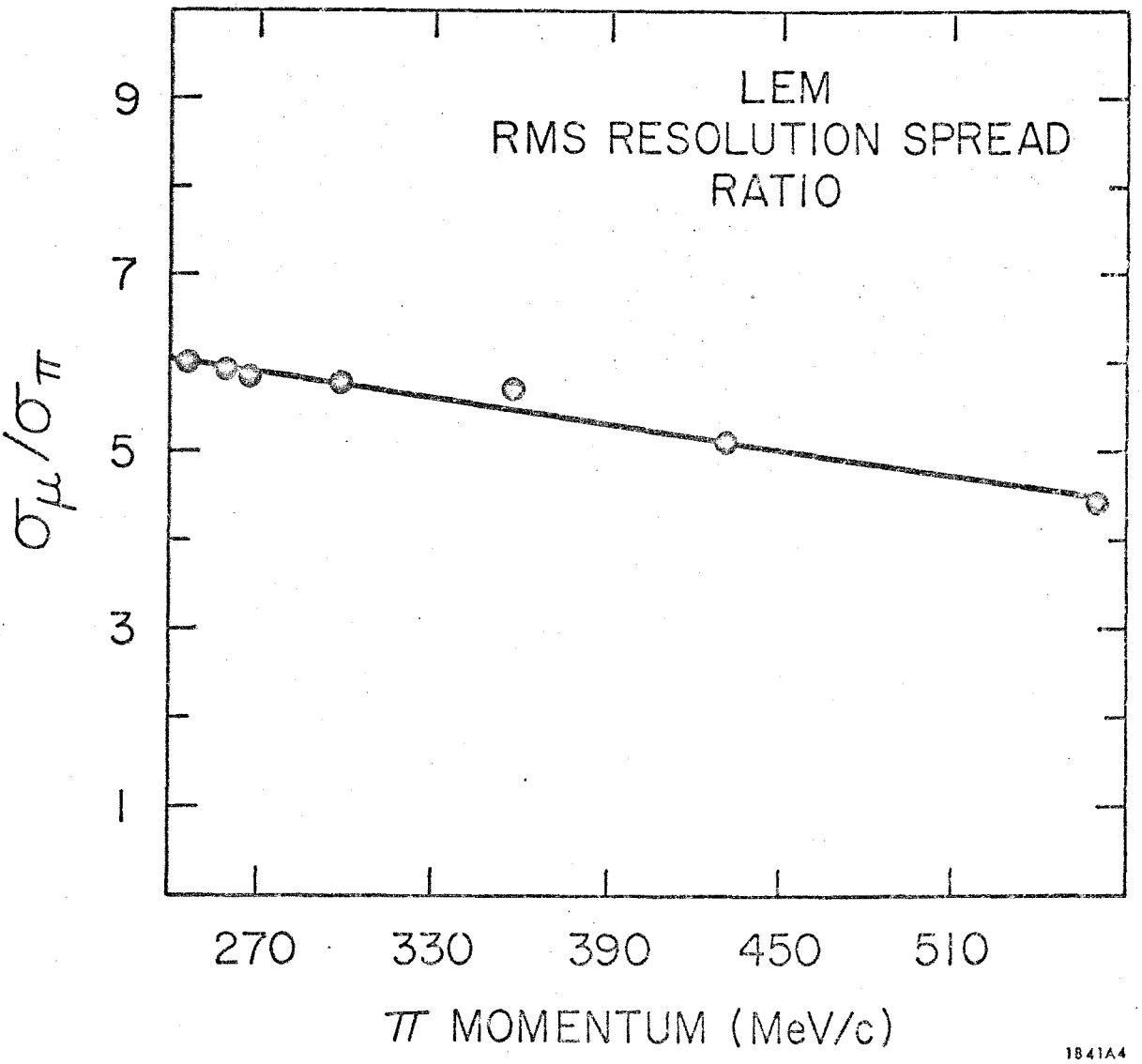
LEM
RMS RESOLUTION SPREAD
RATIO
9
7
5
3
1
σ_μ / σ_π
270
330
390
450
510
π MOMENTUM (MeV/c)
1841A4

FIGURE 25.2

FIGURE 26

MUON TO PION EXPERIMENTAL RESPONSE RATIO

(KAPPA MU/ KAPPA PI) is identical to κ_μ/κ_π in the text.

ML/PT is identical to $\mu L_0/ < q > \tau$ in the text.

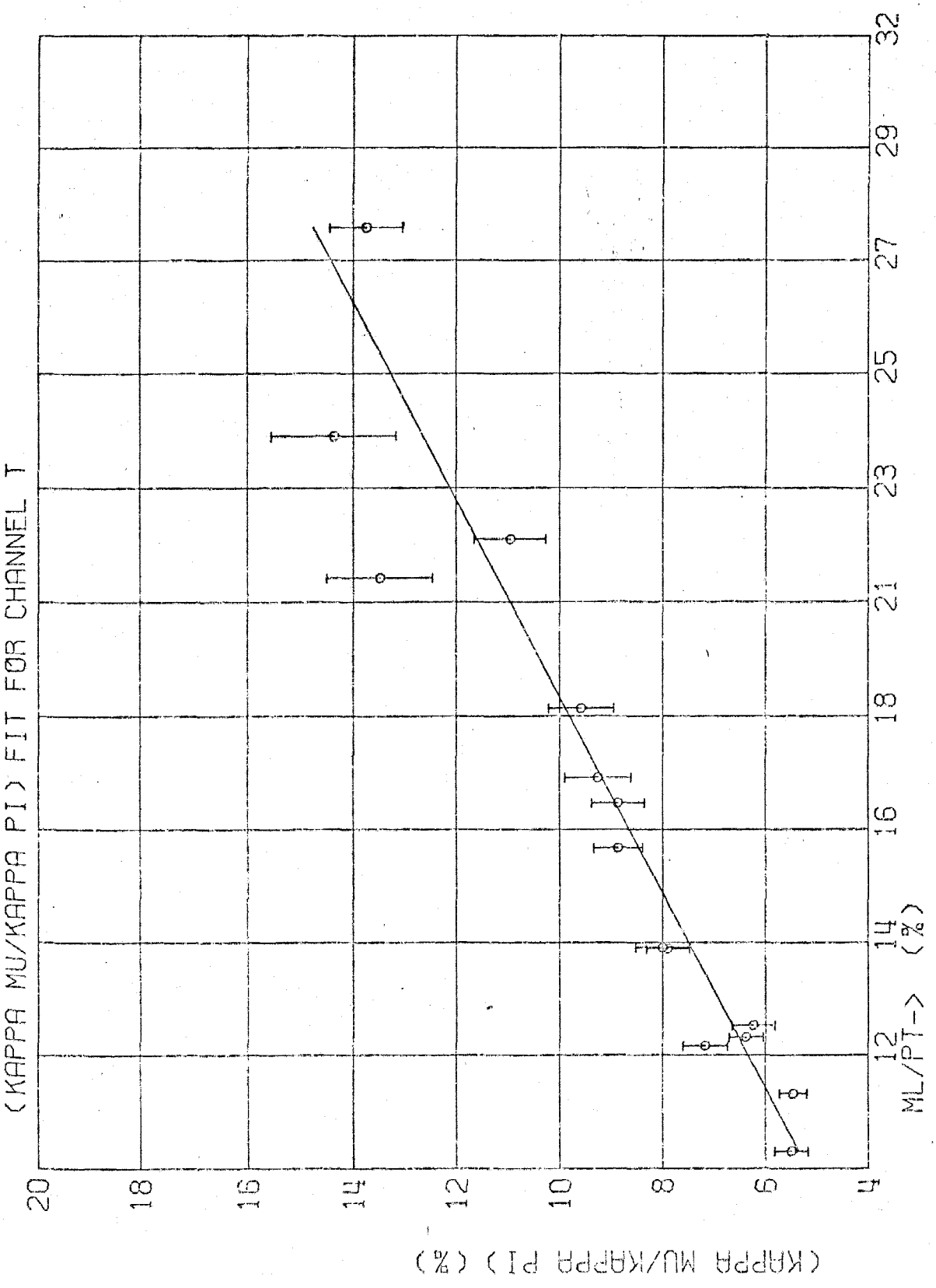
(KAPPA MU/KAPPA PI) FIT FOR CHANNEL T
(KAPPA MU/KAPPA PI) (%)
ML/PT-> (%)
20
18
16
14
12
10
8
6
4
12
14
16
18
21
23
25
27
29
32

FIGURE 26.1

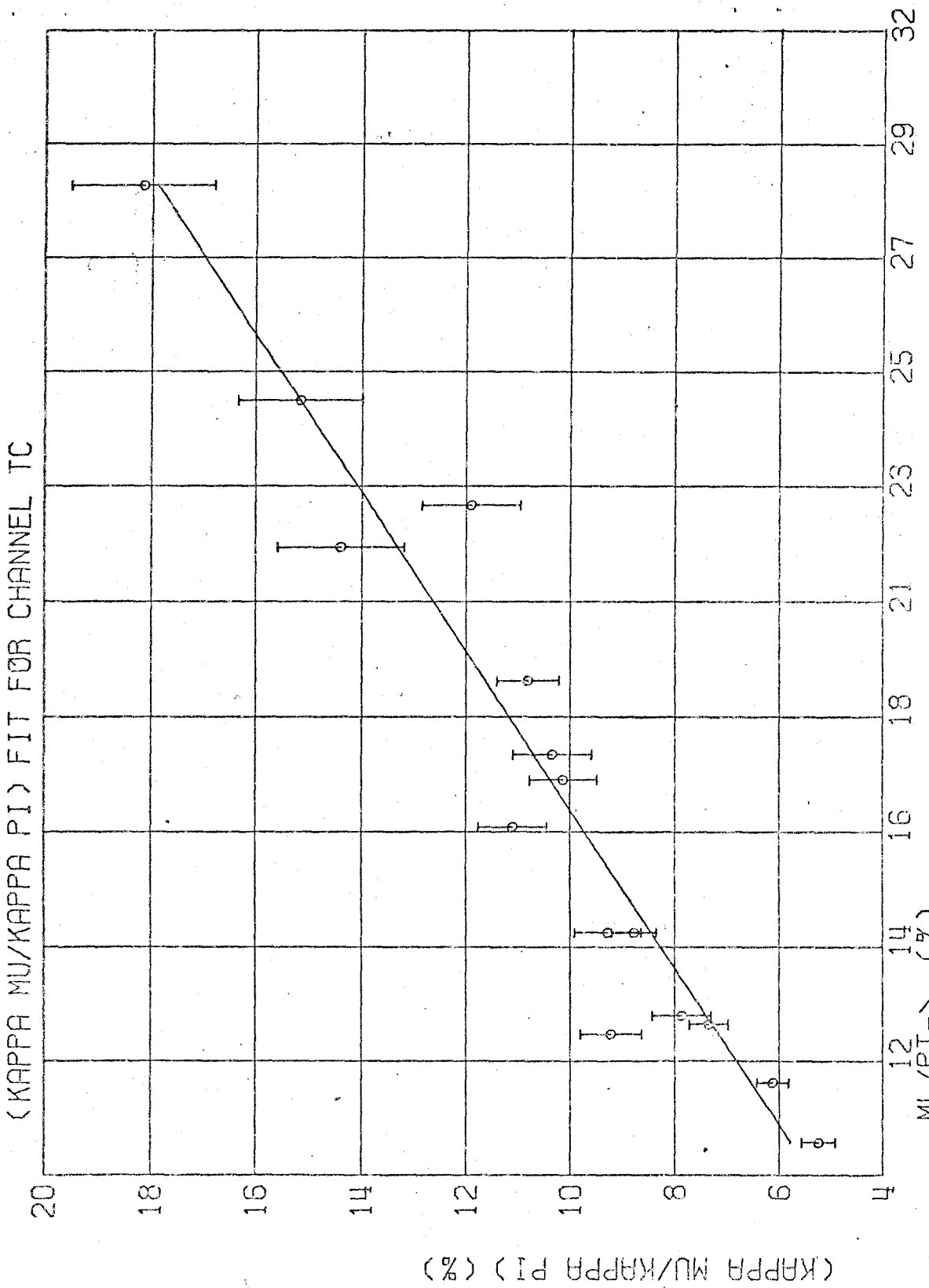
(KAPPA MU/KAPPA PI) FIT FOR CHANNEL TC
(KAPPA MU/KAPPA PI) (%)
20
18
16
14
12
10
8
6
4
12
14
16
18
21
23
25
27
29
32
ML/PT-> (%)

FIGURE 26.2

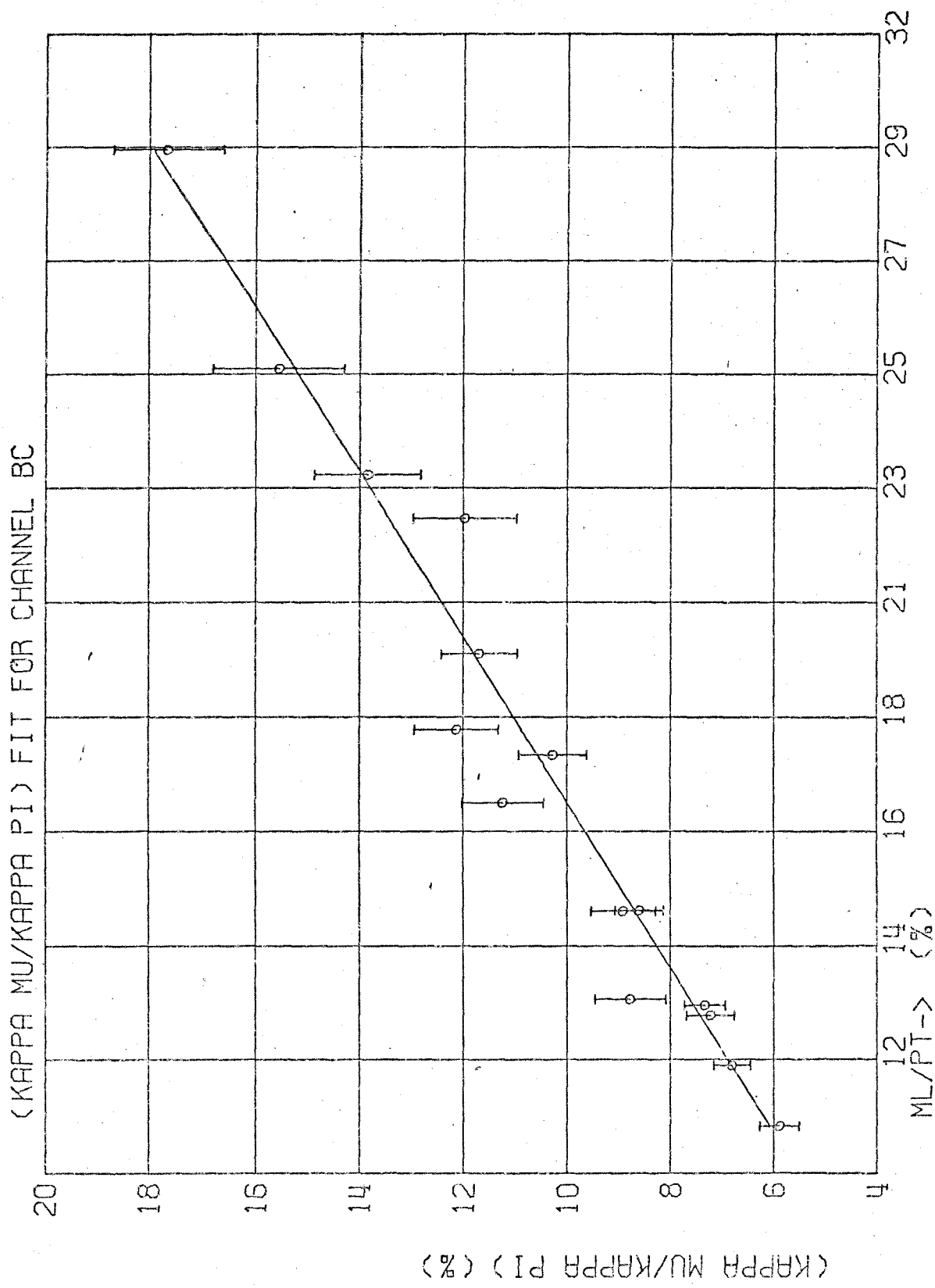
(KAPPA MU/KAPPA PI) FIT FOR CHANNEL BC
(KAPPA MU/KAPPA PI) (%)
ML/PT-> (%)
20
18
16
14
12
10
8
6
4
12
14
16
18
21
23
25
27
29
32

FIGURE 26.3

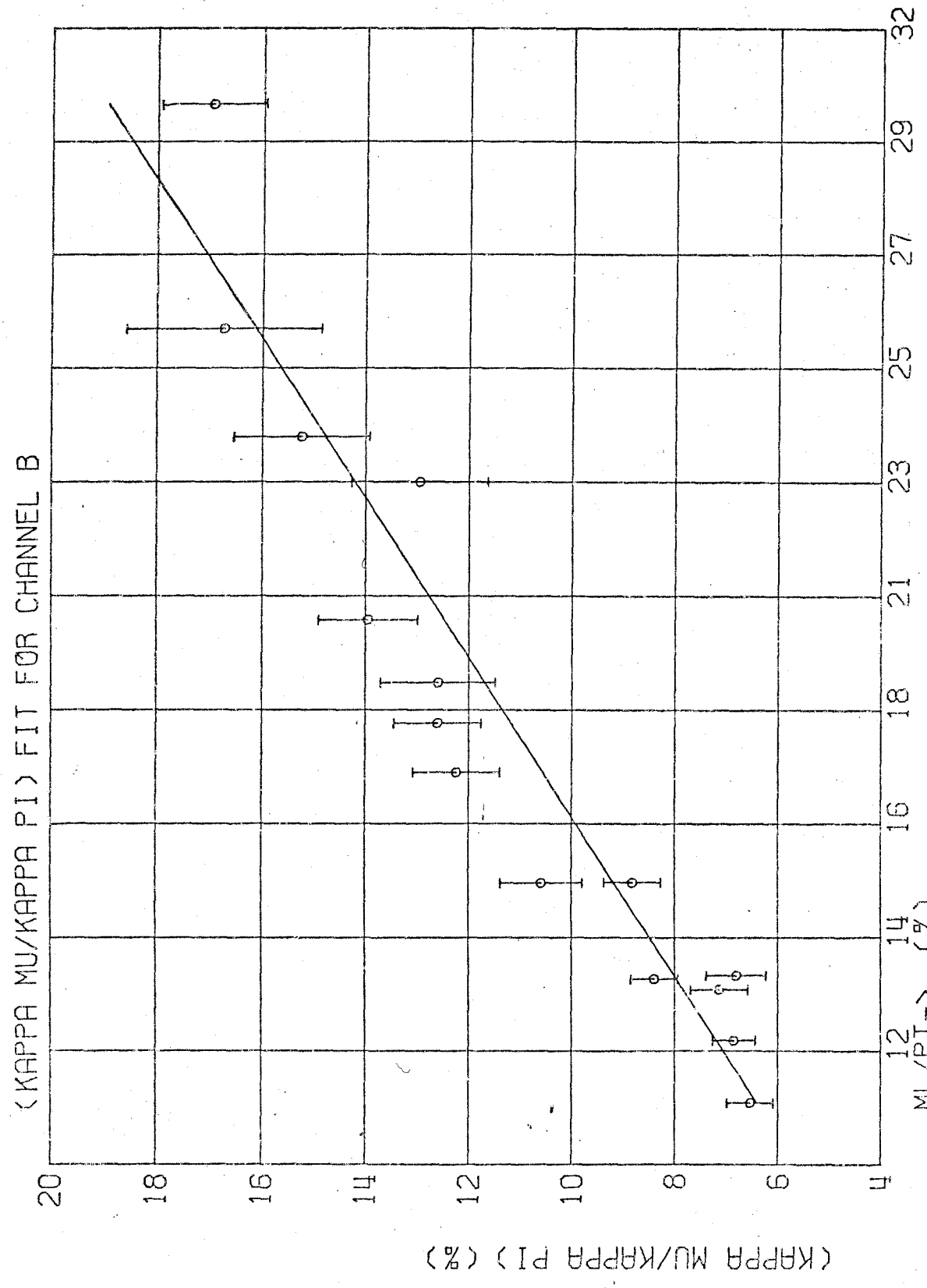
(KAPPA MU/KAPPA PI) FIT FOR CHANNEL B
(KAPPA MU/KAPPA PI) (%)
20
18
16
14
12
10
8
6
4
12
14
16
18
21
23
25
27
29
32
ML/PT-> (%)

FIGURE 26.4

APPENDIX V

SPECTROMETERS

In this experiment three spectrometer configurations were used: HEMA, OUTR, and LEM with maximum effective momentum of 1200, 1670, and 600 MeV/c respectively. HEMA and OUTR used the same magnet system, but differed in the positions of the counter telescope. The LEM configuration used another magnet system. All three configurations had four counters which defined four momentum channels, T, TC, BC, and B. The T channel detected the highest momentum, and the B channel, the lowest. Information regarding field measurements, focusing properties, calibration, etc., will be found in other sources [36,37,10,11,12,13,5], and the information will not be repeated here. Only details particular to this experiment will be discussed.

Before the experiment commenced, it was felt that the existing 7 channel momentum counters [10] on the LEM were far too small for the resolutions that would be achieved in this experiment, so it was decided to replace them. The dimensions of the 4 new counters are given in Figure (27). The area they cover is approximately the same as the area covered by the old counters.

The new counters necessitated a recalculation of the LEM resolution functions and acceptance properties. There existed a program, HAT009B [38], that performed this calculation. The resolution functions for 10 and 15 k G can be seen in Figures (28) and (29). The resolution functions give the vertical angle acceptance as a function of the relative momentum, $Q = (P-P_0)/P_0$, where P_0 is the central spectrometer momentum. The horizontal angle acceptance, $\Delta\theta$, which lies on a plane parallel to the spectrometer field is unaffected

by Q . The acceptance properties for LEM averaged over the 10 and 15 k G resolutions are summarized in Table 12.

To run the Monte Carlo processes discussed in Appendices II and IV it was necessary to relate counter and target positions to particle momentum and direction. This information was not directly available from the spectrometer reports. [36,37]

From the report by F. Wolverton [37] the following third order polynomial fits were available for HEMA and OUTR.

$$\left.\begin{aligned} Q &= F(\beta, \zeta, Z) \\ \beta &= G(Q, \alpha, Z) \end{aligned}\right\} \tag{5.1}$$

where

Z	verticle position of the target
α	verticle position in aperature counter
ζ	verticle position in momentum counters.

For a particle produced in the beam spot center of the target with momentum P_0, and $\beta = 0$ the (Z, α, ζ) coordinates would be (0, 0, 0).

However, to be of use in the Monte Carlo programs, polynomial fits of the form

$$\left.\begin{aligned} Q &= f(Z, \alpha, \zeta) \\ \beta &= g(Z, \alpha, \zeta) \end{aligned}\right\} \tag{5.2}$$

were needed. A program, LITTLE, was written that randomly generated quintuplets $(Q, \beta, Z, \alpha, \zeta)$ from (5.1). LITTLE then produced the fits (5.2) from a least squares fit to the generated quintuplet data. These fits are tabulated in Tables 13 and 14.

To check that these fits were sufficiently accurate, the above process was reversed (i.e., the (5.2) fits were used to regenerate the (5.1) fits). This output was compared to the original (5.1) fits. For the most significant coefficients the comparison was accurate to less than one percent, and the overall accuracy was around a few percent. This showed that the coefficients were uniquely reproducible to a sufficient degree.

For LEM there was no information on how the position in the aperature counter, α, affected Q and β. It was therefore assumed that the $\Delta\beta$ window reported by Thiessen was independent of Q and Z. The polynomial fit given by Thiessen [36]

$$\zeta = (Z, \beta, Q) \tag{5.3}$$

was still inappropriate for use. The same process described previously was used to generate the more useful polynomial fit

$$Q = h(\beta, \zeta, Z) , \tag{5.4}$$

except in this case random sets of quadruplets (Q, β, ζ, Z) were generated as the data. This fit is presented in Table 15 The reversed process again reproduced the input with sufficient accuracy.

As an added check to confirm the trust in the generated fits (5.2) and (5.3) a Monet Carlo program, ACCEPTED, was used to compute the $\Delta Q \Delta \Omega$ acceptances of the spectrometer configurations. The results are presented in Table 16. The agreement there is well within the Monte Carlo accuracy.

TABLE 12

LEM Acceptance Properties

9.5 × 2.75 inch aperature counter

1.25 inch momentum counters

Momentum Channel	Mean Q	$\Delta\beta$ radians	ΔQ	$\Delta\beta\Delta Q$ radians	$\Delta\theta$ radians	$\Delta\Omega$ steradians	$\Delta Q\Delta\Omega$ steradians
T	0.0384	0.1120	0.0262	0.00294	0.0289	3.24×10^{-3}	8.49×10^{-5}
TC	0.0112	0.1120	0.0250	0.00280	0.0289	3.24×10^{-3}	8.10×10^{-5}
BC	-0.0147	0.1120	0.0239	0.00268	0.0289	3.24×10^{-3}	7.74×10^{-5}
B	-0.0394	0.1120	0.0229	0.00257	0.0289	3.24×10^{-3}	7.43×10^{-5}

TABLE 13

HEMA Trajectory Fits

β in radians — Z, α, ζ in inches

	Q fit			β fit	
	Coefficient	Term		Coefficient	Term
A_0	0.5721874E-04	1	B_0	-0.6955100E-04	1
A_1	0.1880500E-01	Z	B_1	-0.7550798E-02	Z
A_2	0.5253148E-03	α	B_2	0.8497495E-02	α
A_3	0.2049600E-01	ζ	B_3	-0.1853500E-02	ζ
A_4	0.3551198E-03	ZZ	B_4	0.2548494E-04	ZZ
A_5	-0.5477499E-03	Zα	B_5	0.5623499E-04	Zα
A_6	0.7159649E-03	Zζ	B_6	-0.9556847E-05	Zζ
A_7	-0.8864001E-05	$\alpha\alpha$	B_7	0.2795648E-04	$\zeta\zeta$
A_8	-0.6909049E-03	$\alpha\zeta$	B_8	-0.2654149E-04	$\zeta\alpha$
A_9	0.5000997E-03	$\zeta\zeta$	B_9	0.1314349E-04	$\alpha\alpha$
A_{10}	-0.3770499E-04	ZZZ	B_{10}	0.1735949E-03	ZZZ
A_{11}	0.6679649E-04	ZZα	B_{11}	0.4171599E-04	ZZα
A_{12}	0.4175999E-04	ZZζ	B_{12}	0.1984001E-05	ZZζ
A_{13}	-0.6137046E-05	Z$\alpha\alpha$	B_{13}	-0.5402600E-05	Z$\alpha\alpha$
A_{14}	-0.4585448E-04	Z$\alpha\zeta$	B_{14}	0.6902399E-05	Z$\alpha\zeta$
A_{15}	-0.1437998E-05	Z$\zeta\zeta$	B_{15}	-0.8853589E-05	Z$\zeta\zeta$
A_{16}	-0.7616300E-05	$\alpha\alpha\alpha$	B_{16}	0.1766749E-05	$\alpha\alpha\alpha$
A_{17}	0.2046749E-04	$\alpha\alpha\zeta$	B_{17}	-0.8633947E-06	$\alpha\alpha\zeta$
A_{18}	-0.3291598E-04	$\alpha\zeta\zeta$	B_{18}	-0.3067800E-06	$\alpha\zeta\zeta$
A_{19}	0.1950579E-04	$\zeta\zeta\zeta$	B_{19}	0.9235396E-06	$\zeta\zeta\zeta$

Example: $Q = A_0 + A_1 Z + A_2 \alpha + A_3 \zeta + \ldots + A_{19} \zeta\zeta\zeta = f(Z, \alpha, \zeta)$

$\beta = B_0 + B_1 Z + B_2 \alpha + B_3 \zeta + \ldots + B_{19} \zeta\zeta\zeta = g(Z, \alpha, \zeta)$

TABLE 14

OUTR Trajectory Fits

β in radians — Z, α, ζ in inches

	Q fit			β fit	
	Coefficient	Term		Coefficient	Term
A_0	-0.1547043E-03	1	B_0	0.4093298E-03	1
A_1	0.2262900E-01	Z	B_1	-0.7470299E-02	Z
A_2	0.9224347E-03	α	B_2	0.7528197E-02	α
A_3	0.1542400E-01	ζ	B_3	-0.9227499E-03	ζ
A_4	0.6519249E-03	ZZ	B_4	-0.3359148E-04	ZZ
A_5	-0.8004350E-03	Zα	B_5	0.3707349E-04	Zα
A_6	0.7200749E-03	Zζ	B_6	0.1338250E-05	Zζ
A_7	-0.1991448E-03	$\alpha\alpha$	B_7	0.2100799E-04	$\alpha\alpha$
A_8	-0.4932848E-03	$\alpha\zeta$	B_8	-0.7018549E-05	$\alpha\zeta$
A_9	0.2035149E-03	$\zeta\zeta$	B_9	0.3592999E-05	$\zeta\zeta$
A_{10}	0.3729349E-03	ZZZ	B_{10}	0.4637554E-04	ZZZ
A_{11}	-0.5653799E-04	ZZα	B_{11}	0.7806346E-05	ZZα
A_{12}	0.1502549E-04	ZZζ	B_{12}	0.6319894E-05	ZZζ
A_{13}	0.1853050E-04	Z$\alpha\alpha$	B_{13}	0.6257696E-06	Z$\alpha\alpha$
A_{14}	-0.5919849E-04	Z$\alpha\zeta$	B_{14}	-0.2042650E-05	Z$\alpha\zeta$
A_{15}	-0.1970649E-04	Z$\zeta\zeta$	B_{15}	-0.1401854E-04	Z$\zeta\zeta$
A_{16}	-0.2363799E-04	$\alpha\alpha\alpha$	B_{16}	0.2644500E-05	$\alpha\alpha\alpha$
A_{17}	0.7175049E-05	$\alpha\alpha\zeta$	B_{17}	-0.7258250E-06	$\alpha\alpha\zeta$
A_{18}	-0.1865349E-04	$\alpha\zeta\zeta$	B_{18}	-0.3144148E-06	$\alpha\zeta\zeta$
A_{19}	0.4240139E-04	$\zeta\zeta\zeta$	B_{19}	-0.2505550E-05	$\zeta\zeta\zeta$

Example: $Q = A_0 + A_1 Z + A_2 \alpha + A_3 \zeta + \ldots + A_{19} \zeta\zeta\zeta = f(Z, \alpha, \zeta)$

$\beta = B_0 + B_1 Z + B_2 \alpha + B_3 \zeta + \ldots + B_{19} \zeta\zeta\zeta = g(Z, \alpha, \zeta)$

TABLE 15

LEM Trajectory Fits

β in radians — Z, α, ζ in inches

Q fit

	Coefficient	Term
A_0	-0.4843849E-04	1
A_1	-0.4131997E-01	β
A_2	0.1943800E-01	ζ
A_3	0.2134050E-01	Z
A_4	-0.1771649E 01	$\beta\beta$
A_5	-0.5689248E-01	$\beta\zeta$
A_6	-0.1189600E 00	βZ
A_7	0.3365697E-03	$\zeta\zeta$
A_8	-0.6432849E-04	ζZ
A_9	-0.8605348E-03	ZZ
A_{10}	0.5105399E 01	$\beta\beta\beta$
A_{11}	0.1003200E 00	$\beta\beta\zeta$
A_{12}	0.3343949E 00	$\beta\beta$Z
A_{13}	-0.2727199E-02	$\beta\zeta\zeta$
A_{14}	-0.3252350E-02	$\beta\zeta$Z
A_{15}	0.2543800E-02	βZZ
A_{16}	0.9712843E-05	$\zeta\zeta\zeta$
A_{17}	-0.4785649E-05	$\zeta\zeta$Z
A_{18}	-0.2925949E-04	ζZZ
A_{19}	-0.1118580E-03	ZZZ

Example: $Q = A_0 + A_1\beta + A_2\zeta + A_3Z + \ldots + A_{19}ZZZ = h(\beta, \zeta, Z)$

TABLE 16

Comparison of Spectrometer Acceptances
Computed by Numerical and Monte Carlo Methods

Acceptance $\Delta Q \Delta \Omega$ (steradians)
HAT009B Numerical Integration Acceptance
ACCEPTED Monte Carlo Integration Acceptance

HEMA

Channel	HAT009B	ACCEPTED
T	4.30×10^{-5}	4.32×10^{-5}
TC	4.08×10^{-5}	4.09×10^{-5}
BC	3.90×10^{-5}	3.90×10^{-5}
B	3.73×10^{-5}	3.71×10^{-5}

Approximate error in ACCEPTED 0.05×10^{-5}

OUTR

Channel	HAT009B	ACCEPTED
T	3.23×10^{-5}	3.22×10^{-5}
TC	3.05×10^{-5}	3.08×10^{-5}
BC	2.95×10^{-5}	2.95×10^{-5}
B	2.94×10^{-5}	2.93×10^{-5}

Approximate error in ACCEPted 0.04×10^{-5}

LEM

Channel	HAT009B	ACCEPTED
T	8.49×10^{-5}	8.52×10^{-5}
TC	8.10×10^{-5}	8.13×10^{-5}
BC	7.74×10^{-5}	7.73×10^{-5}
B	7.43×10^{-5}	7.43×10^{-5}

Approximate error in ACCEPTED 0.10×10^{-5}

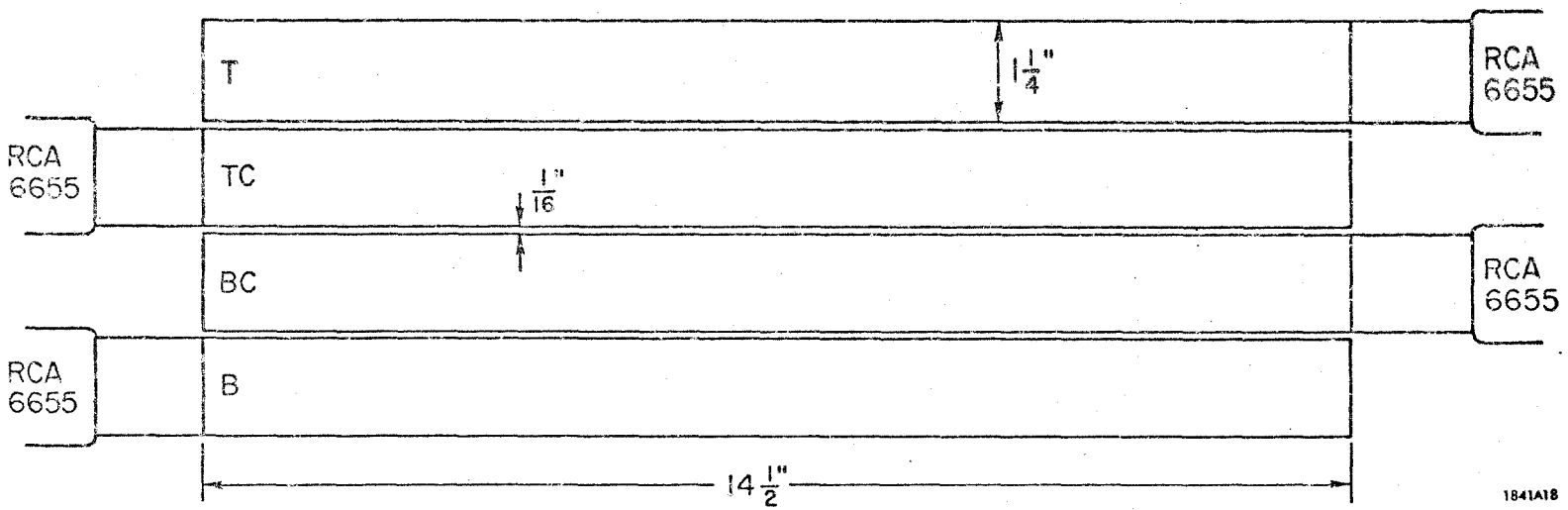

FIGURE 27

The LEM Momentum Counters

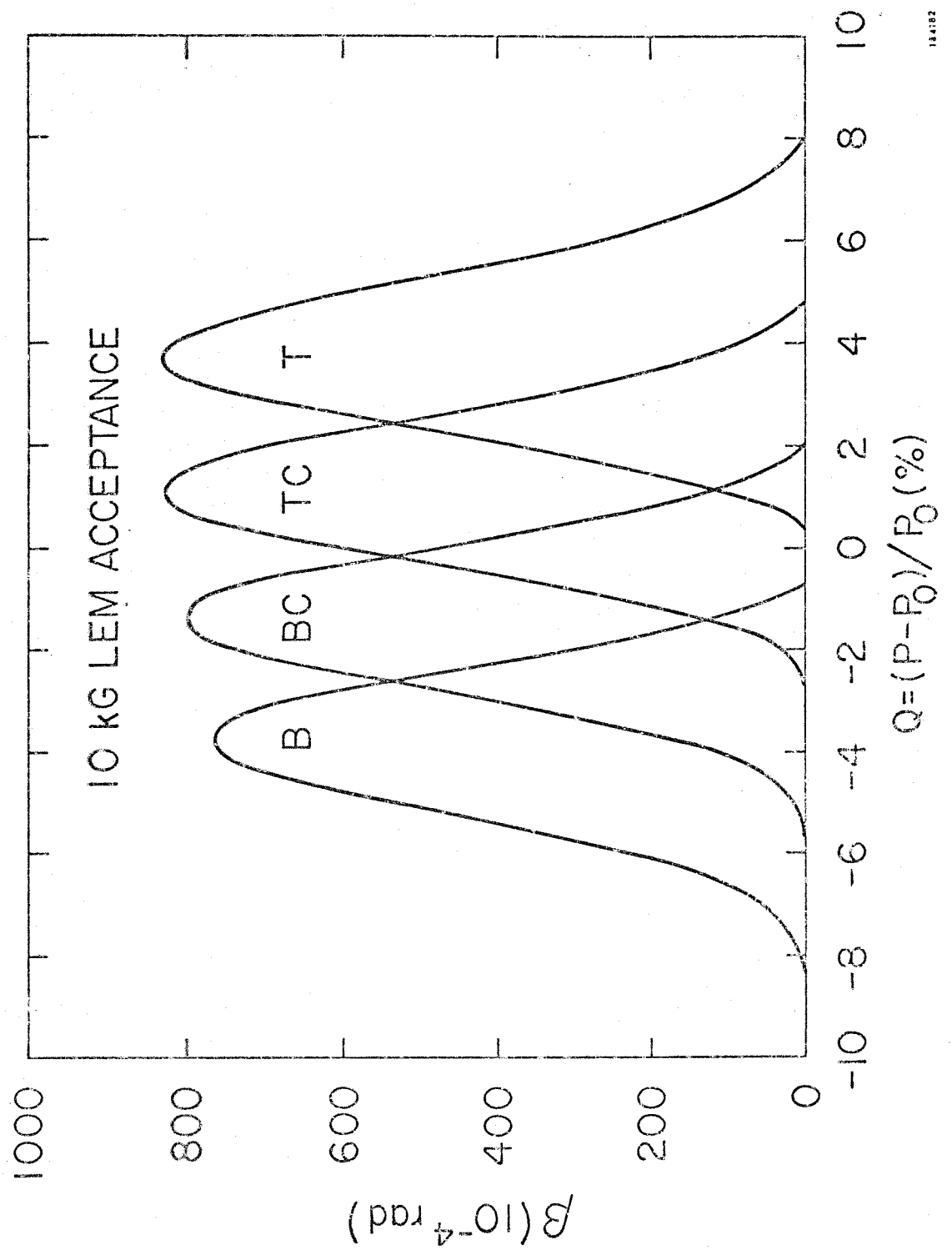
10 KG LEM ACCEPTANCE
B
BC
TC
T
1000
800
600
400
200
0
-10
-8
-6
-4
-2
0
2
4
6
8
10
β (10^{-4} rad)
$Q=(P-P_0)/P_0$ (%)
184182

FIGURE 28

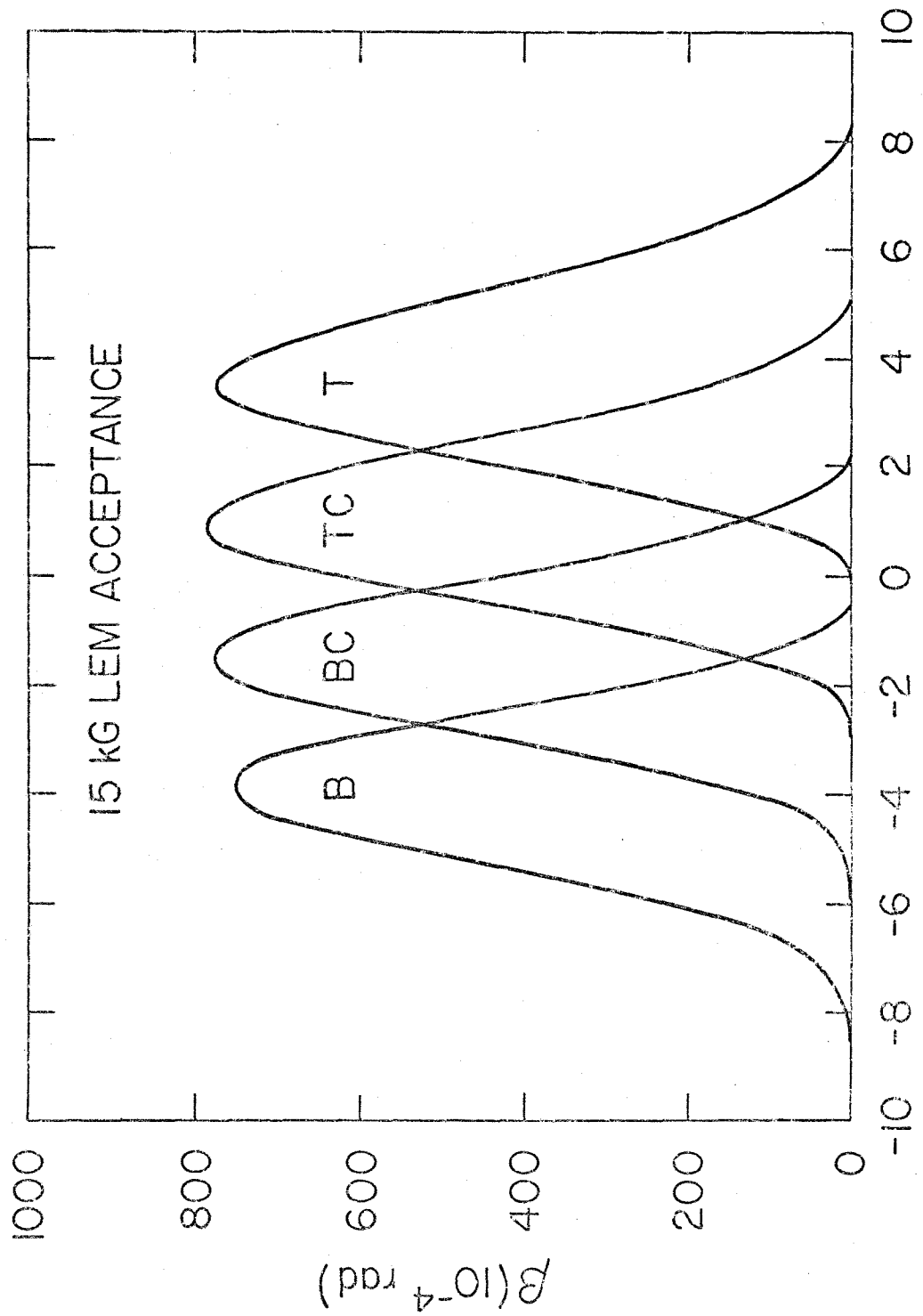
15 kG LEM ACCEPTANCE
B
BC
TC
T
1000
800
600
400
200
0
β (10^{-4} rad)
-10
-8
-6
-4
-2
0
2
4
6
8
10
$Q = (P-P_0)/P_0$ (%)

FIGURE 29

APPENDIX VI

NUCLEAR ABSORPTION

In this experiment the pions and protons which were detected in the spectrometers had to traverse a considerable path length before triggering all the counters required for a successful event. Even though there was as little matter as possible in the particle's path a significant fraction of the particles were nevertheless lost due to interactions.

In previous experiments using the same apparatus there was concern for two types of interactions, multiple scattering and nuclear absorption.

Multiple scatters refers to cumulative small angle Coulomb scattering by atomic nucleii in the material the particle is traversing. These interactions result in small angle scattering and usually a negligible loss of particles. Multiple scattering does cause a broadening of the spectrometer's resolution, but this broadening is small compared to the broadening caused by the deuteron target, so this effect was ignored for this experiment.

Nuclear absorption is a broad category that includes all wide angle scattering of nuclei as well as absorptive reactions. The scattering interaction can result in the particles missing the next counter and failing to be detected.

For this experiment we could take advantage of the fact that the predecessors who had used the same apparatus had already made the necessary nuclear absorption measurements. These measurements also included small multiple scattering losses. In the case of Ecklund and Thiessen, the measurements were presented in the form of a fit and a short table, respectively. These were easy to incorporate into a small computer subroutine which would calculate the nuclear

absorption correction for the cross section calculation (see (2.27)). Wolverton's nuclear absorption for the proton were in the form of bulky tables. To make his data more amenable for rapid calculation in the same subroutine, a third order polynomial was fitted to his data. Wolverton's data and the present fit can be seen in Figures (30)-(33). There are four fits, two each for the spectrometers HEMA and OUTR, with a further subdivision as to whether the spectrometer was detecting protons passing through the target's upstream mylar window or its aluminum vacuum jacket. The fits are in the following form

$$N_A = A_0 + A_1(P/100) + A_2(P/100)^2 + A_3(P/100)^3 \qquad (6.1)$$

where N_A is the percentage of particles absorbed, P is the mean proton momentum, and A_i's are the fit coefficients. The coefficients are presented in Table 17.

To check the confidence in the validity of the previous nuclear absorption corrections, a few measurements were made at the end of the running schedule. Ecklund measured the loss of pions due to the placement of 0.5 inches of lead in front of the last HEMA counter, S3, and this was an easy measurement to check. The results can be seen in Figure (34). Note that both π^- and π^+ nuclear absorption as seen in Figure (34) seem identical. The point in worst agreement with Ecklund was a π^+ run, the same case as Ecklund. The disagreement could be statistics or electronics. Scheculing time did not permit pursuing the matter further.

One of Wolverton's proton absorption measurements was checked. HEMA was set to 580 MeV/c and an inch of polyethylene was placed in front of the A2 counter which produced an absorption of 10.62 ± 2.06%. Wolverton's measurement had an inch of polyethylene in front of the A1 counter as well as an inch in

front of A2, and he observed an absorption of 20 ± + %. If both sheets of polyethylene contributed equally, the absorption for one sheet would be 10.55%, very close to the previous measurement.

No check of Thiessen's nuclear absorption was made on the LEM. The check of Ecklund's results seen in Figure (34) indicated that π^- absorption would be identical to π^+ absorption and scheduling time not permitting adequate measurements, Thiessen's results in the low π momentum region were assumed to be correct.

This assumption holds true as long as most of the absorption results from π scattering off nuclei with Z > 1 where there are approximately equal numbers of protons and neutrons. However, near the momentum of 282 MeV/c the $P_{33}(1236)$ resonant amplitude creates a very large πp cross section and according to isospin conservation

$$\sigma(\pi^+ p) = 3\sigma(\pi^- p) . \qquad (6.2)$$

As a result, a large difference between π^+ and π^- absorption could develop, and a calculation was done to estimate its size.

The results gave 12.12% for π^+ absorption and 10.77% for π^- absorption. Thiessen's value was 11.4%. Using Thiessen's result an error of 0.9% is made in the π^+ cross section and an error of 0.7% in the π^- cross section. These errors are smaller than the 1.5-3.0% error quoted by Thiessen for his nuclear absorption measurements. The differences in the π^+ and π^- absorption causes an error of 1.6% in the (π^-/π^+) ratio. This is much smaller than the 7% statistical error expected for most data points. Because these errors are for the worst case, it is clear that Thiessen's π nuclear absorption values can be used without inducing any significant errors.

TABLE 17

Proton Nuclear Absorption Coefficients

Case	A_0	A_1	A_3	A_4
HEMA, MYLAR	41.162	- 9.5994	0.96856	- 0.031155
HEMA, AL	39.433	- 8.8883	0.89198	- 0.028396
OUTR, MYLAR	- 34.897	9.6644	- 0.67252	0.01626
OUTR, AL	13.848	- 1.1644	0.13345	- 0.003616

FIGURES 30 - 33

Proton Nuclear Absorption

The points are from Wolverton's thesis [11] and the solid line is the calculated fit whose coefficients are presented in Table 17.

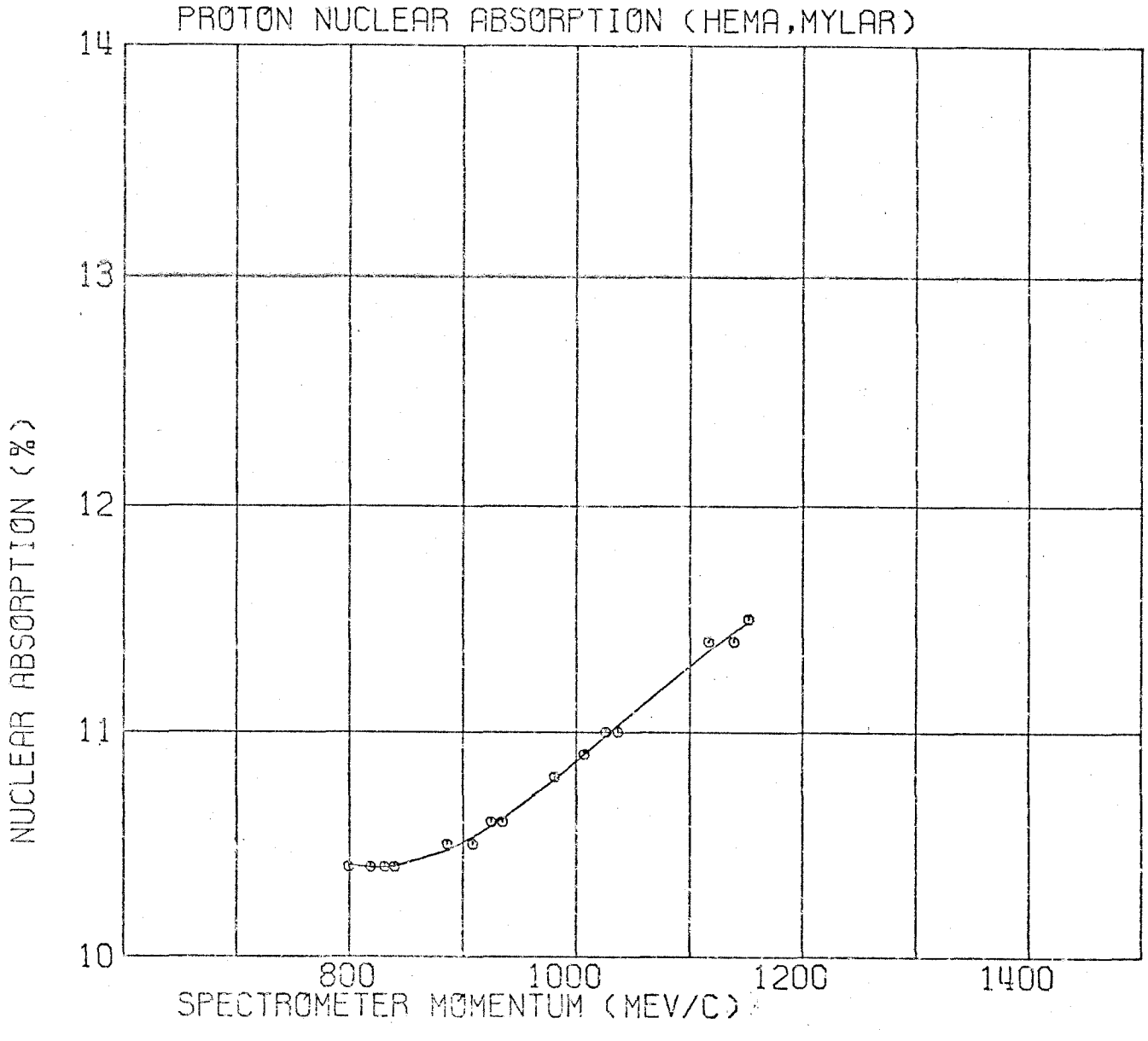
PROTON NUCLEAR ABSORPTION (HEMA,MYLAR)
NUCLEAR ABSORPTION (%)
14
13
12
11
10
800
1000
1200
1400
SPECTROMETER MOMENTUM (MEV/C)

FIGURE 30

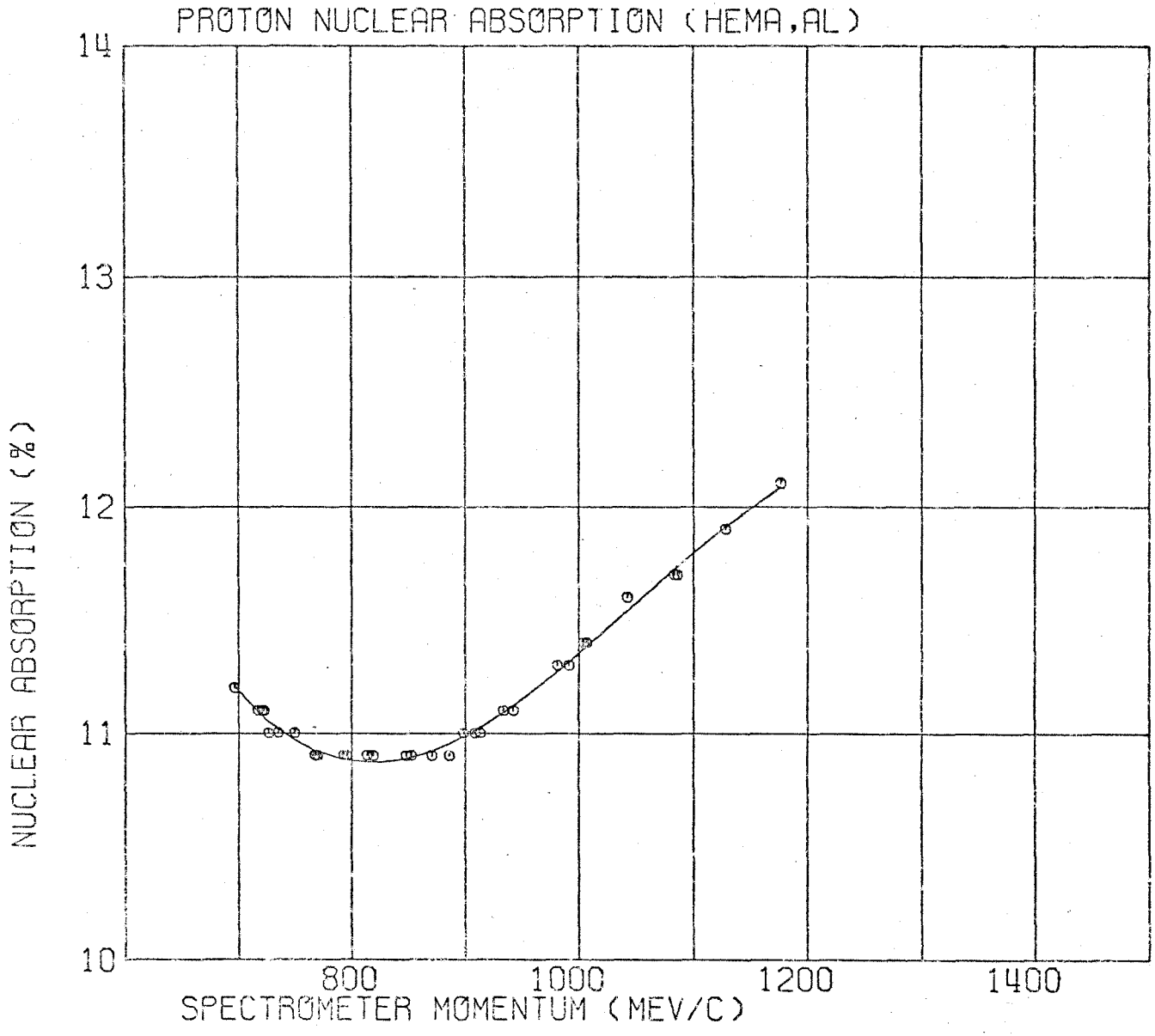
PROTON NUCLEAR ABSORPTION (HEMA,AL)
NUCLEAR ABSORPTION (%)
14
13
12
11
10
800
1000
1200
1400
SPECTROMETER MOMENTUM (MEV/C)

FIGURE 31

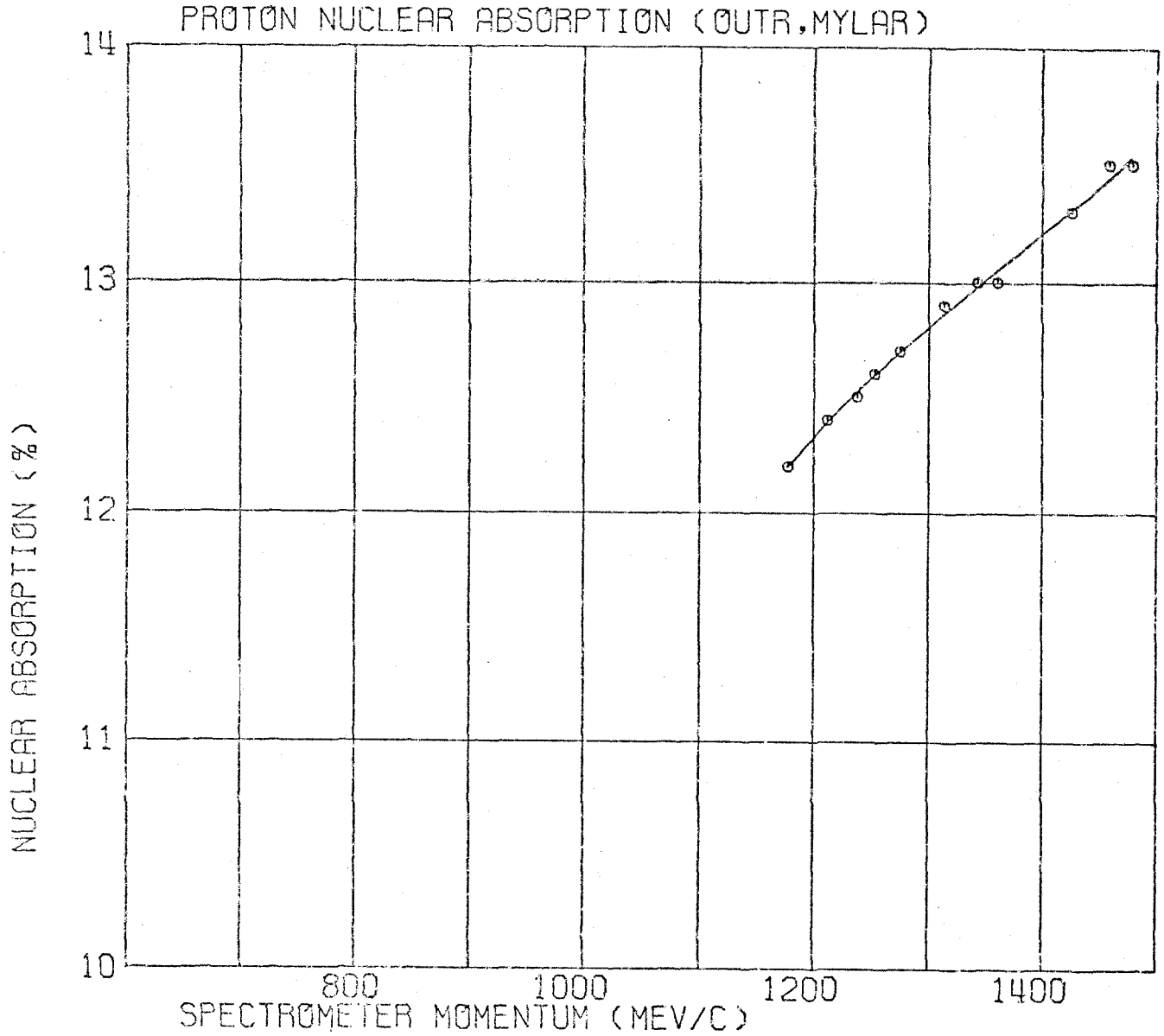
PROTON NUCLEAR ABSORPTION (OUTR,MYLAR)
NUCLEAR ABSORPTION (%)
14
13
12
11
10
800
1000
1200
1400
SPECTROMETER MOMENTUM (MEV/C)

FIGURE 32

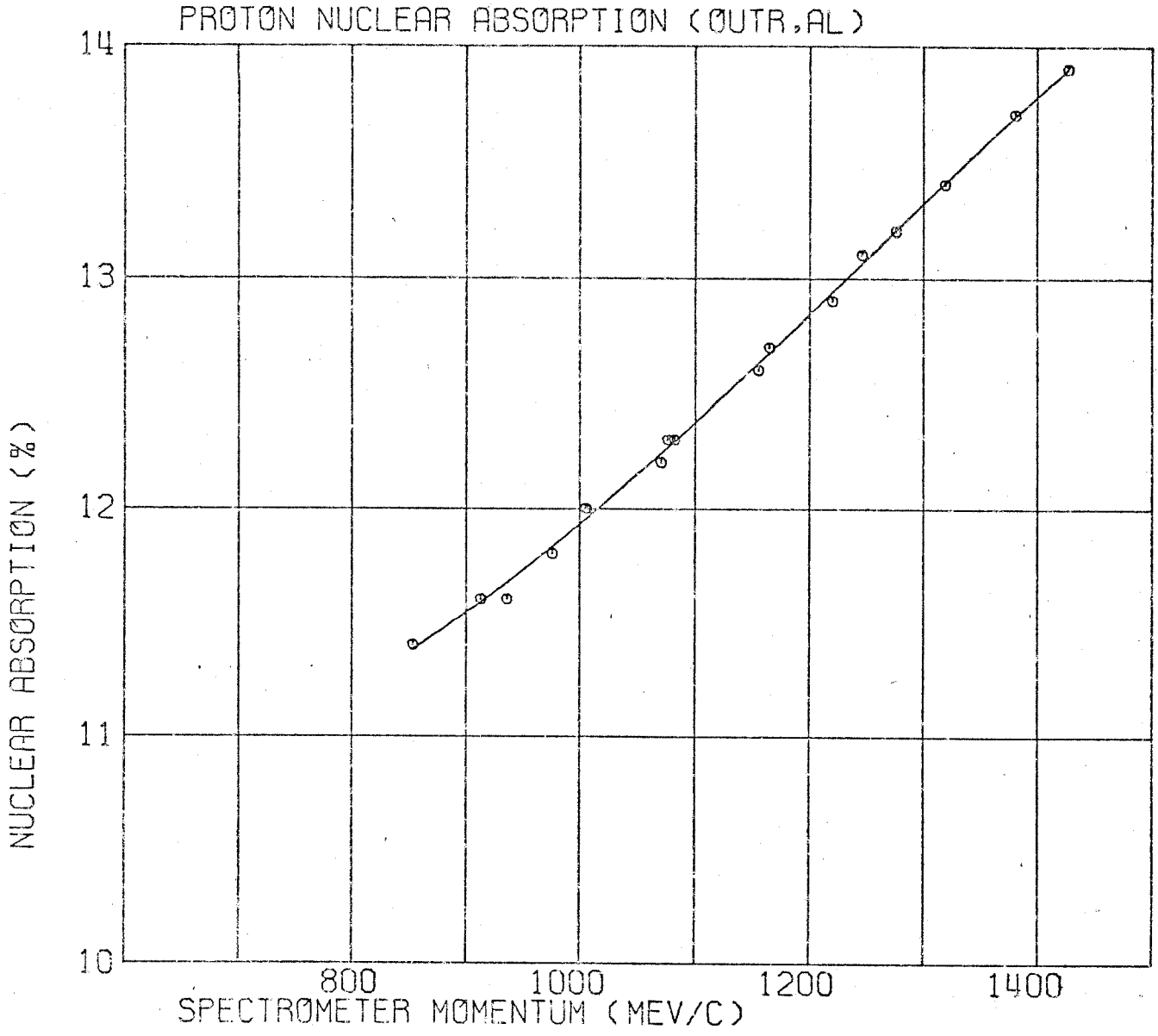
PROTON NUCLEAR ABSORPTION (OUTR,AL)
NUCLEAR ABSORPTION (%)
14
13
12
11
10
800
1000
1200
1400
SPECTROMETER MOMENTUM (MEV/C)

FIGURE 33

FIGURE 34

S3 Miss Rate

S3 = Counts in (HEMA trigger · S3)

S3V = Counts in (HEMA trigger · $\overline{S3}$)

With and Without Pb refers to a 1/2" slab of lead placed in front of counter S3. The fitted lines are from Ecklund [12].

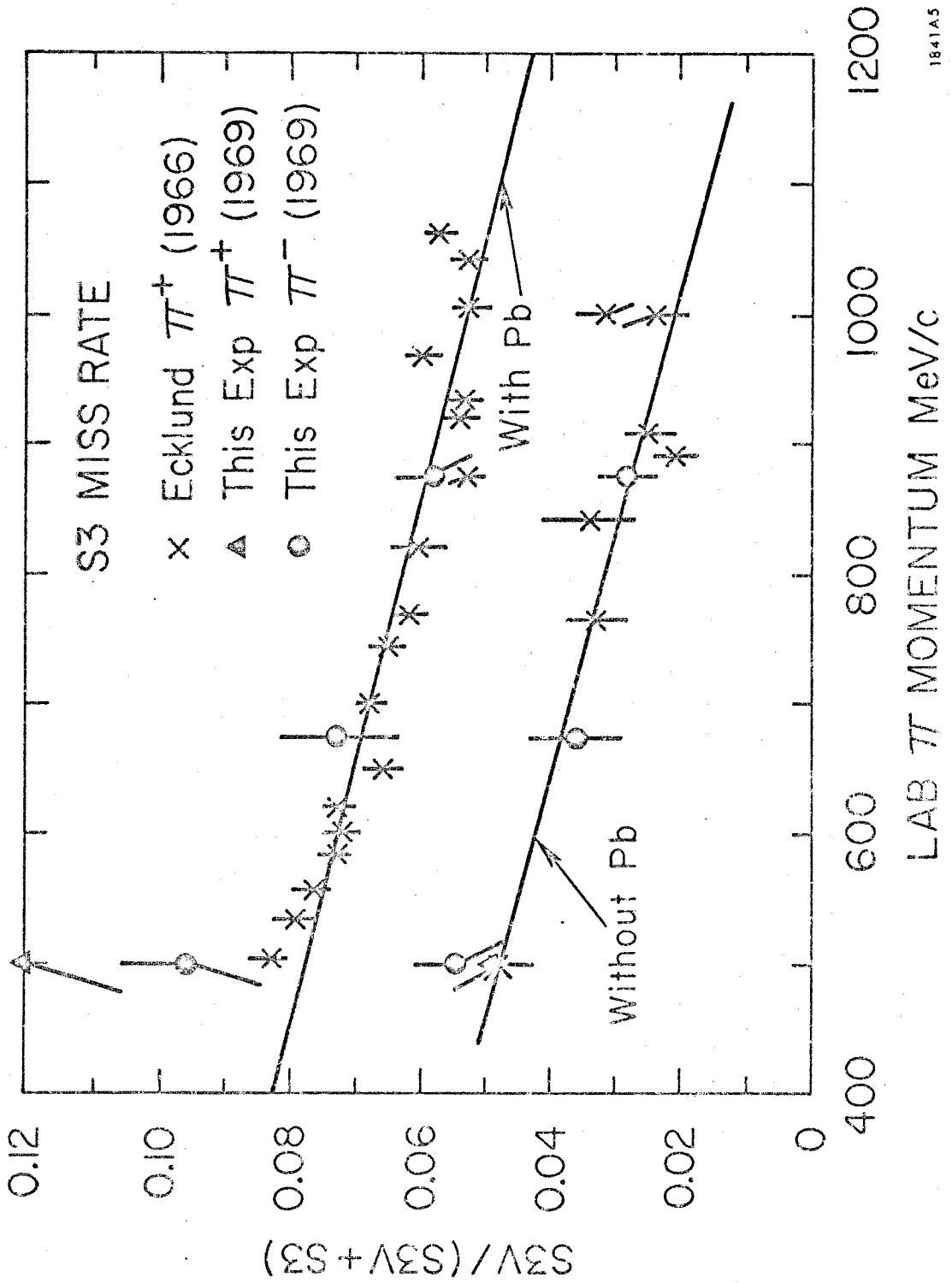
S3 MISS RATE
x Ecklund π^+ (1966)
▲ This Exp π^+ (1969)
o This Exp π^- (1969)
With Pb
Without Pb
S3V/(S3V+S3)
0.12
0.10
0.08
0.06
0.04
0.02
0
400
600
800
1000
1200
LAB π MOMENTUM MeV/c
1841A5

FIGURE 34

APPENDIX VII

2π CONTAMINATION

In this experiment there was considerable concern that 2π photoproduction would significantly contaminate our experimental rates. In previous experiments [5] using a proton target this contamination was eliminated by operating with the bremsstrahlung end point below the 2π threshold for a particular spectrometer setting. This technique also was used in the present experiment. However, it was less effective because the heavier deuteron target lowered the 2π threshold.* There were also experimental indications that the contamination could be significant. The π^0 photoproduction experiment of Wolverton [11] had a large 2π fraction in the rates when just the proton from $\gamma + p \rightarrow \pi^0 + p$ was detected, and the present experiment indicated a possibility of 2π contamination at backward pion angles. For these reasons calculations of the 2π rate for our experiment seemed necessary.

---

* The standard concept used to explain the lowered 2π threshold is the Fermi motion of the deuteron nucleons. However, from energy and momentum conservation the threshold photon energy needed to produce 2π's can be derived without this concept. The threshold is given by

$$K = \frac{4(\mu + M)^2 - M_D^2}{2M_D}$$

where

K = lab photon energy
M = nucleon mass
M_D = deuteron mass
μ = pion mass.

There is no reference to Fermi motion in this equation. Letting $M_D = 2M$ we get

$$K = 2\mu\frac{\mu + 2M}{2M}$$

which is obviously lower than the hydrogen threshold, $K = 2\mu\frac{\mu + M}{M}$.

There are a total of six 2π photoproduction reactions which could contaminate this experiment. They are listed in Table (18). In the region of interest (threshold to 3 GeV) extensive data existed for only the

$$\gamma + p \rightarrow \pi^- + \pi^+ + p \tag{7.1}$$

reaction. The data for this reaction consist of measurements $\partial\sigma/\partial\Omega$ for the following three processes:

$$\begin{aligned} &\gamma + p \rightarrow \pi^- + \Delta^{++} \quad [39, 40, 41] \\ &\gamma + p \rightarrow \rho^o + p \quad [41] \\ &\text{and} \\ &\gamma + p \rightarrow \pi^- + \pi^+ + p \quad \text{(non-resonant)} . \quad [39] \end{aligned} \tag{7.2}$$

Fits were generally available for the cross sections and they were used for the 2π rate calculation described further on. If no fits were available interpolations were done with the data tables. Non-resonant data were only available from Hauser's [39] experiment which covered photon energies 0.9 to 1.3 GeV. His lowest and highest photon energy fits were extended to cover the entire region from threshold to 3 GeV but were normalized to give the proper total non-resonant cross section.

The calculation described later requires the cross section

$$\partial\sigma(W, \theta, M^2)/\partial\Omega\partial M^2 ,$$

where W is the c.m. energy, θ is the c.m. angle between the γ and the π^- or ρ^o, and M is the invariant mass of the other particles. We equate here

$$\frac{\partial\sigma(W,\theta,M^2)}{\partial\Omega\partial M^2} = \frac{\partial\sigma(W,\theta)}{\partial\Omega}\cdot g(W,M^2) \tag{7.3}$$

where $g(W,M^2)$ is the mass distribution of the non-detected particles and is normalized to

$$\int g(W,M^2)\,dM^2 = 1 \ . \tag{7.4}$$

There are three mass distributions, one for each of the processes in (7.2). For the non-resonant process the mass distribution is taken directly from phase space. It is

$$g(W,M^2) = \frac{1}{S}\,\frac{p'}{W}\,\frac{q'}{M} \tag{7.5}$$

where p' is the momentum of the detected particle in the overall c.m. frame, q' is the momentum in the c.m. frame of the non-detected particles, and S is the normalization to force (7.4) to be true. For the resonant processes we use Jackson's [42] phenomenological expression

$$g(W,M^2) = \frac{1}{S}\,\frac{p'}{W}\,\frac{\Gamma(M)}{(M_r-M)^2 - M_r^2\Gamma^2(M)} \tag{7.6}$$

where

$$\Gamma(M) = \Gamma_0\left(\frac{q'}{q'_0}\right)^{2\ell+1}\frac{\rho(M)}{\rho(M_r)} \tag{7.7}$$

and M_r is the resonant mass. Γ_0 is the characteristic width of the resonance, and q' is the momentum in the (π^+,p) c.m. frame for the Δ^{++} process or else momentum in the π's c.m. frame for the ρ^o process. q'_0 is q' evaluated at

$M = M_r$. For the expression $\rho(M)$ Jackson uses

$$\rho(M) = \frac{(M + M_p)^2 - M_\pi^2}{M^2} \tag{7.8}$$

for the Δ^{++} process and

$$\rho(M) = \frac{1}{M} \tag{7.9}$$

for the ρ^o process. For both Δ^{++} and ρ^o processes the orbital angular momentum $\ell = 1$.

To investigate the 2π rates for our experiment, we shall first calculate contamination from reaction (7.1), for which data on cross sections are available. From the calculation about to be described, only approximate answers can be expected. There are many reasons for this. The non-resonant cross sections are largely unknown or else uninteresting enough not to be reported. Decays of Δ^{++} and ρ^o are assumed to be isotropic, which they are not. Also the deuterium effects have perhaps not all been included, although a good attempt has been made.

In the following discussion expressions and conventions used in Appendices I and II will be freely used here. The calculation assumes that a π^- is being detected by the spectrometer. It is a simple matter of substitution for the π^+ and p cases. Also, in order for the calculation to be most efficient with computer time, it was necessary to introduce much complexity. Perhaps a more conceptual approach could have been taken but this would have been expensive.

An expression to calculate the 2π contamination rates is available from the Eq. (2.13) which is

$$C = \int_K \int_\Omega \iint_q \frac{k' M_n}{K E_n} \Phi(K) \frac{2Wq^2}{q_{cm} \omega} \frac{\partial \sigma}{\partial \Omega_{cm}} \delta (\mathscr{P}_R^2 - M_P^2) \left[\phi^2 (P_S) \frac{d^3 P_3}{(2\pi)^3} \right] \eta \, t \, dK \, dq \, d\Omega$$

We claim that

$$\frac{\partial \sigma}{\partial \Omega_{cm}} \delta (\mathscr{P}_R^2 - M_P^2) = \frac{\partial^2 \sigma}{\partial \Omega_{cm} \partial M_P^2} \tag{7.10}$$

because $\delta (\mathscr{P}_R^2 - M_p^2)$ is definitely a mass distribution of the recoil proton and the normalization requirement

$$\int \delta (\mathscr{P}_R^2 - M_P^2) dM_P^2 = 1 \tag{7.11}$$

is true. So for 2π photoproduction we replace $\partial\sigma/\partial\Omega_{cm} \, \delta (\mathscr{P}_R^2 - M_p^2)$ by $\partial^2\sigma/\partial\Omega_{cm} \partial M^2$. Note now that M_n and E_n in (2.13) must be changed to M_p and E_p because now the target nucleon is a proton. We equate

$$\Phi(K) = \frac{H}{E_0} \frac{B(E_0, K)}{K} \tag{7.12}$$

where $B(E_0, K)$ [43] is Hauser's bremsstrahlung function normalized to the targer diameter t. We also define

$$q = P_0 (1 + Q) \tag{7.13}$$

and

$$d\Omega = d\beta \, d\theta \tag{7.14}$$

where P_0 is the central spectrometer momentum, β is the vertical lab angle, and θ is the horizontal lab angle. For a clearer idea of β and θ see Figure (22).

We now have the expression

$$\frac{C}{H} = \eta t \frac{P_0}{E_0} \int_K \int_\Omega \int_Q \int_{\vec{P}_S} \frac{k' M_P}{K E_P} \frac{B(E_0, K)}{K} \frac{2Wq^2}{q_{cm}\omega} \frac{\partial^2\sigma}{\partial\Omega_{cm}\partial M^2} \left[\phi^2(P_S) \frac{d^3P_S}{(2\pi)^3}\right] dQ\, d\beta\, d\theta\, dK \tag{7.15}$$

We can now begin the Monte Carlo process to evaluate Eq. (7.15). The order in which the integration variables are picked is as follows:

1. θ_i limits $\theta_0 - \Delta\theta/2 < \theta_i < \theta_0 + \Delta\theta/2$
2. β_i limits $\pi/2 - \Delta\beta/2 < \beta_i < \pi/2 + \Delta\beta/2$
3. Q_i limits $Q_0 - \Delta Q/2 < Q_i < Q_0 + \Delta Q/2$
4. ϕ_{S_i} limits $0 < \phi_{S_i} < 2\pi$
5. $\cos\theta_{S_i}$ limits $-1 < \cos\theta_{S_i} < 1$
6. P_{S_i} limits $0 < P_{S_i} < \infty$ (weighted as indicated below)

where θ_0 is the lab angle of the spectrometer, Q_0 is the central Q of the momentum channel and ΔQ, $\Delta\beta$ and $\Delta\theta$ are the resolutions of the momentum channel. These latter quantities can be found in Wolverton's spectrometer report [37] and in Appendix V. The spectator neutron momentum is weighted by the function $P_S^2\phi^2(P_S)/(2\pi)^3$ as in Appendices II and IV. Using Eq. (3.4) from the Monte Carlo Appendix (7.15) is now reduced to

$$\frac{C}{H} = \eta t \frac{P_0}{E_0} \frac{\Delta Q \Delta\beta \Delta\theta}{N} \sum_i \int_K \frac{k' M_P}{K E_P} \frac{B(E_0, K)}{K} \frac{2Wq_i^2}{q_{cm}\omega_i} \frac{\partial^2\sigma}{\partial\Omega_{cm}\partial M^2} dK \tag{7.16}$$

It would not be efficient to pick a photon energy between 0 MeV and the end point E_0 because for most of the energy range 2π production is kinematically

impossible. However, there exists for every choice of $\vec{q}$ and $\vec{P}_S$ a K_{min} such that no 2π production is possible below this energy. This value can be derived from the 4-momenta conservation

$$\mathcal{K} + \mathcal{P}_D = \mathcal{Q}_{\pi^-} + \mathcal{Q}_{\pi^+} + \mathcal{P}_R + \mathcal{P}_S \,. \tag{7.17}$$

By taking $\mathcal{Q}_{\pi^-}$ and $\mathcal{P}_S$ to the left hand side, squaring, and equating

$$(\mathcal{Q}_{\pi^+} + \mathcal{P}_R)^2 = (M_\pi + M_P)^2 = M_{min}^2 \tag{7.18}$$

one can obtain

$$K_{min} = \frac{2M_P(\omega + E_S) - 2(\omega E_S - qP_S G) + M_{min}^2 - M_D^2 - m_\pi^2 - M_n^2}{2(M_D - \omega + q\cos\theta_{\pi^-} - E_S + P_S\cos\theta_S)} \,. \tag{7.19}$$

We now pick K between K_{min} and E_0. The final Monte Carlo expression is

$$\frac{C}{H} = \eta t \frac{P_0}{E_0} \frac{\Delta Q \Delta\beta \Delta\theta}{N} \sum_i \frac{k_i' M_P}{K_i E_{P_i}} (E_0 - K_{min_i}) \frac{B(E_0, K_i)}{K_i} \frac{2W_i q_i^2}{q_{cm_i} \omega_i} \frac{\partial^2\sigma(W_i, \theta_i, M_i^2)}{\partial\Omega_{cm_i} \partial M_i^2} \tag{7.20}$$

This equation will be used to calculate the 2π rates expected in our experiment.

The above process works fine if one is calculating rates for particles that are not lumped into a resonance; for example, the π^- with Δ^{++} production, and the proton with ρ^0 production. If one wished to calculate the π^+ rates from Δ^{++} photoproduction the preceeding formula (7.20) would not be adequate. The problem can be stated as follows. If there exist three particles in a final state, say, particles j, k, and l, and the cross section $\partial^2\sigma(W, \theta_j, M_{k\ell}^2)/\partial\Omega_j \partial M_{k\ell}^2$ is completely known, where

$$M_{k\ell}^2 = (\mathcal{P}_k + \mathcal{P}_\ell)^2 \tag{7.21}$$

how is $\partial^2\sigma(W, \theta_\ell, M^2_{jk})/\partial\Omega_\ell\partial M^2_{jk}$ to be computed from this information, where

$$M^2_{jk} = (\mathscr{P}_j + \mathscr{P}_k)^2 \tag{7.22}$$

The problem as stated above does not give sufficient information for its solution. The angular distribution of $M_{k\ell} \rightarrow M_k + M_\ell$ is also required. For our purposes the distribution will be assumed to be isotropic in the rest frame of $M_{k\ell}$. This is not only a saving on computer time, but makes up for a lack of experimental data. With a bit of concentration we can write down the solution

$$\frac{\partial^2\sigma(W, \theta_\ell, M^2_{jk})}{\partial\Omega_\ell\partial M^2_{jk}} = \int dM^2_{k\ell}\int d\Omega_i \int \frac{d\cos x'_{k\ell}}{2} \int \frac{d\phi'_{k\ell}}{2\pi} \frac{\partial^2\sigma(W, \theta_j, M^2_{k\ell})}{\partial\Omega_j\partial M^2_{k\ell}} \times \delta(M^2_{jk} - M^2)\delta(\cos\theta_\ell - \cos\theta)\delta(\phi) \tag{7.23}$$

where $x'_{k\ell}$ is the decay angle of $M_{k\ell}$ and $\phi'_{k\ell}$ is the azimuthal angle corresponding to $x'_{k\ell}$. For clarification of all angles, see Figure (35). The primes of $x_{k\ell}$ and $\phi_{k\ell}$ refer to these values evaluated in the $M_{k\ell}$ rest frame. All primed variables from here on will also be evaluated in this frame. Unprimed values are evaluated in the overall c.m. frame. M, $\cos\theta$, and ϕ are the values of M_{jk}, $\cos\theta_\ell$, and ϕ_ℓ, expressed in terms of the integration variables. If we define a c.m. 4-vector

$$\mathscr{P} = \mathscr{P}_j + \mathscr{P}_k + \mathscr{P}_\ell = (W, \vec{0}) \tag{7.24}$$

M can be expressed by

$$M^2 = (\mathscr{P} - \mathscr{P}_\ell)^2 = W^2 - 2WE_\ell + M^2_\ell \ . \tag{7.25}$$

Expressing E_ℓ in terms of the integration variables we have

$$E_\ell = \frac{1}{M_{k\ell}} (E_{k\ell} E'_\ell + P_{k\ell} P'_\ell \cos x'_{k\ell}) , \tag{7.26}$$

where

$$\mathscr{P}_{k\ell} = \mathscr{P}_k + \mathscr{P}_\ell = (E_{k\ell}, \vec{P}_{k\ell}) . \tag{7.27}$$

E'_ℓ , P'_ℓ , $E_{k\ell}$, $P_{k\ell}$ are dependent on $M_{k\ell}$ only. $\cos\theta$ can be obtained by solving the spherical triangle ABℓ in Figure ( ), and it is

$$\cos\theta = -\cos\theta_j \cos x_{k\ell} + \sin\theta_j \sin x_{k\ell} \cos\phi_{k\ell} . \tag{7.28}$$

To express $x_{k\ell}$ in the proper variables we have

$$\cot x_{k\ell} = \frac{1}{M_{k\ell}} \left(E_{k\ell} \cot x'_{k\ell} + P_{k\ell} E'_\ell / (P'_\ell \sin x'_{k\ell}) \right) \tag{7.29}$$

Finally, we observe

$$\phi'_{k\ell} = \phi_{k\ell} . \tag{7.30}$$

We are now ready to integrate (7.23). We note the results on the following integrations:

$$\int \delta(\phi) d\phi_j = 1 , \tag{7.31}$$

$$\int \delta(\cos\theta_\ell - \cos\theta) d\phi'_{k\ell} = \frac{2}{\sin\theta_j \sin x_{k\ell} \sin\phi_{k\ell}} , \tag{7.32}$$

and

$$\int \delta(M^2_{jk} - M^2) d\cos x'_{k\ell} = \frac{M_{k\ell}}{2W P_{k\ell} P'_\ell} . \tag{7.33}$$

The results of (7.31), (7.32), and (7.33) can be used to reduce (7.23) to

$$\frac{\partial^2\sigma(W,\theta_\ell,M_{jk}^2)}{\partial\Omega_\ell\partial M_{jk}^2}=\frac{1}{4\pi}\int\frac{M_{k\ell}}{WP_{k\ell}P_\ell'}\,dM_{k\ell}^2\int\frac{d\cos\theta_j}{\sin\theta_j\sin x_{k\ell}\sin\phi_{k\ell}}\,\frac{\partial^2\sigma(W,\theta_j,M_{k\ell}^2)}{\partial\Omega_j\,\partial M_{k\ell}^2}. \quad (7.34)$$

We pause here to consider the limits of the final integrations. Taking (7.24), we write

$$(\mathscr{P}-\mathscr{P}_j)^2 = W^2-2WE_j+M_j^2 = (\mathscr{P}_k+\mathscr{P}_\ell)^2 = M_{k\ell}^2\,, \quad (7.35)$$

and we see $M_{k\ell}^2$ depends strictly on E_j. With M_{jk} fixed by the integration (7.33) we can relate E_j to the M_{jk} decay angle x_{jk}^*, by

$$E_j = \frac{1}{M_{jk}}(E_{jk}E_j^*+P_{jk}P_j^*\cos x_{jk}^*)\,, \quad (7.36)$$

where

$$\mathscr{P}_{jk} = (E_{jk},\vec{P}_{jk}) = \mathscr{P}_j+\mathscr{P}_k\,. \quad (7.37)$$

Asterisked quantities refer to an evaluation in the M_{jk} rest frame. From (7.35) and (7.36), we see $M_{k\ell}^2$ depends only on $\cos x_{k\ell}^*$ and by setting $\cos x_{k\ell}^*$ to ± 1 we get the $M_{k\ell}^2$ limits

$$W^2-2W\frac{E_{jk}E_j^*}{M_{jk}}+M_j^2\pm\frac{2WP_{jk}P_j^*}{M_{jk}}\,. \quad (7.38)$$

From (7.25), (7.26), and (7.29) we see that setting M_{jk} and $M_{k\ell}$ fixes $x_{k\ell}$. Thus with $\cos\theta$ fixed at $\cos\theta_\ell$ in (7.28), $\cos\theta_j$ becomes strictly dependent on $\phi_{k\ell}$.

Hence by setting $\cos\phi_{k\ell}$ at ± 1, we get the $\cos\theta_j$ limits

$$\cos(\pi - \theta_\ell \pm x_{k\ell}) \quad . \tag{7.39}$$

With the limits of integration established for $M^2_{k\ell}$ and $\cos\theta_j$, (7.34) can be evaluated by Monte Carlo methods. For N trials picking first $M^2_{k\ell}$ then $\cos\theta_j$ randomly within the limits set by (7.38) and (7.40) we get

$$\frac{\partial^2\sigma(W,\theta_\ell,M^2_{jk})}{\partial\Omega_\ell\,\partial M^2_{jk}} = \frac{1}{\pi}\frac{P_{jk}P^*_j}{M_{jk}}\frac{1}{N}\sum_i \frac{M_{k\ell_i}}{P'_{\ell_i}P_{k\ell_i}}\;\frac{\cos(\theta_\ell - x_{k\ell_i}) - \cos(\theta_\ell + x_{k\ell_i})}{\sin\theta_{j_i}\sin x_{k\ell_i}\sin\phi_{k\ell_i}}\;\frac{\partial^2\sigma(W,\theta_{j_i},M^2_{k\ell_i})}{\partial\Omega_{j_i}\,\partial M^2_{k\ell_i}} \tag{7.40}$$

The problem is now solved. To compute rates for particles decaying from a resonance, for example π^+ rates from Δ^{++} production, Eq. (7.40) can be substituted for the differential cross section in (7.20).

To calculate 2π recoil rates, the recoil products need only to be tested to see if they passed through the recoil counter. Only for events for which the recoils are successful are the factors inside the sum symbols in (7.20) and (7.40) kept.

The preceeding process was used to compute 2π rates at selected spectrometer settings for the processes in (7.2). The results of this calculation can be seen in Table (19). These are the results for the B momentum channel only (see Appendix V) where the largest 2π contamination occurs. Observe that when the π is detected in the spectrometer the contamination is very low, whereas when the proton is detected the contamination is very high. The proton case is worse because protons from 2π reactions are produced from lower photon energies than the corresponding case for π's. The proton case agrees with the results from the π^0 photoproduction experiment of Wolverton.[11] However when

a recoil counter is placed to detect the π^- particle when the proton is detected in the spectrometer the contamination drops to a negligible level. Overall the contamination was much lower than expected. There are two reasons for this. First, the 2π threshold is not considerably lowered between proton and deuteron targets. The difference at 2π threshold is a drop from 320 MeV to 303 MeV. Second, the cross section is suppressed until there is enough energy to form a Δ^{++} final state. This is considerably above threshold.

Contaminations from other 2π processes should increase contamination above what is indicated in Table 19. There are indications that the reaction used for the calculation has the largest cross section over most of the energy region considered However an estimate can be made of the contribution from the other reactions. In Table 18 there is a summary of the 2π contamination for each type of experimental point and below is a formula by which to estimate a total 2π contamination from the (7.1) rates. This total was lowered by a factor of 2/3 because the Frascati bubble chamber measurements [44] indicated that the deuterium 2π cross sections are low. In Table 20 there is a total estimated 2π contamination for the B channel of the spectrometer. We see only a few instances where the contamination becomes significant.

TABLE 18

2π Reactions Contributing to Contamination

I. All 2π reactions

1. $\gamma p \rightarrow \pi^- \pi^+ p$
2. $\gamma p \rightarrow \pi^o \pi^+ n$
3. $\gamma p \rightarrow \pi^o \pi^o p$
4. $\gamma n \rightarrow \pi^- \pi^+ n$
5. $\gamma n \rightarrow \pi^- \pi^o p$
6. $\gamma n \rightarrow \pi^o \pi^o n$

II. Contaminants to π^- direct cross sections

1. $\gamma p \rightarrow \pi^- \pi^+ p$
4. $\gamma n \rightarrow \pi^- \pi^+ n$
5. $\gamma n \rightarrow \pi^- \pi^o p$

III. Contaminants to π^+ direct cross sections

1. $\gamma p \rightarrow \pi^+ \pi^- p$
2. $\gamma p \rightarrow \pi^+ \pi^o n$
4. $\gamma n \rightarrow \pi^+ \pi^- n$

IV. Contaminants to p direct cross sections

1. $\gamma p \rightarrow p \pi^- \pi^+$
3. $\gamma p \rightarrow p \pi^o \pi^o$
5. $\gamma n \rightarrow p \pi^- \pi^o$

V. Contaminants to π^- recoil cross sections

1. $\gamma p \rightarrow \pi^- \pi^+ p$ big
5. $\gamma n \rightarrow \pi^- \pi^o p$ big
4. $\gamma n \rightarrow \pi^- \pi^+ n$ small

VI. Contaminants to π^+ recoil cross sections

1. $\gamma p \rightarrow \pi^+ \pi^- p$ big
4. $\gamma n \rightarrow \pi^+ \pi^- n$ small

VII. Contaminants to p recoil cross sections

1. $\gamma p \rightarrow p \pi^- \pi^+$
5. $\gamma n \rightarrow p \pi^- \pi^o$

Complete Contamination Rates

for π direct rates use $\frac{3}{2}(\pi^- + \pi^+)$ rate of reaction 1

for π^- recoil rates use $2\pi^-$ rate of reaction 1

for π^+ recoil rates use π^+ rate of reaction 1

for p direct rates use 3p rate of reaction 1

for p recoil rates use $\frac{3}{2}$ p rate of reaction 1

TABLE 19

2π Photoproduction Contamination from the Reaction

$$\gamma + P \rightarrow \pi^- + \pi^+ + P$$

θ_{cm}	K	Particle	Total Observed Rate*	Calculated 2π Rate*	% Cont.
20	825	π^-	17.01	4.27×10^{-3}	0.03
20	825	π^+	22.12	1.24×10^{-3}	0.01
75	825	π^-	7.84	1.43×10^{-2}	0.18
75	825	π^- recoil	3.57	2.24×10^{-3}	0.06
75	825	π^+	11.96	8.59×10^{-3}	0.07
105	825	π^-	14.02	1.75×10^{-2}	0.12
105	825	π^- recoil	7.59	5.02×10^{-3}	0.07
105	825	π^+	18.84	2.54×10^{-2}	0.14
150	825	π^-	11.02	2.08×10^{-2}	0.19
150	825	π^+	4.93	6.82×10^{-2}	1.39
150	825	P	67.46	6.97	10.34
150	825	P recoil	7.49	7.80×10^{-2}	1.04
20	1118	π^-	10.71	3.92×10^{-2}	0.36
20	1118	π^+	16.28	2.11×10^{-2}	0.13
110	1118	π^-	4.40	9.03×10^{-2}	2.05
110	1118	π^- recoil	1.46	2.83×10^{-2}	1.94
110	1118	π^+	6.54	1.10×10^{-1}	1.69
150	1118	π^-	4.21	2.30×10^{-2}	0.54
150	1118	π^+	3.57	3.79×10^{-2}	1.06
150	1118	P	14.38	2.40	16.70
150	1118	P recoil	1.17	4.62×10^{-2}	3.95

* Rates are in units of counts per 10^{14} MeV of beam energy.

TABLE 20

Total 2π Photoproduction Contamination

θ_{cm}	K	Particle	Total Observed Rate *	Calculated 2π Rate*	% Cont.
20	825	π^-	17.01	5.51×10^{-3}	0.03
20	825	π^+	22.12	5.51×10^{-3}	0.02
75	825	π^-	7.84	2.28×10^{-2}	0.29
75	825	π^- recoil	3.57	2.99×10^{-3}	0.08
75	825	π^+	11.96	2.28×10^{-2}	0.19
105	825	π^-	14.02	4.29×10^{-2}	0.31
105	825	π^- recoil	7.59	6.71×10^{-3}	0.09
105	825	π^+	18.84	4.29×10^{-2}	0.23
150	825	π^-	11.02	8.91×10^{-2}	0.81
150	825	π^+	4.93	8.91×10^{-2}	1.81
150	825	P	67.46	13.95	20.68
150	825	P recoil	7.49	7.80×10^{-2}	1.04
20	1118	π^-	10.71	6.03×10^{-2}	0.56
20	1118	π^+	16.28	6.03×10^{-2}	0.37
110	1118	π^-	4.40	2.01×10^{-1}	4.57
110	1118	π^- recoil	1.46	3.78×10^{-2}	2.58
110	1118	π^+	6.54	2.01×10^{-1}	3.07
150	1118	π^-	4.21	6.79×10^{-2}	1.61
150	1118	π^+	3.57	6.79×10^{-2}	1.90
150	1118	P	14.38	4.81	33.45
150	1118	P recoil	1.17	4.62×10^{-2}	3.95

* Rates are in units of counts per 10^{14} MeV of beam energy.

THE 3 BODY FINAL STATE SYSTEM

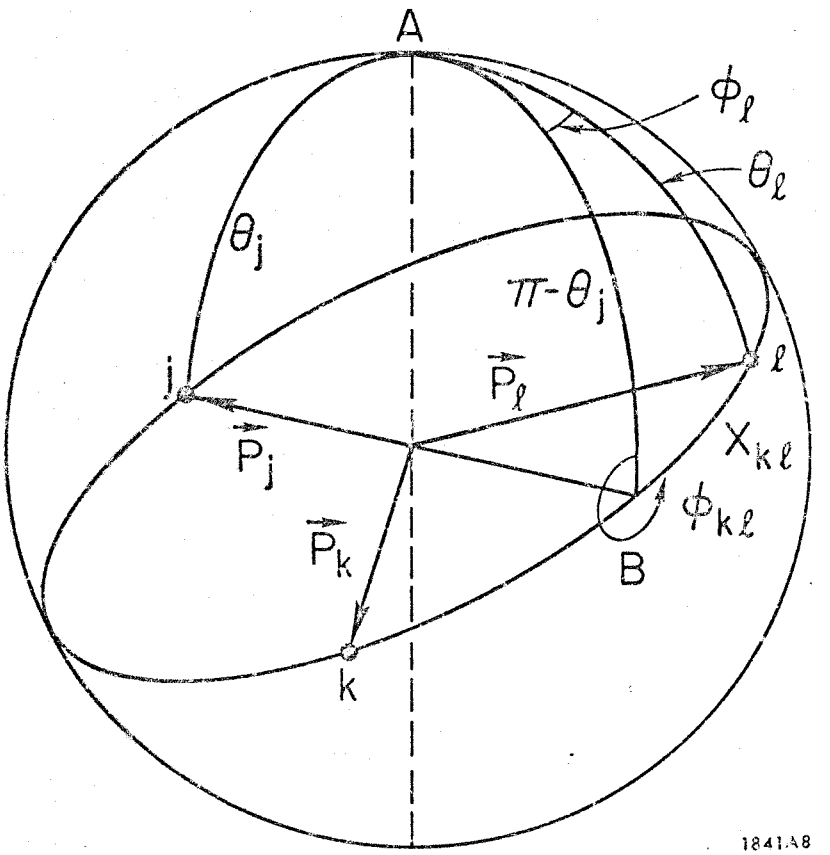

FIGURE 35

APPENDIX VIII

PROTON CORRECTIONS

A. Momentum Loss

When the proton is detected in the spectrometer, the measured momentum must be corrected for the momentum lost by the proton traversing the material from the target to the spectrometer aperature. Using tables of dE/dx prepared by Groom's [45] range-energy program, the momentum loss, ΔP was calculated for proton momenta between 600 MeV/c and 1600 MeV/c at 10 MeV/c, intervals. This exercise was identical to that of Wolverton [11] except the dE/dx tables for hydrogen were replaced by those for deuterium. The results are to be seen in Figure 36. P_{mag} in the figure refers to the momentum at the magnet aperature. To get the momentum at target, P_{source}, we use the equation

$$P_{source} = P_{mag} + \Delta P \quad . \tag{8.1}$$

You will notice there are two cases in Figure 36 labelled aluminum and mylar. The first refers to protons passing through the aluminum jacket of the target and the second to protons passing through the target's upstream mylar window.

A correction must be made not only for momentum loss, but also for the spectrometer acceptance change due to the momentum loss. The experimental acceptance is DP_{source}, the spectrometer acceptance is DP_{mag}, and thus the relation needed is

$$DP_{source} = \left(\frac{DP_{source}}{DP_{mag}}\right) \cdot DP_{mag} \quad . \tag{8.2}$$

The acceptance change (DP_{source}/DP_{mag}) is calculated from differentiating the curve in Figure 36 and using

$$\frac{DP_{source}}{DP_{mag}} = 1 + \frac{D(\Delta P)}{DP_{mag}} \tag{8.3}$$

which is easily derivable from (8.1). The acceptance change as a function of P_{mag} can be seen in Figure 37.

For the cross section calculation in Appendix II and the 2π contamination calculation in Appendix VII, the curves in Figures 36 and 37 were tabularized for the convenience of the computor. For each Monte Carlo event in those calculations provision is made to choose a spectrometer momentum for the detected proton. With the value of P_{mag}, ΔP, and (DP_{source}/DP_{mag}) are obtained from the tables. P_{source} is used for the subsequent kinematical calculations in the event, and (DP_{source}/DP_{mag}) is used as a multiplicative correction to the acceptance for each event.

B. Proton Loss Corrections

At small π^- production angles, the recoil protons come off with very little kinetic energy, and subsequently are very likely to be stopped by the matter between the production point and the last counter of the recoil array. As a result the recoil counters will detect fewer protons than would be expected purely from reaction kinematics and the counters' geometrical size. This effect can be seen in Figure 38 which shows the recoil cross sections dropping below the spectrometer cross sections at the lower photon energies. The

proton momentum at which the recoil cross sections begin to dramatically fall off is around 350 MeV/c.

It was assumed that the observed effect was entirely due to a combination of energy loss and target size. Production points at different positions in the target would result in varying amounts of matter to be traversed by the protons before reaching the recoil counters. Protons produced furthest from the counters would be stopped while those with identical momentum produced closer would not.

To calculate this effect the proton energy loss process was run backwards. That is, starting with a proton of 0 momentum at the last recoil counter, energy was added to the proton as it was moved towards the target by using Groom's dE/dx tables in reverse. The momentum the proton has when it reaches the target is the minimum momentum required to reach the recoil counters. It is denoted P_{min}. The proton is then moved through the target adding energy as it goes until the farthest point of the target is reached. The momentum here is the maximum momentum for which a proton can be stopped. It is denoted P_{max}. The proton momentum at various positions in the target gives a momentum-range curve. Momentum-range curves for various penetrations of the last recoil counter are shown in Figure 39. The labels indicate the penetration. The curves are used as follows. For the $\frac{1}{4}$" curve a target thickness of 0.74 inches corresponds to a proton momentum of 330 MeV/c. This means that a 330 MeV/c proton will not traverse more than 0.74 inches through the target deuterium and trigger the last recoil counter. The curves in Figure 39 were tabularized for computer calculations.

The process used to correct the Monte Carlo calculation of the recoil

response (see Appendix II) for proton losses is as follows: for each Monte Carlo event

1. Determine the production point and the proton recoil momentum $\vec{P}_R$.

2. If $P_R \leq P_{min}$, drop the event.

3. If $P_R > P_{min}$, determine if the proton would hit and trigger the recoil counters. If it does not, drop the event.

4. If (3) is passed, and $P_R \geq P_{max}$, the event is successful.

5. If (4) is not true, determine the proton's path length in the target, L, and determine the proton's deuterium range, L_D, from the range-momentum curve.

6. If $L \geq L_D$, the event fails. If not, it is successful.

It was found that the correction was very sensitive to different penetrations of the last counter in the recoil array. No penetration would under correct. Full penetration would over correct. Penetration through half of the counter, $\frac{1}{4}$ inches, seemed the best choice. That is the correction shown in Figure 38 and was the one used for the final result.

You will notice the four highest photon energy points in Figure 38 are under corrected. However, when the spectrometer cross sections are corrected for background contamination the agreement is very good.

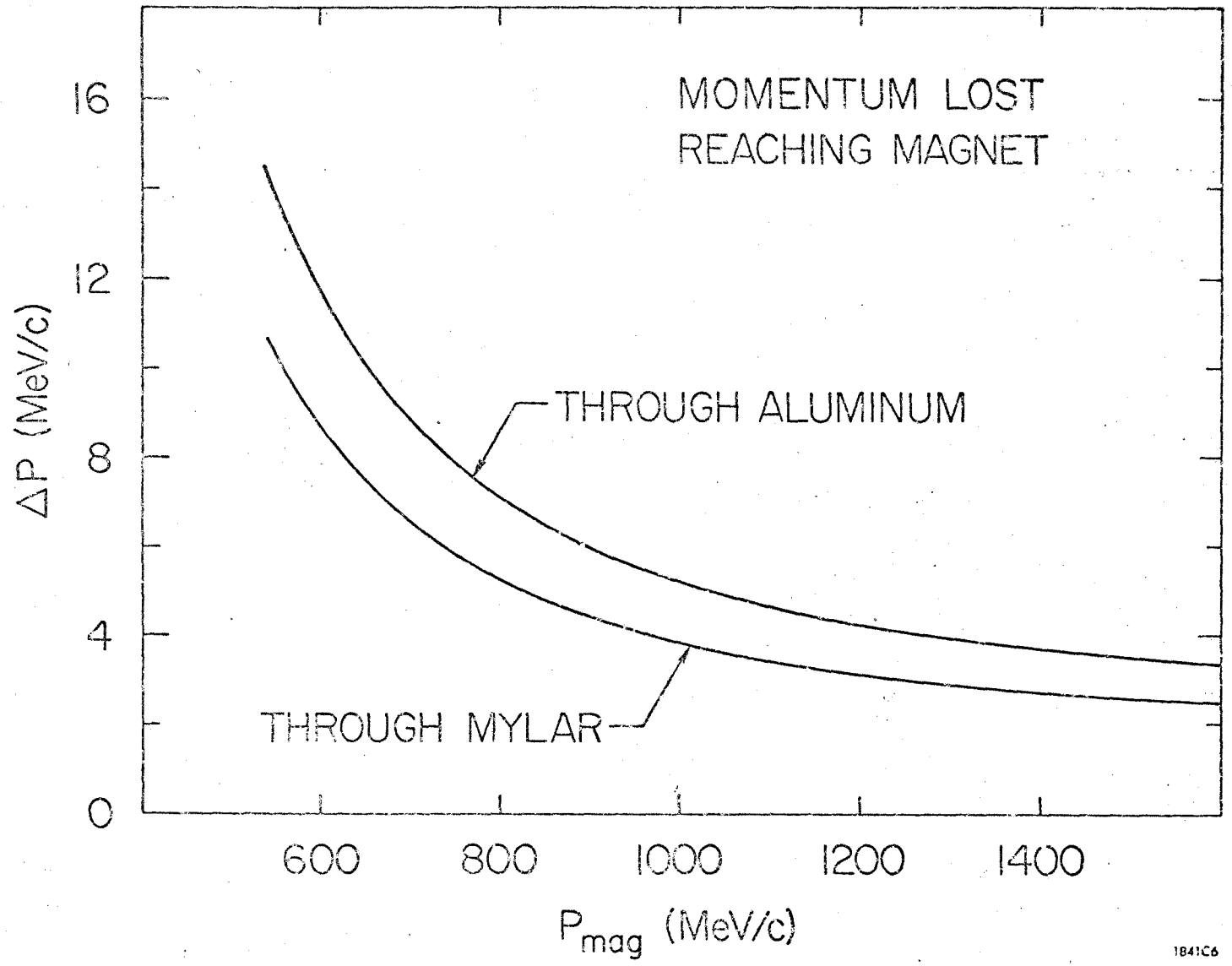
MOMENTUM LOST
REACHING MAGNET
THROUGH ALUMINUM
THROUGH MYLAR
ΔP (MeV/c)
0
4
8
12
16
600
800
1000
1200
1400
Pmag (MeV/c)
1841C6

FIGURE 36

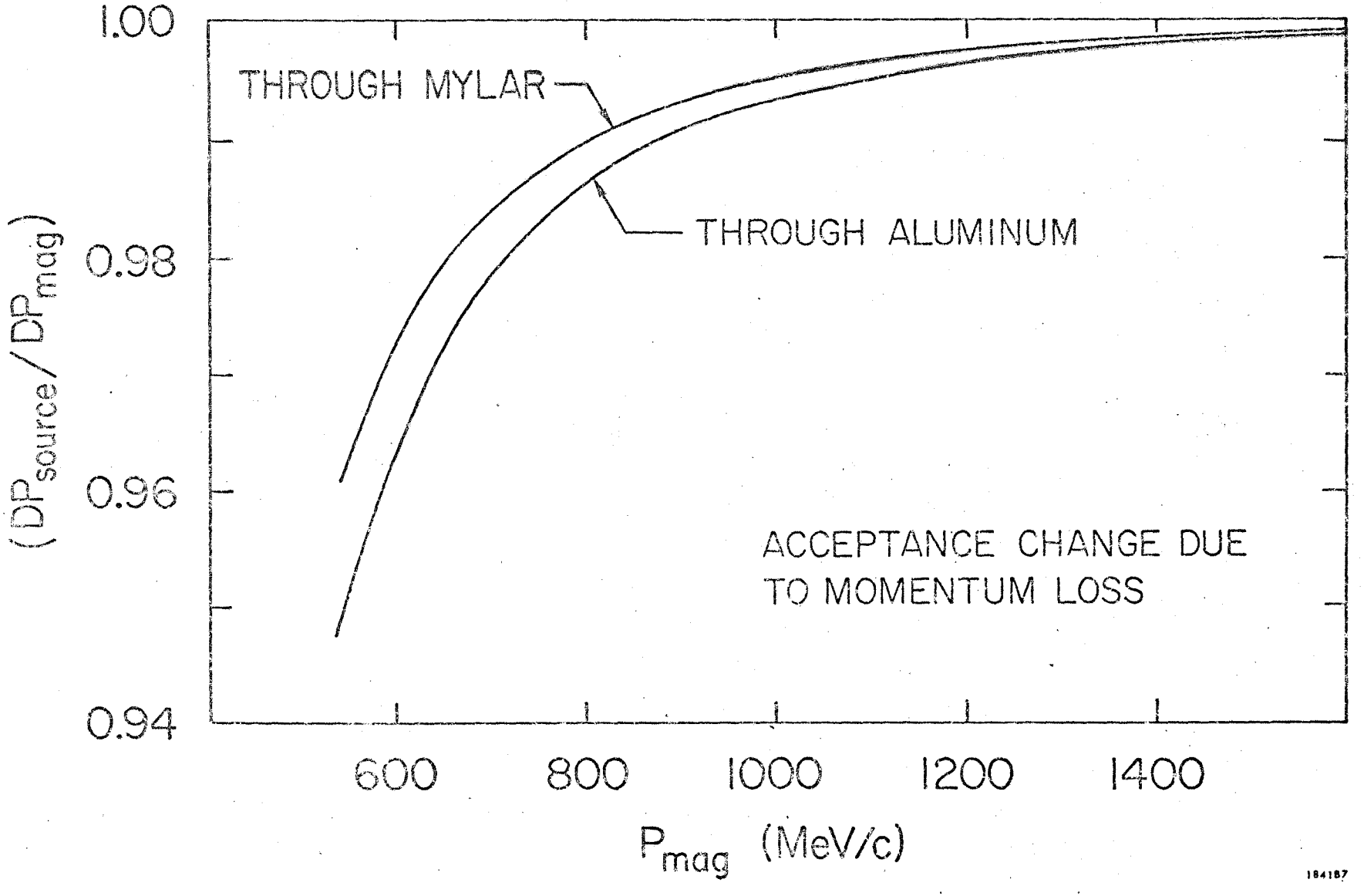
1.00
0.98
0.96
0.94
(DP source / DP mag)
THROUGH MYLAR
THROUGH ALUMINUM
ACCEPTANCE CHANGE DUE
TO MOMENTUM LOSS
600
800
1000
1200
1400
P mag (MeV/c)
184187

FIGURE 37

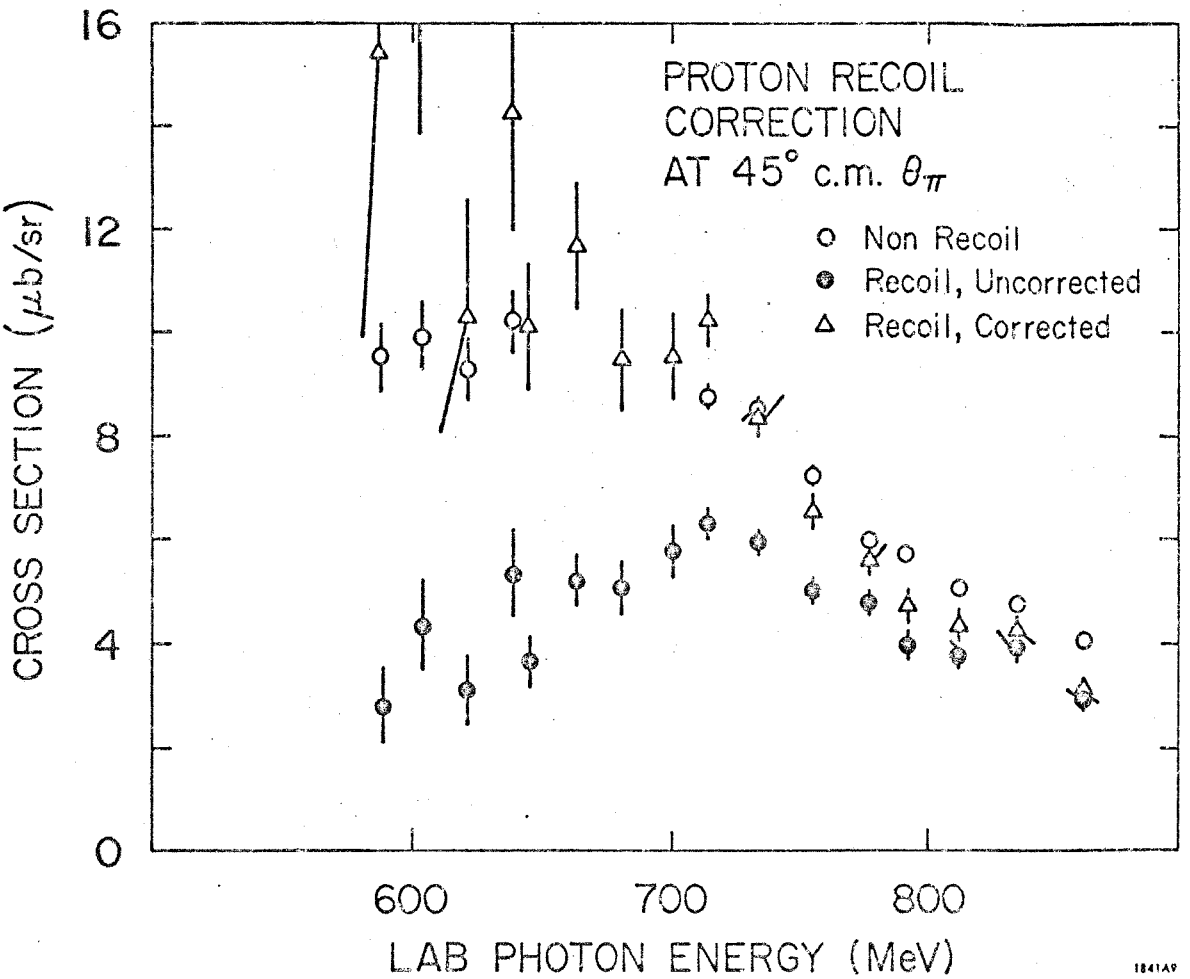
PROTON RECOIL
CORRECTION
AT 45° c.m. θ_π
Non Recoil
Recoil, Uncorrected
Recoil, Corrected
CROSS SECTION (μb/sr)
16
12
8
4
0
600
700
800
LAB PHOTON ENERGY (MeV)
1841A9

FIGURE 38

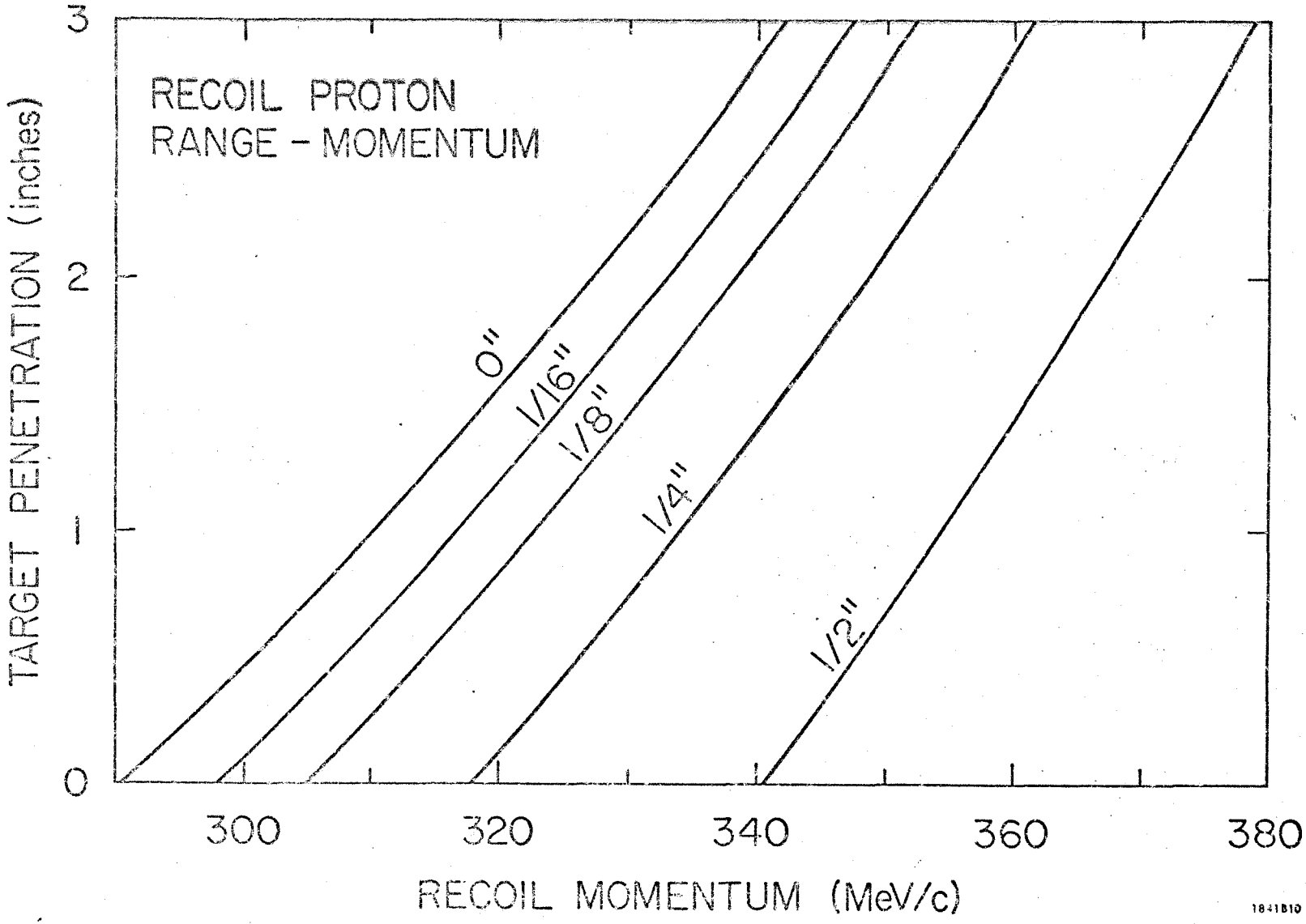
RECOIL PROTON
RANGE - MOMENTUM
TARGET PENETRATION (inches)
0
1
2
3
0"
1/16"
1/8"
1/4"
1/2"
300
320
340
360
380
RECOIL MOMENTUM (MeV/c)
1841B10

FIGURE 39

APPENDIX IX

COUNTERS AND ELECTRONICS

A. Counters

The configuration of the spectrometer counters are illustrated in Figures 2 and 3. The details of their construction have been adequately described in other sources. [5, 10, 11, 12, 13] The only change made to the counters described there was the replacement of the momentum counters in the LEM spectrometer. The new momentum counters are discussed in Appendix V.

The recoil counters were added for this experiment. A drawing of them can be seen in Figure 40. The dimensions of the counters were chosen on the basis of a Monte Carlo study which used a model similar to, but simpler than, the one described in Appendix II.

In this study $\gamma n \rightarrow \pi^- p$ events were randomly generated in which the neutron momentum was distributed according to the Hulthen wave function. For each event the π^- was forced to enter the spectrometer, then the recoil proton was checked to see if it would be detected by a test recoil counter. If the proton was successful the c.m. energy of the reaction would be computed. This process was carried out for a sampling of spectrometer settings and bremsstrahlung end points. The important quantities determined for each run were the efficiency of the test counter and the resolution in the c.m. energy. For the recoil counter design the efficiency of the test counter was not allowed to be much less than 50% in order that the experiment could be run within a reasonable time duration. With this restriction the dimensions of the counter were optimized to give the best resolution of the c.m. energy.

The counter, RC, in Figure 40 was the optimized counter. The large rear counter, RB, was made of a size such that about 80% of the recoil protons would be detected. A coincidence between RC and RB defined a recoil proton. The counters RR and RL were also placed in coincidence with RB. The purpose of these counters was to check the positioning of the recoil array. The average proton efficiency of the recoil array (i. e., RC) was around 40%.

In the HEMA and OUTR spectrometer configurations two Cherenkov counters were used to differentiate between electrons, protons, and pions.

The freon Cherenkov counter, FC, had a threshold $\beta = 0.999$. For the momentum range of this experiment the electron β was always above this threshold and the pion and proton β's were always below. The efficiency of this counter to detect electrons was measured periodically throughout the course of the experiment. This was accomplished by sending a pure electron beam through the spectrometer and recording particle counts with and without FC. The electron beam was produced by placing a pinhole lead collimator in the photon beam and converting the photons by a slab of lead placed in front of the pinhole. The spectrometer was placed at 0° for this measurement. The average efficiency for electrons was 99.70%.

The lucite Cherenkov counter, LC, has a threshold $\beta = 0.9$. The pion β was well above this threshold for all HEMA and OUTR runs. The efficiency for pions was measured using the scalar readings from the π^- data runs. This was possible because the pions and electrons had the same LC efficiency and the protons were not detected because of the polarity of the spectrometer magnet. The efficiency was calculated from the equation

$$\epsilon_\pi = \frac{\pi_S}{\pi_S + P_S} \tag{9.1}$$

where ϵ_π = the LC pion efficiency

π_S = the pion scalar reading

and P_S = the proton scalar reading.

For further details see Appendix X-B. The pion efficiencies as a function of pion momentum are shown in Figure 41 . The fit in that figure is listed in Table 20. The efficiencies given by the fit were used to analyse the π^+ data runs.

The LC ccunter had a non-zero proton efficiency and special runs were required to measure it. For these runs protons were defined independently of LC by the setting of the spectrometer momentum and the time-of-flight requirements of the electronics. The former requirement comes from the knowledge that if a proton and pion have identical momenta, the proton is produced from a lower energy photon. Therefore setting the spectrometer momentum so that the pion's photon energy was slightly greater than the bremsstrahlung end point, eliminated almost all of the pion triggers. The remnant pion contamination was removed by a comparison of the LC pulse height spectrums produced from a π^- beam and the aforementioned proton beam. The formula (9.1) gave the efficiency after π_s and p_s were corrected for π contamination. The results of the proton efficiency measurements are shown in Figure 42, and the fit in that figure is listed in Table 20.

In the LEM spectrometer pions and protons were distinguished by the size of the photomultiplier pulses in S1 and S2. There was no attempt to distinguish pions from electrons in the LEM because the LEM was run at large

lab angles where the electron rates were small. The pulse heights of S1 and S2 were observed in a pulse height analyzer, and using the analyzer the discriminator levels of S1 and S2 were set such that there would be a clean separation between the pion and proton pulse heights. As for the LC pion efficiency, the LEM pion efficiencies could be measured during the π^- runs of the experiment. These results can be seen in Figure 43. The proton efficiencies were measured using a procedure similar to the one used for proton LC efficiencies, and the results of these measurements can be seen in Figure 44. The fits for the LEM pion and proton efficiencies are in Table 20.

B. Electronics

The philosophy behind the electronics was the same as that used by Ecklund [12], Thiessen [10], and Wolverton [11]. In the HEMA electronics of Figure 45 the signal from the S1 counter was placed in a tight coincidence with FAN, A2, and A1, the three counters with the highest counting rate. These signals were combined in the slower electronics to define a particle event which was

$$PAR\cdot\overline{FAN} = (S1\cdot S2\cdot S3\cdot A1)\cdot(S1\cdot A2)\cdot(S1\cdot\overline{FAN}) \quad . \tag{9.2}$$

The $PAR\cdot\overline{FAN}$ signal was put in coincidence with various combinations of the Cherenkov counter signals LC and FC, which defined particles e, p, π, and X.

The X stands for events that triggered FC, but not LC. This signal is impossible physically and indicated the inefficiencies in the Cherenkov counters. The π signal was put into coincidence with each of the S2 counter signals, T, TC, BC, and B, which defined the π rate in each of the four momentum channels.

Provisions were made so that the proton and electron signal could be put in coincidence with the S2 counters instead of the π. The accidental monitoring was done by placing delays of 100 ns on the FAN, A2, and Al signals and setting up parallel electronic circuits which were identical to that of the main trigger. Accidentals will be discussed in more detail in Appendix X.

The LEM electronics illustrated in Figure 46 were set up in a similar fashion as the HEMA electronics except that there is no A2 counter and no Cherenkov counters. The PAR·$\overline{\text{FAN}}$ signal was differentiated into π's and p's using pulse height discrimination on Sl and S2. There was no provision to detect electrons.

The signals from the recoil counter array were picked off with the S (see Figures 45 and 46) and π signals from either the HEMA or the LEM electronics. With the resultant signals a coincidence was made between RC and RB which defined the recoil particle events. This signal was placed in coincidence with each of the four momentum counter signals which came from the same electronics as π and S. The recoil electronics are schematically drawn in Figure 47.

TABLE 21

PARTICLE DETECTION EFFICIENCIES

I. π Efficiencies

fit

$$\epsilon_\pi = A_0 + A_1(P/100)^2 + A_2(P/100)^2$$

where

ϵ_π = efficiency expressed in %

P = spectrometer momentum (MeV/c)

Configuration	A_0	A_1	A_2
HEMA	95.158	1.0711	-0.075639
OUTR	98.28	0	0
LEM	100.20	-0.12596	0

II. P Efficiencies

fit

$$\epsilon_P = A_0 + A_1(P/100) + A_2(P/100)^2 \quad \text{if } P > P_{min}$$

$$\epsilon_P = E_{min} \quad \text{if } P \leq P_{min}$$

where

ϵ_P = efficiency expressed in %

P = spectrometer momentum (MeV/c)

Configuration	A_0	A_1	A_2	P_{min}	E_{min}
HEMR	7.8571	-1.7433	0.10475	832.12	0.604
OUTR	7.8571	-1.7433	0.10475	832.12	0.604
LEM	-28.446	5.28	0	550.0	0.594

THE RECOIL COUNTER

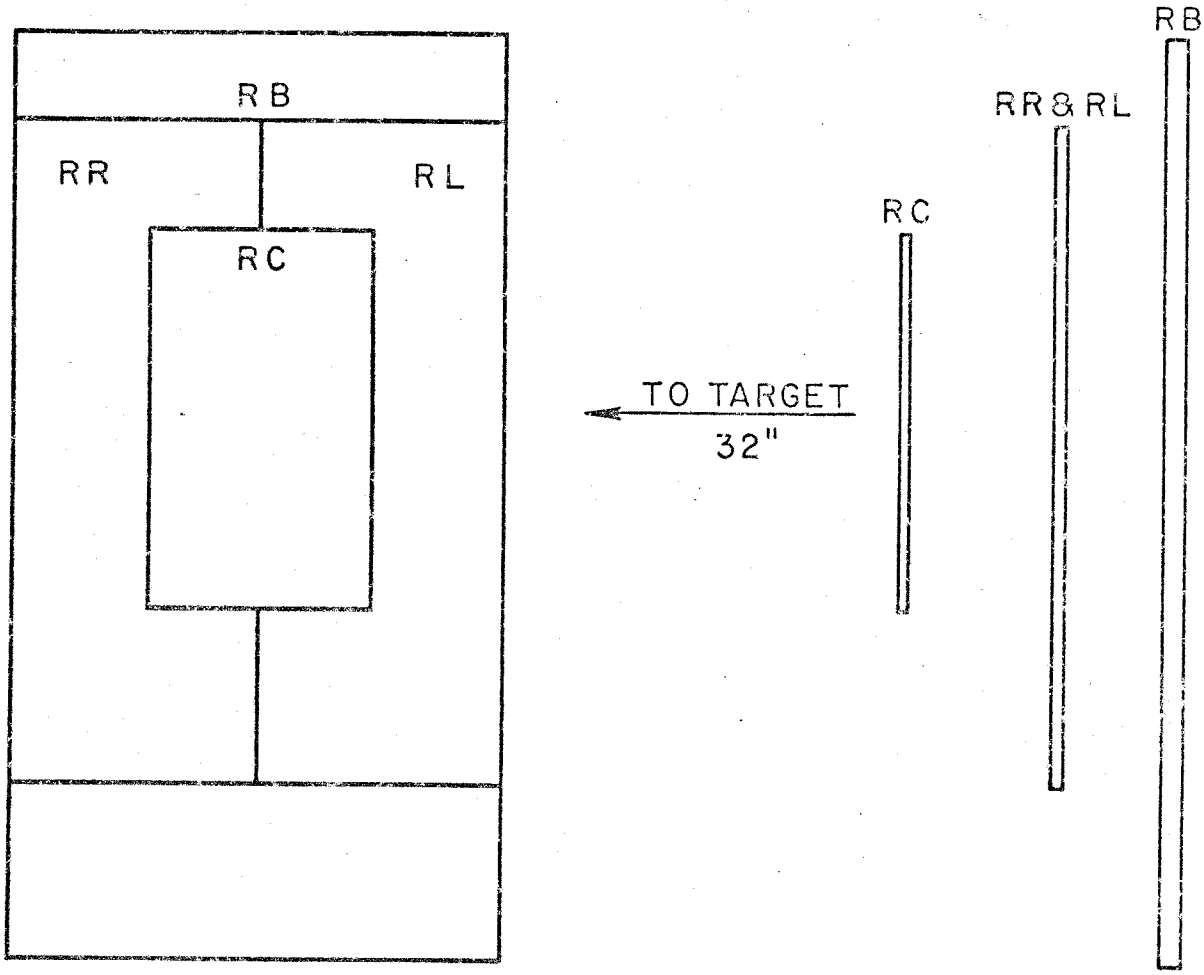

COUNTER DIMENSIONS

RC $5" \times 8\frac{1}{2}" \times \frac{1}{4}"$ RL $5\frac{1}{2}" \times 15" \times \frac{1}{4}"$

RR $5\frac{1}{2}" \times 15" \times \frac{1}{4}"$ RB $11" \times 21" \times \frac{1}{2}"$

1841A12

FIGURE 40

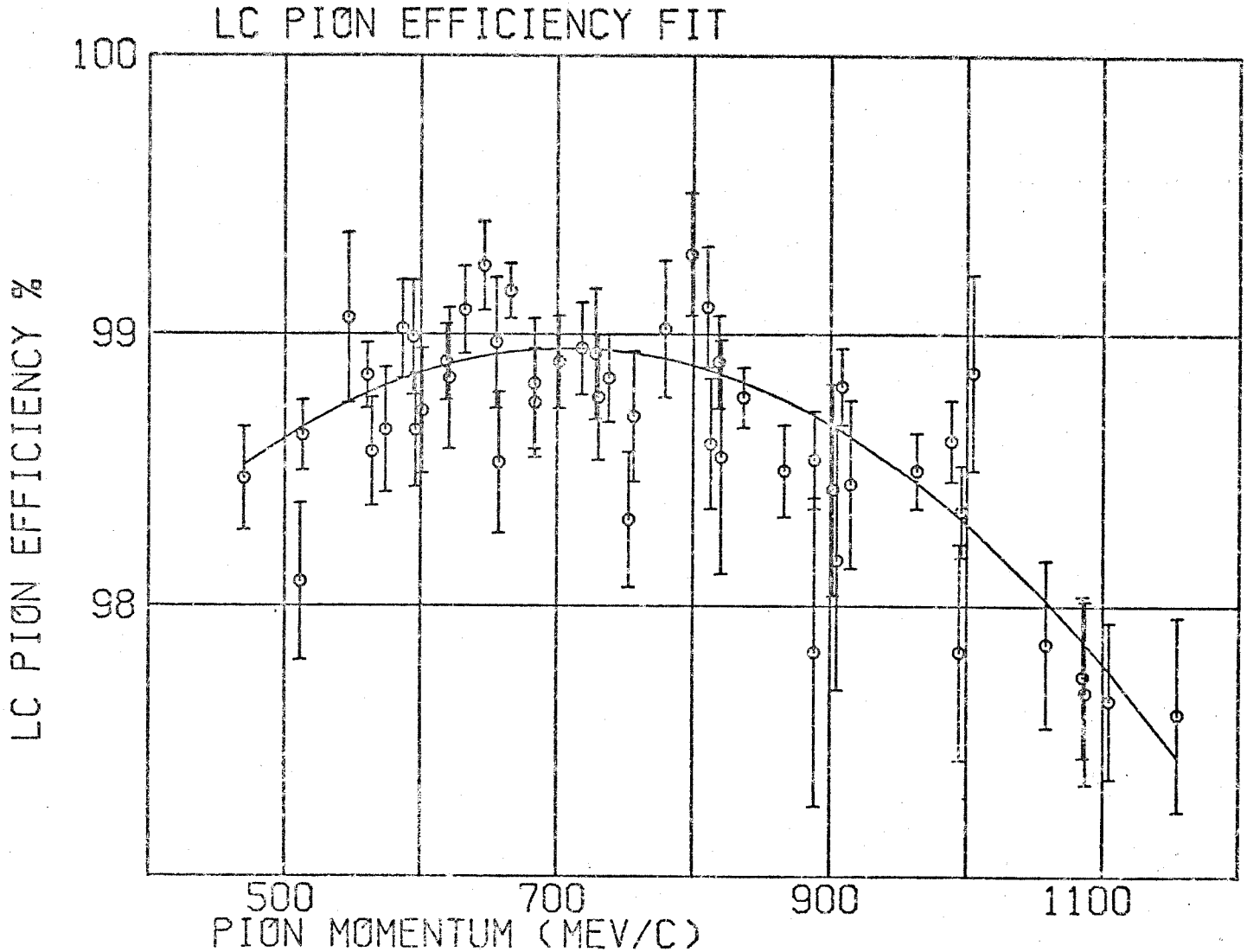
LC PION EFFICIENCY FIT
100
99
98
LC PION EFFICIENCY %
500
700
900
1100
PION MOMENTUM (MEV/C)

FIGURE 41

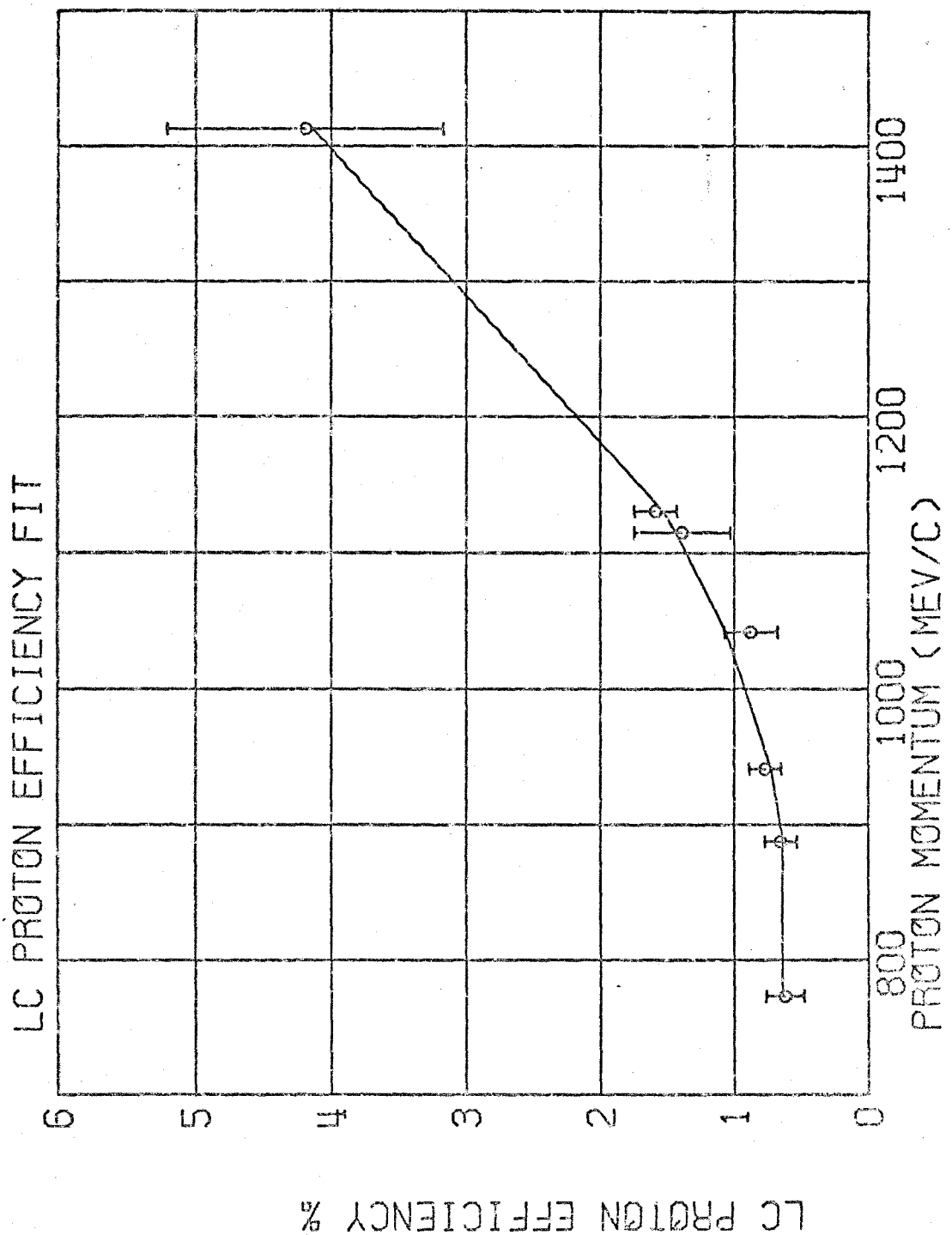
LC PROTON EFFICIENCY FIT
LC PROTON EFFICIENCY %
PROTON MOMENTUM (MEV/C)
0
1
2
3
4
5
6
800
1000
1200
1400

FIGURE 42

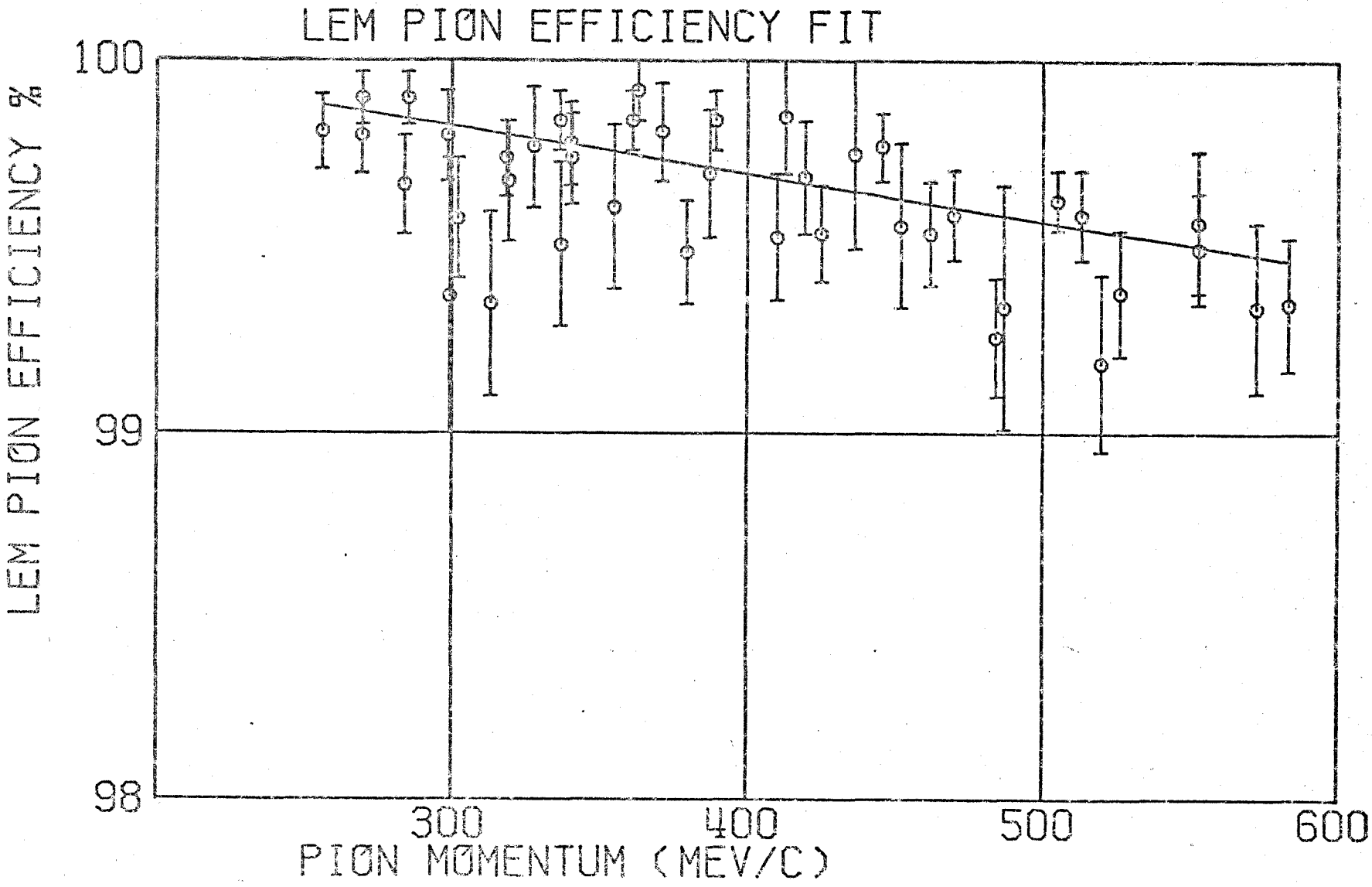
LEM PIØN EFFICIENCY FIT
LEM PIØN EFFICIENCY %
100
99
98
300
400
500
600
PIØN MØMENTUM (MEV/C)

FIGURE 43

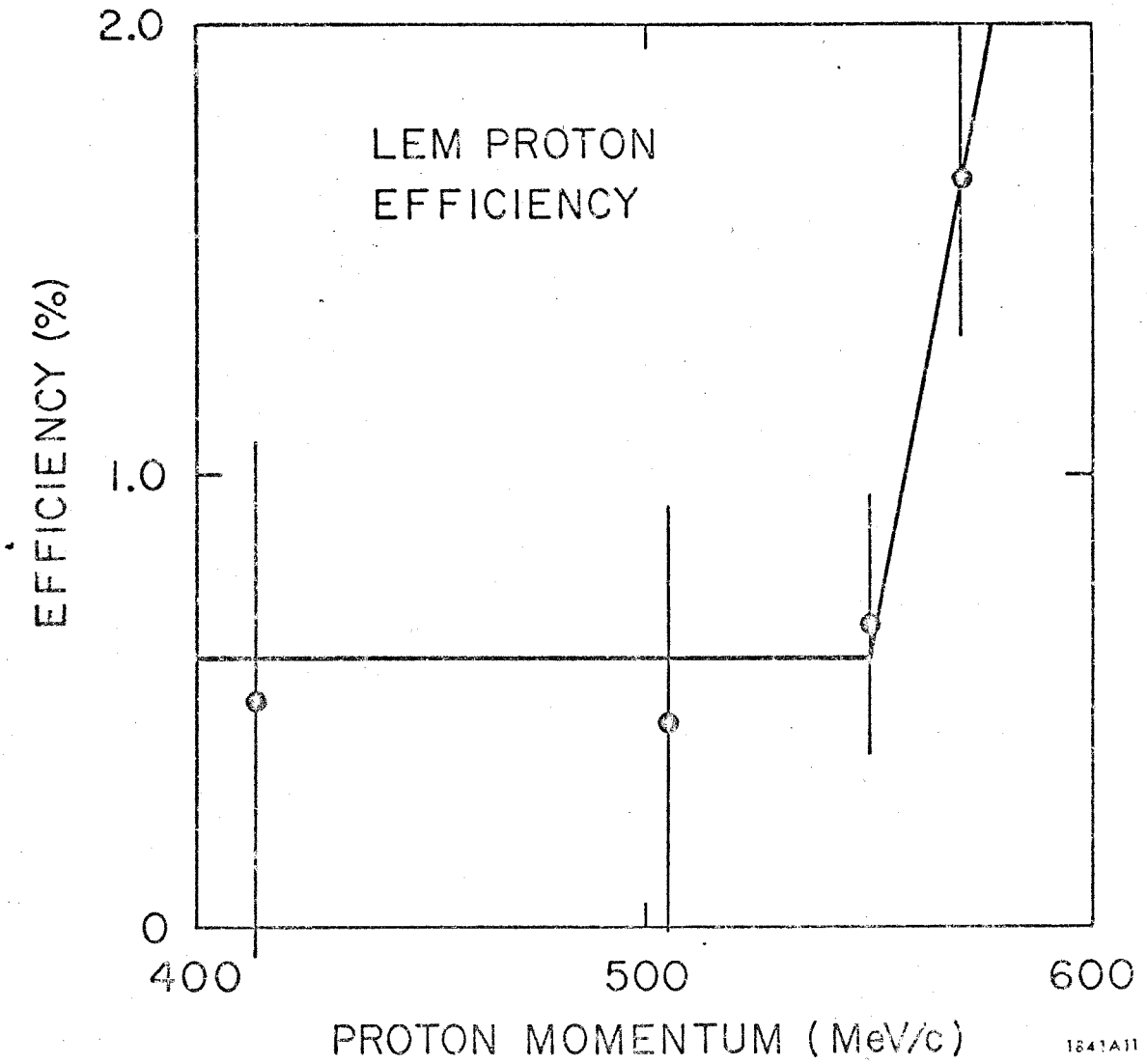
LEM PROTON
EFFICIENCY
EFFICIENCY (%)
2.0
1.0
0
400
500
600
PROTON MOMENTUM (MeV/c)
1841A11

FIGURE 44

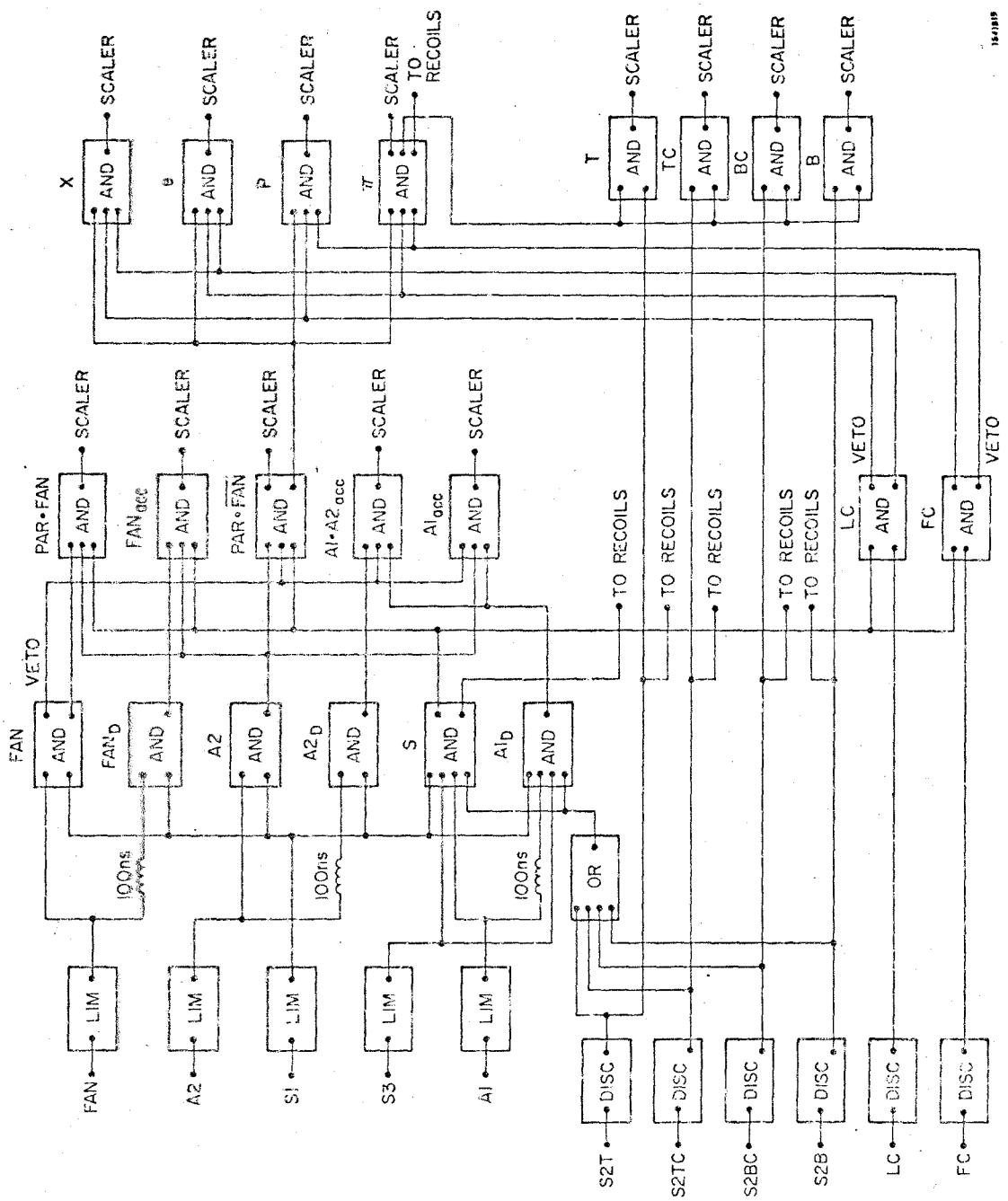

FIGURE 45
The HEMA Electronics

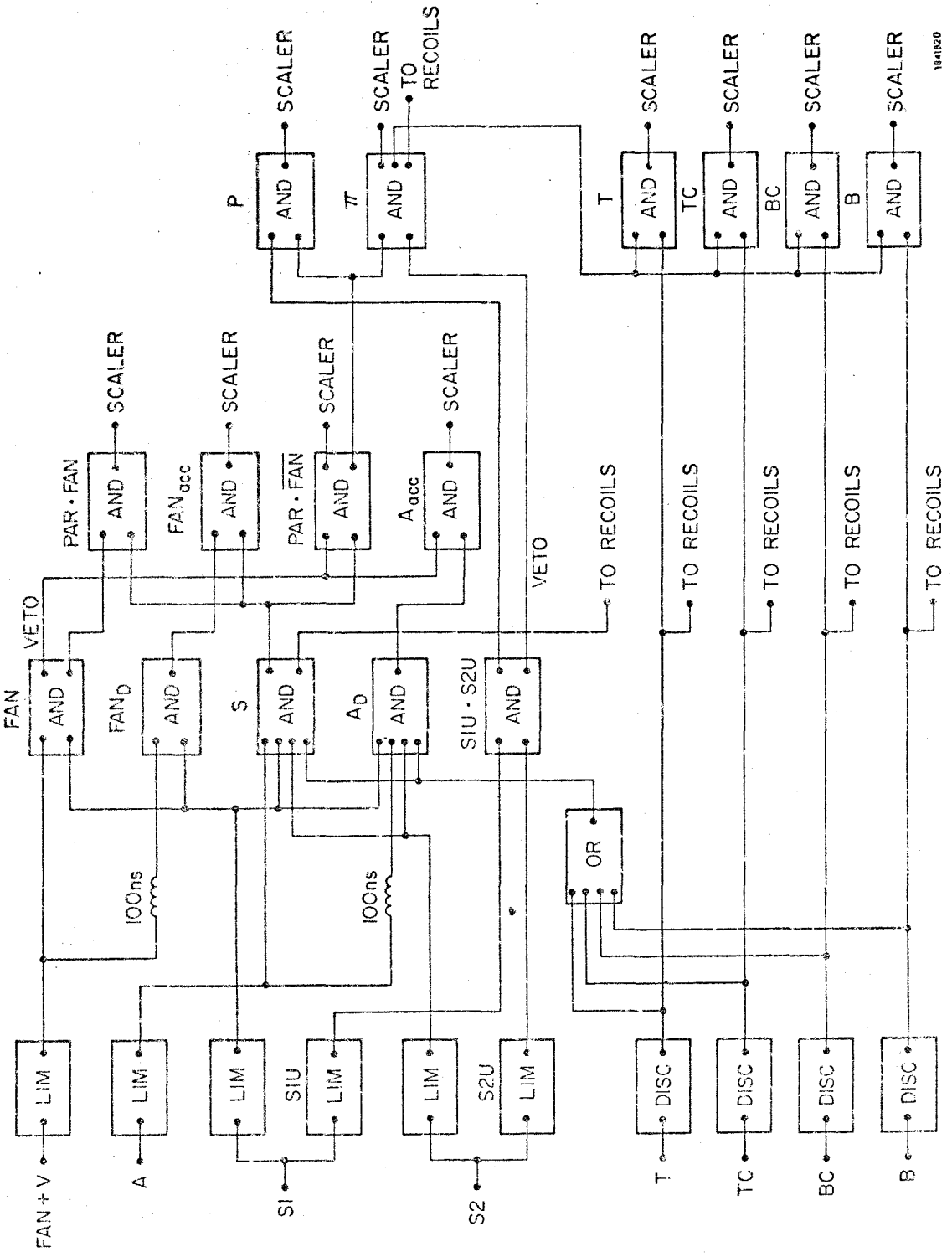

FIGURE 46
The LEM Electronics

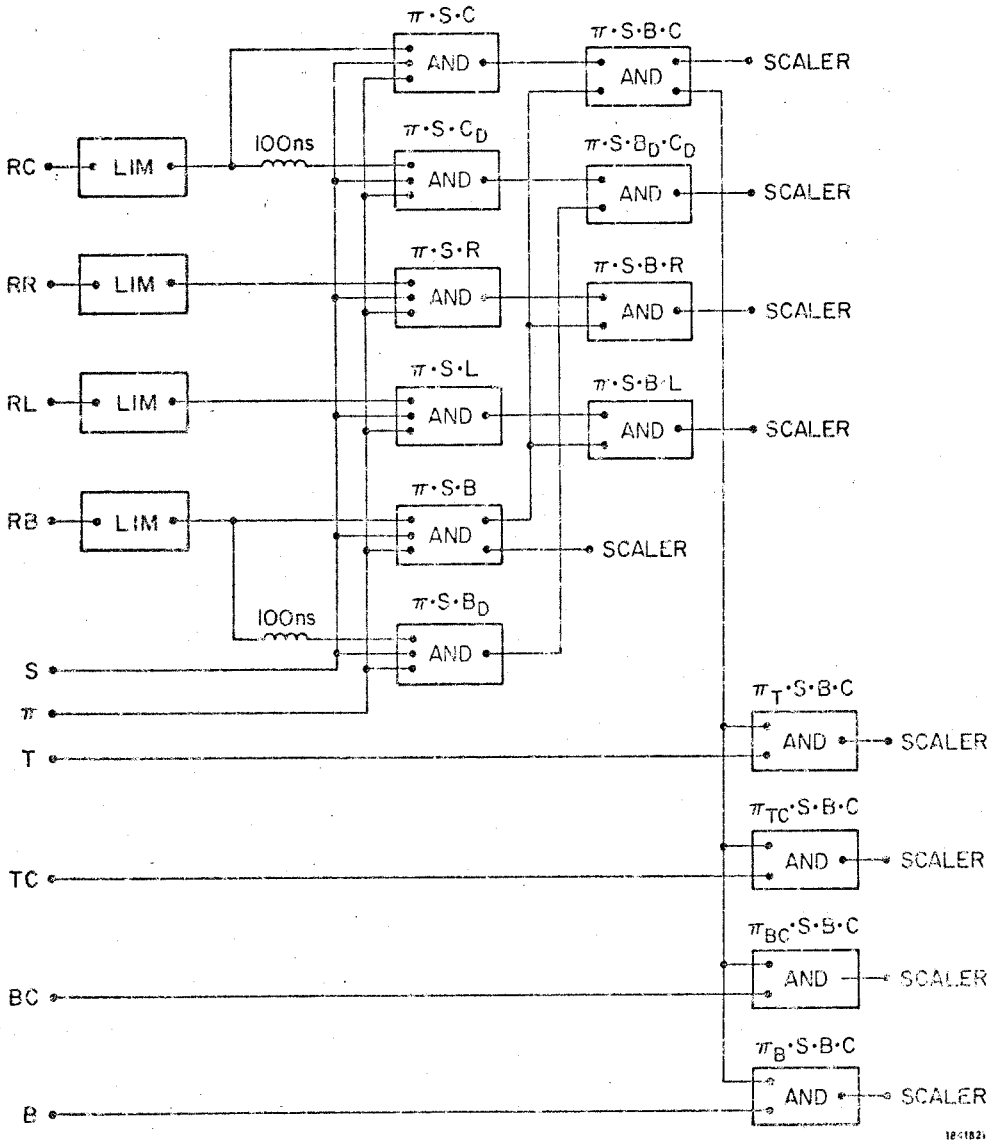

FIGURE 47

The Recoil Electronics

APPENDIX 10

DATA REDUCTION

A. Accidental Corrections

Runs with HEMA electronics (see Appendix 9) had to have the raw particle triggers

$$PAR\cdot\overline{FAN} = (S1\cdot A1\cdot S2\cdot S3)\cdot(S1\cdot S2)\cdot(S1\cdot\overline{FAN}) ,$$

corrected for accidentals caused by the high counting rate in counters FAN, A1, and A2. To monitor these accidentals there were three scalers

$$A1_{acc} = (S1\cdot A1_D\cdot S2\cdot S3)\cdot S1\cdot A2)\cdot(\overline{S1\cdot FAN}) ,$$

$$A1\cdot A2_{acc} = (S1\cdot A1_D\cdot S2\cdot S3)\cdot(S1\cdot A2_D)\cdot(\overline{S1\cdot FAN}) ,$$

and

$$FAN_{acc} = (S1\cdot A1\cdot S2\cdot S3)\cdot(S1\cdot A2)\cdot(\overline{S1\cdot FAN_D}) ,$$

and, in addition, there was a scaler

$$PAR\cdot FAN = (S1\cdot A1\cdot S2\cdot S3)\cdot(S1\cdot A2)\cdot(S1\cdot FAN)$$

which was needed for the accidental analysis. The $A1_D$, $A2_D$, and FAN_D signals were delayed 100 ns with respect to S1. The LEM electronics had the identical setup except there was no equivalent A2 counter, hence no $A1\cdot A2_{acc}$ scaler.

The only accidental corrections actually made were for the FAN_{acc} which were relatively straightforward to analyze. The $A1_{acc}$ and $A1\cdot A2_{acc}$ rates were not used in the analysis because these accidentals cause two different effects, and it was unclear if they should be subtracted from the $PAR\cdot\overline{FAN}$ count as a true accidental or added as a dead time correction. Because of the

ambiguity, $(A1_{acc} + A1 \cdot A2_{acc})$ was included in the error of the corrected $PAR \cdot \overline{FAN}$ count.

For the following analysis the notations to be observed are:

$P \cdot \overline{F}$ = the $PAR \cdot \overline{FAN}$ scaler reading

$P \cdot F$ = the $PAR \cdot FAN$ scaler reading

F_A = the FAN_{acc} scaler reading

α_{FA} = the FAN accidental probability

α_F = the FAN veto probability

R_F = the FAN counting rate

L = the FAN live time per pulse

D = FAN dead time per pulse

T = spectrometer events $(A1 \cdot A2 \cdot S1 \cdot S2 \cdot S3)$

The FAN accidental probability, α_{FA}, can be related to the FAN counting rate by the equation

$$\alpha_{FA} = R_F L \tag{10.1}$$

which is the probability that the FAN counters are on. The probability that the FAN will be off is

$$d = R_F D . \tag{10.2}$$

Careful considerations will give us the relations

$$P \cdot F = (\alpha_F + \alpha_{FA} - \alpha_F(\alpha_{FA} + d))T \tag{10.3}$$

$$T = P \cdot \overline{F} + P \cdot F \tag{10.4}$$

and

$$\alpha_{FA} = F_A / T \,. \tag{10.5}$$

Substituting (10.4) and (10.5) into Eq. (10.3) gives

$$\alpha_F = \frac{P \cdot F - F_A}{T - (F_A + dT)} \,. \tag{10.6}$$

If it is now assumed that L = D then $\alpha_{FA} = d$. A study of the output of the limiter module which transformed the FAN signal into a logic signal made this assumption reasonable. This transforms Eq. (10.6) to

$$\alpha_F = \frac{P \cdot F - F_A}{P \cdot \overline{F} + P \cdot F - 2F_A} \,. \tag{10.7}$$

We have now solved the equations.

With the solutions we can now correct $P \cdot \overline{F}$ for FAN accidentals. The true value is given by

$$P \cdot \overline{F}_T = (1 - \alpha_F) T \tag{10.8}$$

With the proper substitutions we get

$$P \cdot \overline{F}_T = (P \cdot \overline{F} - F_A) \left(\frac{P \cdot \overline{F} + P \cdot F}{P \cdot \overline{F} + P \cdot F - 2F_A} \right) \,. \tag{10.9}$$

The value in (10.10) can be used to correct the counts in the momentum channels (see Part B).

B. π, p and e Calculations

For the HEMA and OUTR spectrometer configurations the LC and FC Cherenkov counters differentiated between π's, p's, and e's. For the LEM spectrometer configuration S1·S2 discriminator bias differentiated between π's and p's (see Appendix IX). The process is not 100% efficient hence the readings in the π, p, and e scalers must be corrected for the inefficiencies. We will use the following notations:

π, p, e will represent the true number of particles

π_s, p_s, e_s will be the scaler readings

ϵ_π = the π and/or e efficiency of LC or S1·S2

ϵ_p = the p efficiency of LC or S1·S2

ϵ_F = the e efficiency of FC

η = the FC accidental probability per spectrometer particle

x_s = the spurion scaler *

We will consider the π^+ runs in the HEMA or OUTR first. Other cases are a subset of this case. Ignoring η we can write the equations:

$$\begin{aligned} \pi_s &= \epsilon_\pi \pi + \epsilon_p p + (1-\epsilon_F)\,\epsilon_\pi e \\ p_s &= (1-\epsilon_\pi)\pi + (1-\epsilon_p)p + (1-\epsilon_F)(1-\epsilon_\pi)e \\ e_s &= \epsilon_F \epsilon_\pi e \\ x_s &= \epsilon_F(1-\epsilon_\pi)e \end{aligned} \qquad (10.10)$$

* This is the x scaler discussed in Appendix IX. The events it recorded indicated inefficiencies with the Cherenkov counters.

The FC counter had a large counting rate ($\sim 10^5$/sec.), so that the effect of its accidental probability, η, was not altogether unnoticeable. However, it has no significant effect on the computed numbers for π, p and e. Its only noticeable effect was to make x_s disproportionately large (i.e., $x_s/e_s >> \epsilon_\pi/(1-\epsilon_\pi)$) for runs where there were a large number of p's. In what follows η could have safely been ignored, but it was included for monitoring purposes. Because of the discriminator used on FC there was also a dead time probability equal to η which must also be included. Putting η into (10.10) we get

$$\begin{aligned}
\pi_s &= (1-\eta)\epsilon_\pi \pi + (1-\eta)\epsilon_p p + (1-\epsilon_F-\eta+2\eta\epsilon_F)\epsilon_\pi e \\
p_s &= (1-\eta)(1-\epsilon_\pi)\pi + (1-\eta)(1-\epsilon_p)p + (1-\epsilon_F-\eta+2\eta\epsilon_F)(1-\epsilon_\pi)e \\
e_s &= \eta\epsilon_\pi \pi + \eta\epsilon_p p + (\epsilon_F+\eta-2\eta\epsilon_F)\epsilon_\pi e \\
x_s &= \eta(1-\epsilon_\pi)\pi + \eta(1-\epsilon_p)p + (\epsilon_F+\eta-2\eta\epsilon_F)(1-\epsilon_\pi)e\,.
\end{aligned} \tag{10.11}$$

In the experimental situation the scaler readings on the left hand side of (10.11) are measured for each run and the efficiencies are known from the measurements described in Appendix IX. The unknowns in (10.11) are the particle counts π, p, and e and the FC accidental probability η. Thus we have four equations and four unknowns and (10.11) can be solved. However, it is not straightforward because the equations in (10.11) are non-linear and have to be solved by an interative method. An initial value of 0 is chosen for η and is plugged into the first three equations of (10.11). These equations are linear in the other unknowns and can be solved to give

$$\pi = \frac{(1-\eta)(1-\epsilon_p)\epsilon'_F\epsilon_\pi - \eta\epsilon_p(1-\epsilon'_F)(1-\epsilon_\pi)}{\epsilon_\pi(\epsilon'_F-\eta)(1-\eta)(\epsilon_\pi-\epsilon_p)}\pi_s - \frac{\epsilon_p}{(1-\eta)(\epsilon_\pi-\epsilon_p)}p_s - \frac{(1-\epsilon'_F)}{\epsilon_\pi(\epsilon'_F-\eta)}e_s$$

$$p = -\frac{(1-\epsilon_\pi)}{(1-\eta)(\epsilon_\pi-\epsilon_p)}\pi_s + \frac{\epsilon_\pi}{(1-\eta)(\epsilon_\pi-\epsilon_p)}p_s \qquad (10.12)$$

$$e = \frac{\eta}{\epsilon_\pi(\epsilon'_F-\eta)}\pi_s + \frac{(1-\eta)}{\epsilon_\pi(\epsilon'_F-\eta)}e_s$$

where

$$\epsilon_F = \epsilon_F + \eta - 2\eta\epsilon_F .$$

The values for π, p, and e in (10.12) can then be substituted into the last equation of (10.11) to get

$$\eta = \frac{x_s - \epsilon_F(1-\epsilon_\pi)e}{((1-\epsilon_\pi)((1-2\epsilon_F)e+\pi)+(1-\epsilon_p)p)} . \qquad (10.13)$$

This value of η can be substituted into the equations in (10.11) which will then give us new solutions for (10.12). These new solutions can be substituted into (10.13) which gives a new value of η. This process is continued until a stable solution is reached (i.e., $0 < \eta < 0.01$). If the solution was unstable, η was set to 0. This only occurred for runs with poor p_s statistics.

For the π^-, HEMA and OUTR, runs protons are not detected by the spectrometer, and this alters Eqs. (10.11) to

$$\begin{aligned}
\pi_s &= (1-\eta)\epsilon_\pi\pi + (1-\epsilon_F-\eta+2\eta\epsilon_F)\epsilon_\pi e \\
p_s &= (1-\eta)(1-\epsilon_\pi)\pi + (1-\epsilon_F-\eta+2\eta\epsilon_F)(1-\epsilon_\pi)e \\
e_s &= \eta\epsilon_\pi\pi + (\epsilon_F+\eta-2\eta\epsilon_F)\epsilon_\pi e \\
x_s &= \eta(1-\epsilon_\pi)\pi + (\epsilon_F+\eta-2\eta\epsilon_F)(1-\epsilon_\pi)e .
\end{aligned} \qquad (10.14)$$

It will be noted that

$$\epsilon_\pi = \frac{\pi_s}{\pi_s + p_s} \tag{10.15}$$

which was used to monitor the LC pion efficiency. If we consider ϵ_π as an unknown in place of p, we have again in (10.14) four equations and four unknowns. However, the equations are not independent, thus are unsolvable. We eliminate an unknown by setting $\eta = 0$. This is justified from the π^+ results where η averaged about 0.25%. We then solve for π and e with the first and third equations of (10.14) and get

$$\begin{aligned} \pi &= \pi_s + p_s - \frac{(1-\epsilon_F)}{\epsilon_\pi - \epsilon_F} e_s \\ e &= \frac{e_s}{\epsilon_\pi \epsilon_F} \end{aligned} \tag{10.16}$$

For the LEM π^+ runs there was no provisions to detect electrons. However, since the LEM runs were always set at wide angles, the electron rate was assumed small. Omitting the references to electrons and the FC counter in (10.11), we solve for π and p and get

$$\begin{aligned} \pi &= \frac{1-\epsilon_p}{\epsilon_\pi - \epsilon_p} \pi_s - \frac{\epsilon_p}{\epsilon_\pi - \epsilon_p} p_s \\ p &= -\frac{1-\epsilon_\pi}{\epsilon_\pi - \epsilon_p} \pi_s + \frac{\epsilon_\pi}{\epsilon_\pi - \epsilon_p} p_s \quad . \end{aligned} \tag{10.17}$$

For the π^- LEM runs we detect on π's assuming that the electron counts are very small. Thus we solve for the pion efficiency as in (10.15) and we solve for the π count which is

$$\pi = \pi_s + p_s \quad . \tag{10.18}$$

For all runs $p_s < 0.01\ \pi_s$.

With the results in this part and in Part A we can now correct the counts in the momentum channel scalers for accidentals and particle detection inefficiencies. If we let M be a momentum channel scaler reading then the corrected reading, M', is

$$M' = \frac{P \cdot \overline{F}_T}{P \cdot \overline{F}} \cdot \frac{\pi}{\pi_s} \cdot M \, . \tag{10.19}$$

The total corrections to M were in the range of + 2% to - 2%.

Where the proton or electron signal is placed in coincidence with the momentum counters, (π/π_s) is replaced by (p/p_s) and (e/e_s) respectively.

C. Doubles Corrections

One might naively expect that the counts in the momentum scalers should add up to the counts in the π scaler or p scaler, which ever type of signal was placed in coincidence with the momentum counters. In practice, this did not prove to be true. The sum of the momentum channel scalers was always somewhat greater than the π scaler reading or p scaler, whichever was relevant. This problem has been encountered before and is extensively discussed by Ecklund [12] who stated that the extra counts were probably due to knock-on electrons. There has to be some correction to remove the extra counts and this is provided by the following simple theory.

We let T, TC, BC, and B represent the counts in the four momentum channels. We assume that the π signal is being sent into the momentum channel coincidences so that the number of doubles is

$$D = (T + TC + BC + B) - \pi \, . \tag{10.20}$$

It will be assumed that the extra counts are caused by the primary particle scattering an electron into an adjacent counter. Therefore the number of doubles in each channel is proportional to the counts in the adjacent channels. We can now write down the doubles corrections for each channel,

$$\begin{aligned} T_d &= TC \cdot D/N \\ TC_d &= (T + BC) \cdot D/N \\ BC_d &= (TC + B) \cdot D/N \\ B_d &= BC \cdot D/N \end{aligned} \tag{10.21}$$

where T_d, etc., are the corrections and N is the normalization which forces

$$T_d + TC_d + BC_d + B_d = D \tag{10.22}$$

to be true. Equations (10.21) and (10.22) give the normalization

$$N = T + 2TC + 2BC + B \, . \tag{10.23}$$

The values calculated in (10.21) are then subtracted from each momentum channel to give the corrected value.

In practice the above process was too simple because particles which missed the momentum counter scattered electrons into T and B. The number of their doubles could not be calculated from Eq. (10.20) and had to be estimated by other means which we shall not go into here. This added correction was about 1% of the total momentum channel counts. The total doubles correction averaged around 2 or 3%.

D. Recoil Calculations

In the recoil electronics there were two scalers, one for the recoil events, the other for the accidental recoil events. The accidentals were defined by delaying the recoil signal an extra 100 ns with respect to the spectrometer trigger. In the following text we shall show how the recoil accidentals were used to correct the recorded recoil events.

We will use the notation

T = number of real π spectrometer triggers

N = number of false π spectrometer triggers

π_S = π scaler reading

π_R = π recoil scaler reading

π_A = accidental π recoil scaler reading

P_R = probability of getting a recoil given a real spectrometer trigger

P_A = probability of getting an accidental recoil given a spectrometer trigger

P_D = probability of losing a recoil because of dead time

It will be noted that if the spectrometer trigger is the π signal then the sum of the real triggers, T, and the false triggers, N, is equal to the counts in the π_S scaler. This is expressed as

$$\pi_S = T + N . \tag{10.24}$$

If we sent the proton spectrometer signal to the recoils instead of the pion signal then the previous sum is equal to the proton scaler. With a little thought we see that the number of counts in the recoil scaler and the number of counts

in the accidental scaler are given by

$$\pi_R = (P_R + P_A - (P_A + P_D)P_R)\,T + P_A N \tag{10.25}$$

and

$$\pi_A = P_A\,(T + N)\,. \tag{10.26}$$

The desired quantity is the number of recoil scaler counts which would result from the real triggers only. This is

$$\pi_T = P_R\,T\,. \tag{10.27}$$

The knowns in the above equations are π_s, π_R, and π_A. We can use Eqs. (10.24) and (10.26) to solve for P_A immediately which gives

$$P_A = \pi_A/\pi_s\,. \tag{10.28}$$

Substituting (10.28) into (10.25) we derive

$$P_R = \frac{\pi_R - \pi_A}{(1-(\pi_A/\pi_s)-P_D)T}\,. \tag{10.29}$$

Using (10.27) in conjuction with (10.29) we derive the number of real recoils which is expressed as

$$\pi_T = (\pi_R - \pi_A)\,\frac{\pi_s}{(\pi_s - \pi_A - P_D\,\pi_s)} \tag{10.30}$$

We are now left with the difficulty of deciding what value to use for the dead time probability P_D. If we assume that all signals from the recoil counters RB and RC (see Figure 40) come directly from the target then RB will fire every time that RC does. Hence the probability for having an accidental is just the RC

live time probability $P_A = R \cdot L$ where R is the RC counting rate and L is the RC live time per count. Since RB has 5.4336 times the area of RC, the RB live time probability, P_B, will be $5.4336 \times P_A$. We will further assume that the dead time of both RB and RC is equal to their live time, which is the same assumption used in Part A for the FAN dead time probability. This assumption will make the live time probability for each counter equal to its dead time probability. The value for P_D is then the probability that either RC or RB will be dead for a given trigger. This is expressed in the equation

$$P_D = P_A + P_B - P_A P_B . \tag{10.31}$$

The above calculation for P_D is not especially accurate but the size of correction it makes to the real recoil events only warrants an order magnitude estimate.

To complete the recoil calculations we must correct the momentum channel recoil counts for the recoil accidentals and the efficiency of detecting the particles. If M is a recoil momentum channel count and M' is the corrected value then the equation needed is

$$M' = \frac{1}{E} \frac{\pi_T}{\pi_R} M \tag{10.32}$$

where

$$E = (1-\eta)\,\epsilon_\pi \text{ for a } \pi^+ \text{ run},$$

$$E = \epsilon_\pi \text{ for a } \pi^- \text{ run},$$

or

$$E = (1-\eta)\,(1-\epsilon_P) \text{ for a proton run.}$$

The equations for E were taken from Part B. Values for (π_T/π_R) were typically 1.035.

E. Data Handling

To reduce the raw scaler readings into cross sections, the raw data had to be first corrected by the analysis described in this appendix, and then reduced to rates by dividing by the amount of beam energy for each run, and finally turned into cross sections. To do this a number of computer programs were written which ran the data through the process indicated in Figure 48.

Before this procedure could be followed all the information recorded in the log books had to be punched onto IBM cards. Although this was a rather crude procedure, the situation was not altogether in the Dark Ages. There was a time-sharing computer console beside the experimental bay which was programmed to give preliminary cross sections as soon as each run was completed. This was generally not done because the time-sharing system was down most of the time, so run data were generally accumulated for a day before being put into the time-sharing system. These preliminary cross sections proved useful not only for detecting erroneous runs quickly but also for giving first indications of the final results.

For the final data the information on the punched cards were first checked by Phase I for any errors in the logging or the punching of the data. Then once all the mistakes detected by Phase I were corrected, as much as possible, the surviving runs were sent into Phase II which performed all the corrections to the raw data described in the first parts of this appendix. Phase II also calculated rates using the beam energies stored in MØNITØR. The information from Phase II was then fed as data into Phase III. Phase III contained a compilation of the experimental responses (see Appendix II) for each experimental

setting and contained the fits for nuclear absorption and muon contamination. With this information Phase III calculated the cross sections using the formula (2.27). The computer punched the output from Phase III onto cards which could then be used as input for the data manipulation routines. These routines were programs to average data, plot graphs, print tables, etc.

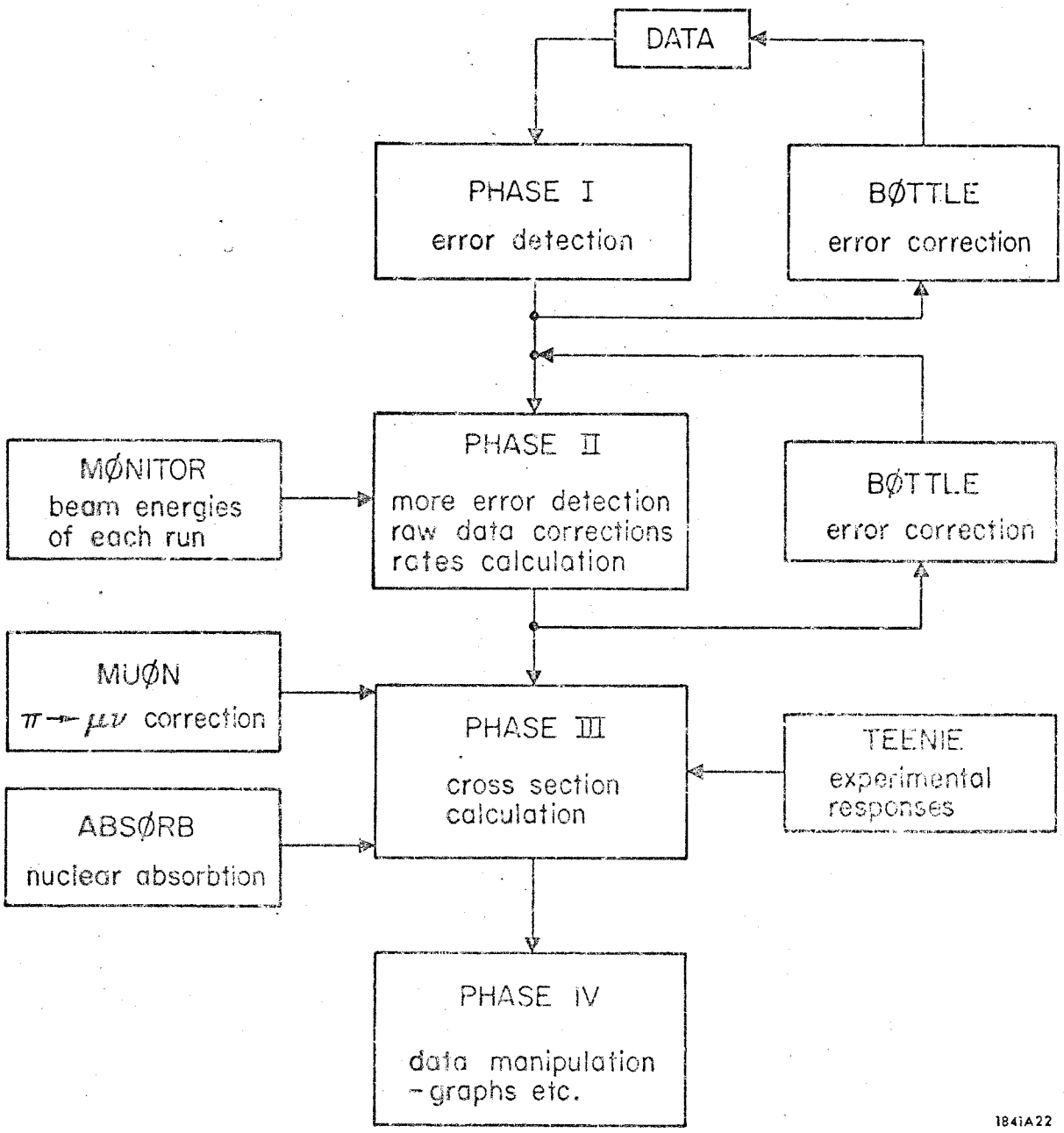

FIGURE 48

Data Handling

APPENDIX 11

BEAM AND TARGET

The layout of the beam area is shown in Figure 1. The photon beam was produced by the electron beam of the synchrotron hitting a 0.2 radiation-length Ta target. The beam passed through a rectangular collimator, scraping walls, and a set of sweeping magnets before reaching the UCLA LH_2 target which was upstream of our LD_2 target. In order to remove interaction particles and electron pairs produced in the UCLA target, the beam had to pass through more scrappers and another sweeping magnet before reaching our target. To decrease number of electron pairs created after the last sweeping magnet a He bag was placed between the last sweeping magnet and the target. The entire beam length was 408 inches and at the target the beam size was 1.5 inches wide by 1.78 inches high. This beam has been used by many experimenters and is more fully described in other sources [5, 10, 11, 12, 13].

The total energy in the bremsstrahlung beam was monitored by six devices. They are:

1. TC-1, a thin-walled ionization chamber placed upstream of the target.
2. TC-2, a second thin-walled ionization chamber placed upstream of the target.
3. 40 MH probe, a device monitoring the amount of electron current in the synchrotron before hitting a Ta radiator.
4. MT, a monitor telescope consisting of two counters which were connected in coincidence in order to record reaction particles produced in the target.
5. BC, an ionization chamber placed downstream of the target.
6. Q, a Wilson-type quantameter [25].

The Q monitor was the primary monitor for the experiment. However, it was not used during any of the data runs. Instead secondary monitors (1-5) were used to monitor beam energy during data runs and some of these (1-3) were intercalibrated with the Q during special quantameter runs which were interspaced between the data runs. The description of the beam monitoring has been brief because the task of computing beam energies was entirely done by Mr. Paul E. Scheffler and the results are reported in his thesis [8].

The target was a three inch diameter vertical cylinder made of 0.005 inch mylar. The deuterium was in a sealed container surrounded by a bath of liquid hydrogen set at one atmosphere plus $\frac{1}{2}$ lb./in^2 pressure. The density of the liquid deuterium was calculated from PVT equations [50] which gave a density of 0.1706 gm/cm^{-3}. This value was confirmed by a reading of -20" Hg pressure inside the sealed liquid deuterium container which the PVT equations predicted to be -19.48" Hg.

REFERENCES

1. Gerry Neugebauer, Walter Wales, and R. L. Walker, Phys. Rev. 119, 1726 (1960).
2. R. L. Walker, Phys. Rev. 182, 1729 (1969).
3. K. M. Watson, Phys. Rev. 85, 852 (1952).
4. A. I. Sanda and Graham Shaw, Phys. Rev. Letters 24, 1310 (1970).
5. S. D. Ecklund and R. L. Walker, Phys. Rev. 159, 1195 (1967).
6. R. L. Walker, in International Symposium on Electron and Photon Interactions at High Energies, Liverpool, England, 1969, edited by D. W. Braben and R. E. Rand (Daresbury Nuclear Physics Laboratory, Daresbury, Lancashire, England, 1970).
7. R. P. Feynman, M. Kislinger, and F. Ravndal, Phys. Rev. D3, 270 (1971).
8. Paul E. Scheffler, private communication.
9. L. A. Copley, G. Karl, and E. Obryk, Nucl. Phys. B13, 303 (1969).
10. H. A. Thiessen, Ph. D. Thesis, California Institute of Technology (1966).
11. F. Wolverton, Ph. D. Thesis, California Institute of Technology (1968).
12. S. D. Ecklund, Ph. D. Thesis, California Institute of Technology (1966).
13. H. A. Thiessen, Phys. Rev. 155, 1488 (1967).
14. G. Gatti et al., Phys. Rev. Letters 6, 706 (1961).
15. P. A. Berardo et al., Phys. Rev. Letters 24, 419 (1970).
16. J. Favier et al., Phys. Letters 31B, 609 (1970).
17. G. F. Chew and H. W. Lewis, Phys. Rev. 84, 779 (1951).
18. R. J. Glaubler, Phys. Rev. 100, 242 (1955).
19. D. O. Caldwell et al., Phys. Rev. Letters 23, 1256 (1969).

20. H. P. Hesse et al., Phys. Rev. Letters 25, 613 (1970).

21. Nathan W. Dean, Phys. Rev. Letters 27, 276 (1971).

22. V. Franco and R. J. Glaubler, Phys. Rev. 142, 1195 (1966).

23. V. Franco and R. J. Glaubler, Phys. Rev. 156, 1685 (1967).

24. David I. Julius, Nucl. Phys. B27, 269 (1971).

25. Robert L. Wilson, Nucl. Inst. 1, 101 (1957).

26. H. G. Hilpert et al., Nucl. Phys. B8, 535 (1968).

27. M. J. Moravcsik, Phys. Rev. 104, 1451 (1956).

28. P. E. Scheffler and P. L. Walden, Phys. Rev. Letters 24, 952 (1970).

29. T. Fujii et al., Phys. Rev. Letters 26, 1672 (1971).

30. R. L. Walker, private communication.

31. F. Wolverton, "Manual for BPAKI, Thick Radiator Bremsstrahlung Computer Program", unpublished (1965).

32. For an adequate treatment of this subject see I. S. Sokolnikoff and R. M. Redheffer, "Mathematics of Physics and Modern Engineering", (McGraw-Hill Book Company, Inc., 1958), p. 667.

33. H. A. Thiessen, "π-μ Decay Analysis Program", unpublished (1964).

34. J. H. Boyden, Ph. D. Thesis, California Institute of Technology (1963).

35. J. R. Kilner, Ph. D. Thesis, California Institute of Technology (1963).

36. H. A. Thiessen, "Calibration of the 600 MeV/c Magnet", CTSL Internal Report No. 27, unpublished (1966).

37. F. Wolverton, "Calibration of the 1200 MeV/c and 1670 MeV/c Magnet", CTSL Internal Report No. 36, unpublished (1966).

38. H. A. Thiessen, "HAT009B/Q-BETA Fit Integration Routine", unpublished (1965).

39. M. G. Hauser, Phys. Rev. 160, 1215 (1967).

40. J. V. Allaby, H. L. Lynch, and D. M. Ritson, Phys. Rev. 142, 887 (1966).

41. R. Erbe et al., DESY 68/8, May 1968.

42. J. D. Jackson, Nuovo Cimento 34, 1644 (1964).

43. M. G. Hauser, "Calculation of Effective Bremsstrahlung Spectrum for a Rectangular Collimator and a Cylindrical Hydrogen Target", CTSL Internal Report No. 26, unpublished (1966).

44. A. Piazza et al., Letters al Nuovo Cimento 3, 403 (1970).

45. Donald E. Groom, "A General Range-Energy-Light Output Program for High Energy Physics", CTSL Internal Report No. 20, unpublished (1965).

46. B. Musgrave; in Proceedings of the Conference on the Phenomenology of Particle Physics, California Institute of Technology, Pasadena, California, March 1971.

47. A. Ito, R. Loe, E. Loh, A. Ramanauskas, D. Ritchie and W. Schmidt, Phys. Rev. Letters 24, 687 (1970).

48. E. Lodi-Rizzini, G. C. Mantovani, A. Piazzoli, L. Fiore, G. Gialanella, V. Rossi, A. Piazza, G. Susino, F. Carbonara, M. Napolitano, and R. Rinzivillo, Lettre al Nuovo Cimento 3, 697 (1970).

49. M. Beneventano, F. de Notaristefani, P. Monacelli, L. Paoluzi, F. Sebastiani, and M. Severi, Lettre al Nuovo Cimento 1, 113 (1969).

50. U. S. National Bureau of Standards, Journal of Research 41, 458 (1948).